ARL-SR-0450 ● JULY 2021

DEVCOM ARMY RESEARCH LABORATORY

Cognition and Neuroergonomics Collaborative Technology Alliance Final Report (Summary Technical Report, June 2010–May 2020)

by Jonathan Touryan and Timothy Lee

Approved for public release: distribution unlimited.

NOTICES

Disclaimers

The findings in this report are not to be construed as an official Department of the Army position unless so designated by other authorized documents.

Citation of manufacturer's or trade names does not constitute an official endorsement or approval of the use thereof.

Destroy this report when it is no longer needed. Do not return it to the originator.

ARL-SR-0450 ● JULY 2021



Cognition and Neuroergonomics Collaborative Technology Alliance Final Report (Summary Technical Report, June 2010–May 2020)

Jonathan Touryan and Timothy Lee
Human Research and Engineering Directorate,
DEVCOM Army Research Laboratory

Approved for public release: distribution unlimited.

REPORT DOCUMENTATION PAGE		Form Approved OMB No. 0704-0188

Public reporting burden for this collection of information is estimated to average 1 hour per response, including the time for reviewing instructions, searching existing data sources, gathering and maintaining the data needed, and completing and reviewing the collection information. Send comments regarding this burden estimate or any other aspect of this collection of information, including suggestions for reducing the burden, to Department of Defense, Washington Headquarters Services, Directorate for Information Operations and Reports (0704-0188), 1215 Jefferson Davis Highway, Suite 1204, Arlington, VA 22202-4302. Respondents should be aware that notwithstanding any other provision of law, no person shall be subject to any penalty for failing to comply with a collection of information if it does not display a currently valid OMB control number.
PLEASE DO NOT RETURN YOUR FORM TO THE ABOVE ADDRESS.

1. REPORT DATE *(DD-MM-YYYY)*	2. REPORT TYPE	3. DATES COVERED (From - To)
July 2021	Summary Technical Report	June 2010–May 2020

4. TITLE AND SUBTITLE	5a. CONTRACT NUMBER
Cognition and Neuroergonomics Collaborative Technology Alliance Final Report (Summary Technical Report, June 2010–May 2020)	5b. GRANT NUMBER
	5c. PROGRAM ELEMENT NUMBER
6. AUTHOR(S) Jonathan Touryan and Timothy Lee	5d. PROJECT NUMBER
	5e. TASK NUMBER
	5f. WORK UNIT NUMBER
7. PERFORMING ORGANIZATION NAME(S) AND ADDRESS(ES) DEVCOM Army Research Laboratory ATTN: FCDD-RLH-FC Aberdeen Proving Ground, MD 21005	8. PERFORMING ORGANIZATION REPORT NUMBER ARL-SR-0450
9. SPONSORING/MONITORING AGENCY NAME(S) AND ADDRESS(ES)	10. SPONSOR/MONITOR'S ACRONYM(S)
	11. SPONSOR/MONITOR'S REPORT NUMBER(S)

12. DISTRIBUTION/AVAILABILITY STATEMENT

Approved for public release: distribution unlimited.

13. SUPPLEMENTARY NOTES

ORCID ID(s): Jonathan Touryan, 0000-0001-7343-7869

14. ABSTRACT

The Cognition and Neuroergonomics (CaN) Collaborative Technology Alliance (CTA) was a 10-year basic science research and technology transition program in the neurosciences. Formed by the US Army Combat Capabilities Development Command Army Research Laboratory in 2010, this program was a collaborative effort among Government, industry, and academic partners. Over its tenure, the CaN CTA made significant advances in neuroscience, neurotechnology, and related fields. The work under the CaN CTA has impacted a number of Army programs using neurotechnology to enhance next-generation Soldier systems. This report provides both a high-level overview of the vision, approach, and impact of the program as well as detailed scientific progress and technical achievements from the member organizations.

15. SUBJECT TERMS

neuroergonomics, neuroscience, neurotechnology, brain–computer interface, cognition, neuroimaging, bioengineering, Summary Technical Report, STR

16. SECURITY CLASSIFICATION OF:			17. LIMITATION OF ABSTRACT	18. NUMBER OF PAGES	19a. NAME OF RESPONSIBLE PERSON
a. REPORT	b. ABSTRACT	c. THIS PAGE			Jonathan Touryan
Unclassified	Unclassified	Unclassified	UU	236	19b. TELEPHONE NUMBER (Include area code) (410) 278-4329

Standard Form 298 (Rev. 8/98)
Prescribed by ANSI Std. Z39.18

Contents

List of Figures ix

List of Tables xvi

1. Introduction 1

1.1 Organization 1

1.2 Technology Transfer 2

1.3 Vision 3

1.4 Journey toward the Vision 6

2. Progression of Research Achievements 11

3. Columbia University 12

3.1 Methods for Analysis and Integration of Neural, Physiological, and Behavioral Data 13

3.1.1 Latent Neural Source Recovery via Transcoding of Simultaneous EEG-fMRI 13

3.1.2 A State-Space Model for Inferring Effective Connectivity of Latent Neural Dynamics 14

3.1.3 Estimation of Phase in EEG Rhythms for Real-Time Applications 15

3.1.4 Ballistocardiogram Artifact Reduction in Simultaneous EEG-fMRI Using Deep Learning 15

3.2 Using VR as an Experimental Platform for Cognitive Neuroscience 16

3.2.1 Regulation of Arousal via Online Neurofeedback Improves Human Performance in a Demanding Sensory-Motor Task 16

3.2.2 Neurally and Ocularly Informed Graph-Based Models for Searching 3-D Environments 17

3.2.3 NEDE, an Open-Source Scripting Suite for Developing Experiments in 3-D Virtual Environments 18

3.3 Understanding the Neural Basis of Decision-Making and Expertise 19

3.3.1 A Multimodal Encoding Model Applied to Imaging Decision-Related Neural Cascades in the Human Brain 19

3.3.2 Perceptual Salience and Reward Both Influence Feedback-Related Neural Activity Arising from Choice 20
3.3.3 Knowing When Not to Swing: EEG Evidence that Enhanced Perception–Action Coupling Underlies Baseball Batter Expertise 21
3.4 Network Configurations in the Human Brain Reflect Choice Bias during Rapid Face 21
3.4.1 Brain Networks for Perceptual Processing 21
3.4.2 Decomposing Simon Task BOLD Activation Using a Drift-Diffusion Model Framework 22
3.5 References 23
3.5.1 Journal Articles 23
3.5.2 Conference Proceedings 24
3.5.3 Archives 25
3.5.4 Patents 26

4. DCS Corporation 27

4.1 Operator Dynamics of Event (ODE) Appraisal 27
4.1.1 Purpose of ODE Study 27
4.1.2 Accomplishments 28
4.2 Informed Multidimensional Independent Components Analysis (IMICA) 32
4.2.1 IMICA BCI 36
4.2.2 Comparison 36
4.2.3 Data Sets 37
4.2.4 BCI Approaches Used 38
4.3 CaN CTA Consortium Data Server (C3DS) 41
4.4 Deep Learning for EEG Feature Extraction and Classification 42
4.5 BCI Test Bed 43
4.6 BCI-Fixation-Related Potential (FRP) 45
4.7 References 48

5. University of Michigan (UMI)/University of Florida (UFL) 50

5.1 Brain and Body Dynamics of Healthy Individuals under Conditions of Cognitive and Physical Stress 50
5.1.1 Cognitive Loading during Walking at Different Speeds 50

5.1.2 Locomotion on Uneven Terrain 51
5.1.3 Large-Scale Integrative Experiment (LSIE) 53
5.1.4 Comparison of Stress Responses in Real-World Environments 53
5.1.5 Electrocortical Effects of Virtual Reality Use during Balance Beam Walking 54
5.1.6 Measurement of Spatial Myoelectric Patterns during Human Locomotion Using High-Density Electromyography 55
5.2 Assessment of Signal-Processing Methods and Approaches for Removing Motion Artifact in Real-World Neuroimaging Technologies 56
5.2.1 Isolation of Gait-Related Motion Artifacts Recorded Using EEG 56
5.2.2 Development of Benchmarks for Data Quality of Real-World Neuroimaging Technologies 58
5.2.3 Electrical Head Phantom with User-Defined, Ground-Truth Sources 58
5.2.4 Effects of Cable Sway, Electrode Surface Area, and Electrode Mass on EEG Signal Quality 59
5.2.5 Dual-Electrode EEG Design for Motion Artifact Removal 60
5.2.6 Integration of Neck Muscle Sources for Muscle Artifact Removal 60
5.2.7 Brain Dynamics during Obstacle Navigation 61
5.3 References (Refereed Journal Articles) 62

6. University of California, San Diego 66

6.1 Advanced Computational Approaches: Neurocomputation 66
6.1.1 First-Year Objectives 66
6.1.2 First-Year Accomplishments 66
6.1.3 NCP Third-Year Objectives 68
6.1.4 Third-Year Accomplishments 69
6.2 Neurocognitive Performance: Large-Scale Experiment (LSE) 72
6.2.1 Research Goals 72
6.2.2 Third-Year Accomplishment 73
6.2.3 LSE Year 4 76
6.3 STRUM Data Analysis (UCSD) 76
6.3.1 ACA LSIE EEG-Focused Analysis (LSIE-EEG) 76

6.3.2 ACA Integrating Multi-Aspect Information (IMAI) 78
6.4 References 79

7. National Chiao Tung University (with UCSD Collaboration) 87

7.1 Neurotechnologies: Effects of Vehicle Motion and Cognitive Fatigue (VMF) 87
7.1.1 VMF Year 1–2 87
7.1.2 VMF Program Year 1 and 2 Accomplishments 87
7.1.3 VMF Year 3 89
7.1.4 VMF Program Year 3 Accomplishments 91
7.1.5 VMF Year 4 94
7.2 Neurotechnologies: Wearable EEG Development and Testing (WDT) 109
7.2.1 WDT Research Goals 109
7.2.2 WDT Year 1–2 110
7.2.3 WDT Year 1–2 Accomplishments 110
7.2.4 WDT Year 3 Accomplishments 111
7.2.5 WDT Year 4 115
7.3 Publications and Transitions (UCSD, NCTU) 117

8. Three-Year Collaborative Research 122

8.1 Real-World Neuroimaging: Understanding Real-World Fatigue in Vehicle Driving Experiments RWN-VDE 122
8.1.1 RWN VDE Background 122
8.1.2 Real-World Driving Experiment Longitudinal Study 124
8.1.3 Simulated Driving Experiment Longitudinal Study 125
8.1.4 Big Data Approach 130
8.2 Brain–Computer Interface: Effects of State Changes on BCI Technologies over Long Time Periods (BCI-GEM) 133
8.2.1 BCI-GEM Goals 133
8.2.2 BCI-GEM Accomplishment 134
8.3 References 146

9. University of Texas, San Antonio 148

9.1 ACA-NSST: ACA Improving EEG-Based Detection of Nonstationary Short-Term Spectral Features with Application to Attention and Fatigue (Robbins) 148

9.2. ACA-SANDR: Standardized Annotated Neurophysiology Data Repository (Robbins) 149

9.3 ACA/BCI/RWN-LARG: Large-Scale EEG Analysis and Validation of Event Tags (Robbins) 151

9.4 ACA Large-Scale Electroencephalography (EEG) Analysis and Exploration of Cognitive Aspects (LARG-II) (Robbins and Huang) 152

9.5 References 154

9.5.1 Journal Articles 154

9.5.2 Papers Submitted to Conferences 155

9.5.3 Extended Abstracts Presented 156

10. University of Pennsylvania 157

10.1 Overall Contribution to the CaN CTA 157

10.2 Real-World Neuroimaging Vehicle Driving Experiment 158

10.2.1 Aim 1 158

10.2.2 Aim 2 159

10.2.3 Further Exploration 160

10.3 Papers Submitted and Under Review 161

10.4 Development of Algorithms for Reading Real-World Brain States 169

10.5 Conference Presentations (from 2018–2020 Supported by ARL Funding) 170

10.6 Top Paper Award 172

10.7 Publications (from 2018–2020 Supported by ARL Funding) 174

11. Syntrogi Inc. 178

11.1 ACA Large-Scale Electroencephalography (EEG) Analysis and Exploration of Cognitive Aspects (LARG-II) 178

11.2 Lab Streaming Layer Development and Maintenance (LSL-DM) 184

11.2.1 Development and Maintenance 184

11.2.2 Application Development 186

11.2.3 Journal Paper 186

11.2.4 Community and Standardization Efforts 186

11.2.5 Transition Opportunities/Standards Initiatives 187

11.2.6 Synergistic Projects 187
11.2.7 Community Outreach 189
11.3 Publication Summary for PY10 191
11.4 References 192

12. University of Maryland, Baltimore County 194
12.1 Human-in-the-Loop Model Refinement for Efficient Deep Reinforcement Learning 194
12.2 Publications 194

13. Bibliography of Representative Publications 198

14. CaN CTA Research Contributors 204

List of Symbols, Abbreviations, and Acronyms 208

Distribution List 218

List of Figures

Fig. 1.1 CaN CTA technical barriers..... 4

Fig. 1.2 Program years 1 and 2..... 7

Fig. 1.3 Program years 3 and 4..... 7

Fig. 1.4 Program years 5 and 6..... 8

Fig. 1.5 Program years 7 and 8..... 9

Fig. 1.6 Program years 9 and 10..... 10

Fig. 3.1 Comparing fMRI transcoded from EEG and real fMRI data: fMRI transcoded from EEG has a spatial resolution of 12 mm × 12 mm × 12 mm, while real fMRI data has a spatial resolution of 2 mm × 2 mm × 2 mm 14

Fig. 3.2 Setup of experiment and study protocol. Study participants alternately guided a virtual aircraft through an easy or hard course of red rectangular boundaries (rings). Both courses were a maximum of 90 s long and increased in difficulty over time as ring sizes decreased. Missing a ring ended the flight trial immediately. Every new flight attempt was randomly assigned one of three feedback conditions. In the main condition, a) BCI, audio feedback from an EEG-based decoder was presented to the participant (closed-loop experiment). During the two control conditions b) sham and c) silence, partly random or no audio signal was presented, respectively. Participants were instructed to down-regulate their arousal as outlined at the bottom left of the panel. 17

Fig. 3.3 Overview of NEDE..... 18

Fig. 3.4 Group-level encoding model weights results show a cascade of neural activation. Subset of thresholded (false discovery rate-corrected, k = 10) group-level statistical parametric maps created by the spatiotemporal threshold-free cluster enhancement (stTFCE) randomization procedure on the encoding model weight matrices. Shown is the progression of spatial activity across the trial. Activation can be seen early in the trial in the occipital regions while progressing more anteriorly later in the trial to executive control areas. Activations in red indicate areas where high stimulus evidence trials had larger activations than low stimulus evidence trials, with blue the inverse relationship..... 20

Fig. 4.1 DCS research progression..... 27

Fig. 4.2 Integration of all data streams for one representative subject..... 29

Fig. 4.3 Accuracy per target type for Game 1 No-Fog, Game 2 No-Fog, Game 1 Fog, and Game 2 Fog sorted by target type (top) and game condition (bottom)..... 30

Fig. 4.4 Reference pairs used to capture EOG artifacts. (Top-left) Horizontal reference based on the position of a bouncing ball the subjects were instructed to visually track. (Top-right) Vertical reference based on the position of a bouncing ball the subjects were instructed to visually track. (Middle-left) Horizontal reference based on eye-tracker recordings during the bouncing ball task. (Middle-right) Vertical reference based on eye-tracker recordings during the bouncing ball task. (Bottom-left) Horizontal EOG during the bouncing ball task. (Bottom-right) Vertical EOG during both the bouncing ball task. 33

Fig. 4.5 Reduction in visual ERP as more components are used to isolate and remove the jaw clench artifact. Performance is measured as correlation values between the original ERP and the ERP obtained after removal of the artifact subspace. For all visual-evoked potentials (VEPs), there was no artifact present during the event. These results show that IMICA better isolated the jaw clench subspace..... 34

Fig. 4.6 Identified component projections for alpha-fog correlation. The first three components (top row) all have strong projections from the occipital cortex, as expected. 35

Fig. 4.7 Plot of normalized alpha (black line) and fog (red line) using components extracted from Fig. 4-6. 35

Fig. 4.8 Comparing IMICA, ICA, and PCA decomposition/component selection for one subject of the MRCP data set. The time-frequency data is plotted for right-hand movements at electrode C3 (i.e., contralateral hemisphere). Top left: Backprojection of selected 14 IMICA components. Top middle: backprojection of 27 components from Infomax ICA-IG. Top right: Backprojection of 47 components selected from PCA-IG. Bottom left: Backprojection of 50 nonselected IMICA components. Bottom middle: Backprojection of 37 nonselected ICA components. Bottom right: Backprojection of 17 nonselected PCA components 40

Fig. 4.9 BCI performance results for the MRCP data set. In each group, the bar on the left (solid color) indicates the MINP condition. The remaining bars indicate performance using the selected components (dark gray) and removing the selected components (light gray). 40

Fig. 4.10 BCI performance results for the RSVP data set. In each group, the bar on the left (solid color) indicates the MINP condition. The remaining bars indicate performance using the selected components (dark gray) and removing the selected components (light gray). 41

Fig. 4.11 Sample P300 evoked response to targets (red line) and non-targets (blue line) 42

Fig. 4.12 Application of EEGNet to leave-one-experiment-out study of P300 variability 43

Fig. 4.13 BCI Test Bed architecture developed by DCS in collaboration with ARL (iconography from Syntrogi Inc.) 44

Fig. 4.14 Operational concept of using a HID to map an external environment 45

Fig. 4.15 BCI scores using a collaborative approach across 16 individuals for target detection in the ODE environment 45

Fig. 4.16 Proposed concept: Fixations from different individuals are co-registered using eye tracking and position/orientation at the time of each fixation. Fixations are classified using the deep learner. As objects are tagged by individuals, the location of those objects are placed in a world map as either "group" or "individual" tagged. Periods of high workload are identified for each individual as they traverse the environment. 46

Fig. 4.17 Implementation of our HID task in Unity3D 47

Fig. 4.18 Object types ranked by aggregate neural score (e.g., EEGNet output) for both the MOTORCYCLES and HUMVEE groups. In both cases, the aggregate scoring correctly uncovers the target object for that group with a predominance of those objects occurring high in the rankings. Mean and standard errors are shown for each object group. 48

Fig. 5.1 Event-related spectral perturbation plots showing power change around the presentation of a stimulus in the central somatosensory association cortex 51

Fig. 5.2 a) Treadmill with the uneven terrain surface attached. b) Schematic of the uneven surface layout, consisting of three alternating heights (arrows indicate the treadmill's long axis). c) Close-up representation of the individual blocks composing each stepping area 52

Fig. 5.3 Net metabolic rate for walking and running on the even and uneven surfaces. Percentages indicate the increases in energetic cost caused by uneven terrain when compared with even walking or running. Asterisks signify a statistically significant difference between the even and uneven walking and running conditions. 52

Fig. 5.4 Percent change in failures per minute, heart rate, and RT. Being in VR increased overall stress metrics and being in the simulated beam walking at a high height increased variability in measures considerably. 54

Fig. 5.5 Time courses of movement artifact and accelerometer data. Time courses of the ground reaction forces for the right and left legs, head accelerations (vertical, mediolateral, and anterior–posterior), and movement artifacts recorded in five electrodes (A1, A19, C18, E12, and G11) for the four walking speeds (0.4, 0.8, 1.2, and 1.6 m s^{-1}) for a single subject. 57

Fig. 5.6 a) Computerized tomography (CT) scan of the plaster phantom head showing the distribution of antennae. b) We broadcast artificial "neural" signals from three antennae at varying frequencies. c) We recorded high-density EEG data using three different systems for comparison. 59

Fig. 5.7 a) BioSemi active pin type electrode, b) custom dual-electrode pair (BioSemi active pin type electrode and inverted flat type electrode). 60

Fig. 5.8 Cortical clusters and event-related spectral perturbation plots by speed in the a) supplementary motor area, b) premotor cortex, and c) posterior parietal cortex. 62
Fig. 6.1 STRUM apparatus 73
Fig. 6.2 IMAI source space modeling. (Left) Scalp, skull, CSF, and brain surfaces for one subject including the measured 128 scalp electrode locations. (Right) High-resolution Freesurfer cortical source space for the same subject. 79
Fig. 7.1 Magnitude of connectivity observed in every pair of brain regions ... 95
Fig. 7.2 Significant information flow of alpha band (8–12 Hz) in four different arousal levels 96
Fig. 7.3 The summary reaction time of 31 preliminary behavioral data. (Upper panel) Average RT for DAS and (lower panel) average RT for driving; (right) visual condition and (left) auditory condition. 98
Fig. 7.4 EEG data were decomposed and grouped to some frontal, motor, parietal, and occipital clusters 99
Fig. 7.5 Design of EEG signal acquisition, processing, and analysis system 100
Fig. 7.6 Weighted spectral power estimation 101
Fig. 7.7 Temporal changes in a) the vigilance level predicted by the proposed system, b) the vehicle trajectory, and c) the RT observed during a 70-min experiment. 102
Fig. 7.8 The behavioral relationships between participants' responses to the lane-deviation and math problems in the distracted driving 104
Fig. 7.9 The specific frequency bands in the lane-deviation driving and problem-solving mathematic tasks 105
Fig. 7.10 The significant difference and selected frequency bands were marked in the PSD from six brain areas 106
Fig. 7.11 The estimated FOA by the SVMRBF during the driving-math dual tasks and the relationship between the ST and the estimated FOA on driving 108
Fig. 7.12 4-channel MINDO headband 115
Fig. 7.13 MINDO 32 116
Fig. 7.14 64-channel MINDO-64 117
Fig. 8.1 RW vehicle driving DAQ 124
Fig. 8.2 NCTU MVS 125
Fig. 8.3 NCTU VDE experiment design 126
Fig. 8.4 The tonic EEG dynamics images with respect to normalized RT depicted for four brain components under three different fatigue groups, respectively (vertical axis, frequency, Hz; horizontal axis, RT-sorted index, and the corresponding normalized RT) 127

Fig. 8.5 The trends of parietal channels (P1, P2, and Pz) pre-stimulus EEG log power mean depicted for four frequency bands, respectively, and results of the correlation spectrum in parietal channels (vertical axis, Pearson's R-value; horizontal axis, frequency, Hz)..... 128

Fig. 8.6 The trends of occipital channels (O1, O2, and Oz) pre-stimulus EEG log power mean depicted in four frequency bands, respectively, and results of the correlation spectrum in occipital channels (vertical axis, Pearson's R-value; horizontal axis, frequency, Hz)..... 128

Fig. 8.7 MVS vehicle driver brain network dynamics. 131

Fig. 8.8 The flowchart of the experimental protocol (left panel) and the criteria for delivering warning feedback to drivers during driving tasks (right panel)..... 132

Fig. 8.9 Structure of the developed BCI-GEM and the acquired relative data 134

Fig. 8.10 Rapid ERP detection. a) Radial basis function network applied to ERP-based BCI. b) RSVP paradigm. The uppercase letters randomly present to subjects who are instructed to respond to the target (i.e., the letter "G"). Performance comparison of the ERP was estimated by evolutionary algorithm (EA) and DR-RBFN algorithm. c) ERP estimated by applying EA on 80 epochs. Red and blue traces represent the target- and non-target-evoked ERPs, respectively. d) Target-evoked ERP estimated by applying DR-RBFN on 20 (green), 40 (black), 60 (blue), and 80 (red) epochs. 135

Fig. 8.11 Two platforms were set for acquiring physiological data as executing BCI-GEM..... 136

Fig. 8.12 EyeTribe tracker was tested for monitoring the eye movement 136

Fig. 8.13 Polynomial model ($r^2 = 0.41$ incl. all subjects) of resting upper alpha–MI accuracy relationship. On y-axis, MI Accuracy changes; on x-axis, resting upper alpha variations between sessions..... 138

Fig. 8.14 Dynamic TW and MutInf relationship in upper alpha between untrained data set (blue) and trained (orange). 140

Fig. 8.15 (top) ERD and (bottom) ERSP 141

Fig. 8.16 ERP maps for learning and fatigue, where FH = first half data of session, SH = second half data of session; ERP – O (Oct) and ERP – N (Nov) are data from two continuous months with a gap of four weeks..... 142

Fig. 8.17 Scores earned by subjects in the attention task..... 142

Fig. 8.18 Boxplot of maximal GFP values (y-axis) over experimental time course in lower alpha. Boxplot of maximal GFP values (y-axis) over experimental time course in lower alpha. The x-axis represents four experimental conditions: (from left to right) 1: untrained data set at beginning of gameplay, 2: untrained data set at end of gameplay, 3:

trained data set at beginning of gameplay, 4: trained data set at end of gameplay. 143

Fig. 8.19 Lower alpha: dynamic TW and MutInf. Lower alpha: dynamic TW and MutInf mean values across time (mean ± std from 15 scalp derivations). Untrained data set in blue, trained data set in violet.... 144

Fig. 8.20 Upper alpha: dynamic TW and MutInf. Upper alpha: dynamic TW and MutInf mean values across time (mean ± std from 15 scalp derivations). Untrained data set in blue, trained data set in violet.... 144

Fig. 8.21 Upper alpha mean of instantaneous phase shifts over FC3, FCz, FC4, C3, Cz, C4, CP3, CP4, and CPz. Upper alpha mean of instantaneous phase shifts over FC3, FCz, FC4, C3, Cz, C4, CP3, CP4, and CPz (same electrodes as Fig. 8.9). Phase differences seem to be more sustained in the intra-session variables of the trained data set (71% of epoch points in the trained data set have a higher instantaneous phase difference). 145

Fig. 9.1 Composite screenshots of the new online HED validator 150

Fig. 10.1 The degree to which the pattern of brain activity for each individual banner matches predefined maps for negative and positive emotion, as well as vividness is linked to the population-level click-through rate generated by the same banners. Banners that prompt brain activity patterns that better match negative emotion and vividness signatures tend to have lower population-level click-through-rates. All analyses are based on ranked similarity and click-through-rate scores, respectively. 162

Fig. 10.2 Neural activation during Balloon Analogue Risk Task (BART) balloon inflation in the VS and the ventromedial prefrontal cortex (VMPFC) is associated with the number of social network clusters. 163

Fig. 10.3 Relationship between ISC in participants' neural activity during ad watching and similarity between participants' a) ad effectiveness ratings and b) verbal ad evaluation. a) Regions in which ISC was significantly associated with similarities in participants' ad effectiveness ratings. Significant clusters include regions associated with higher-order visual processing such as the occipital-temporal cortex and socio-semantic processing regions such as the temporoparietal junction. b) Regions in which ISC was significantly associated with similarities in participants' verbal ad evaluation. Significant clusters include regions associated with higher-order visual processing, as well as midline structures associated with self-related and valuation (e.g., VMPFC). 164

Fig. 10.4 ROIs and how their neural activation in the BART related to changes in risky driving in the simulated driving task. No relationship was found between stake-modulated VS activation and changes in risky driving: a) passenger type marginally moderated the relationship between stake-modulated neural activation and changes in risky driving; b) additional analyses that investigated each subcluster of stake-modulated separately showing a significant interaction between

the ACC cluster of stake-modulated and passenger type, with a significant simple effect for the risky peer condition in that stake-modulated ACC activation is associated with more risky driving with a risky peer passenger; and c) *: simple effect $p < 0.05$. 166

Fig. 10.5 Visualization of the strength of EEG signal responses to the hue and value/luminance of the color being shown on screen (Panel A) or being imagined (Panel B). Brain signals are divided into four frequency bands: delta (blue), theta (red), alpha (yellow), beta (purple), and gamma (green). Here, offset refers to a data manipulation technique to ensure that 0 value represents the target value to achieve and any deviation from 0 represents noise. Panel A represents the viewing task, where we showed solid colors on a screen to the participant. Panel B represents the imagination task, where the participant imagined a color of their own choice and then indicated the color on a color palette. 170

Fig. 11.1 LARG-II poster presented at IEEE SMC 2019 181

Fig. 11.2 Scatter plots of estimated BFs (red traces) vs. RT for each of eight subjects. Dotted lines show linear and quadratic polynomial functions fit to the (BF, RT) data. Larger values of the BF indicate greater evidence for TPN activation relative to that of the DMN. 189

Fig. 12.1 Demonstration of five real-world environments with our proposed techniques in RL 194

Fig. 12.2 Autonomous agent training with video input and human feedback. Comparison of the backflip in the real-world video demonstration and by our agent. a) Frames of YouTube video of person performing backflip, b) backflip performed by our agent (AAMAS 2019). 195

List of Tables

Table 3.1 Open-source tools developed by the Sajda Lab under CTA funding . 13
Table 4.1 AUC values for each subject using multimodal models 31
Table 4.2 Performance of the IMICA algorithm using different reference signals vs. other common EEG decomposition approaches (Infomax, FastICA, JADE, SOBI, principal component analysis [PCA]) 34
Table 7.1 Behavioral performances in the math and driving task 103
Table 7.2 The classification performance by SVMRBF 107
Table 7.3 The classification performance by RVM 107
Table 8.1 Classified performances of SSVEP developed by NCTU 136
Table 8.2 GFP during mental preparation recordings 139
Table 8.3 MutInf and dynamic TW in upper alpha 140
Table 11.1 HED tags meeting minimum criteria 182

1. Introduction

The Cognition and Neuroergonomics (CaN) Collaborative Technology Alliance (CTA) has been the US Army's flagship basic science research and technology transition program in the neurosciences. Over the past few decades, progress in the neurosciences has greatly advanced our knowledge of how brain function underlies behavior, providing the modern foundations for understanding how we sense, perceive, and interact with the world. These understandings have provided and continue to provide revolutionary advances, fostering technological solutions to address Army needs.

Launched in May 2010, the CaN CTA brought together world-class researchers, experienced industry partners, and some of the US Army Combat Capabilities Development Command Army Research Laboratory's brightest scientists to harness the vast, worldwide investment in neuroscience research and development. The CaN CTA's program of scientific research and development has been aimed at advancing and accelerating the maturation of neuroscience-based approaches to understanding Soldier performance in operational environments and enhancing next-generation adaptive Soldier systems.

This report summarizes and highlights the achievements across the alliance during the past 10 years. Additional information, including video demonstrations and software tools can be found on the DEVCOM Army Research Laboratory CaN CTA website: https://www.arl.army.mil/cast/CaNCTA. Likewise, Section 13 of this report contains a representative list of 50 high-impact publications that have resulted from collaborative research under the CaN CTA.

1.1 Organization

Modern neuroscience research is a truly multidisciplinary endeavor. Across the world's leading research institutions, neuroscience research is conducted by scientists from diverse fields, including, but not limited to, neuroscience and neurobiology, genetics, psychology, kinesiology, statistics, applied mathematics, physics, computer science, and engineering. These research efforts depend upon the collaborative relationships that are at the heart of ARL's CTAs. With partner institutions from Taiwan to Germany, the CaN CTA truly embodied the CTA concept, bringing together leading academics from world-class research organizations from around the globe.

Led by its industry partner, DCS Corporation (DCS), the CaN CTA Consortium has included institutions that are widely recognized as leaders in the academic

research world. In the course of its 10-year execution, the CaN CTA Consortium and its partners have included the following: Columbia University, Carnegie Mellon University (CMU), University of California, San Diego (UCSD), University of California, Santa Barbara (UCSB), University of Texas at San Antonio (UTSA), University of Florida (UFL), University of Michigan (UMI), University of Maryland Baltimore County (UMBC), University of Pennsylvania (UPenn), Johns Hopkins University (JHU), National Chiao Tung University (Taiwan) (NCTU), University of Technology Sydney (Australia) (UTS), University of Osnabruck (Germany) (UOs), University of Pompeu Fabra (Spain) (UPF), and Syntrogi (now Intheon).

1.2 Technology Transfer

Even into the final year of the program, the CaN CTA continues to overcome a variety of challenges to real-world neuroimaging and modeling human performance in natural environments that can be applied to facilitate a broad range of neurotechnologies. Some of these efforts have resulted in tools and concepts transitioning to academic, government, and industry partners within and outside the CTA. Following are some examples:

- CTA partners have developed novel machine learning (ML) approaches to explore and exploit neurophysiology data as never before. CTA partners have demonstrated a proof of concept of artificial intelligence that detects the perception of mission-relevant objects in unstructured environments using classification models trained across multiple disparate data collections and no user-specific calibration.
- CTA partners have transitioned innovative solutions for dry-electrode electroencephalography (EEG) with prototypes to ARL, other academic labs, as well as industry. ARL has tested and integrated the wireless dry-electrode systems into the instrumentation for multiple applied research projects. In addition, several commercial dry-electrode EEG products have leveraged this research and are being used by multiple educational institutions. These institutions include UCSD, University of Malaysia, University of British Columbia, and Korea Advanced Institute of Science and Technology. Moreover, some of the dry-electrode products and evaluation methodologies have been transitioned to the laboratories of large and small industry stakeholders such as Nissan Motor Co. (Japan), NeuroRex Inc. (US), Alchemy (Taiwan), Neurocare (Singapore), Google X (US), and Intel (US).

- Lab streaming layer (LSL), a multi-aspect data acquisition (DAQ) and synchronization software backbone, is being adopted by Neurobehavioral Systems for integration into the commercial stimulus presentation tool, Presentation. Additionally, LSL has become a key integration and synchronization technology for a number of ARL projects, including large-scale research efforts supported by the Next Generation Combat Vehicle and Soldier Lethality Cross-Functional Teams. Importantly, LSL is now being used by a growing number of academic and industry labs around the world to create a unified ecosystem for human sensing.
- CTA partners have developed a wide array of other software tools useful for noninvasive investigations of brain function (using EEG and other modalities). Many of these tools are incorporated into larger tool suites such as BCILAB (i.e., a platform for brain–computer interface [BCI]) and EEGLAB, which are made available to the research community and utilized by many institutions.
- The CaN CTA has also pursued technology transfer and integration targets both within and outside government laboratories. In particular, we have conducted translational research toward enabling future advances in human autonomy integration in automotive environments. We have progressed our driving research by moving the investigation into real cars on real roads while also adding real-world social effects. In parallel, we have coordinated with an applied research project that is investigating the brain processes as a driver interacts with modern driving aid technologies.
- CaN CTA efforts have resulted in a new applied research program, utilizing several of the above technologies, that will refine and validate a novel concept for enhancing tactical situational awareness of mounted and dismounted Soldiers through opportunistic sensing of signals related to visual perception, across multiple individuals. This program leverages deep learning approaches trained on prior data sets to enable calibration-free operation, in addition to other computational techniques, to synergistically improve computer vision algorithms given human-labeled data. The goal of this technology is to improve unit effectiveness through seamless human–autonomy integration without added cognitive burden on the Soldier.

1.3 Vision

Recent progress in the cognitive neurosciences has greatly advanced our knowledge of how brain function underlies behavioral performance. However, there are inherent limitations in the methodological and analytical approaches utilized in the

vast majority of research efforts to date in the human sciences, including those in cognitive neuroscience. These limitations, which are encapsulated in the technical barriers identified by the CaN CTA (Fig. 1.1), have resulted in an understanding of how the human brain works in highly constrained tasks performed in highly controlled laboratory settings. In turn, this has meant that previous systems-development approaches and methods for technological advancement cannot adequately account for the capabilities and limitations of the neurocognitive abilities of Soldier operators.

Technical Barriers

The restriction of experimental designs to highly controlled and impoverished stimulus–response paradigms and environments.

The lack of portable, user-acceptable, minimally invasive, and robust systems for monitoring brain and body dynamics.

The failure to record the whole of the behavior that the brain controls, and the physical and socio-cultural effects of the environment that impact brain function, in sufficient detail and across a sufficient breadth of circumstances.

The lack of mathematical modeling methods and software to find statistical relationships between moment-to-moment variations in environmental, behavioral, and functional brain.

The lack of sufficient data archives and resources to systematically study relationships between individualized models derived for cognitive monitoring and individual differences in performance across diversity of tasks.

Lack of principles and approaches to utilize real-time measures of physiological signals to influence operator cognitive state or inform adaptive technologies to improve human–system performance over time and across individuals.

Fig. 1.1 CaN CTA technical barriers

The skilled cognitive and sensorimotor performance that underlies effective mission utilization of advanced technological capabilities is clearly organized at the level of the nervous system. In particular, technological advances in sensor deployment, automation, and communications bandwidth will intensify the information processing demands placed on the Soldier. Mission success will depend on how well Soldiers can recognize the significance of accumulating information in relation to unfolding events and on their ability to integrate relevant information into a situational awareness that can support effective decisions and actions. Conversely, Soldier cognitive failures in comprehension and decision-making in the face of an ever more complex information stream will be a critical bottleneck in the effective utilization of advanced battlefield technologies. These challenges will only intensify as Soldiers interact with more adaptive and "intelligent" systems on the battlefield.

In this context, the scientific vision of the CaN CTA, therefore, asserted that to address critical Soldier needs, Army neuroscience efforts must be able to provide and leverage a clear working understanding of how the human brain functions when faced with real-world tasks in real-world operational settings. This vision was derived from well-established theoretical foundations in ecological psychology and concepts of embodied or situated cognition, which argue that it is literally impossible to understand natural, motivated behavior in artificial scenarios that divorce the individual from their context.

To fulfill this vision, new approaches to neuroscientific inquiry and new capabilities to enable neuroscience research in operationally relevant environments were needed. The CaN CTA addressed these six technical barriers directly through the following:

- Development of experimental paradigms that capture the unfolding nature of multisensory stimulus streams experienced in real-world environments
- Development and employment of novel, wearable sensor suites for monitoring brain and body dynamics during naturalistic behavior, as well as software systems to enable integrated monitoring capabilities
- Acquisition and processing of high-dimensional data sets that characterize physical, mental, and physiological behavior, as well as its environmental context, in sufficient detail and across a sufficient breadth of circumstances
- Discovery of models and novel methods for the identification and interpretation of statistical relationships among high-dimensional data sets characterizing the dynamics of environment, behavior, and brain function during complex task performance
- Acquisition and analysis of data from a large participant sample allowing characterization of inter- and intra-individual variation to systematically study relationships between individualized models derived for cognitive monitoring and for individual differences in performance, cognitive ability, and personality
- A conceptual framework and functional architecture enabling the acquisition and interpretation of multi-aspect data for real-time integration into human–agent systems

Successes since the launch within this approach, in turn, have led to the establishment of principles on which to base advances in neuroscience in terms of the translation of fundamental research to military-relevant domains, that is, to establish and articulate fundamental translational principles. These principles have

guided the development of technology solutions that work in harmony with the capabilities and limitations of the human nervous system as situated within its dynamic, complex environment.

1.4 Journey toward the Vision

Since the beginning of the program, the CaN CTA has been mindful of the vision described previously and strove to lower the barriers. In the course of the program, the CaN CTA has lowered the barriers through the following:

- Unique developments in advanced computational approaches to extract neuro signal correlates of real-world behavior, and a resultant set of diverse software tools to enable research and application
- Unprecedented multimodal data collection of minimally constrained or unconstrained subjects in diverse realistic simulation, or in real-world environments
- Advancements in nonintrusive and mobile sensors for EEG, and the development of methodologies to facilitate sensor performance assessment
- Formulation and testing of concepts to leverage all of the above to augment Soldier-system capabilities

These achievements can be seen as series of research stages that built upon the previous stage throughout the duration of the program. Here, we highlight these stages of the program.

Program Year 1: The CTA worked to lay out a collaborative program vision and research projects to seed many of the research ideas, and lay a foundation for a more ambitious exploration in future years. This is the stage where the program defined the vision and the scientific barriers articulated previously. As depicted in Fig. 1.2, research was categorized into three groups: neurocognitive performance, advanced computational approaches, and neurotechnologies. Noninvasive neuroimaging in realistic and progressively more complex settings, paired with advances in computational methods to explore the data, were the underlying themes.

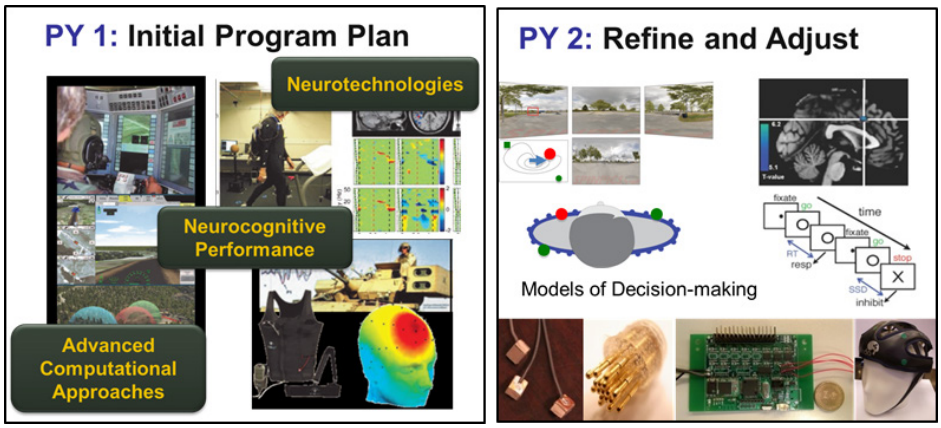


Fig. 1.2 Program years 1 and 2

Program Year 2: The research plans and progress were reevaluated and adjusted to achieve better efficiencies, and enable more effective transitions. Further, the CTA started to detail plans for a CTA-wide collaborated neurophysiological data collection in less-constrained experimental paradigms. In the move toward more realistic environments that address Army contexts, some experiments were designed to represent mounted (in vehicle) environments, and others were designed for dismount, ambulatory environments. Concurrently, smaller experiments and analyses requiring less preparation for the methods continued across the CTA.

Program Year 3: Research in computational methods coalesced into tools made available to the community, and experimental apparatus for the CTA-wide neurophysiological data collections were implemented (Fig. 1.3). The CTA developed multi-subject and single-subject vehicle operation crew stations, each with multimodal data collection (including high-channel EEG) and one with motion simulation. Further, the CTA implemented a single-subject ambulatory apparatus for collecting data in the lab as well as outdoors. In addition, the CTA continued to refine methods of collecting, organizing, and managing the data and approaches to facilitate exploration of large and diverse set of multimodal neurophysiology data.

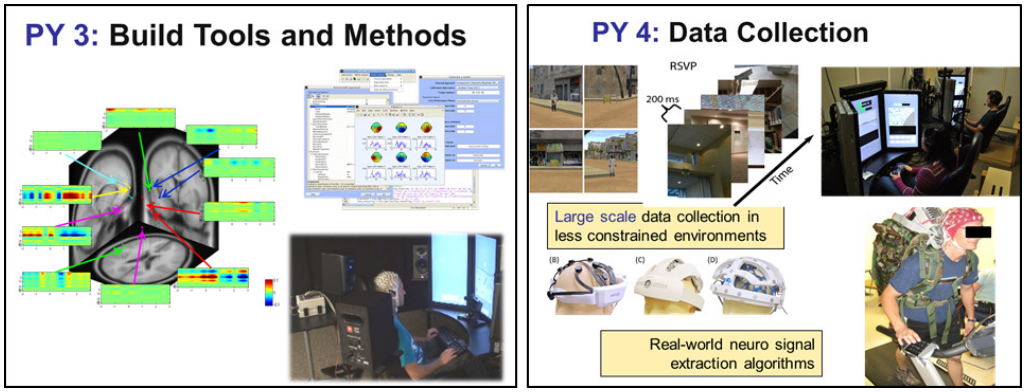


Fig. 1.3 Program years 3 and 4

Program Year 4: The unique experimental systems and data collection tools were put to use across multiple CTA sites to collect multimodal data in real or realistic environments (see Fig. 1.3). In conjunction, advances continued in computational methods, real-world sensors, and acquisition methods to facilitate exploration of the data.

Program Years 5–6: The cumulative research of the first four years to advance holistic sensing and exploration of real-world brain–body data was refocused to more directly address transitional goals. In particular, research was reorganized as depicted in Fig. 1.4, to close the gaps in enabling more robust brain–computer interaction technologies (BCITs). As remaining large-scale data collections finished, the program realigned its projects into three new science areas: advanced computational approaches (ACAs), BCIT, and real-world neuroimaging (RWN). As more and more multimodal, realistic behavior neurophysiology data became available, more emphasis was placed on methods to organize, manage, explore, and exploit the data sets. Thus, the ACA area remained, but with a more direct linkage to the other two science areas. Also, recognizing that significant research efforts take at least two years from start to finish, the program planning cycle was lengthened to a biennial cycle, and some significant projects were planned for three-year execution.

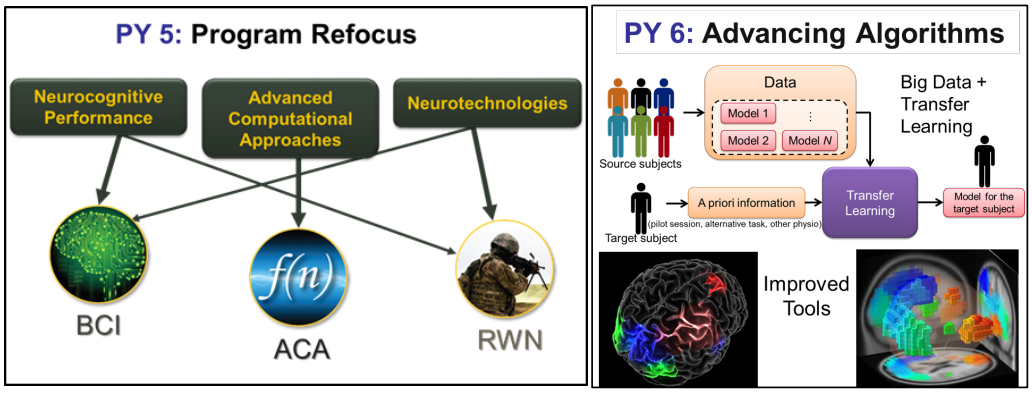


Fig. 1.4 Program years 5 and 6

The driving questions behind the three new science areas were the following:

- *ACAs*: What is the optimal way to decode, track, and fuse neural and non-neural sources of information to infer state?
- *RWN*: How does the brain function in the real world, outside the constraints of the lab?
- *BCI*: How do we use neural signals to improve human interactions with computers, autonomous agents, their environment, and even other humans?

In turn, the three areas were interconnected by an overarching goal:

- Continuous and robust estimate of cognitive state in complex tasks and real-world environments

Program Years 7–8: This stage focused attention on robust BCIT (Fig. 1.5). This effort produced promising research in closed-loop BCI systems, which laid the groundwork for the exploitation of real-time neural activity to optimize joint human–system performance. In parallel, as the collaborators continued to wrestle with large volumes of disparate RWN data (consisting largely of EEG and other surface sensor data), approaches to tag and preprocess were standardized for the benefit of the broader research community.

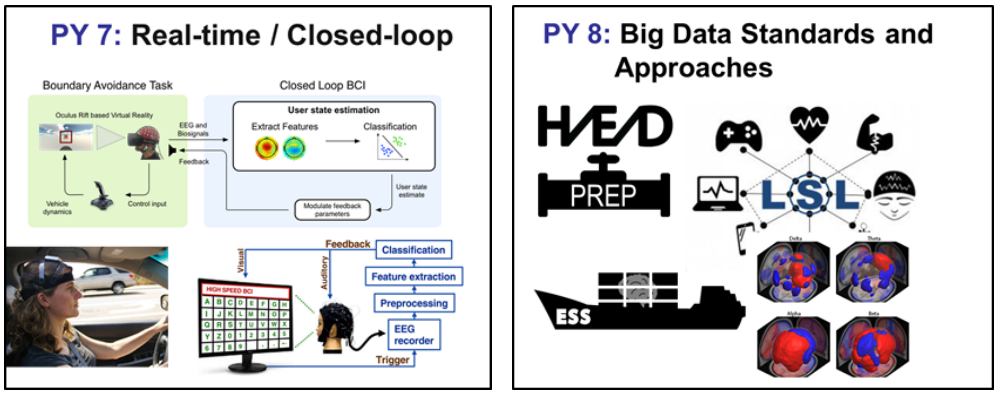


Fig. 1.5 Program years 7 and 8

Program Years 9–10: The alliance focused research efforts in real-world experimentation (such as freeway driving), while earlier methods for exploring and exploiting neuroimaging data reach the maturity levels required for real-world applications. In particular, ML approaches for interpreting multimodal human neuro and physiological data were refined and tested in the context of passive, closed-loop technologies to enhance Soldier situational awareness (mounted or dismount) and operational safety (Fig. 1.6). Further, the DAQ and synchronization middleware, LSL, gained widespread acceptance across industry and academia; and was integrated into the Army's applied and advanced research projects investigating manned–unmanned teaming in future mounted operations.

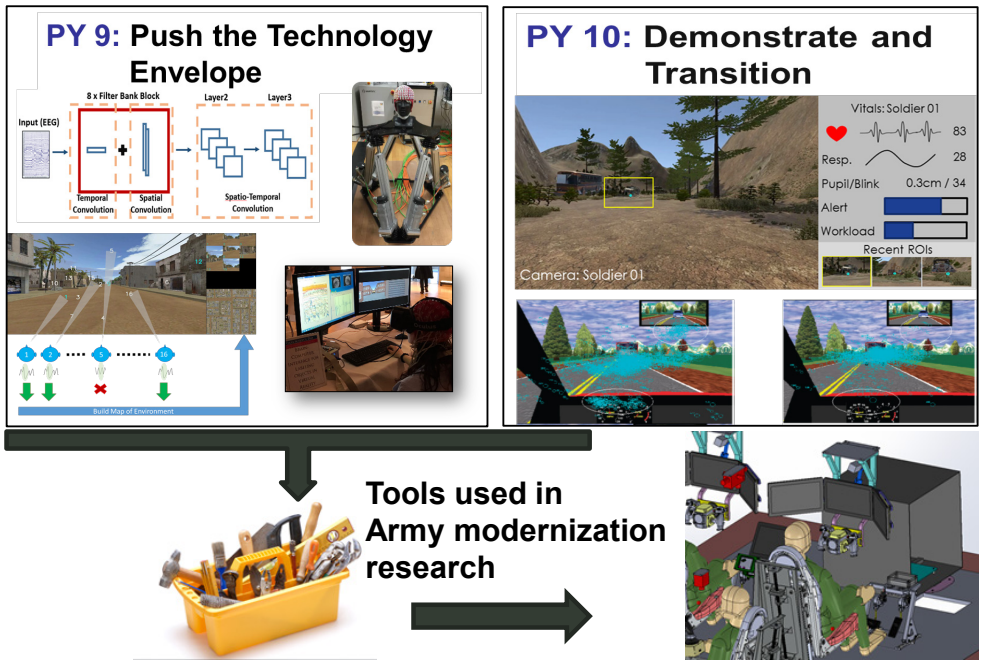


Fig. 1.6 Program years 9 and 10

2. Progression of Research Achievements

This section details the progression and accomplishments of key research by major consortium members and partners. For each project, effort is made to articulate how the project addressed the barriers to advancement of the scientific vision. To re-iterate, the barriers are the following:



B1. The restriction of experimental designs to highly controlled and impoverished stimulus/response paradigms and environments.



B2. The lack of portable, user-acceptable (e.g., comfortably wearable), and robust systems for routinely monitoring brain and body dynamics.



B3. The failure to record the whole of physical, mental, and physiological behavior that the brain controls, and the physical and socio-cultural effects of the environment that impact brain function, in sufficient detail and across a sufficient breadth of circumstances.



B4. The lack of mathematical modeling methods to find statistical relationships among the moment-to-moment variations in environmental, behavioral, and functional brain dynamics.



B5. The lack of sufficient data archives and resources to systematically study relationships between individualized models derived for cognitive monitoring and individual differences in performance, cognitive ability, and personality, relationships that could optimize performance of cognitive monitoring systems while lowering requirements for collecting individual-subject training data.



B6. Lack of principles and approaches to utilize real-time measures of physiological signals to influence operator cognitive state or inform adaptive technologies to improve human–system performance over time and across individuals.

3. Columbia University

The CaN CTA was established with the goal of leveraging neuroscience approaches to understand and improve human behavioral performance, particularly in realistic, complex environments.

Columbia University's work has focused on addressing technical barriers B1, B3, and B4, specifically through the following three thrust areas:

- Developing methods for analysis and integration of multi-model neural, physiological, and behavioral data. (B3 and B4)
- Using virtual reality (VR) as an experimental platform. (B1 and B3)
- Understanding the neural basis of decision-making and expertise (B1, B3, and B4)

Columbia has had very successful cross-collaborations with many CTA partners and ARL researchers. Over the course of the project, Columbia has had a number of joint appointments and embedded personnel with ARL including the following:

- Jason Sherwin, PhD: embedded postdoc at ARL
- Nick Waytowich, PhD: joint Columbia–ARL postdoc embedded at ARL and who transitioned to an ARL civilian.
- Kanika Bansal, PhD: joint ARL–Columbia postdoc embedded at Columbia
- Josef Faller PhD: ARL postdoc at Columbia

The remainder of this section is organized as follows. We first summarize the most important accomplishments in each thrust area. This summary is then followed by list of publications and other products, including open-source tools (Table 3.1).

Table 3.1 Open-source tools developed by the Sajda Lab under CTA funding

Tool	Description	Link
NEDE	A scripting suite designed to leverage the capabilities of the Unity3D game engine into the neuroscientific study of realistic scenarios.	http://www.nede-neuro.org
SigViewer	Application for visualizing multimodal signals stored in Extensible Data Format (XDF).	https://github.com/cbrnr/sigviewer
BrainFlight Data	Data and code for reproducing results in J.13.	https://ieee-dataport.org/open-access/regulation-arousal-online-neurofeedback-improves-human-performance-demanding-sensory
py_eegepe	Python code base to test ML approaches for EEG rhythm phase prediction.	https://github.com/jrmxn/py_eegepe
Malleable SSM	A MATLAB toolbox that allows for rapid prototyping of sequential sampling models (SSMs) for analysis of decision-making data.	https://github.com/jrmxn/malleable-ssm
State-space modeling for simultaneous EEG/fMRI	MATLAB code and data for reproducing C.10.	https://github.com/taotu/VBLDS_Connectivity_EEG_fMRI

Note: fMRI = functional magnetic resonance imaging.

3.1 Methods for Analysis and Integration of Neural, Physiological, and Behavioral Data

3.1.1 Latent Neural Source Recovery via Transcoding of Simultaneous EEG-fMRI

Simultaneous EEG–fMRI is a multimodal neuroimaging technique that provides complementary spatial and temporal resolution for inferring a latent source space of neural activity. We addressed this inference problem within the framework of transcoding—mapping from a specific encoding (modality) to a decoding (the latent source space) and then encoding the latent source space to the other modality. Specifically, we develop a symmetric method consisting of a cyclic convolutional transcoder that transcodes EEG to fMRI and vice versa. Without any prior knowledge of either the hemodynamic response function or lead field matrix, the method exploits the temporal and spatial relationships between the modalities and latent source spaces to learn these mappings. We have shown, for real EEG–fMRI data, how well the modalities can be transcoded from one to another (Fig. 3.1.) as well as the source spaces that are recovered, all on unseen data. In addition to enabling a new way to symmetrically infer a latent source space, the method can

also be seen as low-cost computational neuroimaging (i.e., generating an "expensive" fMRI blood oxygen level-dependent [BOLD] image from "low cost" EEG data). *This work was submitted to NeurIPS 2020 and a preliminary version published in the Institute of Electrical and Electronics Engineers (IEEE) NER'19.*

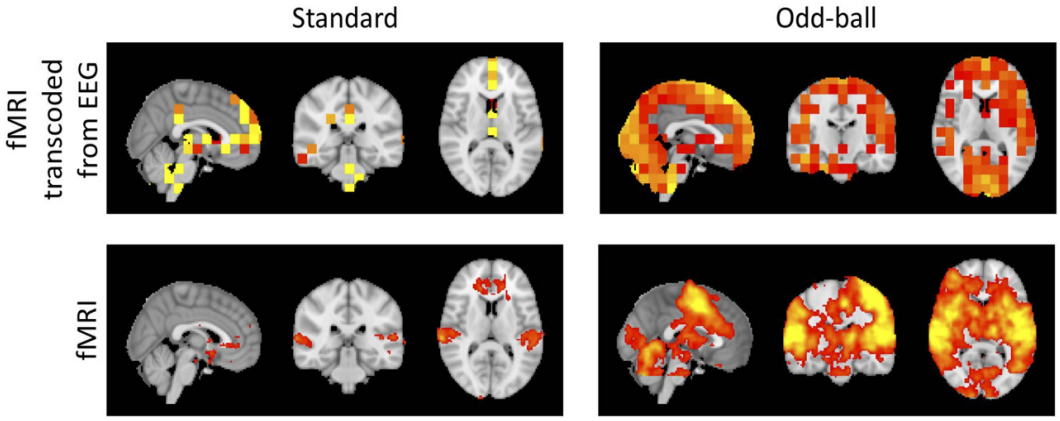


Fig. 3.1 Comparing fMRI transcoded from EEG and real fMRI data: fMRI transcoded from EEG has a spatial resolution of 12 mm × 12 mm × 12 mm, while real fMRI data has a spatial resolution of 2 mm × 2 mm × 2 mm

3.1.2 A State-Space Model for Inferring Effective Connectivity of Latent Neural Dynamics

Inferring effective connectivity between spatially segregated brain regions is important for understanding human brain dynamics in health and disease. Noninvasive neuroimaging modalities, such as EEG and fMRI, are often used to make measurements and infer connectivity. However, most studies do not consider integrating the two modalities, even though each is an indirect measure of the latent neural dynamics and each has its own spatial and/or temporal limitations. We developed a linear state-space model to infer the effective connectivity in a distributed brain network based on simultaneously recorded EEG and fMRI data. Our method first identifies task-dependent and subject-dependent regions of interest (ROIs) based on the analysis of fMRI data. Directed influences between the latent neural states at these ROIs are then modeled as a multivariate autogressive (MVAR) process driven by various exogenous inputs. The latent neural dynamics give rise to the observed scalp EEG measurements via a biophysically informed linear EEG forward model. We use a mean-field variational Bayesian approach to infer the posterior distribution of latent states and model parameters. The performance of the model has been evaluated on two sets of simulations. Our results emphasize the importance of obtaining accurate spatial localization of ROIs from fMRI. Finally, we applied the model to simultaneously recorded EEG–fMRI data from 10 subjects during a face-car-house visual categorization task and compared

the change in connectivity induced by different stimulus categories. Our results show an increase in effective connectivity when a house is presented relative to when the stimulus is a face. *This work was published in NeurIPS 2019.*

3.1.3 Estimation of Phase in EEG Rhythms for Real-Time Applications

We identified two linked problems related to estimating the phase of the alpha rhythm when the signal after a specific event is unknown (real-time case) or corrupted (offline analysis). We propose and develop methods to estimate the phase prior to such events. Using an ML approach to mimic a non-causal signal-processing chain with a purely causal one, we demonstrate the ability of these methods to estimate the instantaneous phase from an EEG signal subjected to very minor preprocessing with higher accuracy than more standard signal-processing methods. Phase estimation of EEG rhythms is a challenge due to nonstationarity and a low signal-to-noise ratio (SNR). The methods presented and developed by our group enable scientists and engineers to achieve relatively low error by optimizing causal phase estimation on a non-causally processed signal for a real-time experiments and offline analysis. *This work was published in* The Journal of Neural Engineering.

3.1.4 Ballistocardiogram Artifact Reduction in Simultaneous EEG-fMRI Using Deep Learning

The concurrent recording of EEG and fMRI is a technique that has received much attention due to its potential for combined high temporal and spatial resolution. However, the ballistocardiogram (BCG), a large-amplitude artifact caused by cardiac-induced movement, contaminates the EEG during EEG-fMRI recordings. Removal of BCG in software has generally made use of linear decompositions of the corrupted EEG. This is not ideal as the BCG signal is nonstationary and propagates in a manner that is nonlinearly dependent on the electrocardiogram (ECG). We developed a novel method for BCG artifact suppression using recurrent neural networks (RNNs). Specifically, EEG signals were recovered by training RNNs on the nonlinear mappings between the ECG and BCG-corrupted EEG. We evaluated our model's performance against the commonly used optimal basis set (OBS) method at the level of individual subjects, and investigated generalization across subjects. Results show that our algorithm can generate larger average power reduction of the BCG at critical frequencies, while simultaneously improving task-relevant EEG-based classification. The presented deep learning architecture can be used to reduce BCG-related artifacts in EEG–fMRI recordings. *This work was published in* IEEE Transactions in Biomedical Engineering.

3.2 Using VR as an Experimental Platform for Cognitive Neuroscience

3.2.1 Regulation of Arousal via Online Neurofeedback Improves Human Performance in a Demanding Sensory-Motor Task

Our state of arousal can significantly affect our ability to make optimal decisions, judgments, and actions in real-world dynamic environments. The Yerkes–Dodson law, which posits an inverse-U relationship between arousal and task performance, suggests that there is a state of arousal that is optimal for behavioral performance in a given task. We showed that we can use online neurofeedback to shift an individual's arousal from the right side of the Yerkes–Dodson curve to the left, toward a state of improved performance. Specifically, we use a BCI that uses information in the EEG to generate a neurofeedback signal that dynamically adjusts an individual's arousal state when they are engaged in a boundary-avoidance task (BAT) that is presented in VR (Fig. 3.2). The BAT is a demanding sensory-motor task paradigm that we implement as an aerial navigation task in VR and that creates cognitive conditions that escalate arousal and quickly result in task failure (e.g., missing or crashing into the boundary). We demonstrate that task performance, measured as time and distance over which the subject can navigate before failure, is significantly increased when veridical neurofeedback is provided. Simultaneous measurements of pupil dilation and heart-rate variability (HRV) show that the neurofeedback indeed reduces arousal. Our work demonstrates a BCI system that uses online neurofeedback to shift arousal state and increase task performance in accordance with the Yerkes–Dodson law. *This work was published in the Proceedings of the National Academy of Sciences (PNAS).*

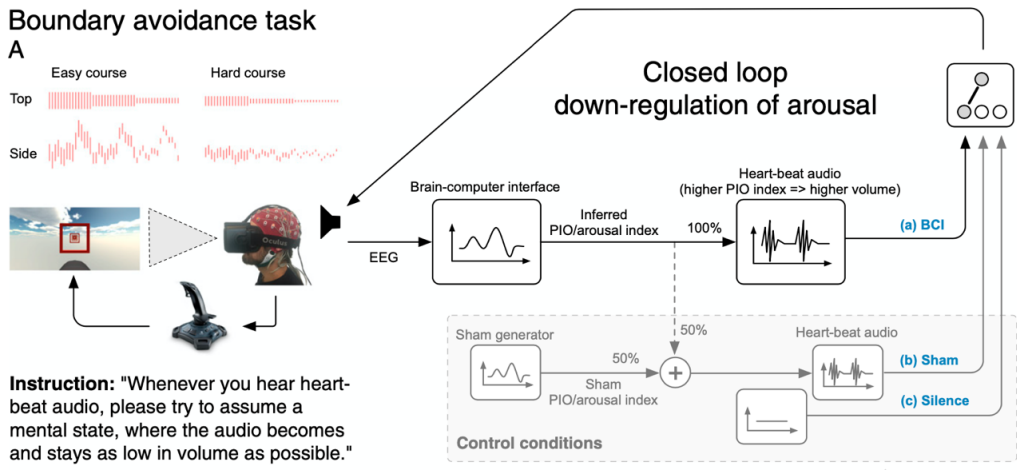


Fig. 3.2 Setup of experiment and study protocol. Study participants alternately guided a virtual aircraft through an easy or hard course of red rectangular boundaries (rings). Both courses were a maximum of 90 s long and increased in difficulty over time as ring sizes decreased. Missing a ring ended the flight trial immediately. Every new flight attempt was randomly assigned one of three feedback conditions. In the main condition, a) BCI, audio feedback from an EEG-based decoder was presented to the participant (closed-loop experiment). During the two control conditions b) sham and c) silence, partly random or no audio signal was presented, respectively. Participants were instructed to down-regulate their arousal as outlined at the bottom left of the panel.

3.2.2 Neurally and Ocularly Informed Graph-Based Models for Searching 3-D Environments

As we move through an environment, we are constantly making assessments, judgments, and decisions about the things we encounter. Some are acted upon immediately, but many more become mental notes or fleeting impressions—our implicit "labeling" of the world. In this section, we use physiological correlates of this labeling to construct a hybrid brain–computer interface (hBCI) system for efficient navigation of a 3-D environment. First, we recorded EEG, saccadic, and pupillary data from subjects as they move through a small part of a 3-D virtual city under free-viewing conditions. Using ML, we integrated the neural and ocular signals evoked by the objects they encounter to infer which ones are of subjective interest to them. These inferred labels are propagated through a large computer vision graph of objects in the city, using semi-supervised learning to identify other, unseen objects that are visually similar to the labeled ones. Finally, the system plots an efficient route to help the subjects visit the "similar" objects it identifies.

We showed that by exploiting the subjects' implicit labeling to find objects of interest instead of exploring naively, the median search precision is increased from 25% to 97%, and the median subject need only travel 40% of the distance to see 84% of the objects of interest. We also find that the neural and ocular signals contribute in a complementary fashion to the classifiers' inference of subjects'

implicit labeling. In summary, we showed that neural and ocular signals reflecting subjective assessment of objects in a 3-D environment can be used to inform a graph-based learning model of that environment, resulting in an hBCI system that improves navigation and information delivery specific to the user's interests. *This work was published in the* Journal of Neural Engineering.

3.2.3 NEDE, an Open-Source Scripting Suite for Developing Experiments in 3-D Virtual Environments

As neuroscientists endeavor to understand the brain's response to ecologically valid scenarios, many are leaving behind hyper-controlled paradigms in favor of more realistic ones. This movement has made the use of 3-D rendering software an increasingly compelling option. However, mastering such software and scripting rigorous experiments requires a daunting amount of time and effort. To reduce these startup costs and make virtual environment studies more accessible to researchers, we demonstrate a naturalistic experimental design environment (NEDE) that allows experimenters to present realistic virtual stimuli while still providing tight control over the subject's experience. NEDE is a suite of open-source scripts built on the widely used Unity3D game development software, giving experimenters access to powerful rendering tools while interfacing with eye tracking and EEG, randomizing stimuli, and providing custom task prompts (Fig. 3.3).

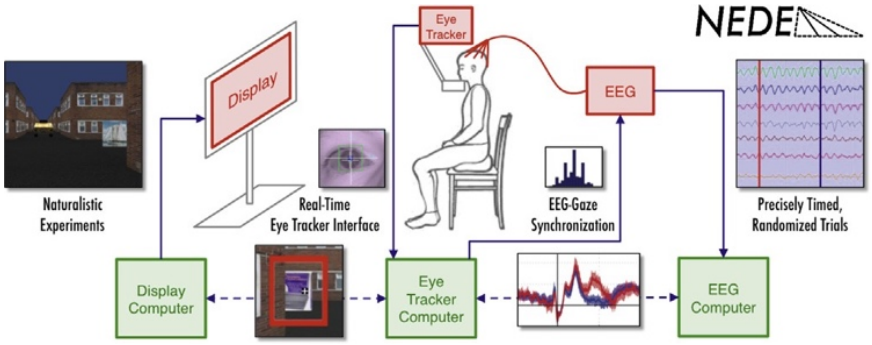


Fig. 3.3 Overview of NEDE

Researchers using NEDE can present a dynamic 3-D virtual environment in which randomized stimulus objects can be placed, allowing subjects to explore in search of these objects. NEDE interfaces with a research-grade eye tracker in real time to maintain precise timing records and sync with EEG or other recording modalities. In comparison with existing methods, Python offers an alternative for experienced programmers who feel comfortable mastering and integrating the various toolboxes available. NEDE combines many of these capabilities with an easy-to-use interface and, through Unity's extensive user base, a much more substantial body of assets and tutorials. Our flexible, open-source experimental design system lowers the

barrier to entry for neuroscientists interested in developing experiments in realistic virtual environments. *This work was published in the* Journal of Neuroscience Methods.

3.3 Understanding the Neural Basis of Decision-Making and Expertise

3.3.1 A Multimodal Encoding Model Applied to Imaging Decision-Related Neural Cascades in the Human Brain

Perception and cognition in the brain are naturally characterized as spatiotemporal processes. Decision-making, for example, depends on coordinated patterns of neural activity cascading across the brain, running in time from stimulus to response and in space from primary sensory regions to the *frontal lobe*. Measuring this cascade is key to developing an understanding of brain function. We demonstrated a novel methodology that employs *multimodal imaging* for inferring this cascade in humans at unprecedented spatiotemporal resolution. Specifically, we developed an encoding model to link simultaneously measured *EEG* and *fMRI* signals to infer high-resolution spatiotemporal brain dynamics during a perceptual decision.

After demonstrating replication of results from the literature, we report previously unobserved sequential reactivation of a substantial fraction of the pre-response network whose magnitude correlates with a proxy for decision confidence (Fig. 3.4). Our encoding model, which temporally tags BOLD activations using time-localized *EEG* variability, identifies a coordinated and spatially distributed neural cascade that is associated with a perceptual decision. In general, the methodology illuminates complex brain dynamics that would otherwise be unobservable using *fMRI* or *EEG* acquired separately. *This work was published in* Neuroimage.

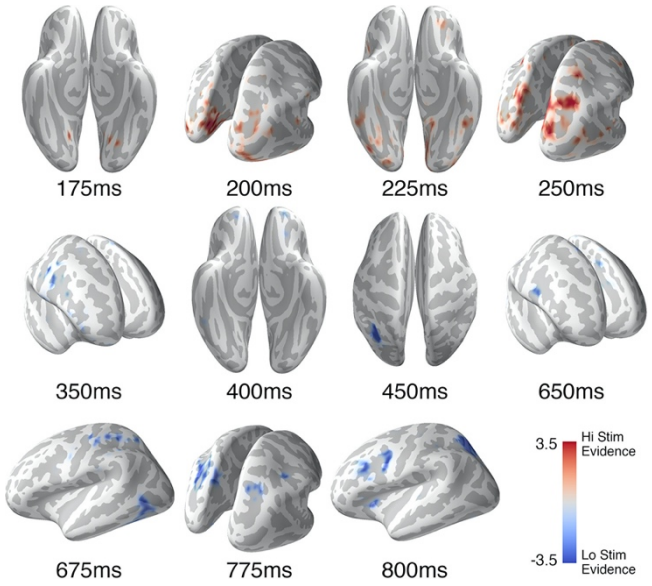


Fig. 3.4 Group-level encoding model weights results show a cascade of neural activation. Subset of thresholded (false discovery rate-corrected, k = 10) group-level statistical parametric maps created by the spatiotemporal threshold-free cluster enhancement (stTFCE) randomization procedure on the encoding model weight matrices. Shown is the progression of spatial activity across the trial. Activation can be seen early in the trial in the occipital regions while progressing more anteriorly later in the trial to executive control areas. Activations in red indicate areas where high stimulus evidence trials had larger activations than low stimulus evidence trials, with blue the inverse relationship.

3.3.2 Perceptual Salience and Reward Both Influence Feedback-Related Neural Activity Arising from Choice

For day-to-day decisions, multiple factors influence our choice between alternatives. Two dimensions of decision-making that substantially affect choice are the objective perceptual properties of the stimulus (e.g., salience) and its subjective value. Here we measure EEGs in human subjects to relate their feedback-evoked EEG responses to estimates of prediction error given a neurally derived expected value for each trial. Unlike in traditional reinforcement learning (RL) paradigms, in our experiment, the reward itself is not probabilistic; rather, it is a fixed value, which, when combined with the variable stimulus salience, yields uncertainty in the choice. We find that feedback-evoked event-related potentials (ERPs), specifically those classically termed feedback-related negativity, are modulated by both the reward level and stimulus salience. Using single-trial analysis of the EEG, we show stimulus-locked EEG components reflecting perceived stimulus salience can be combined with the level of reward to create an estimate of expected reward. This expected reward is used to form a prediction error that correlates with the trial-by-trial variability of the feedback ERPs for negative, but not positive, feedback. This suggests that the valence of prediction error is more important than the valence of the actual feedback, since only positive rewards were

delivered in the experiment (no penalty or loss). Finally, we show that these subjectively defined prediction errors are informative of the riskiness of the subject's choice on the subsequent trial. In summary, our work shows that neural correlates of stimulus salience interact with value information to yield neural representations of subjective expected reward. *This work was published in* The Journal of Neuroscience.

3.3.3 Knowing When Not to Swing: EEG Evidence that Enhanced Perception–Action Coupling Underlies Baseball Batter Expertise

Given a decision that requires less than half a second, like evaluating the characteristics of the incoming pitch and generating a motor response, hitting a baseball potentially requires unique perception–action coupling to achieve high performance. We designed a rapid perceptual decision-making experiment modeled as a go/no-go task yet tailored to reflect a real scenario confronted by a baseball hitter. For groups of experts (Division I baseball players) and novices (non-players), we recorded EEG while they performed the task. We analyzed evoked EEG single-trial variability, contingent negative variation (CNV), and pre-stimulus alpha power with respect to the expert versus novice groups.

We found strong evidence for differences in inhibitory processes between the two groups, specifically differential activity in supplementary motor areas (SMAs), indicative of enhanced inhibitory control in the expert (baseball player) group. We also found selective activity in the fusiform gyrus (FG) and orbital gyrus in the expert group, suggesting an enhanced perception–action coupling in baseball players that differentiates them from matched controls. In sum, our results show that EEG correlates of decision formation can be used to identify neural markers of high-performance athletes. *This work was published in* Neuroimage.

3.4 Network Configurations in the Human Brain Reflect Choice Bias during Rapid Face

3.4.1 Brain Networks for Perceptual Processing

Network interactions are likely to be instrumental in processes underlying rapid perception and cognition. Specifically, high-level and perceptual regions must interact to balance preexisting models of the environment with new incoming stimuli. Simultaneous EEG and fMRI (EEG–fMRI) enables temporal characterization of brain–network interactions combined with improved anatomical localization of regional activity. In this section, we use simultaneous EEG–fMRI and multivariate dynamical systems (MDS) analysis to characterize network relationships between constitute brain areas that reflect a subject's choice for a face

versus non-face categorization task. Our simultaneous EEG and fMRI analysis on 21 human subjects (12 males, 9 females) identifies early perceptual and late frontal subsystems that are selective to the categorical choice of faces versus non-faces. We analyze the interactions between these subsystems using an MDS in the space of the BOLD signal.

Our main findings show that differences between face-choice and house-choice networks are seen in the network interactions between the early and late subsystems, and that the magnitude of the difference in network interaction positively correlates with the behavioral false-positive rate of face choices. We interpret this to reflect the role of saliency and expectations likely encoded in frontal "late" regions on perceptual processes occurring in "early" perceptual regions. *This work was published in* The Journal of Neuroscience.

3.4.2 Decomposing Simon Task BOLD Activation Using a Drift-Diffusion Model Framework

The Simon effect is observed in spatial conflict tasks where the response time (RT) of subjects is increased if stimuli are presented in a lateralized manner so that they are incongruous with the response information that they symbolically represent. Previous studies have used fMRI to investigate this phenomenon, and while some have been driven by considerations of an underlying model, none have attempted to directly tie model and BOLD response together. It is likely that this is due to Simon models having been predominantly descriptive of the phenomenon rather than capturing the full spectrum of behavior at the level of individual subjects. SSMs, which capture full response distributions for correct and incorrect responses, have recently been extended to capture conflict tasks.

In this study, we use our freely available framework for fitting and comparing non-standard SSMs to fit the Simon effect SSM (SE-SSM) to behavioral data. This model extension includes specific estimates of automatic response bias and a conflict counteraction parameter to individual subject behavioral data. We apply this approach in order to investigate whether our task-specific model parameters have a correlate in BOLD response. Under the assumption that the SE-SSM reflects aspects of neural processing in this task, we go on to examine the BOLD correlates with the within trial expected decision-variable.

We find that the SE-SSM captures the behavioral data and that our two conflict-specific model parameters have clear across-subject BOLD correlates, while other model parameters, as well as more standard behavioral measures, do not. We also find that examining BOLD in terms of the expected decision-variable leads to a

specific pattern of activation that would not be otherwise possible to extract. *This work was published in* Scientific Reports.

3.5 References

3.5.1 Journal Articles

1. Conroy BR, Walz JM, Sajda P. Fast bootstrapping and permutation testing for assessing reproducibility and interpretability of multivariate fMRI decoding models. PloS one. 2013;8(11):e79271.

2. Jangraw DC, Johri A, Gribetz M, Sajda P. NEDE: An open-source scripting suite for developing experiments in 3D virtual environments. J Neurosci Methods. 2014;235:245–251.

3. Jangraw DC, Wang J, Lance BJ, Chang S-F, Sajda P. Neurally and ocularly informed graph-based models for searching 3D environments. J Neural Eng. 2014;11(4):046003.

4. Lou B, Hsu W-Y, Sajda P. Perceptual salience and reward both influence feedback-related neural activity arising from choice. J Neurosci. 2015;35(38):13064–13075.

5. Muraskin J, Sherwin J, Sajda P. Knowing when not to swing: EEG evidence that enhanced perception–action coupling underlies baseball batter expertise. NeuroImage. 2015;123:1–10.

6. Sherwin JS, Muraskin J, Sajda P. Pre-stimulus functional networks modulate task performance in time-pressured evidence gathering and decision-making. NeuroImage. 2015;111: 513–525.

7. Muraskin J., Sherwin J, Lieberman G, Garcia JO, Verstynen T, Vettel JM, Sajda P. Fusing multiple neuroimaging modalities to assess group differences in perception–action coupling. Proceedings of the IEEE. 2016;105(1):83–100.

8. Saproo S, Shih V, Jangraw DC, Sajda P. Neural mechanisms underlying catastrophic failure in human–machine interaction during aerial navigation. J Neural Eng. 2016;13(6):066005.

9. Tu T, Schneck N, Muraskin J, Sajda P. Network configurations in the human brain reflect choice bias during rapid face processing. J Neurosci. 2017;37(50):12226–12237.

10. Delis I, Dmochowski JP, Sajda P, Wang Q. Correlation of neural activity with behavioral kinematics reveals distinct sensory encoding and evidence

accumulation processes during active tactile sensing. Neuroimage. 2018;175:12–21.

11. Muraskin J, Brown TR, Walz JM, Tu T, Conroy B, Goldman RI, Sajda P. A multimodal encoding model applied to imaging decision-related neural cascades in the human brain. NeuroImage. 2018;180: 211–222.

12. Waytowich N, Lawhern V, Garcia JO, Cummings J, Faller J, Sajda P, Vettel JM. Compact convolutional neural networks for classification of asynchronous steady-state visual evoked potentials. J Neural Eng. 2018;15(6):066031.

13. Faller J, Cummings J, Saproo S, Sajda P. Regulation of arousal via online neurofeedback improves human performance in a demanding sensory-motor task. Proc Natl Acad Sci. 2019;116(13):6482–6490.

14. McIntosh JR, Yao J, Hong L, Faller J, Sajda P. Ballistocardiogram artifact reduction in simultaneous EEG-fMRI using deep learning. IEEE Trans Biomed Eng. Forthcoming 2019.

15. McIntosh JR, Sajda P. Estimation of phase in EEG rhythms for real-time applications. J Neural Eng. 2020;17(3):034002.

16. McIntosh JR, Sajda P. Decomposing Simon task BOLD activation using a drift-diffusion model framework. Sci Rep. 2020;10(1):1–11.

3.5.2 Conference Proceedings

1. Jangraw DC, Sajda P. Feature selection for gaze, pupillary, and EEG signals evoked in a 3D environment. Proceedings of the 6th workshop on Eye gaze in intelligent human machine interaction: gaze in multimodal interaction; 2013.

2. Zhang JR, et al. Correlating speaker gestures in political debates with audience engagement measured via EEG. Proceedings of the 22nd ACM international conference on Multimedia; 2014.

3. Faller J, Zhang JR, Sherwin J, Dmochowski J, Sajda P, Kender JR. Closed-loop regulation of user state during a boundary avoidance task. 2016 IEEE International Conference on Systems, Man, and Cybernetics (SMC); 2016. IEEE.

4. Waytowich NR, Faller J, Garcia JO, Vettel JM, Sajda P. Unsupervised adaptive transfer learning for steady-state visual evoked potential brain-computer interfaces. 2016 IEEE International Conference on Systems, Man, and Cybernetics (SMC); 2016. IEEE.

5. Shih V, Jangraw D, Saproo S, Sajda P. Deep reinforcement learning using neurophysiological signatures of interest. in Proceedings of the Companion of the 2017 ACM/IEEE International Conference on Human-Robot Interaction. 2017.

6. Delis I, Dmochowski JP, Sajda P, Wang Q. Correlations of neural activity with behavioral kinematics during active tactile decision making. Proceedings of the 10th Hellenic Conference on Artificial Intelligence; 2018.

7. Delis I, Ince RAA, Sajda P, Wang Q. Information-theoretic characterization of the neural mechanisms of active multisensory decision making. International Conference on NeuroRehabilitation; 2018. Springer.

8. Lapborisuth P, Faller J, Koss J, Waytowich NR, Touryan J, Sajda P. Investigating evoked EEG responses to targets presented in virtual reality. 2019 41st Annual International Conference of the IEEE Engineering in Medicine and Biology Society (EMBC); 2019. IEEE.

9. Liu X, Sajda P. A convolutional neural network for transcoding simultaneously acquired EEG-fMRI data. In: 2019 9th International IEEE/EMBS Conference on Neural Engineering (NER); 2019. IEEE.

10. Tu T, Paisley J, Haufe S, Sajda P. A state-space model for inferring effective connectivity of latent neural dynamics from simultaneous EEG/fMRI. Advances in Neural Information Processing Systems; 2019.

11. Tu T, Sajda P. Simultaneous EEG-fMRI study reveals separate bias mechanisms modulated by stimulus evidence during rapid face processing. 2019 41st Annual International Conference of the IEEE Engineering in Medicine and Biology Society (EMBC); 2019. IEEE.

3.5.3 Archives

1. Muraskin J, Brown TR, Walz JM, Conroy B, Goldman RI, Sajda P. Imaging decision-related neural cascades in the human brain. bioRxiv. 2016;050856.

2. Faller J, Hong L, Cummings J, Sajda P. A comparison of single-trial EEG classification and EEG-informed fMRI across three MR compatible EEG recording systems. arXiv preprint arXiv:1707.08077. 2017.

3. Shih V, Jangraw DC, Sajda P, Saproo S. Towards personalized human AI interaction-adapting the behavior of AI agents using neural signatures of subjective interest. arXiv preprint arXiv:1709.04574. 2017.

4. Sherwin JS, Sajda P**.** Parameterized expertise: evidence for gradations of musical expertise from electroencephalographic monitoring of auditory decision-making. bioRxiv. 2018;370379.

5. Liu X, Sajda P. Unsupervised sparse-view backprojection via convolutional and spatial transformer networks. arXiv preprint arXiv:2006.01658. 2020.

3.5.4 Patents

Chang S-F, Wang J, Sajda P, Pohlmeyer E, Hanna B, Jangrew D, inventors. Columbia University, assignee. Rapid image annotation via brain state decoding and visual pattern mining. United States patent. US 9,665,824, 2017 May 30.

Jangrew D, Sajda P, inventors. Mobile, neurally-assisted personal assistant. United States patent application. Col. IR #CU13178; File docket no. 070050.5087, 2014 Jan 23.

Muraskin J, Sherwin J, Sajda P, inventors. Columbia University, assignee. Systems and methods for identifying and tracking neural correlates of baseball pitch trajectories. United States patent application. US10299695B2, 2019 May 28.

Sajda P, inventor. Systems and methods for deep reinforcement learning using a brain-artificial intelligence interface. United States patent application. 16/149,785, pending.

4. DCS Corporation

DCS' work focused on addressing barriers B1, B2, B3, B4, and B5 through a diversity of projects and development efforts over the past 10 years. Figure 4.1 highlights a selection of projects and development efforts that were performed. Also shown is the conceptual linkage needed to understand 1) how these projects intertwined, 2) the barriers addressed by each, and 3) the logical flow from project to major CaN CTA transition. The projects highlighted in light green are described in more detail in this report.

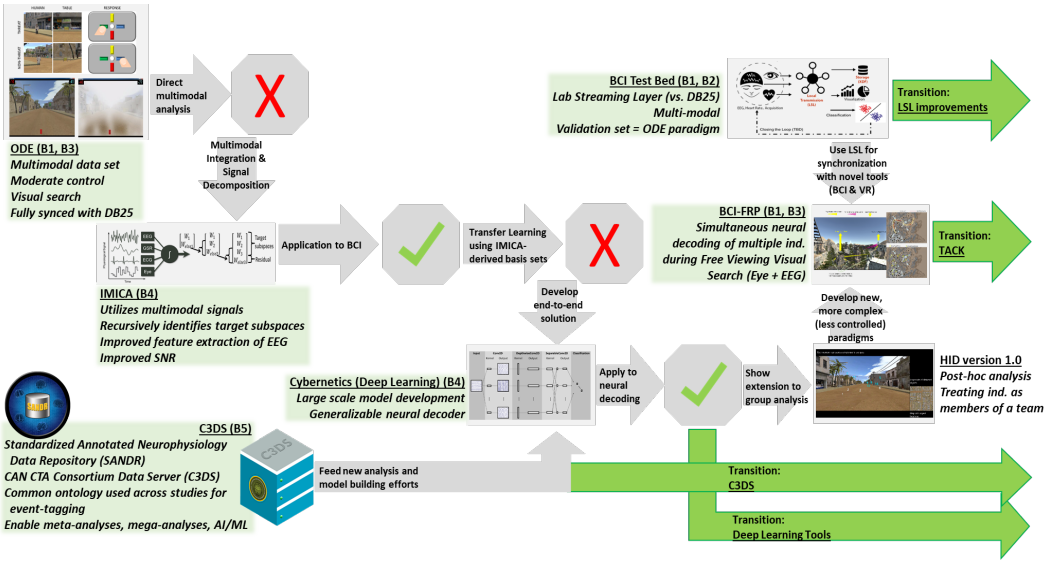


Fig. 4.1 DCS research progression

4.1 Operator Dynamics of Event (ODE) Appraisal

Barriers B1, B3

4.1.1 Purpose of ODE Study

The overarching goal of the ODE study was to develop and validate methods analyzing operator event appraisal processes as reflected in changes observed in cognitive and emotional state variables during the execution of tasks in operational environments. The study was intended to address barriers B1 (i.e., limitation of current study designs to impoverished stimuli) and B3 (i.e., failure to record the whole physical, mental, and physiological behavior). To this end, three specific aims were identified:

- **Aim #1.** To develop and experimentally validate an integrated system capable of recording and synchronizing high-density, multimodal data on human physiology and behavior. To enable system validation, we will

record and explore the patterns of correlation and co-variance among a variety of psycho-physiological and behavioral response variables. Measures will be derived from EEG, electrooculography (EOG), electromyography (EMG), ECG, and electrodermal activity (EDA); limb, head, and gaze position tracking; facial expressions; verbalizations; salivary samples; and subject responses to the tasks using the mouse, keyboard, and/or response pad.

- **Aim #2.** To develop computational strategies that will facilitate sensor management to enhance the acquisition and processing of multimodal data for studies of human neurocognitive performance in operational environments. Our approach will involve applying an intentionally selected set of algorithms to human physiologic and behavioral data, which, when performing reliably, will enhance the online acquisition of complex data sets as well as their later offline processing. We will also apply several ML algorithms to characterize individual data streams with respect to various data quality measures in order to establish their reliability and robustness.
- **Aim #3 (Barrier B4).** To develop an understanding of the factors that influence event appraisal processes, which are expected to be revealed by subjective changes in affect and task-specific motivation and satisfaction, and their relationship to performance. To achieve this, we will leverage our multimodal recording and analysis techniques to enable the classification of changes in human appraisal processes using cognitive and affective state variables derived from physiological and behavioral measures during the performance of simple and complex tasks in operationally relevant environments.

4.1.2 Accomplishments

4.1.2.1 Aim #1

For this study we successfully integrated a wide range of sensors and devices including 1) BioSemi DAQ system to measure EEG, EOG, EMG, ECG, and galvanic skin response (GSR), 2) a Trigno DAQ system to measure EMG and accelerometry, 3) a faceLAB eye-tracking system to record eye gaze and head movements, 4) a networked video camera to record facial movements, 5) USB audio to record sounds, and 6) an experiment control system including video display, experimental events, and user responses. Integration and synchronization was achieved using both network communications as well as traditional transistor-transistor logic (TTL) systems (i.e., parallel port). Figure 4.2 shows an example of the physiological integration performed. In addition, we developed in-house

strategies to integrate 1) the Trigno system, which had no native capability for traditional parallel port integration, and 2) the network camera, which also did not provide an interface for standard parallel port integration.

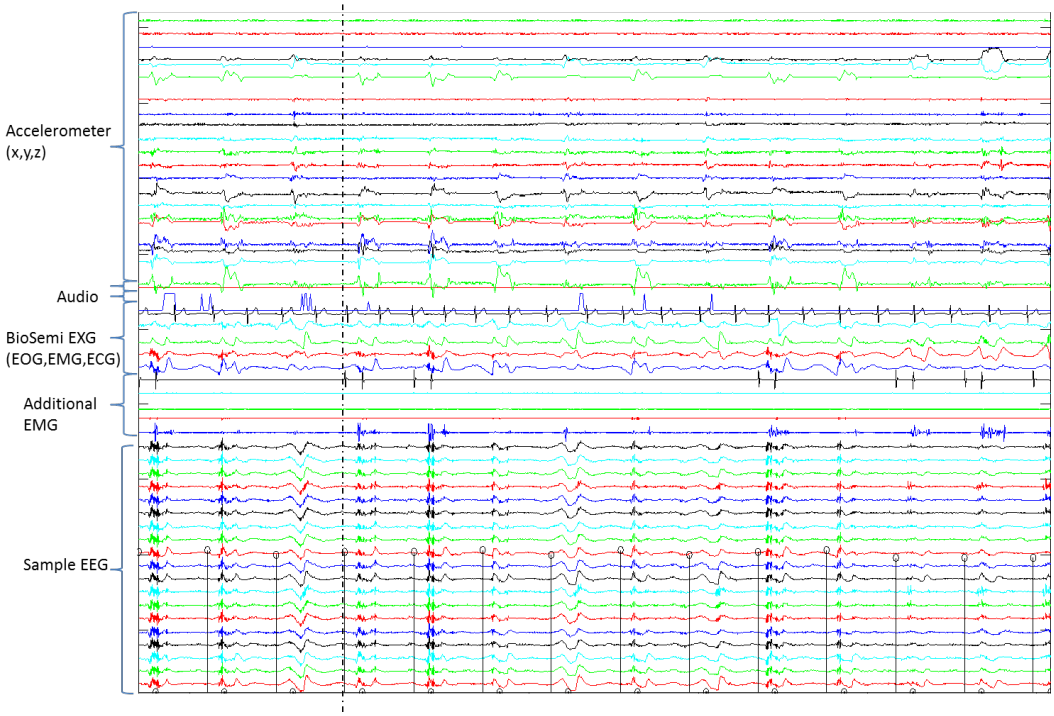


Fig. 4.2 Integration of all data streams for one representative subject

To integrate the Trigno, we built a custom printed-circuit board (PCB). We connected this board to the parallel port's least significant bit through a 1/100 voltage divider. We then placed on of the Trigno sensors directly on this board, which enabled the system to catch the rising edge and falling edge of the parallel port's least significant bit. In a similar fashion, we sent the same least significant bit to a red LED, which was strategically positioned in view of the network camera. We then wrote image processing software to extract the LED state changes from the raw video feed.

The only system that could not be integrated directly with the parallel port was the faceLAB eye-tracking system. This system provided no means to interface with standard TTL, and it was determined that obscuring the faceLAB cameras with an LED would pose too much of a risk to the integrity of the eye-tracking data. This system was integrated through a local area network, and the data was sent over this network to another computer that was connected to the parallel port.

Note: This development was performed *before* the emergence of online synchronization tools, such as LSL.

4.1.2.2 Aim # 2

Using the multimodal data that we obtained from this experiment, we worked on developing methods to improve integration of multimodal physiological data. This is described in detail in Section 4.2.

4.1.2.3 Aim # 3

The final aim was to develop an understanding of factors that influence task-specific motivation and the relationship between these factors and performance. The two versions of the game used in this experiment were designed to have similar dynamics, but in one version, the virtual competitor was set to "easy", while in the other condition the virtual competitor was set to "hard". Through the appearance of competition, we hoped to be able to modulate perceived task difficulty as well as performance on the task.

We assessed performance on the task by analyzing accuracy and RT for each of the different types of targets (threat humans, nonthreat humans, threat tables, nonthreat tables) in each of the two conditions (easy: Game 1 and hard: Game 2). We also included Fog and No-Fog since it was expected that this would have an effect on performance. Figure 4.3 shows average accuracy per target type across the four conditions. With the exception of nonthreat tables, there was very little difference in performance across Game 1 No-Fog and Game 2 No-Fog. Interestingly, however, if one considers target accuracy to be an indicator of difficulty, then there is a general trend of increasing difficulty along the curve: Game 1 No-Fog → Game 2 No-Fog → Game 1 Fog → Game 2 Fog, which suggests that Game 1 is less difficult than Game 2 and that No-Fog is less difficult than Fog.

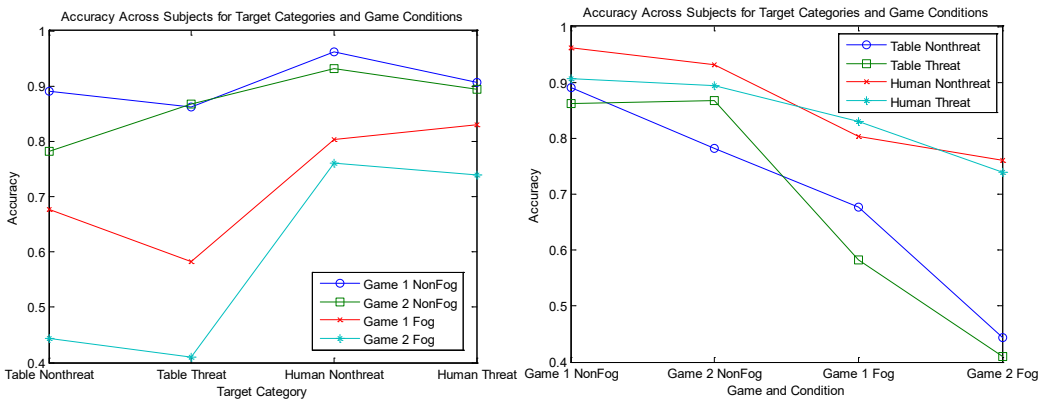


Fig. 4.3 Accuracy per target type for Game 1 No-Fog, Game 2 No-Fog, Game 1 Fog, and Game 2 Fog sorted by target type (top) and game condition (bottom).

Next, we performed comparisons of different modality-specific features to performance. We started by looking at eye behavior using the Nearest Neighbor

Index (NNI)—a measure of the randomness of an individual's search pattern—and blink rate. We compared NNI and blink rate to RT for combined Game 1 and Game 2, combined Game 1 Fog and Game 2 Fog, and combined Game 1 No-Fog and Game 2 No-Fog. We baseline corrected the RT for each target by subtracting the average RT for that target across all subjects. We did this in an effort to account for effects related to target type and location. We then computed NNI, blink rate, and RT values for each subject-game session.

Finally, we attempted to integrate the information contained in multiple different streams of data to predict alertness (as measured by high/low RT). To do this, we used the baseline corrected RT values for each subject. We constructed a feature vector utilizing the eye features NNI and blink rate, EEG features such as average alpha and beta power, and heart rate. We computed each of these features over the following windows time-locked to each target response: [–60, 0], [–45, 0], [–30, 0], [–15, 0], [–5, 0]. We combined the data from Game 1 and Game 2 and performed fourfold cross-validation. Within each fold, we used forward feature selection to determine the optimal feature set (by performing another round of cross-validation within the training set only). We then built a model using this feature set and tested the performance of that model on the remaining data. Table 4.1 shows the performance using 13 subjects (3 subjects had incomplete data). In this table, performance is measured using area under the curve (AUC).

Table 4.1 AUC values for each subject using multimodal models

Subject	Fold 1	Fold 2	Fold 3	Fold 4	Average (subject)
S1	0.650749	0.619656	0.682771	0.677955	**0.657782611**
S2	0.709596	0.636878	0.712704	0.658541	**0.679429808**
S3	0.733276	0.681074	0.686494	0.646852	**0.686923863**
S4	0.604513	0.617316	0.685165	0.634026	**0.635254912**
S5	0.697824	0.600152	0.583679	0.645022	**0.631669032**
S6	0.74	0.629528	0.612794	0.670168	**0.663122561**
S7	0.609141	0.672429	0.582863	0.615152	**0.619896088**
S8	0.628889	0.614545	0.617059	0.67982	**0.635078357**
S9	0.587108	0.555647	0.652144	0.571042	**0.591485222**
S10	0.691012	0.771479	0.729853	0.727015	**0.729839551**
S11	0.610859	0.605455	0.600932	0.590083	**0.601832044**
S12	0.625185	0.607727	0.623542	0.58987	**0.611581064**
S13	0.650427	0.647633	0.69907	0.618889	**0.654004884**
Average (folds)	**0.656814**	**0.635348**	**0.651467**	**0.640341**	**0.645992308**

4.2 Informed Multidimensional Independent Components Analysis (IMICA)

Barrier B4

One of the lessons learned from our initial ODE analysis was that integrating disparate streams of data into a cohesive whole was a non-trivial issue for a multitude of reasons including, but not limited to, different sampling rates, different temporal trajectories, different underlying cognitive influences, different SNRs, and different dimensionalities. Therefore, we began to focus efforts on integrating specific aspects of the multimodal picture. In other words, we pivoted toward improving our mathematical modeling tools (Barrier B4). Following the initial ODE multimodal analysis, we pursued the development of an improved method for EEG decomposition. This method, termed Informed Multidimensional Independent Components Analysis (IMICA), was developed using data from the ODE-PRACTB and allows incorporation of external information into the EEG decomposition process. Using this method, we were able to show that better EOG-like components could be extracted from the original EEG by incorporating information from the eye-tracking system. In addition, we showed that similar performance could be achieved by incorporating visual target position from the screen. The results that we obtained showed less residual blink after EOG component removal and greater correlation between the EOG-like components and the actual EOG channels than the best projections obtained using more traditional independent components analysis (ICA) decomposition algorithms (e.g., Infomax, FastICA, Joint Approximation Diagonalization of Eigenmatrices [JADE], Second Order Blind Identification [SOBI]). These results were accepted for publication to the *Journal of Neuroscience Methods*. A representative example is included in Fig. 4.4 and Table 4.2.

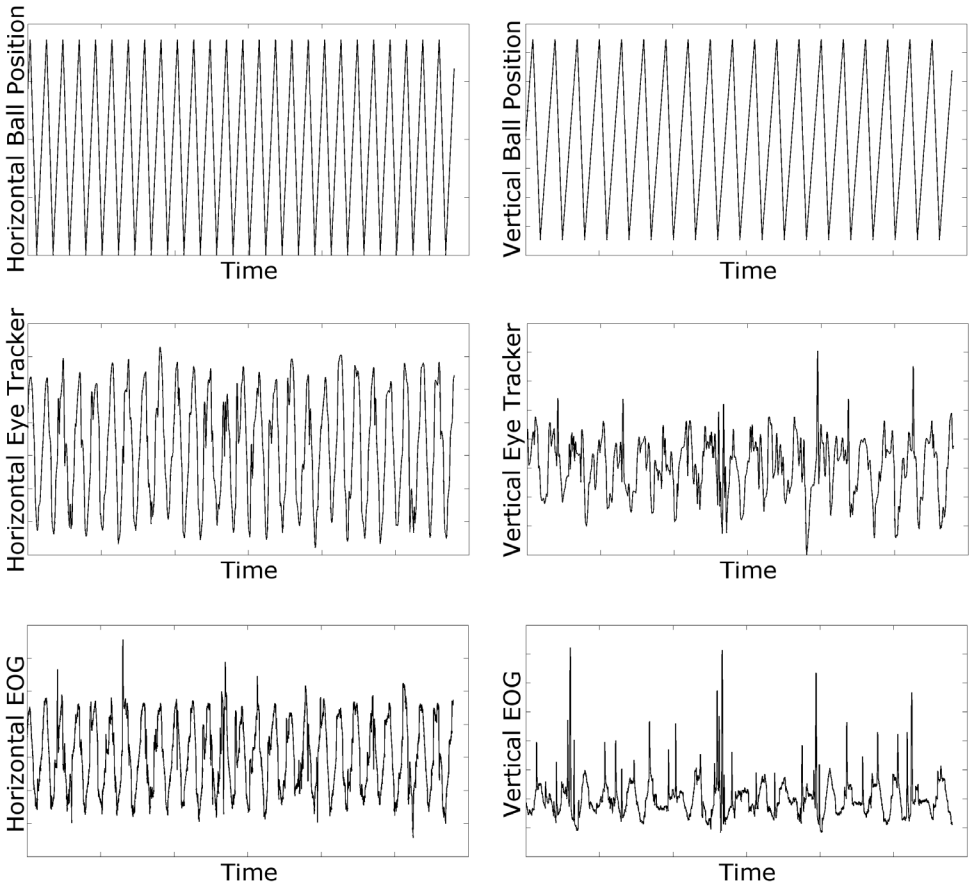


Fig. 4.4 Reference pairs used to capture EOG artifacts. (Top-left) Horizontal reference based on the position of a bouncing ball the subjects were instructed to visually track. (Top-right) Vertical reference based on the position of a bouncing ball the subjects were instructed to visually track. (Middle-left) Horizontal reference based on eye-tracker recordings during the bouncing ball task. (Middle-right) Vertical reference based on eye-tracker recordings during the bouncing ball task. (Bottom-left) Horizontal EOG during the bouncing ball task. (Bottom-right) Vertical EOG during both the bouncing ball task.

Table 4.2 Performance of the IMICA algorithm using different reference signals vs. other common EEG decomposition approaches (Infomax, FastICA, JADE, SOBI, principal component analysis [PCA])

Projection method	(1) Residual blink amplitude remaining after removal (%)	(2) R^2 using modeled blink activity	(3) Correlation with HEOG channel	(4) Correlation with VEOG channel	(5) Correlation with horizontal eye tracker	(6) Correlation with vertical eye tracker
IMICA: EOG	**0.1567**	0.9408	**0.9034**	0.6660	0.6040	**0.2470**
IMICA: EyeTracker + blink	0.1859	**0.9529**	0.8423	0.5228	0.5916	0.1316
IMICA: SmoothPursuit + blink	0.1864	**0.9529**	0.8754	0.5381	**0.6063**	0.1345
Infomax	0.5157	0.5676	0.4466	0.4621	0.2932	0.1483
FastICA	0.6567	0.4388	0.4532	0.4500	0.3066	0.1527
JADE	0.6940	0.4128	0.4484	0.4297	0.2758	0.1498
SOBI	1.3346	–1.0658	0.7966	**0.7046**	0.5461	0.2125
PCA	0.7345	0.2534	0.8539	0.6359	0.5864	0.1736

Note: HEOG = horizontal EOG, VEOG = vertical EOG.

In the same effort, we also extended the IMICA method to capture spectral components, which allowed us to model and remove EMG artifacts. As with the EOG artifacts, we saw improved performance using the IMICA method versus traditional EEG decomposition methods. IMICA was able to capture more of the EMG activity using fewer components. This allows IMICA to retain more of the original neural data, when EMG components were removed from the entire experiment. A representative result is shown in Fig. 4.5.

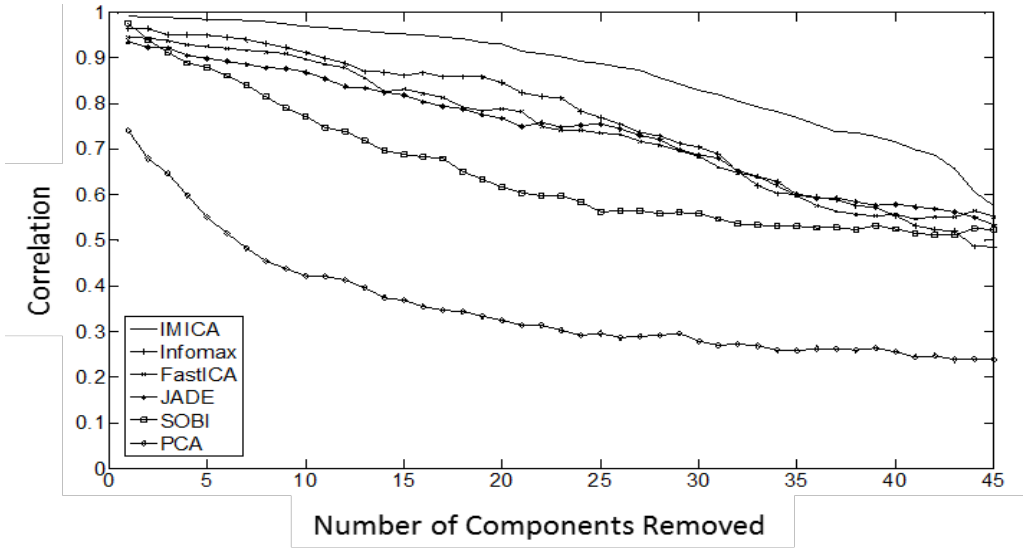


Fig. 4.5 Reduction in visual ERP as more components are used to isolate and remove the jaw clench artifact. Performance is measured as correlation values between the original ERP and the ERP obtained after removal of the artifact subspace. For all visual-evoked potentials (VEPs), there was no artifact present during the event. These results show that IMICA better isolated the jaw clench subspace.

As a final test for the IMICA algorithm, we used it to extract alpha-power changes in response to the experimental conditions of Fog/No-Fog that occurred in the ODE data. In other words, we used the predefined state changes derived from experimental conditions as a reference signal to extract independent components (ICs) whose alpha power maximally correlated with those changes. This was not presented in the paper but was done as a proof of concept. For the majority of subjects, these components yielded an increase in correlation between the best IC and the Fog/No-Fog state change versus the best channel and the Fog/No-Fog state change, when trained and tested on the two different versions of the game. In addition, for all subjects, the best alpha IC was identified over the occipital cortex, which was consistent with our prior expectations. A representative example is shown in Figs. 4.6 and 4.7.

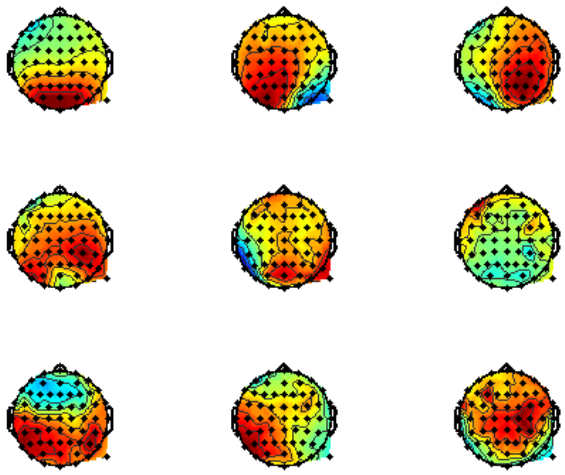


Fig. 4.6 Identified component projections for alpha-fog correlation. The first three components (top row) all have strong projections from the occipital cortex, as expected.

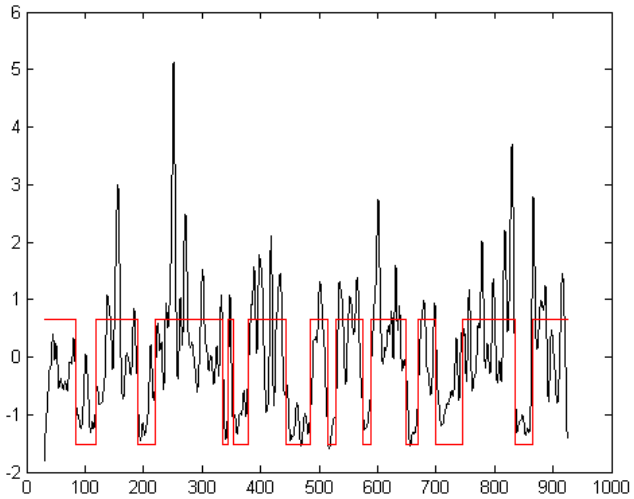


Fig. 4.7 Plot of normalized alpha (black line) and fog (red line) using components extracted from Fig. 4.6.

4.2.1 IMICA BCI

Given that the IMICA algorithm was shown to produce more optimal decompositions, thus improving overall SNR, and that it could trained using multimodal data, we investigated the use of such preprocessing for BCI purposes. In order to use IMICA for BCI, we needed a template of the event-related and band-specific neural dynamics. For this, we used each subject's labeled training data. After learning the IMICA weights, we then used $\mathbf{W}^{\text{final}}$ to keep only those subspaces that capture the neural dynamics, where $\mathbf{z}^{\text{final}} = [\mathbf{z}_1, \mathbf{z}_2, \ldots, \mathbf{z}_K]$, $K = \Sigma\ N_j$, and j indexes the target subspaces:

$$\mathbf{z}^{\text{final}} = \mathbf{W}^{\text{final}} \times \mathbf{y}. \quad (1)$$

For this work, we used the correlation between the projected components, $\mathbf{z}$, and reference signals derived from the available training data for the different frequency bands of interest to implement, $\boldsymbol{g}(\mathbf{z})$. Thus, the prior knowledge encoded with our approach is the time course and frequency band of neural features related to the event of interest. For example, for motor control activity, there are often alpha (~8–13 Hz) and beta (~14–30 Hz) desynchronizations prior to and re-synchronizations immediately following the motor event (Pfurtscheller and Aranibar 1977). These occur primarily in the contralateral motor cortex and are accompanied by low-frequency (0.5–3 Hz) readiness and somatosensory response potentials.

4.2.2 Comparison

4.2.2.1 Information Gain and Genetic Algorithm Feature Selection

Filter feature selection methods evaluate features prior to learning, whereas wrapper methods rely on the classification approach. Filters are thus faster to compute, but wrappers have the potential to better fit the problem space (O'Keefe and Koprinska 2009).

For our filter method, we implemented information gain (IG): IG(f) of feature f is the expected reduction in entropy, H, caused by observing feature f given a set of classes $C=\{c_i,\ldots,c_k\}$ (Cover 1999). The continuous-valued EEG features are properly discretized using the standard Minimum Description Length (MDL) approach. IG of each feature f is then calculated using Eqs. 2–4.

We compute IG values for each time point of each component and select only those components whose summed IG values are greater than 0:

$$IG(f) = H(C) - H(C|f), \quad (2)$$

$$H(C) = -\sum_{i=1}^{2} P(c_i) log P(c_i), \quad (3)$$

and

$$H(C|f) = -P(f) \sum_{i=1}^{2} P(c_i|f) log P(c_i|f). \quad (4)$$

The wrapper method we implemented was a genetic algorithm (GA) with a 0.0001 mutation probability, a 1 crossover probability, and clamping. From the available training data, split into two continuous halves, we performed a twofold cross-validation (CV) for each classifier and decomposition method. The fitness of each subset of components in the population (n = 30) was the average AUC across CV folds. The GA ran for 100 generations or until the fitness function plateaued.

4.2.2.2 IMICA for Feature Extraction

We analyzed the effects of using 1) minimally processed data in which only bandpass filtering and channel selection were performed (minimal preprocessing [MINP]), 2) PCA and Infomax ICA using IG to select components (PCA-IG and ICA-IG), 3) the same PCA and ICA decompositions but performing component selection via GA (PCA-GA and ICA-GA), and 4) IMICA preprocessing. For each decomposition method, the selected components were backprojected to the scalp so the same channel set could be used for all tests.

To further evaluate the different preprocessing methods, we also analyzed BCI performance when the selected components were *removed* from the data rather than kept. This additional step allows us to determine the amount of classification-related information carried by the selected components.

4.2.3 Data Sets

4.2.3.1 Movement-Related Cortical Potential (MRCP)

The first data set we analyzed was from a motor tapping study. In this study, 13 subjects performed self-paced finger movements using the left index, left middle, right index, or right middle fingers. The subjects performed eight sessions of four blocks. Each block contained a single 2-min run of self-paced finger movements. This produced the well-known alpha and beta synchronizations (i.e., increases in power) and desynchronizations (i.e., decreases in power), most clearly observed over the contralateral motor cortex (Pfurtscheller and Aranibar 1977). The data were originally recorded using a 256-channel BioSemi Active II at 1024 Hz. The data were referenced to average mastoids, bandpass filtered between 0.3 and 50 Hz, and then down-sampled to 128 Hz. We further down-sampled the channel space to the standard 64-channel BioSemi montage. For this data set, the classification task

that was used was left-hand movements (left index or left middle finger) versus right-hand movements (right index or right middle finger).

4.2.3.2 Rapid Serial Visual Presentation (RSVP)

The second data set that we analyzed was from an RSVP task, which has been described in a previous study (Marathe et al. 2015). In this study, 13 subjects observed a sequence of images presented at 2 Hz. The images depicted an urban landscape. Approximately 10% of images contained a target stimulus, in this case, a person with a weapon. Subjects were instructed to mentally count the number of targets observed. The data were recorded using a 64-channel BioSemi Active II at 1024 Hz. The data were referenced to average mastoids, bandpass filtered between 0.1 and 50 Hz, and then down-sampled to 128 Hz.

4.2.4 BCI Approaches Used

We analyzed the impact of our different preprocessing routines using multiple feature extraction (FE) and classification (CL) pairs. For both the MRCP and RSVP data sets, we used 1) hierarchical discriminant components analysis (HDCA) (Sajda et al. 2010), 2) xDAWN with Bayesian linear discriminant analysis (Rivet et al. 2009), and 3) Riemannian geometry (minimum distance to Riemannian mean [MDRM]) (Barachant et al. 2013). In addition, for the MRCP data set, we also included the Common Spatial Patterns (CSPs) (Blankertz et al. 2008) with linear discriminant analysis (LDA) FE/CL pair, which is common for motor imagery/execution BCI.

For both data sets, we downselected the channel space after decomposition, component selection, and backprojection but prior to FE/CL. We found that this produced better classification results for all tasks and FE/CL pairs.

The final channels used for BCI classification were 1) for MRCP, {FC3, FC1, C3, CP3, CP1, Cz, Pz, CP2, CP4, C4, FC2, FC4} and 2) for RSVP, {C1, C2, CPz, Pz, POz, Oz, O1, P1, P5, O2, P2, P6}. These channels were selected due to their proximity to the cortical regions of interest (i.e., for MRCP, over the motor strip, and for RSVP, over the occipital/parietal regions).

4.2.4.1 IMICA Subspace Design

We preset the size of each IMICA subspace, rather than use the likelihood curve approach of Gordon et al. (2015). For the MRCP data set, we used three subspaces to capture 1) the delta/theta [0.1–7] Hz response, 2) alpha [8–13] Hz response, and 3) the beta [14–30] Hz response. We preset the subspace sizes to be 2, 6, and 6

components, respectively. This is based on our prior analysis of this data described in full in Gordon et al. (2015).

For the RSVP data, we designed three subspaces to capture 1) delta/theta [0.1–7] Hz response for targets, 2) delta/theta response for non-targets, and 3) alpha [8–13] Hz response for targets. We used four components for each of these subspaces.

4.2.4.2 Statistical Analysis

We model the data using repeated measures analysis of variance (RM-ANOVA) with two factors, one for algorithm type (HDCA, xDAWN, MDRM, and CSP) and one for preprocessing type (MINP, PCA-IG, PCA-GA, ICA-IG, ICA-GA, and IMICA), and the interaction between these two factors. When the assumption of sphericity is violated, we use the Huynh–Feldt (HF) correction. If the interaction term was not significant, we refitted the model without the interaction. The *p*-values reported for the remainder the manuscript are the HF-corrected *p*-values when necessary.

4.2.4.3 Results

We first demonstrate the effects of component selection on the neural response for one sample subject. Figure 4.8 shows the time-locked evoked-response in the time-frequency domain for one subject from the MRCP data set for the downward motion of the finger. The top row shows the projection to the contralateral hemisphere from the components created and selected using three of our chosen preprocessing methods. The bottom row shows the projection to the contralateral hemisphere using only the residual components from those same preprocessing methods. The data is shown for the right-hand movements over the contralateral hemisphere, electrode C3 in the standard 10-10 montage.

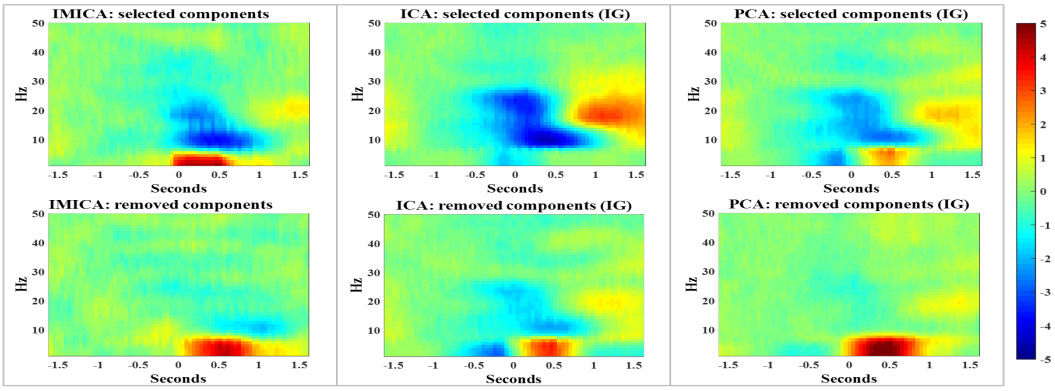


Fig. 4.8 Comparing IMICA, ICA, and PCA decomposition/component selection for one subject of the MRCP data set. The time-frequency data is plotted for right-hand movements at electrode C3 (i.e., contralateral hemisphere). Top left: Backprojection of selected 14 IMICA components. Top middle: backprojection of 27 components from Infomax ICA-IG. Top right: Backprojection of 47 components selected from PCA-IG. Bottom left: Backprojection of 50 nonselected IMICA components. Bottom middle: Backprojection of 37 nonselected ICA components. Bottom right: Backprojection of 17 nonselected PCA components

Figure 4.9 shows the performance of each preprocessing method for the MRCP data set for each FE/CL pair. Within each group, the bars on the far left (solid color) indicate MINP. For the remaining bars, dark-gray values show the BCI performance using only the selected components. Light-gray values show the BCI performance when those same components are removed rather than kept.

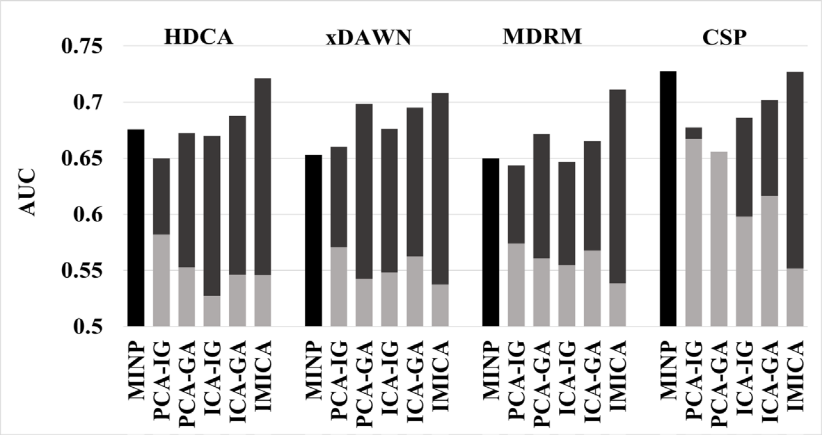


Fig. 4.9 BCI performance results for the MRCP data set. In each group, the bar on the left (solid color) indicates the MINP condition. The remaining bars indicate performance using the selected components (dark gray) and removing the selected components (light gray).

For the MRCP data set, the RM-ANOVA revealed a significant effect for preprocessing type ($p < 0.0001$) and interaction between algorithm and preprocessing type ($p < 0.0001$), with IMICA preprocessing providing the most gains in performance (dark-gray values) over the MINP condition (Fig. 4.9, left). Furthermore, removal of the 14 IMICA components (light-gray values) negatively

impacts the performance as much, if not more, than removal of those components computed using PCA or ICA. This is despite the selected PCA and ICA subsets consisting of substantially more components. The only MRCP conditions in which IMICA is not the clear top performer is the MINP condition for CSP and PCA-GA for xDAWN.

Figure 4.10 shows the results for the RSVP data set. The RM-ANOVA showed a non-significant interaction between algorithm type and preprocessing type. Upon refitting the model without the interaction, only the preprocessing factor was significant ($p < 0.0001$). Like the MRCP data set, IMICA is consistently a top performer; however, the other preprocessing methods, especially PCA-GA, also perform well. IMICA performed better when compared to the ICA preprocessing methods (ICA-IG and ICA-GA), but did not perform better than the PCA preprocessing methods (PCA-IG and PCA-GA).

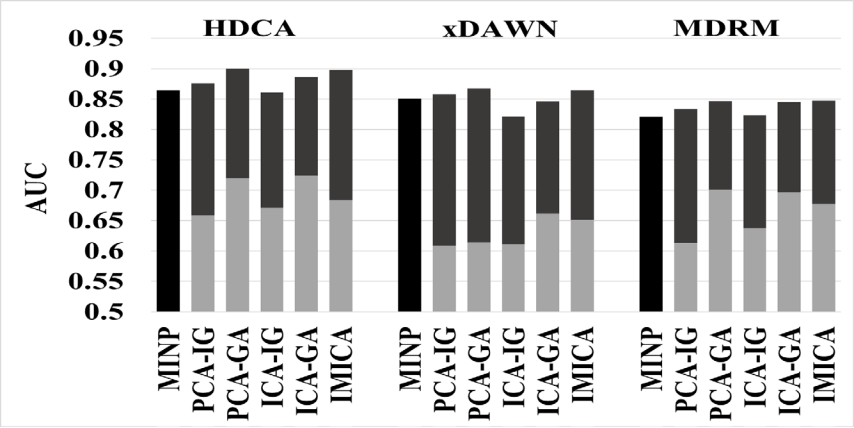


Fig. 4.10 BCI performance results for the RSVP data set. In each group, the bar on the left (solid color) indicates the MINP condition. The remaining bars indicate performance using the selected components (dark gray) and removing the selected components (light gray).

4.3 CaN CTA Consortium Data Server (C3DS)

Barrier B5

In parallel to our efforts to develop advanced signal-processing tools for the analysis of multimodal, multidimensional data, DCS began work on the C3DS. This work was in partnership with other CTA members, most notably UTSA and Syntrogi (now Intheon), and was intended to address Barrier B5 (i.e., lack of sufficient data archives). C3DS is an ARL data server located at DCS and maintained by DCS engineers. Data sets representing different studies are searchable based on description, principal investigator (PI), modalities, and so on. A web user-interface (Data Catalog) has been developed to allow users to query datasets stored in C3DS by hierarchical event descriptors (HED) tags in addition to

the other attributes. The back-end search service was intended to be accessible directly through a web application programming interface (API) for others to build applications on. As programmatic decisions are made regarding data-use policies and authorship rights, user access will be adjusted accordingly. C3DS was originally developed as part of the Standardized Annotated Neurophysiological Data Repository (SANDR) project.

One of the main goals of the SANDR project was to produce a large collection of well-annotated, synchronized data for shared analysis efforts. Moreover, given the complexity of real-world research, SANDR was intended to be a resource for supporting complex, large-scale analyses. C3DS and SANDR produced advanced capabilities for members of the CaN CTA to perform cutting-edge cross-experiment analysis and model building.

C3DS has been a key component to the development of large-scale deep learning-based analyses within ARL, DCS, and the broader CaN CTA.

4.4 Deep Learning for EEG Feature Extraction and Classification

Barrier B4

Following our initial success with the IMICA algorithm, in particular the application to BCI, we attempted to develop transfer learning approaches using IMICA-defined subspaces. However, all of our attempts to do so failed to produce statistically meaningful improvements in BCI performance on transfer tasks. We realized that one failure of IMICA was that it was still tailored to the individual and unable to learn invariant representations of the data. Therefore, we shifted focus, again (in partnership with collaborators from ARL), to investigating deep convolutional networks for data mining. This collaborative work produced EEGNet (Lawhern et al. 2018), arguably the first compact, convolutional network for EEG analysis.

We fined-tuned this model using the well-known P300 response in EEG studies of visual-evoked processing (Fig. 4.11).

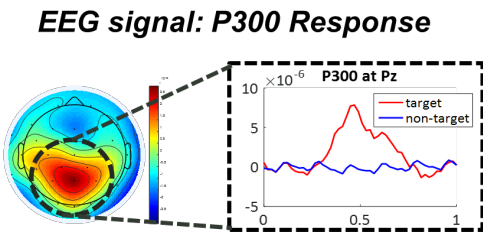


Fig. 4.11 Sample P300 evoked response to targets (red line) and non-targets (blue line)

Using the C3DS system, we performed a comprehensive leave-one-experiment-out analysis with the EEGNet architecture to study P300 variability (Fig. 4.12) and found that the convolutional model could faithfully capture the underlying variability in the signal while exhibiting invariance to both subjects and experiments. To the best of our knowledge, this type of large-scale model building and analysis effort had not been done. Our results were published in Solon et al. (2019) and have fed multiple follow-on studies.

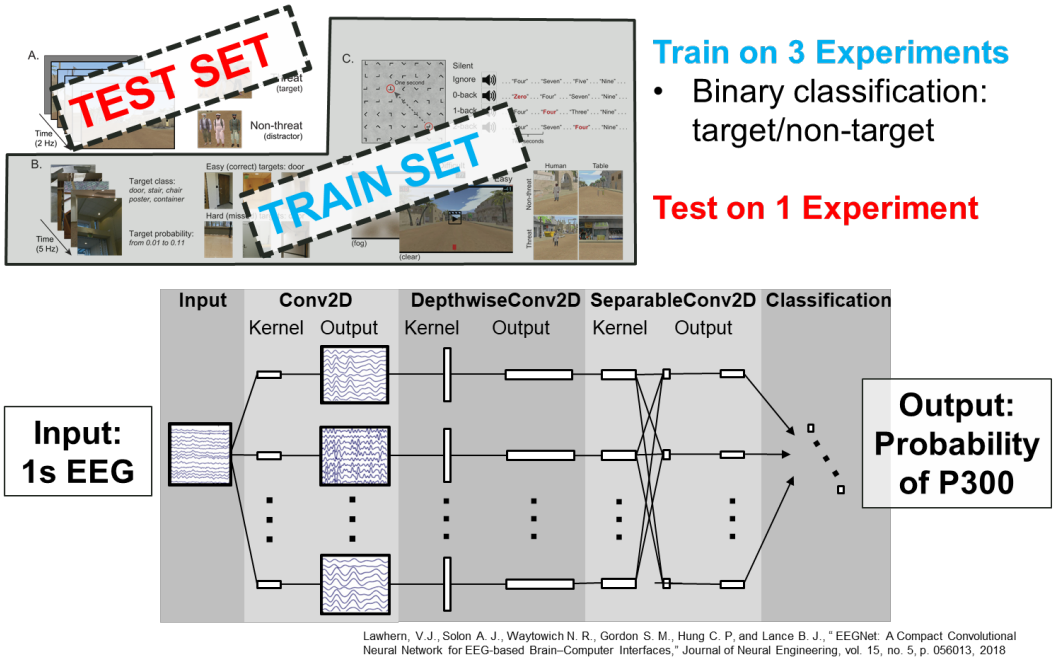


Fig. 4.12 Application of EEGNet to leave-one-experiment-out study of P300 variability

This convolutional approach to neural decoding provided a new approach for EEG analysis, specifically, we could now build models from prior data that use those models to interrogate new, unseen data. This interrogation was based on the compression of the multidimensional EEG data into a probability estimate that evolved over time and described a specific latent aspect of the subject's internal state.

4.5 BCI Test Bed

Barriers B1 and B2

In parallel to our development efforts on C3DS and EEGNet, we began working on general tools for BCI algorithm development and validation. Chief among these tools was a "test bed" to enable real-time application and assessment of BCITs. The BCI Test Bed project, which addresses Barriers B1 and B2, grew out of our prior work with ODE. In the ODE project, we used an intricate implementation of

parallel ports and signal converter technology to facilitate millisecond-level synchronization between disparate data streams. This approach was unwieldy and impractical. Building on efforts initiated by scientists at UCSD, we refined the LSL tool for providing real-time multimodal physiological integration.

In collaboration with ARL scientists we developed software tools for DAQ, streaming, and synchronization; a software architecture to support the integration of novel signal-processing and ML algorithms (developed by other parties); and software components for reintegrating the output of the classification system with different experimental paradigms.

The system was designed for event-based reactive BCIT in a naturalistic setting and supported plug-and-play functionality with different physiological sensors for recording EEG and eye tracking. An overview of the BCI Test Bed system is given in Fig. 4.13.

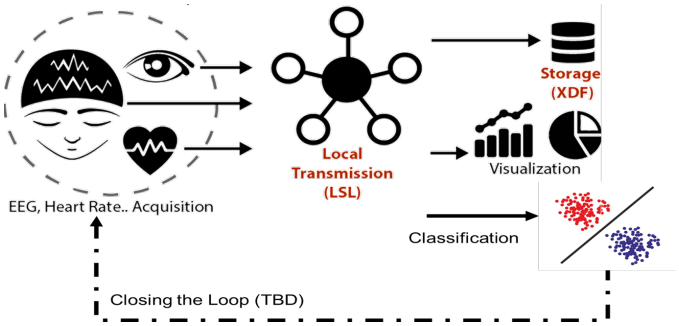


Fig. 4.13 BCI Test Bed architecture developed by DCS in collaboration with ARL (iconography from Syntrogi Inc.)

For the development of the test bed system, we first evaluated currently available solutions to identify those components that could be immediately leveraged for system development. This initial analysis also helped to identify gaps in current approaches. Alternative systems, and/or components, that we were investigated include, BCI2000, OpenEEG, BCILAB, and NeuroPype.

Our first test of the BCI Test Bed involved neural decoding from individuals participating in the ODE paradigm. This test leveraged multiple components that had been developed through the CaN CTA, including the following:

1) ODE paradigm and software tools
2) BCI Test Bed, including the LSL backend
3) Fully trained EEGNet model for analysis of fixation-locked potentials
    a. EEGNet was trained using data from SANDR

4) Implementation of various real-time signal-processing approaches for detecting eye movements and saccades

The test was successful and led to the development of the first human interest detector (HID) for mapping an external environment, which was subsequently published in IEEE Conference for Systems, Man, and Cybernetics in 2018 (Solon et al. 2018). Figures 4.14 and 4.15 provide an overview of the HID concept, along with collaborative BCI performance.

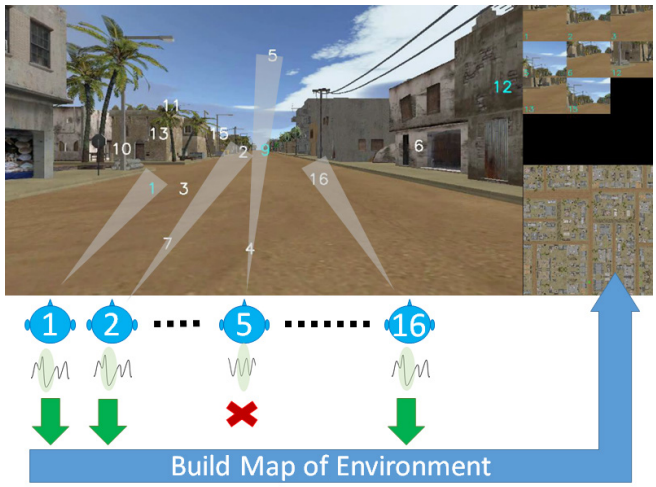


Fig. 4.14 Operational concept of using a HID to map an external environment

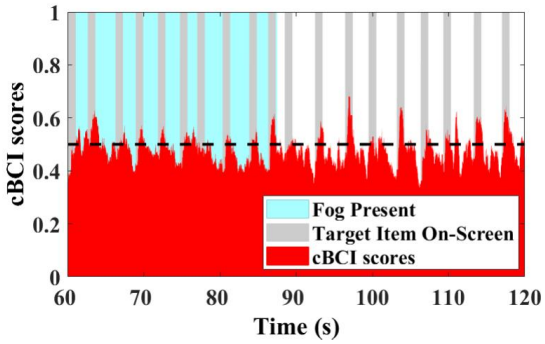


Fig. 4.15 BCI scores using a collaborative approach across 16 individuals for target detection in the ODE environment

4.6 BCI-Fixation-Related Potential (FRP)

Barriers B1 and B3

The success of the BCI Test Bed, EEGNet (trained using C3DS), and the initial HID led to the development of our final project under the CaN CTA: BCI-FRP.

There were several goals for this research project. First, we investigated the neural responses to naturalistic stimuli in a naturalistic environment using integrated eye

tracking, known object locations, and deep models to measure the data. Second, we investigated the contribution of task relevance versus visual salience when participants fixated upon, and presumably visually processed, specific stimuli. Third, based on these results, we showed that we can exploit the common task structure of a team of individuals in an environment in order to reconstruct, as we did in the HID test, the location of task-relevant stimuli in that environment without any prior knowledge of the task or location of specific objects. A high-level overview of this concept is shown in Fig. 4.16.

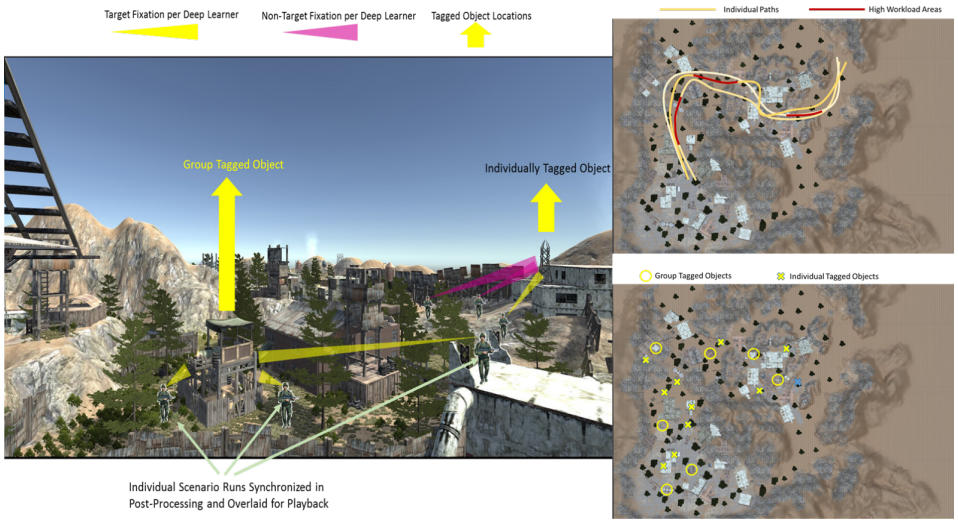


Fig. 4.16 Proposed concept: Fixations from different individuals are co-registered using eye tracking and position/orientation at the time of each fixation. Fixations are classified using the deep learner. As objects are tagged by individuals, the location of those objects are placed in a world map as either "group" or "individual" tagged. Periods of high workload are identified for each individual as they traverse the environment.

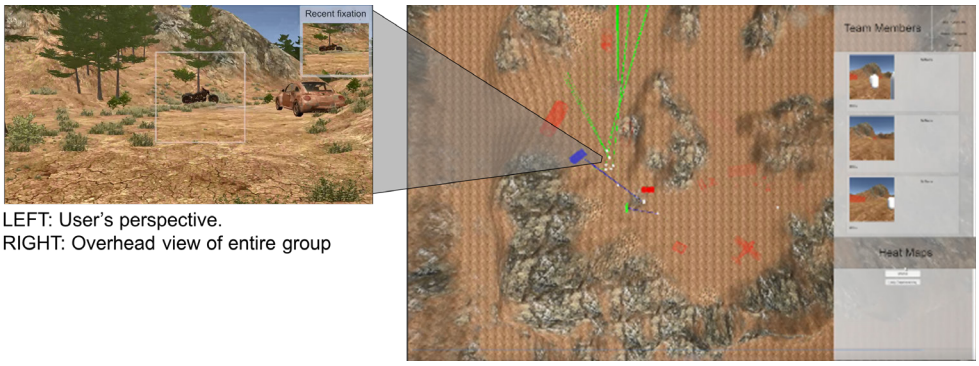
Our scenario was developed in the Unity3D game engine (Fig. 4.17). We used software libraries from Tobii eye tracking for integration with the environment to map fixations to specific stimuli.

The scenario that we developed involved the following:

1) *Baseline data collection using a standard RSVP go/no-go task*. This was limited to approximately 10 min, or two sessions of 5 min, and was used primarily to evaluate the accuracy of the deep model for each participant. In one session, the participants performed just the visual go/no-go task. In the second session, participants performed the go/no-go task while also performing a simultaneous auditory task. We are not planning to use this data to train our deep models, but we will perform a comparison of our generalized models to subject-specific models trained on this task as part of our final analysis.

2) *VR environment exploration*. Participants were divided into two groups. Each group had a specific task. Each task required that the participants identify/locate certain objects in the environment. The objects needed by each group were different. The participants were allowed to freely explore the environment while generally moving between two waypoints. We recorded each participant's location in the environment as well as their eye-tracking data. At one point during the experiment, participants were given the same simultaneous auditory task that occurred in the baseline session.

The data were synchronized using LSL implemented via our approach in the BCI Test Bed. We used two groups of participants. Each group was given a specific target object. The first group was told to search for "MOTORCYCLES". The second group was told to search for "HUMVEES". Each group searched the same environment and, thus, were exposed to the same stimuli. The only difference in the groups was the target object of interest.



LEFT: User's perspective.
RIGHT: Overhead view of entire group

Fig. 4.17 Implementation of our HID task in Unity3D

We used EEGNet, previously trained on data from C3DS, to decode the fixations from each individual. We used raycasts from the Tobii eye tracker to assign fixations to specific stimuli. We then aggregated the neural responses from each group for each stimulus in the environment. Finally, we sorted per group the stimuli based on the aggregate neural response.

The results from our primary analysis on group detection of target objects and their locations are shown in the Fig. 4.18.

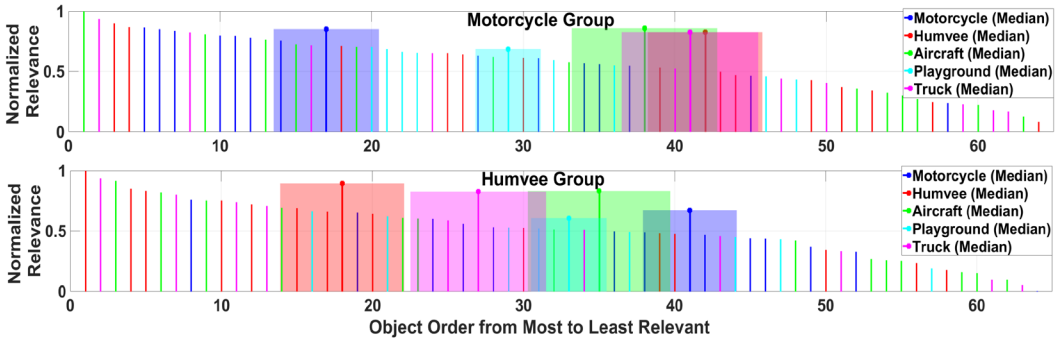


Fig. 4.18 Object types ranked by aggregate neural score (e.g., EEGNet output) for both the MOTORCYCLES and HUMVEE groups. In both cases, the aggregate scoring correctly uncovers the target object for that group with a predominance of those objects occurring high in the rankings. Mean and standard errors are shown for each object group.

4.7 References

Barachant A, Bonnet S, Congedo M, Jutten C. Classification of covariance matrices using a Riemannian-based kernel for BCI applications. Neurocomputing. 2013;112:172–178.

Blankertz B, Kawanabe M, Tomioka R, Hohlefeld F, Müller KR, Nikulin VV. Invariant common spatial patterns: Alleviating nonstationarities in brain-computer interfacing. Advances in neural information processing systems; 2008. p. 113–120.

Cover TM. Elements of information theory. John Wiley & Sons; 1999.

Gordon SM, Lawhern V, Passaro AD, McDowell K. Informed decomposition of electroencephalographic data. J Neurosci Meth. 2015;256:41–55.

Lawhern VJ, Solon AJ, Waytowich NR, Gordon SM, Hung CP, Lance BJ. EEGNet: a compact convolutional neural network for EEG-based brain–computer interfaces. J Neural Eng. 2018;15(5):056013.

Marathe AR, Lawhern VJ, Wu D, Slayback D, Lance BJ. Improved neural signal classification in a rapid serial visual presentation task using active learning. IEEE Trans Neural Syst Rehabilitation Eng. 2015;24(3):333–343.

O'Keefe T, Koprinska I. December. Feature selection and weighting methods in sentiment analysis. Proceedings of the 14th Australasian Document Computing Symposium; 2009; Sydney. p. 67–74.

Pfurtscheller G, Aranibar A. Event-related cortical desynchronization detected by power measurements of scalp EEG. Electroencephalography and Clinical Neurophysiology. 1977;42(6): 817–826.

Rivet B, Souloumiac A, Attina V, Gibert G. xDAWN algorithm to enhance evoked potentials: application to brain–computer interface. IEEE Transactions on Biomedical Engineering. 2009;56(8):2035–2043.

Sajda P, Pohlmeyer E, Wang J, Parra LC, Christoforou C, Dmochowski J, Hanna B, Bahlmann C, Singh MK, Chang SF. In a blink of an eye and a switch of a transistor: cortically coupled computer vision. Proceedings of the IEEE. 2010;98(3):462–478.

Solon A, Gordon S, McDaniel J, Lawhern V. Collaborative brain-computer interface for human interest detection in complex and dynamic settings. 2018 IEEE International Conference on Systems, Man, and Cybernetics (SMC); 2018, Oct. IEEE. p. 970–975.

Solon AJ, Lawhern VJ, Touryan JO, McDaniel JR, Ries AJ, Gordon SM. Decoding P300 variability using convolutional neural networks. Front Hum Neurosci. 2019;13:201.

5. University of Michigan (UMI)/University of Florida (UFL)

The UMI/UFL team focused our efforts on developing the use of EEG in dynamic, mobile environments to better understand cognition during human locomotion. In doing so, we were able to address technical barriers B1–B4 with the following areas of research:

- Brain and body dynamics of healthy individuals under conditions of cognitive and physical stress (B1–B3)
- Assessment of signal-processing methods and approaches for removing motion artifacts in RWN technologies (B1, B4)

5.1 Brain and Body Dynamics of Healthy Individuals under Conditions of Cognitive and Physical Stress

5.1.1 Cognitive Loading during Walking at Different Speeds

When humans walk in everyday life, they typically perform a range of cognitive tasks while they are on the move. We used high-density EEG to determine if electrocortical activity mirrored changes in cognitive performance across speeds. Subjects stood (0.0 m/s) and walked (0.4, 0.8, 1.2, and 1.6 m/s) with and without performing a Brooks spatial working memory task. Across speeds, the spatial working memory task caused subjects to step more widely compared with walking without the task. This is typically a sign that humans are adapting their gait dynamics to increase gait stability. Several cortical areas exhibited power fluctuations time-locked to memory encoding during the cognitive task. In the somatosensory association cortex, alpha power increased prior to stimulus presentation and decreased during memory encoding (Fig. 5.1). There were small significant reductions in theta power in the right superior parietal lobule and the posterior cingulate cortex (PCC) around memory encoding. However, the subjects did not show a significant change in cognitive task performance or electrocortical activity with walking speed. These findings indicate that in young, healthy subjects walking speed does not affect performance of a spatial working memory task. The subjects devoted adequate cortical resources to spatial cognition when needed, regardless of walking speed.

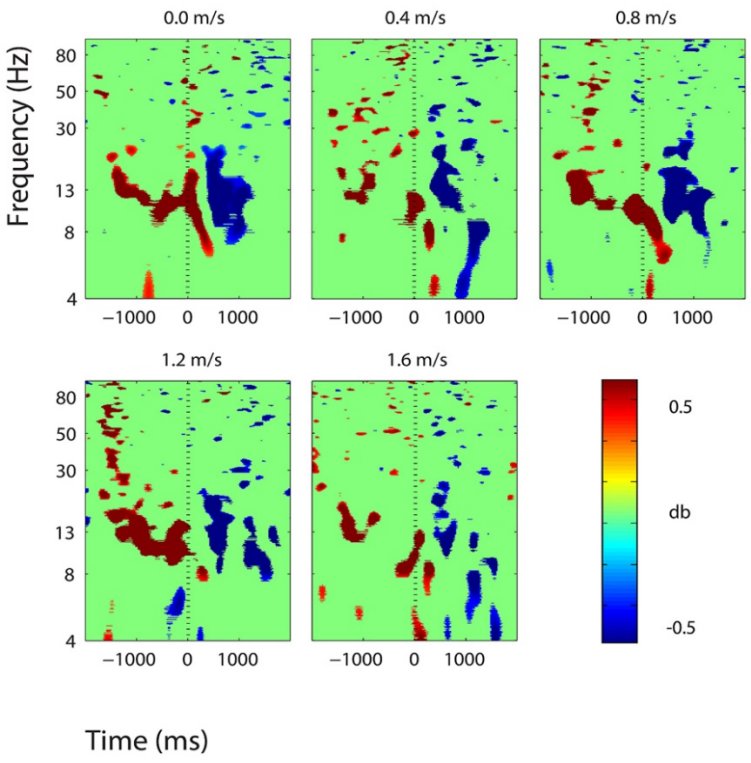


Fig. 5.1 Event-related spectral perturbation plots showing power change around the presentation of a stimulus in the central somatosensory association cortex

5.1.2 Locomotion on Uneven Terrain

Walking on uneven terrain is more energetically costly than walking on smooth ground, but the biomechanical factors that contribute to this increase are unknown. To identify possible factors, we constructed an uneven terrain treadmill (Fig. 5.2) that allowed us to record biomechanical, EMG, and metabolic energetics data from human subjects during walking and running (Voloshina et. al 2013; Voloshina and Ferris 2019). We tested healthy subjects (N = 11) walking at 1.0 m s^{-1}, and found that, when walking on uneven terrain with up to 2.5-cm variation, subjects decreased their step length by 4% and did not significantly change their step width, while both step length and width variability increased significantly (22% and 36%, respectively; $p < 0.05$). Uneven terrain walking caused a 28% and 62% increase in positive knee and hip work, respectively, and a 26% greater magnitude of negative knee work (0.0106, 0.1078, and 0.0425 J kg^{-1}, respectively; $p < 0.05$). Mean muscle activity increased in seven muscles in the lower leg and thigh ($p < 0.05$). These changes caused overall net metabolic energy expenditure to increase by 0.73 W kg^{-1} (28%; $p < 0.0001$). Much of that increase could be explained by the increased mechanical work observed at the knee and hip. Greater muscle co-activation could also contribute to increased energetic cost but to an unknown

degree. The findings provide insight into how lower-limb muscles are used differently for natural terrain compared with laboratory conditions.

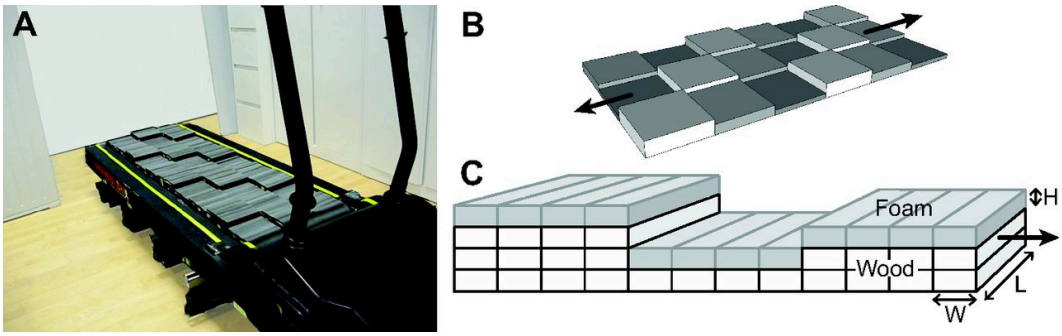


Fig. 5.2 a) Treadmill with the uneven terrain surface attached. b) Schematic of the uneven surface layout, consisting of three alternating heights (arrows indicate the treadmill's long axis). c) Close-up representation of the individual blocks composing each stepping area.

To build on these results, we then quantified the biomechanical and energetic effects of running on uneven terrain (Voloshina and Ferris 2015). We tested healthy subjects (N = 12) running at 2.3 m/s on both uneven and even surfaces. Subjects showed an energetic increase of 5% (0.68 W/kg; $p < 0.05$) when running on uneven terrain compared to smooth terrain (Fig. 5.3). Step width and length variability increased by 27% and 26%, respectively ($p < 0.05$). Positive and negative ankle work decreased by 22% (0.413 J/kg) and 18% (0.147 J/kg), respectively ($p = 0.0001$ and $p = 0.0008$). Mean muscle activity increased for only three muscles in the thigh ($p < 0.05$). All but three muscles showed a minimum of 15% increase in muscle activity variability ($p < 0.05$). About half of the increase in energetic cost can be explained by changes in mechanical work due to up- and down-steps on the uneven surface. These results provide insight into the changes in lower-limb biomechanics on more natural surfaces and their effects on energetic cost.

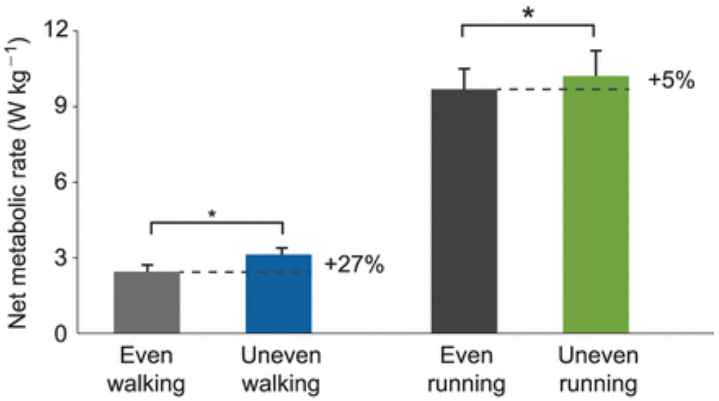


Fig. 5.3 Net metabolic rate for walking and running on the even and uneven surfaces. Percentages indicate the increases in energetic cost caused by uneven terrain when compared with even walking or running. Asterisks signify a statistically significant difference between the even and uneven walking and running conditions.

5.1.3 Large-Scale Integrative Experiment (LSIE)

The goal of the ambulatory LSIE was to push brain and body mobile imaging into settings that are close to operational environments and compare/contrast useful information from these measurements. We recruited 51 young, healthy subjects and obtained electrocortical dynamics and whole-body kinematics via limb-mounted inertial measurement units (IMUs) during active locomotion in two different environmental settings: a VR laboratory setting and a natural outdoor setting. While the subjects walked in each setting, they completed a visual search task where they had to identify dark green flags placed in the environment (or VR display). Light-green flags were also present, albeit less numerous (about one-third the number of dark-green flags), and registered as a visual oddball with a concomitant P300 EEG ERP. For each dark-green flag they successfully identified, subjects received an additional $0.50. During the stressor period (a 10-min window within each environment), subjects were told that they lost $3.00 for each dark-green flag they missed. There was an audio cue when they missed a dark-green flag during the experiment, signaling the subject just lost the $3.00 of extra financial payment. Unbeknown to the subject, the experimenter signaled a missed dark-green flag on average 1 per minute regardless of whether the subject missed a dark-green flag or not. The continued signaling of losing money was intended to induce a stressful condition. We collected salivary cortisol levels at intervals throughout the experiment to verify that the stressor condition produced measurable changes in physiological stress (i.e., salivary cortisol).

5.1.4 Comparison of Stress Responses in Real-World Environments

The goal of this project was to determine the possibility of using EEG signals to monitor stress responses in real-world environments. A noninvasive method to measure stress with good temporal resolution and few side effects would enhance our ability to study human physiology, especially in realistic settings. While other approaches to measure acute and/or chronic stress are either relatively invasive (blood or urine cortisol levels) or have poor temporal resolution (salivary cortisol), electrocortical signals may have the potential to bridge these gaps. To explore this potential, we recorded 128-channel EEG data from 11 subjects while they performed a stationary shooting task with an airsoft rifle in our laboratory (Schlink et al. 2017). In the Control condition, subjects aimed the rifle at a target 12 m away and fired one shot (repeating this process 50 times). In the Stress condition, subjects performed the same protocol while a second experimenter randomly fired shots in the subject's direction. We observed significantly higher skin conductance responses and salivary cortisol levels ($p < 0.05$ for both) during the stressful conditions, indicating that we had successfully induced an adequate level of acute stress. We located ICs in five regions throughout the cortex, most notably in the

dorsolateral prefrontal cortex, a region previously shown to be affected by increased levels of stress. This area showed a significant decrease in spectral power in the theta and alpha bands less than a second after the subjects pulled the trigger. Overall, our results suggest that EEG with ICA and source localization has the potential of monitoring acute stress in real-world environments.

5.1.5 Electrocortical Effects of Virtual Reality Use during Balance Beam Walking

In a series of related experiments, we examined how VR affects motor behavior compared to real-world conditions. In the first experiment, we recorded 128-channel EEG, heart rate, skin conductance, and RT from 19 subjects walking on an over-ground balance beam to assess the effects of high height exposure in VR on physical and cognitive performance (Peterson et al. 2018a). We found that virtual high heights exposure increased stress compared to virtual low heights as measured by HRV (Fig. 5.4). VR use also impaired balance performance and increased cognitive loading compared to unaltered viewing.

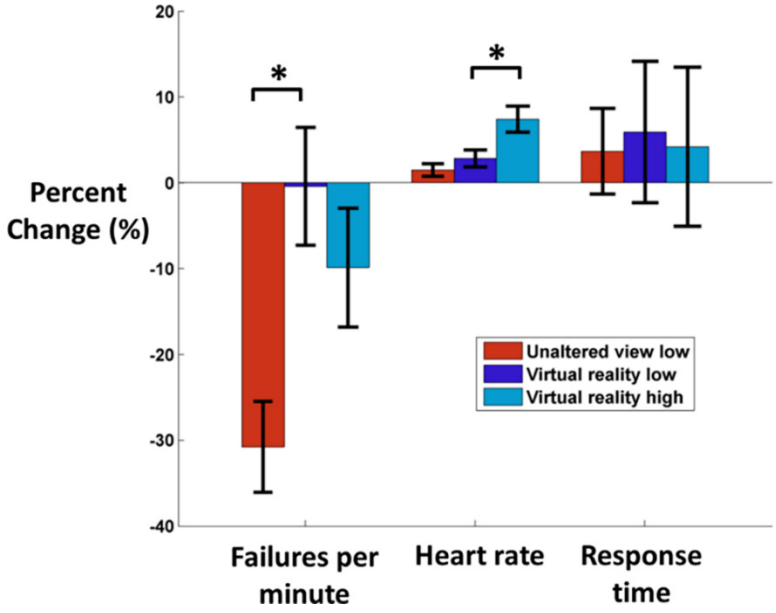


Fig. 5.4 Percent change in failures per minute, heart rate, and RT. Being in VR increased overall stress metrics and being in the simulated beam walking at a high height increased variability in measures considerably.

In our next experiment, we tested the effects of half-second field-of-view rotations during pass-through VR on balance performance (Peterson et al. 2018b). Thirty subjects walked on a treadmill-mounted balance beam. Using 128-channel source-localized EEG, we found that subjects exposed to visual rotations showed decreased alpha (8–13 Hz) power in parietal/occipital regions and had a fourfold

improvement in balance performance when compared to subjects who were not exposed to the rotations in VR. These transient visual perturbations in VR can improve motor learning via cognitive change, potentially minimizing the balance impairments caused by VR.

We further explored how sensorimotor perturbations affect electrocortical activity during walking and standing on a treadmill-mounted balance beam (Peterson and Ferris 2018b). We recorded 128-channel EEG, motion capture, lower-leg EMG, and neck EMG from 30 subjects exposed to brief 20° field-of-view rotations and mediolateral pulls at the waist. Using source localization via ICA, we found that these two perturbation types induced transient spectral power increases in theta (4–8 Hz) and decreases alpha-beta (8–30 Hz) bands across multiple cortical regions. The spectral pattern was strongest in sensorimotor regions during physical pulls and in occipito-parietal regions during visual rotations. This suggests similar time-frequency electrocortical patterns when responding to sensorimotor conflict, but different cortical region involvement depending on the perturbation type.

In addition to analyzing cortical regions separately with spectral power, we wanted to quantify the connectivity among regions during sensorimotor perturbations (Peterson and Ferris 2018a). First, we tested potential connectivity measures using ground-truth signals from antennae embedded inside a phantom head. We mounted the phantom head to a motion platform that mimicked recorded human head motion while walking at speeds up to 2.0 m/s. We assessed how well ICA recovered the ground-truth signals during head motion. ICA reconstructed the original signals well, with cross-correlations above 0.8 and SNRs close to 10 dB across all walking speeds. Connectivity measures using these ICs were typically able to identify ground-truth interconnections, but many measures were susceptible to spurious high-frequency connections. Based on these results, we quantified multi-subject electrocortical connectivity during our human EEG recordings using direct directed transfer function (dDTF), a connectivity measure that performed consistently well during our phantom experiment (Peterson and Ferris 2019). We found increased connectivity during physical pull perturbations in central regions and decreased occipito-parietal connectivity during visual rotations. We also found evidence for connectivity from the cortex to lower-leg muscles during physical balance perturbations.

5.1.6 Measurement of Spatial Myoelectric Patterns during Human Locomotion Using High-Density Electromyography

Our success in advancing EEG as a viable technology for recording brain dynamics during locomotion suggested we branch out to other biosignal recording systems. Electrical muscle activity is typically measured via bipolar surface sensors, which

have poor spatial resolution for measuring intramuscular variations in myoelectric activity. High-density EMG improves upon this by using a grid of electrodes to measure both the temporal and spatial properties of a muscle, but it has been primarily used in stationary conditions. We first developed an electrical lower-limb phantom to quantify the effects of crosstalk and motion artifacts (Schlink and Ferris 2019). We found that motion artifacts do not affect all areas of the EMG array uniformly, and traditional filtering measures may not fully remove these artifacts. To address this issue, we compared the effectiveness of standard EMG signal processing and alternative signal-processing methods at removing motion artifacts from high-density EMG data during locomotion (Schlink et al. 2020a). Canonical correlation analysis (CCA) decomposition provided the greatest reduction in signal content associated with artifacts. We then applied this signal-processing approach to EMG signals recorded from five lower-limb muscles across a range of walking and running speeds (Schlink et al. 2020b). We found heterogeneous spatial EMG activation patterns, evidenced by contrasting spatial entropy and EMG barycenter locations among the muscles. Finally, we assessed how localized muscle fatigue affected spatial myoelectric patterns in the medial gastrocnemius during locomotion (Schlink et al. 2020b). Peak EMG activity during locomotion significantly decreased when the subjects' gastrocnemius was fatigued, and the barycenter of EMG activity shifted from its pre-fatigue location, suggesting an altered neuromuscular recruitment pattern in response to fatigue. Together, these studies establish high-density EMG as an effective tool for studying muscle activity in dynamic environments.

5.2 Assessment of Signal-Processing Methods and Approaches for Removing Motion Artifact in Real-World Neuroimaging Technologies

5.2.1 Isolation of Gait-Related Motion Artifacts Recorded Using EEG

The relative contributions of movement artifact and electrocortical activity in scalp EEG data are difficult to quantify. To better characterize the movement artifact recorded by EEG electrodes, we used a novel experimental method to isolate the motion artifact by blocking electrophysiological signals using a silicone swim cap (Kline et al. 2015). We then simulated an electrically conductive scalp on the top of the swim cap using a wig coated with conductive gel. We recorded motion artifact EEG data from nine young adults walking at a range of speeds (0.4–1.6 m/s). Movement artifacts varied considerably across speed, subject, and electrode location (Fig. 5.5). The artifacts recorded with EEG electrodes did not correlate well with head acceleration. Standard artifact removal methods attenuated low-frequency noise but did not completely remove the movement artifact. We also

observed spectral power fluctuations in the movement artifact data that resembled data from previously published studies of normal EEG during walking, suggesting that EEG data recorded during walking likely contains substantial movement artifacts. Further analysis using ICA and dipole fitting was able to accurately localize 99% of the ICs as non-neural (Snyder et al. 2015), though ICs in cortical locations were still identified despite no actual cortical dipolar sources being present.

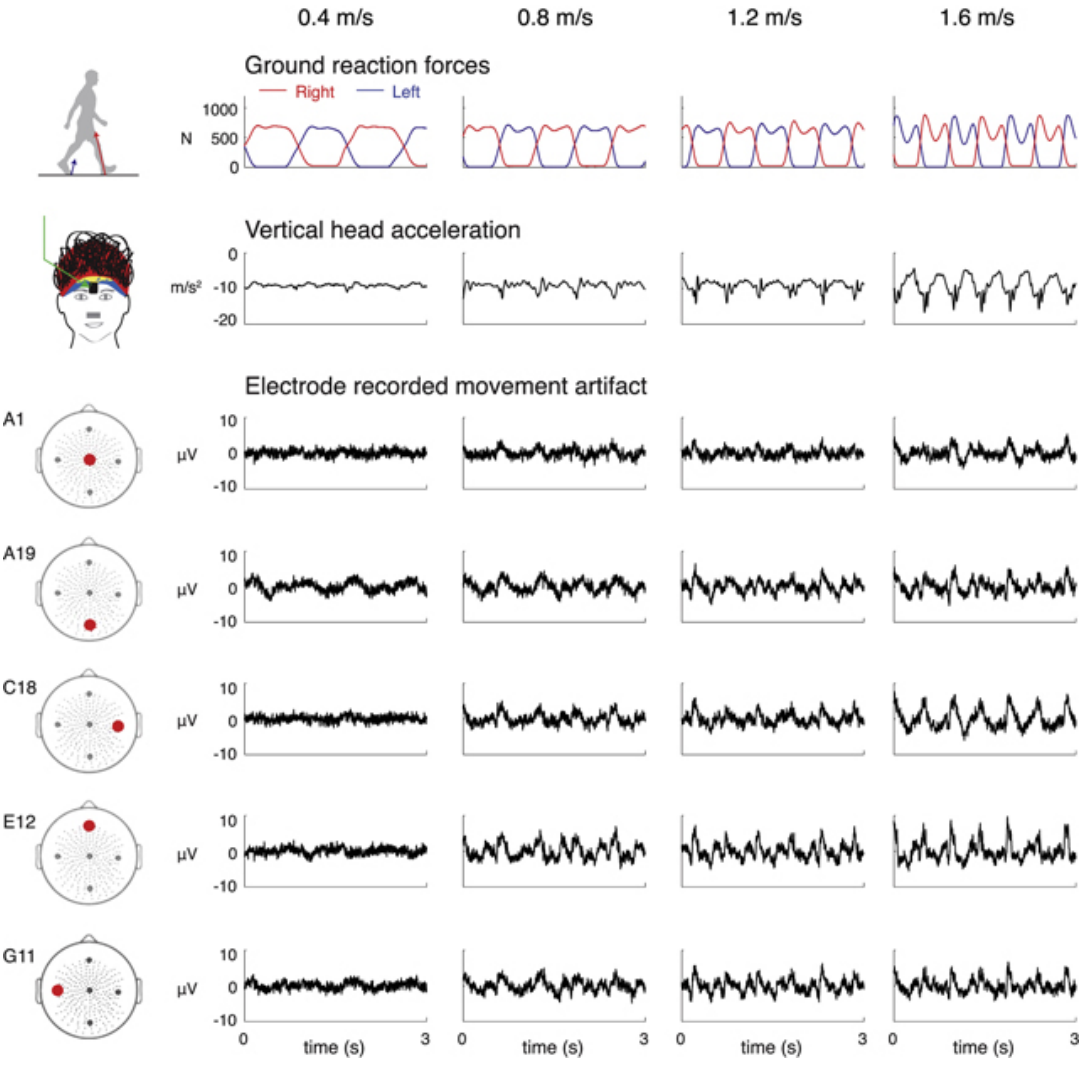


Fig. 5.5 Time courses of movement artifact and accelerometer data. Time courses of the ground reaction forces for the right and left legs, head accelerations (vertical, mediolateral, and anterior–posterior), and movement artifacts recorded in five electrodes (A1, A19, C18, E12, and G11) for the four walking speeds (0.4, 0.8, 1.2, and 1.6 m s^{-1}) for a single subject.

5.2.2 Development of Benchmarks for Data Quality of Real-World Neuroimaging Technologies

A major roadblock to more widespread acceptance of new neurotechnology systems is that we often do not have a clear understanding of how well these systems work. The large variety of commercially available EEG systems contrasts with the lack of established methods for objectively describing their performance during whole-body motion. Our goal was to develop repeatable and reliable benchmarks for assessing EEG technology. Subjects performed an auditory oddball task seated and while walking using three different EEG systems (Oliveira et al. 2016). We calculated EEG epoch rejection rate, pre-stimulus noise (PSN), SNR, and EEG amplitude variance across the P300 event window (CV_{ERP}) from a subset of 12 channels common to all systems. We also calculated test-retest reliability and the subject's level of comfort while using each system. All three systems performed similarly during the seated condition, but we found differences among the three EEG systems in rejection rates, PSN, and SNR during the mobile conditions. Subjects also reported less discomfort and were motivated for longer recording periods when wearing wet EEG systems compared to the dry system we evaluated. Our method was successful in identifying differences across systems that are mostly caused by motion-related artifacts and usability issues. We concluded that the extraction of the selected metrics from an auditory oddball paradigm may be used as a benchmark method for testing the performance of different EEG systems in mobile conditions.

5.2.3 Electrical Head Phantom with User-Defined, Ground-Truth Sources

The efficacy of using ICA to separate motion artifacts from EEG recordings is difficult to judge given that there is no ground truth for human EEG recordings. To investigate the effects of motion artifacts on an invariant EEG source, we constructed a phantom head composed of dental plaster and sodium propionate (Oliveira et al. 2016). Eight electrical dipoles were embedded within the plaster, and we broadcasted artificial neural signals from three antennae to simulate varying sources of brain activity (Fig. 5.6). We used a custom-built platform to induce sinusoidal vertical motions of the phantom and recorded EEG signals with three different acquisition systems. ICA was able to successfully isolate the three dipolar sources across all conditions and systems. The SNR was significantly higher for the IC activation in comparison to the channel data, thereby attenuating the effects of motion on the SNR.

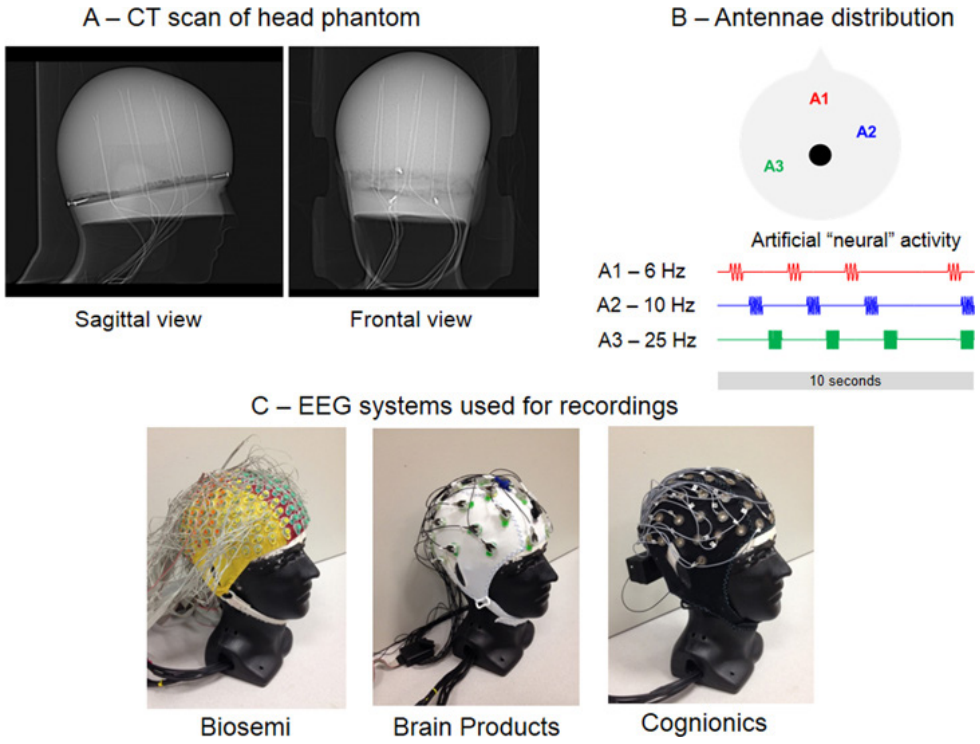


Fig. 5.6 a) Computerized tomography (CT) scan of the plaster phantom head showing the distribution of antennae. b) We broadcast artificial "neural" signals from three antennae at varying frequencies. c) We recorded high-density EEG data using three different systems for comparison.

To build upon these results, we purchased a 6 degree-of-freedom robotic hexapod (Notus). We also began using a new version of the head phantom developed by Dr Hairston's group at ARL (Oliveira et al. 2016a) composed mainly of ballistics gelatin.

5.2.4 Effects of Cable Sway, Electrode Surface Area, and Electrode Mass on EEG Signal Quality

To quantify the causes of mobile EEG motion artifacts, we conducted basic science experiments to isolate the effects of electrode mass, electrical surface area, and cable sway on EEG signal quality during motion (Symeonidou et al. 2018). Pilot testing suggested cable movements were a major contributor to motion artifacts in mobile EEG recordings, particularly when using the most commonly used commercially available mobile EEG system, BioSemi ActiveTwo. We modified BioSemi ActiveTwo electrodes by doubling and tripling the mass of standard BioSemi electrodes and by altering electrode surface area using larger-diameter silver (Ag)/silver chloride (AgCl) pellets. Recordings from the ARL ballistics gel head phantom showed that increasing electrode surface area marginally improved signal quality during motion on the Notus hexapod. Altering electrode mass had no

effect on signal quality. Cable motions, however, were a large contributor to motion artifacts, justifying the use of dual-electrode EEG configurations for noise cancellation, which relies on matched noise-only electrode pairs and bundled cables that experience equivalent cable artifacts.

5.2.5 Dual-Electrode EEG Design for Motion Artifact Removal

Novel EEG electrode designs are needed to improve upon current limitations in real-world mobile brain and body imaging. We proposed to design and fabricate novel EEG electrode prototypes that could facilitate studies of motion artifact contamination during real-world EEG recording. Our first iteration of the dual-electrode array consisted of eight scalp electrodes recording normal EEG and eight mechanically coupled and inverted secondary electrodes that were electrically isolated from the scalp EEG sensors, recording only motion artifacts and electrical noise, without artificial neural signals (Fig. 5.7; Nordin et al. 2018). We recorded artificial neural signals broadcast from antennae in the phantom head during continuous vertical sinusoidal movements (stationary, and 1.00-, 1.25-, 1.50-, 1.75-, and 2.00-Hz movement frequencies). Signal quality was restored following noise cancellation when compared to single-electrode EEG measurements collected with no phantom head motion. We achieved substantial motion artifact attenuation using secondary electrodes for noise cancellation.

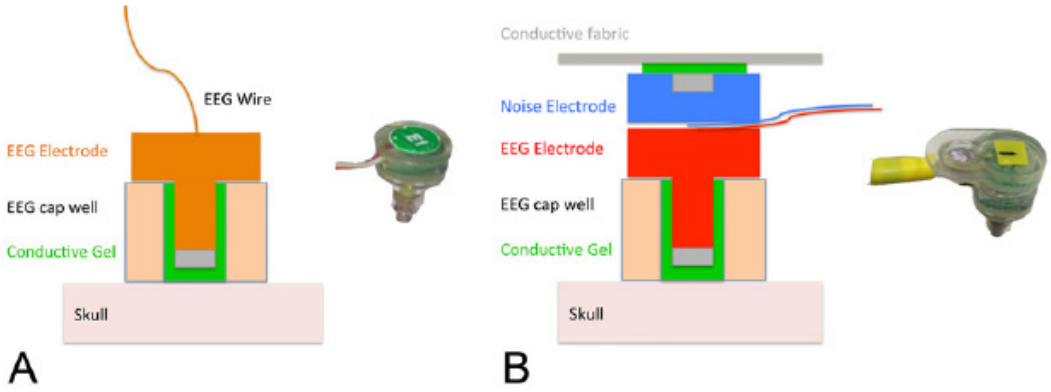


Fig. 5.7 a) BioSemi active pin type electrode, b) custom dual-electrode pair (BioSemi active pin type electrode and inverted flat type electrode)

5.2.6 Integration of Neck Muscle Sources for Muscle Artifact Removal

Because muscle artifacts can also corrupt dynamic mobile EEG recordings, we developed an electrical head phantom with artificial brain and neck muscle sources to test approaches for muscle artifact removal during motion. Similar to our approach for motion artifact removal, we included isolated neck muscle recordings with scalp EEG corrupted by muscle activity in an ICA decomposition and were able to improve artificial brain signal source separation (Richer et al. 2020). We

recorded 128-channel dual-layer EEG and 8-channel neck EMG from the head phantom during motion. We evaluated ground-truth electrocortical source signal recovery from artifact-contaminated data using ICA. By including isolated noise and EMG recordings in the ICA decomposition, we more effectively recovered ground-truth artificial brain signals. A reduced subset of 32-noise and 6-EMG channels showed equivalent performance compared to including the complete arrays. Artifact Subspace Reconstruction (ASR) improved source separation, but this was contingent on muscle activity amplitude. CCA also improved source separation. Merging noise and EMG recordings into the ICA decomposition, with ASR and CCA preprocessing, improved source signal recovery.

5.2.7 Brain Dynamics during Obstacle Navigation

Using the knowledge gained from the dual-electrode design and phantom experiments, we applied these data-processing procedures to human EEG recordings during an obstacle avoidance task (Nordin et al. 2019a, 2019b, 2019c). We dropped unexpected obstacles on a treadmill belt while subjects walked and ran at a range of speeds (0.5–2.5 m/s). We merged 128-scalp EEG channels, 40-matched noise pairs, and 8-single channel neck EMG signals into ICA to recover brain sources involved in overcoming unexpected obstacles. Electrocortical activity in supplementary motor area and premotor cortex showed spectral power increases soon after obstacles appeared on the treadmill belt (Fig. 5.8). Posterior parietal cortex activity showed later spectral power increases that maintained similar distance to contact with the approaching obstacle.

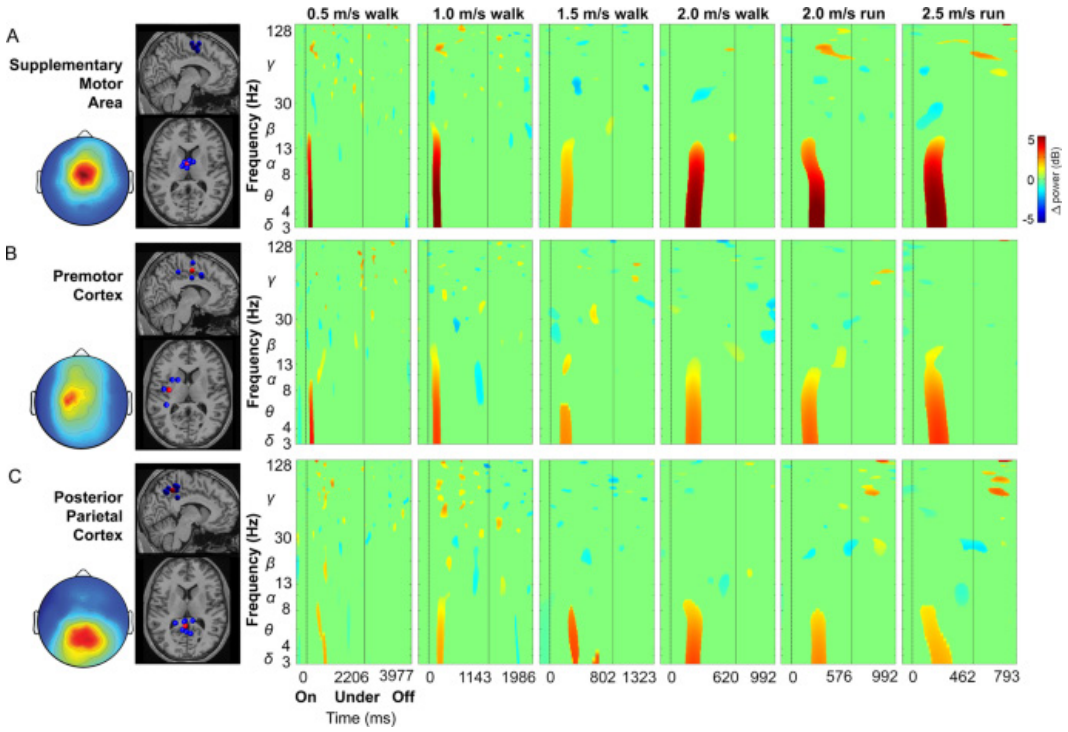


Fig. 5.8 Cortical clusters and event-related spectral perturbation plots by speed in the a) supplementary motor area, b) premotor cortex, and c) posterior parietal cortex.

5.3 References (Refereed Journal Articles)

Bradford JC, Lukas J, Ferris DP. Electrocortical activity distinguishes between uphill and level walking in humans. J Neurophysiol. 2016;115:958–966.

Gwin JT, Ferris DP. An EEG-based study of discrete isometric and isotonic human lower limb muscle contractions. J Neuroeng Rehabil. 2012a;9:35.

Gwin JT, Ferris DP. Beta- and gamma-range human lower limb corticomuscular coherence. Front Hum Neurosci. 2012b;6:258.

Gramann K, Ferris DP, Gwin JT, Makeig S. Imaging natural cognition in action. Int J Psychophysiol. 2014;91:22–29.

Gramann K, Gwin JT, Ferris DP, Oie K, Jung TP, Lin CT, Liao LD, Makeig S. Cognition in action: imaging brain/body dynamics in mobile humans. Rev Neurosci. 2011;22:593–608.

Gramann K, Jung T, Ferris DP, Lin C, Makeig S. Towards a new cognitive neuroscience: Modeling natural brain dynamics. Front Hum Neurosci. 2014;8:444.

Kline JE, Huang HJ, Snyder KL, Ferris DP. Isolating gait-related movement artifacts in electroencephalography during human walking. J Neural Eng. 2015;12(4):046022.

Kline JE, Huang HJ, Snyder KL, Ferris DP. Cortical spectral activity and connectivity during active and viewed arm and leg movement. Front Neurosci. 2016;10:91.

Kline JE, Poggensee K, Ferris DP. Your brain on speed: cognitive performance of a spatial working memory task is not affected by walking speed. Front Hum Neurosci. 2014;8:288.

Lau TM, Gwin JT, Ferris DP. Walking reduces electrocortical sensorimotor network connectivity compared to standing. J Neuroeng Rehabil. 2014;11:14.

Lau TM, Gwin JT, Ferris DP. How many electrodes are really needed for EEG-based mobile brain imaging? J Behav Brain Sci. 2012;2:387–393.

Lau TM, Gwin JT, McDowell K, Ferris DP. Weighted phase lag index stability as an artifact resistant measure to detect cognitive EEG activity during locomotion. J Neuroeng Rehabil. 2012;9:47.

Nordin AD, Hairston WD, Ferris DP. Dual-electrode motion artifact cancellation for mobile electroencephalography. J Neural Eng. 2018;15(5):056024.

Nordin AD, Hairston WD, Ferris DP. Faster gait speeds reduce alpha and beta EEG spectral power from human sensorimotor cortex. IEEE Trans Biomed Eng. 2019a;67(3):842–853.

Nordin AD, Hairston WD, Ferris DP. Faster gait speeds suppress human auditory electrocortical responses. 2019 IEEE International Conference on Systems, Man, and Cybernetics; 2019b. IEEE. p. 235–240.

Nordin AD, Hairston WD, Ferris DP. Human electrocortical dynamics while stepping over obstacles. Sci Rep. 2019c;9(1):4693.

Oliveira A, Schlink BR, Hairston WD, Konig P, Ferris DP. Induction and separation of motion artifacts in EEG data using a mobile phantom head device. J Neural Eng. 2016a;13(3):036014.

Oliveira A, Schlink BR, Hairston WD, Konig P, Ferris DP. Proposing metrics for benchmarking novel EEG technologies towards real-world measurements. Front Hum Neurosci. 2016b;10:188.

Oliveira AS, Schlink BR, Hairston WD, Konig P, Ferris DP. A channel rejection method for attenuating motion-related artifacts in EEG recordings during walking and running. Front Neurosci. 2017a;11:225.

Oliveira AS, Schlink BR, Hairston WD, Konig P, Ferris DP. Restricted vision increases sensorimotor cortex involvement in human walking. J Neurophysiol. 2017b;118(4):1943–1951. (Won 2nd place in Brain Products MOBI Prize, https://www.mobi-award.com/)

Peterson SM, Ferris DP. Combined head phantom and neural mass model validation of effective connectivity measures. J Neural Eng. 2018a;16(2):026010.

Peterson SM, Ferris DP. Differentiation in theta and beta electrocortical activity between visual and physical perturbations to walking and standing balance. eNeuro, 2018b;5(4).

Peterson SM, Ferris DP. Group-level cortical and muscular connectivity during perturbations to walking and standing balance. NeuroImage. 2019;198:93–103.

Peterson SM, Furuichi E, Ferris DP. Effects of virtual reality high heights exposure during beam-walking on physiological stress and cognitive loading. PloS One. 2018a;13(7):e0200306.

Peterson SM, Rios E, Ferris DP. Transient visual perturbations boost short-term balance learning in virtual reality by modulating electrocortical activity. J Neurophysiol. 2018b;120(4):1998–2010.

Richer N, Downey RJ, Nordin AD, Hairston WD, Ferris DP. Adding neck muscle activity to a head phantom device to validate mobile EEG muscle and motion artifact removal. 2019 9th International IEEE/EMBS Conference on Neural Engineering (NER); 2019 Mar. IEEE. p. 275–278.

Richer N, Downey RJ, Hairston WD, Ferris DP, Nordin AD. Motion and muscle artifact removal validation using an electrical head phantom, robotic motion platform, and dual layer mobile EEG. IEEE Trans Neural Syst Rehabilit Eng. 2020;28(8):1825–1835.

Schlink BR, Ferris DP. A lower limb phantom for simulation and assessment of electromyography technology. IEEE Trans Neural Syst Rehabil Eng. 2019;27(12):2378–2385.

Schlink BR, Nordin AD, Ferris DP. Comparison of signal processing methods for reducing motion artifacts in high-density electromyography during human locomotion. IEEE Open J Eng Medicine Biol. 2020a;1:156–165.

Schlink BR, Nordin AD, Ferris DP. Human myoelectric spatial patterns differ among lower limb muscles and locomotion speeds. Physiological Rep. 2020b:8(23):e14652

Symeonidou ER, Nordin AD, Hairston WD, Ferris DP. Effects of cables sway, electrode surface area, and electrode mass on EEG signal quality during motion. Sensors. 2018;18(4):1073.

Schlink BR, Peterson SM, Hairston WD, Konig P, Ferris DP. Independent component analysis and source localization on mobile EEG data can identify increased levels of acute stress. Front Hum Neurosci. 2017;11:310.

Snyder KL, Kline JE, Huang HJ, Ferris DP. Independent component analysis of gait-related movement artifact recorded using EEG electrodes during treadmill walking. Front Human Neurosci. 2015;9:639.

Voloshina AS, Ferris DP. Biomechanics and energetics of running on uneven terrain. J Exper Biol. 2015;218:711-9.

Voloshina AS, Ferris DP. Design and validation of an instrumented uneven terrain treadmill. J Applied Biomech. 2019;34(3):236–239.

Voloshina A, Kuo AD, Daley MA, Ferris DP. Biomechanics and energetics of walking on uneven terrain. J Exper Biol. 2013;216:3963–3970.

6. University of California, San Diego

The CaN CTA consortium founding member UCSD has performed a large volume of research projects covering diverse topics addressing scientific barriers, and has produced tools that have been used by the alliance and the global research community. In the interest of brevity, two of their research projects are highlighted in this section based on compilation of research plan objectives and progress reports.

6.1 Advanced Computational Approaches: Neurocomputation

The activity supported to overcome barriers was the following:

- Discovery of models and novel methods for the identification and interpretation of statistical relationships among high-dimensional data sets characterizing the dynamics of environment, behavior, and brain function during complex task performance.

6.1.1 First-Year Objectives

The primary goal of the first two years was to develop algorithms that can extract information-bearing constellations of cortical activity patches from noisy mobile brain/body imaging (MoBI) data that is robust to a lack of idealized models and sensor calibrations. We wanted the ability to further process these patterns of activity into features that are informative for discerning and prediction human cognitive performance across subjects and tasks in complex environments. Years 1 and 2 were focused on the development and testing of such algorithms, and toolboxes that allow the algorithms to be tested in a variety of real-world settings. In subsequent years, these algorithms were applied in the laboratory and in the field and used to develop theories of human cognitive performance in extreme situations.

6.1.2 First-Year Accomplishments

Measure Projection. In Year 1 of the CaN CTA, we enhanced the Measure Projection method and implemented its core features in a toolbox as an open-source plugin for EEGLAB. Measure Projection Toolbox (MPT) is currently in beta version and available for download at http://sccn.ucsd.edu/wiki/MPT.

Exploiting Anatomical Priors. We have developed an automated framework for the use of human subject-specific anatomical priors as part of (real-time) predictive models. The current implementation relies on ICA to obtain biologically distinct signal components from EEG measurements (Palmer et al. 2008), the use of DIPFIT software (Delorme and Oostenveld 2019) to obtain each derived signal

component's equivalent dipole coordinates in a standardized brain space, as well as on an anatomical structure atlas to derive the probability of a component being localized in some anatomical brain structure. Support for both Talairach (Lancaster et al. 2000) and LONI LBPA40 brain atlases has been implemented and integrated with BCILAB.

Enhancement of the Neuroelectromagnetic Forward Head Modeling Toolbox (NFT). NFT is a toolbox running under MATLAB for generating realistic head models and computing numerical solutions for the forward problem of EEG source imaging. NFT runs either as a plugin to EEGLAB or as a standalone toolbox and includes electrical modeling of human head, segmentation, mesh generation, and electrode co-registration, and warping of a template head model (MNI head model), forward problem solution using boundary element method (BEM). The first version was released in 2009 (Acar and Makeig 2010). In Year 1 of the project, we released version 2.0 of the NFT toolbox in which enhancements have been added, which will be useful for facilitating the use of subject-specific anatomical priors in the development of source location algorithms. Among others, extensions of the inverse estimation method by Zhilin Zhang (Zhang and Rao 2011) and Cheng Chao (publication planned), respectively, were added in Year 2.

BCI in the Spectral Domain. We have developed a natural extension of a current state-of-the-art framework for EEG-based BCI (Tomioka and Mueller 2010) into the spectral domain (Spectral Dual-Augmented Lagrangian method [Spec-DAL]; paper in revision), using spatial filters learned via ICA (while the approach generalizes to beamforming, as well) and per-component derived discrete Fourier-transform (DFT) features (also applicable to wavelet features). We have successfully applied a further refined lineage of the method under other funding on a workload task (Kothe and Makeig 2011).

Mixture-of-Learner ICA. Using Spec-DAL as a building block, we have demonstrated a construction in which any ICA-based learner with support for weighted data can be used as a mixture of learners in a multiple-mixture ICA model (AMICA), allowing it to capture a richer structure in the data (Makeig et al. 2012a, 2012b). The idea is to simultaneously use multiple alternative decompositions that explain different aspects of the recorded data. This approach has been tested successfully on a workload task under other funding (Kothe and Makeig 2011), and more recently, also on the attention-shifting data of the dynamic attention-shifting (DAS) project.

Regularized Spatio-Spectral Dynamics (RSSD)-based ICA. In follow-up research to Spec-DAL, we have developed a generalized linear model capturing the joint spatial, spectral, and temporal structure of IC-decomposed EEG signals

(RSSD). The key component, which allows one to capture the spatio-spectral dynamics of the data in full extent while avoiding severe model overfitting, is a structured sparse matrix norm, which has become efficiently implementable with recent advances in convex optimization (in particular dual-augmented Lagrangian methods and related proximal/accelerated-gradient methods [Tomioka et al. 2011]). Separately from the captured structure and employed regularization, the method has been designed from the outset with support for rich anatomical, spectral, and temporal priors, using the anatomical-priors framework. The method has been implemented as a component in BCILAB and supports its parallel computation infrastructure to scale to compute clusters. The implementation is available to collaborators.

Other. Dr Jason Palmer released a new version of his AMICA algorithm software for computing multiple ICA models with the possibility of shared components. The integration of the parallel AMICA solver into BCILAB and the related cluster management, as well as testing, have been done as part of neurocomputation (NCP) research. Tim Mullen released his Source Information Flow Toolbox (SIFT) toolbox for source-level information flow network analysis of EEG data.

Combining Soldier, Task, and Environmental Event data in Unstructured Environments. A critical bottleneck to the development of effective data-driven human cognitive state identification and prediction algorithms is the practical problem of not having enough data collection trials for every possible fixed experimental condition. This indicates the need for a method to simultaneously detect and associate statistically relevant variables and simultaneously occurring, nonorthogonal experimental conditions with many possible cognitive factors and event types so they can be further analyzed by various computational approaches being developed under ACA.

To address this challenge, in Year 1, we have initiated exploration of a promising approach, based on the "representational similarity analysis (RSA)" statistical method introduced in Kriegeskorte et al. (2008).

6.1.3 NCP Third-Year Objectives

In Year 3, we investigated ways to improve BCI performance by using priors obtain from measure projection of other subject classifiers: we explored multiple ways in which information from other subjects, associated with their ICs and dipoles, can be exploited to increase the performance and robustness of BCI classification on new subjects. This was a joint project between BCILAB and MPT developers. We utilized data from the MBF1 task for this investigation.

A major focus in the second half of Year 3 was multimodal inference methods as the data necessary for analysis became available. This includes hierarchical Bayesian methods, as well as extensions of the dictionary learning and other unsupervised learning frameworks (such as various types of auto-encoders).

In Year 3, we began to investigate the use of graph-theoretic tools to attempt to discover features associated with the directed graphs provided by the SIFT toolbox that are (ideally) invariant to or, at least, robust to variations in calibration, subject, environment, and so on. This task was originally planned for Year 2 but was deferred due to delays in the availability of robust real-time connectivity estimates.

In Year 3, we carried out qualitative assessments of different variants of the independent component sparse decomposition (ICSD) algorithm by feeding existing BCI algorithms with the component activations recovered by ICSD. A goal here was to improve the classification performance of the whole RSSD pipeline, which handles the derivation of component activations from multi-model AMICA decomposition with a relatively simple approach compared to the ICSD algorithms. Of particular interest was data where AMICA model changes play a crucial role, in which case we hoped ICSD would capture those model (component) changes. On the theoretical side, we integrated model likelihoods into the ICSD framework and performed component selection using this prior information.

6.1.4 Third-Year Accomplishments

In Year 3, we developed methods, software tools, file formats, and schemas to analyze currently recorded CTA data and in preparation for the analysis of data to soon be produced by the LSIE:

- *HED tags* and associated MATLAB and Java tools have been developed to enable describing events and paradigms using combination of user-friendly tags. A compatible Java user interface and associated set of MATLAB tools have been developed by Dr Kay Robbins and her group at UTSA to facilitate associating event codes with HED tags. (Nima Bigdely-Shamlo, Kay Robins, Christian Kothe, and Jessica Hsi)

  A first demonstration of the use of HED-tagged EEG data mining to retrieve similarities between brain source-level, event-related EEG responses in different task paradigms has been offered by Mr Bigdely-Shamlo (Makeig and Bigdely-Shamlo).

- The *EEG Study Schema (ESS)* was developed to encapsulate study-level (metadata) information (e.g., subject-group associations, event descriptions,

subject-file associations, and so on) in a standard manner. (Nima Bigdely-Shamlo and Jessica Hsi)

- Several robust ICA preprocessing (artifact cleaning) methods were designed and their performance compared to each other and to data hand-cleaning (12 methods compared on 51 data sets from two studies). In at least 95% of cases, one of the automatic methods outperformed hand-cleaning (robust estimation of the amount of mutual information removed from the channel data by ICA decomposition). (Christian Kothe and Nima Bigdely-Shamlo)
- An internally robust Infomax-ICA calculation method ("Robust Extica") using the geometric median was implemented and its performance evaluated on more than 20 data sets. Remarkably, the method can often produce high-quality ICA decompositions even without any artifact data cleaning. (Christian Kothe and Nima Bigdely-Shamlo)
- A robust method for calculating EEG dynamic measures such as ERP and event-related spectrum perturbation (ERSP) from outlier-contaminated trials was developed and performance of these methods investigated. These geometric median-based methods automatically down-weight outlier trials and produce virtually identical results even when, for example, 10% of the trials are replaced by outlier (noise) trials with 100× the amplitude of the true trial signals. (Nima Bigdely-Shamlo and Christian Kothe)
- Multiple regression algorithms based on a 2011 UCSD PhD dissertation by Matthew Smith were implemented for separating event-locked EEG dynamics in dense experimental paradigms in which there is a significant temporal overlap among event responses. Our initial results using L2 regression suggest that more variance in the data can be explained by regression-based ERPs compared to average-based ERPs. A paper on this method and results was submitted to the IEEE Engineering in Medicine and Biology Conference (EMBC) in June 2013. (Nima Bigdely-Shamlo and Mathew Burns)
- Multi-subject inference using measure projection analysis (for ERP, ERSP, inter-trial coherence (ITC), and mean power spectral measures) and network projection analysis (for pairwise network connectivity features calculated in SIFT and similar software tools) were devised and implemented to enable investigation of commonalities as well as individual differences in EEG dynamics associated with different experimental conditions. A paper on the measure projection approach was published in *NeuroImage*. (Nima Bigdely-Shamlo)

- An automatic eye IC detector based solely on scalp map information was created. This uses an algorithm similar to the semi-automated CORRMAP method but does not require user involvement. Instead, EyeCatch uses a database of 3400+ exemplar eye scalp maps learned by analyzing over half-a million IC scalp maps drawn from all the EEG data sets on Swartz Center for Computational Neuroscience (SCCN) servers. The performance of the method is comparable to CORRMAP. A paper on this algorithm was submitted to the 2013 IEEE EMBC conference. (Nima Bigdely-Shamlo)
- A method for joint EEG/body motion capture analysis using N-way partial least squares was developed. The method is a generalization of PCA to multiple dimensions. It allows finding latent factors in EEG spectral perturbations correlated with kinematic profiles obtained by motion capture. The method has been applied successfully in finding common patterns of movement and brain dynamics involved in the expression of musical feelings. The results of this work were submitted in an abstract to Society for Music Perception and Cognition Conference (SMPC) 2013. (Alejandro Ojeda)
- A method for EEG source localization in real time was developed and demonstrated. The method estimates the current source density constrained to the cortical surface, spatial smoothness among neighboring patches of cortex, is used as prior constrain. It uses maximum a posteriori (MAP) updating rules for hyperparameters controlling the amount of regularization needed at each time point. The method was used in a pipeline for online information flow analysis and visualization. The results of this work were submitted to the International BCI Meeting, June 2013. An extension of this work is being submitted to the IEEE EMBC 2013. (Alejandro Ojeda, Christian Kothe, and Tim Mullen)
- A new online motion artifact correction method for EEG (first demonstrated live at the IEEE EMBC meeting in 2012 using dry/wireless headsets from MINDO and Cogionics) has been further developed. Also, real-time Granger-causal connectivity estimation using SIFT and BCILAB has been demonstrated at the 2013 BMBI satellite workshop, also using dry/wireless EEG hardware. (Christian Kothe)
- A wavelet-based method for robust ERP estimation has been implemented. This method is a further improvement of the work of Quiroga and Garcia (2003), which is an elegant adaptive filter technique suitable for application to epoched data at the single trial level. (Alejandro Ojeda)

- Two methods for performing ICSD have been developed. One method uses a robust version of multi-step sparse Bayesian learning; the other performs a large number of mutual information reduction calculations to choose between alternative sparse patterns. In ICSD, first a dictionary of IC scalp maps is constructed by concatenating scalp maps from different models learned by multi-model ICA (AMICA). Then a sparse subset of these ICs (with a scarcity level equal to the rank of the recorded EEG data) is selected for each approximately 4-s (overlapping) window. Our simulations show that the resulting decomposition can capture the true dynamic scarcity pattern with low error rate at various noise levels. (Nima Bigdely-Shamlo and Ozgur Balkan)

6.2 Neurocognitive Performance: Large-Scale Experiment (LSE)

Activities supported to overcome barriers include the following:

- Development of experimental paradigms that capture the unfolding nature of multisensory stimulus streams experienced in real-world environments
- Development and employment of novel, wearable sensor suites for monitoring brain and body dynamics during naturalistic behavior, as well as software systems to enable integrated monitoring capabilities
- Acquisition and processing of high-dimensional data sets that characterize physical, mental, and physiological behavior, as well as its environmental context, in sufficient detail and across a sufficient breadth of circumstances

6.2.1 Research Goals

The goal was to develop a two-subject, high-information, crewstation-like experimental apparatus in the Command Environment Simulator (CES) at UCSD and collect high-dimensional data that characterize physical, mental, and physiological behavior, as well as its environmental context. The LSE experiment was used to acquire a rich set of neurophysiological and behavioral data from subjects performing two-person team and individual tasks in high-information, multitasking environments. The LSE team's goal in the experiment design was to establish a paradigm that would test the viability of multiple cognitive state assessment (CSA) factors in realistic multisensory input, multitasking environment. The CSA factors of interest were in monitoring of alertness and attention shifts in target stimulus recognition, stimulus stream comprehension, multiscale spatial situational awareness, decision-making and self-error detection, and teammate comprehension.

6.2.2 Third-Year Accomplishments

As of the end of Year 3, the LSE team had completed the development of the experiment apparatus and the experiment design, had conducted pilot tests, and was training subjects for data collection. The experiment apparatus involved programming of a new simulation game within the SCCN Experimental Recording, Interactive Control and Analysis (ERICA) framework to run on the CES multi-screen crewstation environment. This simulation game, the Small Team Reconnaissance and Urban Surveillance Missions (STRUM), was developed with features to exercise the operator's multi-screen and multimodal attention shifts, vigilance, sensorimotor decision-making, navigational reference frame switching, text and audio comprehension, and inter-subject communication, all within the context of 3-D VR multiple robotic vehicle operation (both ground and air). During Year 3, the team has utilized the pilot testing, analysis, as well as feedback from subjects and researchers to refine, debug, and validate the STRUM simulation game and the DAQ system.

Figure 6.1 shows a summary of the STRUM game design.



Fig. 6.1 STRUM apparatus

Participants are told that in this game they are a member of a two-person reconnaissance and surveillance team stationed at a central command post in a coastal city. Each team member must navigate a robotic surveillance vehicle through the city in order to accomplish a series of primary missions, often in parallel

with one or more side tasks. Three to five primary missions, each lasting between 8–15 min, are combined within a single game "block" lasting approximately 45 min. Blocks are separated by "rest" periods during which participants are instructed to sit quietly and simply monitor their consoles so as to respond when needed to Danger/Alert signals. Total game time is 3 h (four game blocks). The different types of tasks are described here.

Primary Mission

Primary missions require constant attention and continuous user input/ performance; in addition, some missions are cooperative in that partners must coordinate their actions to complete mission tasks:

1) **Checkpoints Mission:** Players must navigate their robot vehicle through the city streets to reach checkpoints. Both players have access to a satellite map that shows the location of the current checkpoint. In the cooperative version, players must communicate with their partner in order to keep their robots close together while traveling; in the individual version, one player navigates through the city while the other performs side tasks only.

2) **Perimeter Defense:** Players defend a command post from close inspection by drones. Players navigate a limited area around the command post and "warn off" the drones by pushing a button on the video game controller to activate an alarm. Both players have access to a satellite map that shows drone locations. Player coordination is needed to ensure maximum coverage and prevent repeat warnings to the same drone (which incurs a penalty).

3) **Aerial Guidance:** In this cooperative mission, one player operates an aerial robot, relaying directions to their grounded partner below as that player navigates the city looking for checkpoints. Information about checkpoint locations is only available to the player controlling the aerial robot.

4) **Panning Surveillance:** In this individual mission, the player's robot remains in a fixed location. This player detects incoming alien drones by panning the 360° environment, then warning them off by sounding an alarm. The other player performs side tasks only.

Side Tasks

Participants' ability to divide/distribute attention across multiple stimulus streams will be gauged by the periodic addition of one or more side tasks concurrent with the primary task. Along with distributed attention, these side tasks increase working memory load (visual, auditory, spatial, and verbal) and assess speech comprehension:

1) ***Curbside Objects:*** Various objects are positioned near the street in the central Primary Mission screen (e.g., trash can, suitcase, and so on). Periodically, players are queried (via the text box on the Primary Mission screen) about the location of the object after it has disappeared from the display. Players respond by touching the "left", "center", "right", or "skip" buttons.

2) ***Satellite Map Icons:*** Different icons are displayed, one at a time, on the satellite map shown on the right touch screen. Periodically, players are queried (the relevant response buttons beneath the satellite map will flash red to indicate a response is needed) about the icon's direction (NSEW) in respect to their robot, or icon color (red, green, blue, yellow). Players may indicate uncertainty by choosing "skip" (earning a smaller point penalty than a miss).

3) ***Symbolic Sounds:*** Players listen for several types of environmental sounds presented in a left front, left rear, center front, right front, or right rear auditory location. Periodically, players are queried (via an appropriate auditory cue) about the location of the most recent sound. Players may again indicate uncertainty by choosing "skip".

4) ***Spoken Sentences:*** Periodically, players are asked (via another spoken sentence beginning with their code name, "Delta" or "Echo", respectively) a yes/no comprehension question about the most recently presented sentence. Players respond by touching either the "yes", "no", or "skip" button.

5) ***Written Sentences:*** Players read written sentences displayed in a text box on the left touch screen, attending to the sentences beginning with their code name. Periodically, players are asked (via a written sentence beginning with their code name) a yes/no comprehension question about the most recently presented sentence. Players respond by touching the "yes", "no", or "skip" button.

Alerting Task

This task, meant to monitor vigilance, requires only that participants respond to the illumination of a large red warning screen "button" by touching the button as quickly as possible. Players are informed that the warning light may be illuminated at any time during the game, including during the rest periods.

Rest Periods

Rather than operate using discrete (recorded) task blocks separated by (not recorded) rest periods, the high-demand task blocks in STRUM game are interrupted by low-demand (near-rest) periods. During these "rest" periods, players are permitted to stretch their arms and legs within a restricted range (so as not to dislodge the recording equipment), but are instructed to continue to monitor and respond as needed to the warning light.

6.2.3 LSE Year 4

In Year 4, data was collected from 38 participants in the STRUM experiment. Structural brain imaging data (T1, T2, and diffuse tensor imaging [DTI] structural magnetic resonance) have been collected from 16 of these participants. Individual electrical finite-element method (FEM) forward head models for these subjects are under construction.

SCCN collected 17 sessions (on 34 participants) with dual EEG, eye gaze, and ground force tracking. In an additional 12 sessions (24 participants), for technical reasons, eye tracking was performed only on one of the participants. In an additional five sessions (10 participants), eye-tracking data was available for neither participant. A further three sessions (six participants) gave data that was not acceptable for various technical reasons. This gives a total of 37 sessions recorded from 74 participants.

6.3 STRUM Data Analysis (UCSD)

Beginning Year 5 (PY5), consortium members started collaborative research in exploring the rich data that was acquired in the STRUM experiments (described in Section 2.4.2). This section summarizes some of the analysis and exploration conducted at UCSD.

6.3.1 ACA LSIE EEG-Focused Analysis (LSIE-EEG)

During PY5 of the project, we have curated the LSIE STRUM data set previously collected under the LSE project (PY4) and defined five cognitive variables based on event markers present in the data sets ("response errors", "target perception", "attention focus", "alertness", and "task load" as defined in the Annual Program Plan [APP]), including some with several subtypes (such as perception of different kinds of stimuli and discretized and continuous subject performance measures). We have then implemented data analysis scripts for a large-scale batch analysis covering all cognitive variables and a total of 20 methods plus infrastructure for running these analyses efficiently on a cluster. The data set, curation scripts, and

data analysis scripts have been shared with any interested parties within the CaN CTA (DCS, Columbia, Syntrogi) for use in the other projects.

Throughout the first half of the program year, we have completed the batch analyses proposed under Tasks 1 and 3, namely, a within-subject 5x cross-validation for each subject and cognitive variable, using all originally proposed methods for these respective variables, with the exception of Disciplined Cross-Spectral Regression (which we found to be prohibitively slow to compute). Two mid-course adjustments were to replace the multi-window Common Spatio-Spectral Patterns (mwCSSP; Lemm et al. 2005) method with the multi-window Filter-Bank Common Spatial Patterns (mwFBCSP; Ang et al. 2008) method, which we have found to perform better, and second, to replace an originally planned gaze-dependent visual spatial attention variable with a newly introduced task load variable since only 35 subjects had a working eye tracker and preprocessing these data to the required quality level proved to be challenging.

We have computed AUC/standardized mean square error (SMSE) performance measures, performed statistical tests to compare method performances in line with the project plan, and performed a first triage of the (many) results. All result files have also been transferred to DCS. The outcomes of computations from Tasks 1 and 3 have been assessed and were reported at the PY5 all-hands meeting and midpoint review meeting. Among others, it was found that response errors could be predicted at rather good accuracies (AUC = 0.79) across all side tasks, which was rather unexpected due to the complexity and variability of errors across all these tasks. Other cognitive variables, such as the alertness variable, were found to be harder to predict accurately using the chosen methods (with AUCs around 0.6). In the case of the "target perception" cognitive variable specifically, we observed a strong dependence between achievable accuracy and stimulus type for reasons yet to be investigated.

Following the completion of these tasks, we have implemented and ramped up the data analysis for Tasks 2 and 4, in which cross-subject transfer learning methods were applied to the LSIE STRUM corpus for subsequent continuation by Syntrogi after Mr Kothe had transitioned to that institution.

Based on the Task 1 and 3 results, we have performed a number of in-depth follow-up analyses of some of the cognitive variables (Task 6) in order to find fruitful directions for further study in PY6 research and beyond; notably, we have found on a preliminary subset of the data that it was possible to predict response errors ahead of time at above-chance accuracy based on cortical idle oscillations preceding the response. These early results became the basis for the PY6 direction of the project.

6.3.2 ACA Integrating Multi-Aspect Information (IMAI)

Tasks 1 and 2: In PY5, we curated the LSIE STRUM data set for analysis with multimodal fusion methods, with a focus on EEG and EMG, gaze parameters, and motion capture parameters, and preprocessed the data of all 35 subjects who had all measures. We worked closely with the Columbia team in the areas of preprocessing and cognitive variable definition, and exchanged marker extraction and data cleaning scripts. We investigated the various cognitive variables that have previously been studied in the LSIE-EEG project with respect to their potential use in a multimodal fusion context. For this, we tested a number of simple baseline methods on all five cognitive variables to identify promising areas for further research.

Task 3.1: We investigated commission of user errors across all experimental side tasks in response to potentially misperceived target stimuli as the most promising first direction, and implemented a three-level HDCA-based multimodal fusion approach that integrates information from both EEG and gaze parameters (including gaze coordinates and pupil parameters) relative to the stimulus presentation. Using this HDCA method, we found that incorrect responses can be predicted ahead of time at above-chance level when fusing EEG and gaze parameters, and that the fusion using this method yields a (modest but significant) empirical performance advantage over the EEG-only model measures across all subjects in the corpus (29 subjects analyzed, 6 with bad/missing data not included). Other methods in the generalized linear model (GLZ) framework were also tested, including logistic regression with various types of sparsity, but were found to be less performant.

Toward the end of PY5, we have begun work on a paper with the Columbia team and Syntrogi, which has independently analyzed a related scientific question, although a somewhat different cognitive variable and subset of side tasks. We have also exchanged analysis approaches with DCS with the intent of transferring some analyses between the ODE data set and the STRUM data set.

Generation of 4-layer head models and high-resolution source space: At the UCSD fMRI center, we acquired whole-head T1-weighted MR images with 1-mm^3 voxel resolution for 15 of the LSIE STRUM subjects using a 3-T GE MRI system. For these subjects, we generated four-layer realistic head tissue models via the NFT toolbox (Acar 2010) that models scalp, skull, CSF, and brain tissues. We generated both BEM and FEM head models. We also generated high-resolution cortical surface source spaces containing 80,000 sources for each subject using Freesurfer (Dale et al. 1999). The median surface area of the face of the elements on the source space mesh was 0.8 mm^2. The tissue surface and cortical source space meshes for

one subject, as well as the locations of the 128 scalp electrodes, are shown in Fig. 6.2.

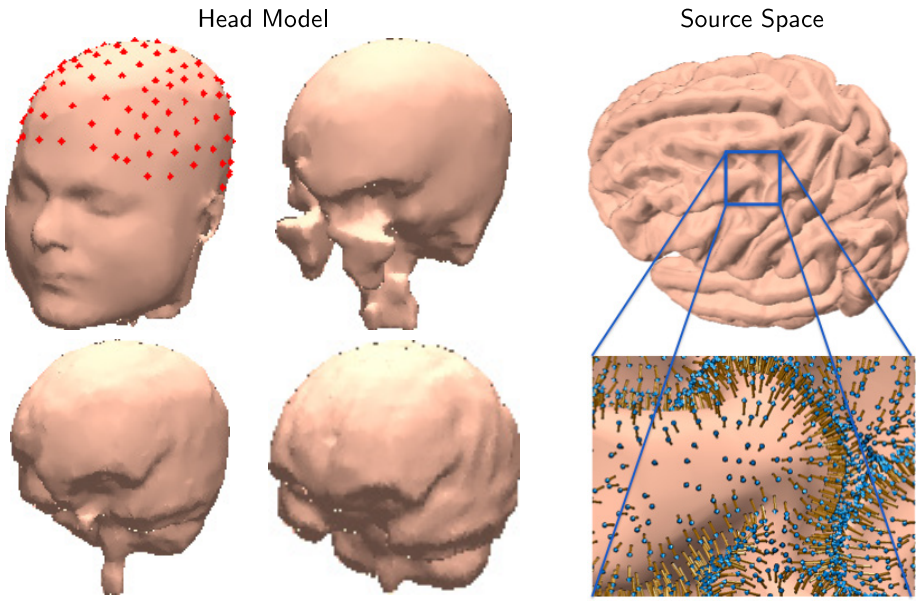


Fig. 6.2 IMAI source space modeling. (Left) Scalp, skull, CSF, and brain surfaces for one subject including the measured 128 scalp electrode locations. (Right) High-resolution Freesurfer cortical source space for the same subject.

6.4 References

Acar ZA, Makeig S. Neuroelectromagnetic forward head modeling toolbox. J Neurosci Meth. 2010;190:258–270.

Ang KK, Chin ZY, Zhang H, Guan C. Filter Bank Common Spatial Pattern (FBCSP) in brain-computer interface. 2008 IEEE International Joint Conference on Neural Networks (IEEE World Congress on Computational Intelligence); 2008. pp. 2390–2397. doi: 10.1109/IJCNN.2008.4634130.

Bigdely-Shamlo N. EyeCatch: Data-mining over half a million EEG independent components to construct a fully-automated eye-component detector. EMBC. 2013.

Bigdely-Shamlo N, Mullen T, Kothe C, Su K-M, Robbins K. The PREP pipeline: standardized preprocessing for large-scale EEG analysis. Frontiers Neuroinformatics. 2015. https://doi.org/10.3389/fninf.2015.00016

Bigdely-Shamlo N, Mullen T, Kreutz-Delgado K, Makeig S. Measure projection analysis: a probabilistic approach to EEG source comparison and multi-subject analysis. NeuroImage. 2013;72:287–303.

Chang H-Y, Stevenson CE, Jung T-P, Ko L-W. Stress-induced effects in resting EEG spectra predict the performance of SSVEP-based BCI. IEEE Trans Neural Syst Rehab Eng. 2020;28(8):1771–80.

Chen SA, Lin FC, Shen TK, Ko LW, Jung TP, Lin CT. An EEG-based self-constructed neural fuzzy system to estimate driver's cognitive state. Australian J Intellig Information Process Syst. 2010;11(3).

Chen X, Wang Y, Gao S, Jung T-P, Gao X. Filter bank canonical correlation analysis for implementing a high-speed SSVEP-based brain-computer interface. J Neural Eng. 2015;12:046008. https://doi.org/10.1088/1741-2560/12/4/046008.

Chi YM, Jung T-P, Cauwenberghs G. Dry-contact and noncontact biopotential electrodes. IEEE Rev Biomed Eng. 2010, 3, 106–119.

Chi YM, Wang Y-T, Wang Y, Jung T-P, Cauwenberghs G. Dry and non-contact EEG sensors for mobile brain-computer interfaces. IEEE Trans Neural System and Rehabilit Eng. 2012;20(2):28–235.

Chien YY, Lin FC, Zao JK, Chou CC, Huang YP, Kuo HY, Wang Y, Jung T-P, Shieh HP. Polychromatic SSVEP stimuli with subtle flickering adapted to brain-display interactions. J Neural Eng. 2017;14(1):016018.

Chiu T-C, Gramann K, Ko L-W, Duann J-R, Jung T-P, Lin C-T. Alpha modulation in parietal and retrosplenial cortex correlates with navigation performance. Psychophysiology. 2012;1:43–55.

Chuang C-H, Lin Y-P, Ko L-W, Jung T-P, Lin C-T. Independent component ensemble of EEG for brain-computer interface. IEEE Trans Neural Syst Rehabil Eng. 2014;22(2):230–8. https://doi.org/10.1109/TNSRE.2013.2293139.

Chuang S-W, Ko L-W, Lin Y-P, Huang R-S, Jung T-P, Lin C-T. Co-modulatory spectral changes in independent brain processes are correlated with task performance. NeuroImage. 2012;62(3):1469–1477.

Dale AM, Fischl B, Sereno MI. Cortical surface-based analysis: 1. segmentation and surface reconstruction. NeuroImage. 1999;9:179–194.

Delorme A, Miyakoshi M, Jung T-P, Makeig S. Grand average ERP-image and statistics: A method for comparing variability in event-related single-trial EEG activities across subjects and conditions. J Neurosci Meth. 2014. https://doi.org/10.1016/j.jneumeth.2014.10.003.

Delorme A, Mullen T, Kothe C, Zeynap AA, Bigdely-Shamlo N, Vankov A, Makeig S. EEGLAB, SIFT, NFT, BCILAB, and ERICA: new tools for advanced EEG processing. Comput Intell Neurosci. 2011;10:130714.

Delorme A, Oostenveld R. DIPFIT. GitHub; 2019 Sep 10 [accessed 2021 July]. https://github.com/sccn/dipfit.

Doty TJ, Kellihan B, Jung T-P, Zao JK, Litvan I. The wearable multimodal monitoring system: a platform to study falls and near-falls in the real-world. 2015.

Gramann K, Ferris DP, Gwin J, Makeig S. Imaging natural cognition in action. Int J Psychophysiol. 2014;91(1), 22–9.

Gramann K, Gwin JT, Ferris DP, Oie K, Jung T-P, Lin C-T, Liao L-D, Makeig S. Cognition in action: imaging brain/body dynamics in mobile humans. rev Neurosci. 2011;22(6):593–608.

Gramann K, Jung TP, Ferris DP, Lin CT, Makeig S. Toward a new cognitive neuroscience: modeling natural brain dynamics. Front Hum Neurosci. 2014;8(444).

Gramann K, Shang W, Jung T-P, Viirre E, Riecke BE. Switching spatial reference frames for yaw and pitch navigation. Spatial Cognition and Computation: An Interdisciplinary Journal. 2001 Jan;(2-3).

Gu X, Cao Z, Jolfaei A, Xu P, Wu D, Jung T-P, Lin C-T. EEG-based brain-computer interfaces (BCIs): a survey of recent studies on signal sensing technologies and computational intelligence approaches and their applications. n.d.

Hajinoroozi M, Mao Z, Jung T-P, Lin C-T, Huang Y. EEG-based prediction of driver's cognitive performance by deep convolutional neural network. Signal Processing: Image Communication. 2016;47:549–55.

Hsu S-H, Jung T-P. Monitoring alert and drowsy states by modeling EEG source nonstationarity. J Neural Eng. 2017;14(5).

Huang KC, Huang T-Y, Chuang C-H, King J-T, Wang Y-K, Lin C-T, Jung T-P. An EEG-based fatigue prediction and mitigation system. International J Neural Syst. 2016.

Huang Y-K, Jung T-P, Lin C-T. Theta and alpha oscillations in attentional interaction during distracted driving. Front Behav Neurosci. In press. https://doi.org/10.3389/fnbeh.2018.00003.

Ide JS, Shenoy P, Yu AJ, R L-C-S. Bayesian prediction and evaluation in the anterior cingulate cortex. J Neurosci. 2013;33(5):2039–2047.

Jeng PY, Wei CS, Jung TP, Wang LC. Low-dimensional subject representation-based transfer learning in EEG decoding. IEEE J Biomed Health Informatics. 2020.

Ko L-W, Komarov O, Hairston WD, Jung T-P, Lin C-T. Sustained attention in real classroom settings: an EEG study. Front Hum Neurosci. ; 2017;11:article 388.

Ko L-W, Komarov O, Lai W-K, Liang W-G, Jung T-P. Eyeblink recognition improves fatigue prediction from single-channel forehead EEG in a realistic sustained attention task. J Neural Eng. 2020;17:036015. https://iopscience.iop.org/article/10.1088/1741-2552/ab909f/meta.

Komarov O, Ko L-W, Jung T-P. Associations among emotional state, sleep quality, and resting-state EEG spectra: a longitudinal study in graduate students. IEEE Trans Neural Syst Rehab Eng. 2020;28(4):795–804. https://doi.org/10.1109/TNSRE.2020.2972812.

Kothe CA, Makeig S. Estimation of task workload from EEG data: new and current tools and perspectives. Annu Int Conf IEEE Eng Med Biol Soc. 2011;2011:6547-51. doi: 10.1109/IEMBS.2011.6091615.

Kriegeskorte N, Mur M, Bandettini P. Representational similarity analysis - connecting the branches of systems neuroscience. Front Syst Neurosci. 2008 Nov 24;2:4. doi: 10.3389/neuro.06.004.2008.

Lancaster JL, Woldorff MG, Parsons LM, Liotti M, Freitas CS, Rainey L, Kochunov PV, Nickerson D, Mikiten SA, Fox PT. Automated Talairach atlas labels for functional brain mapping. Hum Brain Mapp. 2000 Jul;10(3):120-31. doi: 10.1002/1097-0193(200007)10:3<120::aid-hbm30>3.0.co;2-8.

Lemm S, Blankertz B, Curio G, Müller KR. Spatio-spectral filters for improving the classification of single trial EEG. IEEE Trans Biomed Eng. 2005 Sep;52(9):1541-8. doi: 10.1109/TBME.2005.851521.

Liao L-D, Lin C-T, McDowell K, Gramann K, Jung T-P, Ko L-W, Chang J-Y. Biosensor technologies for augmented brain–computer interfaces in the next decades. Proceedings of the IEEE. 2012;100:1553–1556.

Lin C-L, Shaw Z-Z, Young K-Y, L C-T, Jung T-P. EEG correlates of haptic feedback in a visuomotor tracking task. NeuroImage. n.d.

Lin C-T, Huang K-C, Chao C-F, Chen J-A, Chiu T-W, Ko L-W, Jung T-P. Tonic and phasic EEG and behavioral changes induced by arousing feedback. NeuroImage. 2010;52:633–42.

Lin C-T, Huang K-C, Chuang K, L-W, Jung T-P. Can arousing feedback rectify lapses in driving? : prediction from EEG power spectrum. J Neural Eng. 2013;10. https://doi.org/10.1088/1741-2560/10/5/056024.

Lin Y-P, Hsu S-H, Jung T-P. Exploring day-to-day variability in the relations between emotion and EEG signals. Foundations of augmented cognition; Springer; 2015a.

Lin Y-P, Hsu S-H, Jung T-P. Exploring day-to-day variability in the relations between emotion and EEG signals. In: Rouillard J. editor. Augmented cognition. 2015b.

Lin Y-P, Wang Y, Jung T-P. Assessing the feasibility of online SSVEP decoding in human walking using a consumer EEG headset. J NeuroEng Rehabil. 2014;11(119). https://doi.org/10.1186/1743-0003-11-119.

Lin Y-P, Wang Y, Wei C-S, Jung T-P. A Mobile Brain-computer interface for freely moving humans. In: Kurosu M, editor. Human-computer interaction. towards intelligent and implicit interaction, Lecture Notes in Computer Science. 2013;8008:448–453.

Lin Y-P, Wang Y, Wei C-S, Jung T-P. Assessing the quality of steady-state visual-evoked potentials for moving humans using a mobile electroencephalogram headset. Front Hum Neurosci. 2014. https://doi.org/10.3389/fnhum.2014.00182.

Makeig S, K CA, Mullen T, Bigdely-Shamlo N, Kreutz-Delgado K. Evolving signal processing for brain-computer interface design IEEE Centennial Celebration issue. 2012a.

Makeig S, K CA, Mullen T, Bigdely-Shamlo N, Kreutz-Delgado K. Evolving signal processing for brain-computer interface design. Proceedings of the IEEE. 2012b;100:1567–1584.

Molina E, Sanabria D, Jung T-P, Correa A. Electroencephalographic and peripheral temperature dynamics during a prolonged psychomotor vigilance task, Accident Analysis & Prevention. 2017;S0001–4575(17):30370–6. https://doi.org/10.1016/j.aap.2017.10.014.

Mullen T, Khalil A, Ward T, Iversen J, Leslie G, Warp R, Whitman M, Minces V, McCoy A, Ojeda A. MindMusic: playful and social installations at the

interface between music and the brain. More Playful User Interfaces. Springer; 2015.

Nakanisha M, Wang Y, Wang Y-T, Mitsukura Y, Jung T-P. A high-speed brain speller using steady-state visual evoked potentials. Int J Neural Syst. 2014a;24(6).

Nakanisha M, Wang Y, Wang Y-T, Mitsukura Y, Jung T-P. Generating Visual flickers for eliciting robust steady-state visual evoked potentials at flexible frequencies using monitor refresh rate. PLoS ONE. 2014b;11;9(6):e99235. https://doi.org/10.1371/journal.pone.0099235.

Nakanishi M, Wang Y, Chen X, Wang Y-T, Gao X, Jung T-P. Enhancing detection of SSVEPs for a high-speed brain speller using task-related component analysis. IEEE Trans Biomed Eng. 2018;65(1):104–112,.

Nakanishi M, Wang Y, Jung T-P. Spatial filtering techniques for improving template-based SSVEP detection. In: Mahnaz TTA, editor. Signal processing and machine learning for brain-machine interfaces. Institute for Engineering and Technology (IET); 2018.

Nakanishi M, Wang YT, Jung TP, Zao JK, Chien YY, Diniz-Filho A, Medeiros FA. Detecting glaucoma with a portable brain-computer interface for objective assessment of visual function loss. JAMA Ophthalmology. 2017;135(6):550–557.

Ojeda A, Bigdely-Shamlo N, Makeig S. MoBILAB: An open source toolbox for analysis and visualization of mobile brain/body imaging data. Front Hum Neurosci. 2014;8(121). https://doi.org/10.3389/fnhum.2014.00121.

Palmer JA, S. Makeig, K. Kreutz-Delgado, and B. D. Rao, Newton Method for the ICA Mixture Model, in Proceedings of the 33rd IEEE International Conference on Acoustics and Signal Processing (ICASSP 2008), Las Vegas, NV, pp. 1805-1808, 2008.

Shenoy P, Yu AJ. Rational decision-making in inhibitory control. Front Hum Neurosci. 2011;5(48). https://doi.org/10.3399/fnhum.2011.00048.

Szu H, Hsu C, Moon G, Yamakawa T, Tran BQ, Jung T-P, Landa J. Smartphone household wireless electroencephalogram hat. Appl Computational Intell Soft Comput. 2013;8. https://doi.org/10.1155/2013/241489.

Tomioka R, Suzuki T, Hayashi K, Kashima H. Statistical performance of convex tensor decomposition. In: Advances in Neural Information Processing Systems 24 (NIPS 2011); 2011. pp. 972–980.

Tomioka R, Müller KR. A regularized discriminative framework for EEG analysis with application to brain-computer interface. Neuroimage. 2010 Jan 1;49(1):415-32. doi: 10.1016/j.neuroimage.2009.07.045.

Tsai AC, Jung T-P, Chien V, Savostyanov AN, Makeig S. Cortical surface alignment in multi-subject spatiotemporal independent EEG source imaging. NeuroImage. 2014;87:297–310. https://doi.org/10.1016/j.neuroimage.2013.09.045.

Wang Y, Jung TP. Improving brain–computer interfaces using independent component analysis. Towards practical brain-computer interfaces. Springer; 2012. p. 67–83.

Wang Y, Jung T-P. A collaborative brain-computer interface for improving human performance. PLoS ONE. 2011;6(5):20422. https://doi.org/10.1371/journal.pone.0020422.

Wang YK, Jung TP, Lin CT. EEG-based attention tracking during distracted driving. IEEE Trans on Neural Syst Rehabil Eng. 2015.

Wang Y, Wang Y-T, Jung T-P. Translation of EEG spatial filters from resting to motor imagery using independent component analysis. PLoS ONE. n.d.;7(5):37665. https://doi.org/10.1371/journal.pone.0037665.

Wang Y, Wang Y-T, Jung T-P, Gao X, G S. A collaborative brain-computer interface. Proceedings of the 4th International Conference on Biomedical Engineering and Informatics; 2011. p. 583–6.

Wang Y-T, Huang K-C, Wei C-S, Huang T-Y, Ko L-W, Lin C-T, Cheng CK, Jung T-P. Developing an EEG based on-line closed-loop lapse detection and mitigation system. Front Neuroscie Neuroprosthetics. 2014;8(321). https://doi.org/10.3389/fnins.2014.00321.

Wang Y-T, Nakanishi M, Wang Y, Wei C-S, Cheng C-K, Jung T-P. An online brain-computer interface based on SSVEPs measured from non-hair-bearing areas. IEEE Trans Neural Syst Rehabil Eng. 2017;25(1):11–18.

Wang Y-T, Wang Y, Jung T-P. A cell-phone based brain-computer interface for communication in daily life. J Neural Eng. 2011;8(2).

Wei CS, Wang YT, Lin CT, Jung TP. Toward drowsiness detection using non-hair-bearing EEG-based brain-computer interfaces. IEEE Trans Neural Syst Rehabil Eng. 2018;26(2):400–406.

Wei C-S, Lin Y-P, Wang Y-T, Lin C-T, Jung T-P. Towards plug-and-play brain state decoding for drowsiness with large-scale data and baseline calibration. NeuroImage. 2018;174:407–419.

Wu D, King JT, Chuang CH, Lin CT, Jung TP. Spatial filtering for EEG-based regression problems in brain–computer interface (BCI. IEEE Trans Fuzzy Syst. 2017;26(2):771–781.

Wu D, Lance BJ, Lawhern VJ, Gordon S, Jung TP, Lin CT. EEG-based user reaction time estimation using Riemannian geometry features. IEEE Trans Neural Syst Rehabil Eng. 2017;25(11):2157–2168.

Xu M, Wang Y, Nakanishi M, Wang Y-T, Qi H, Jung T-P, Ming D. Fast detection of covert visuospatial attention using hybrid N2pc and SSVEP features. J Neural Eng. 2016;13(066003).

Zhang Z, Jung T-P, Makeig S, Rao BD. Compressed Sensing of EEG for Wireless Telemonitoring with low energy consumption and inexpensive hardware. IEEE Trans Biomed Eng. 2013;60(1):221–224.

Zhang Z, Jung T-P, Makeig S, Rao BD, Pi Z. Spatiotemporal sparse Bayesian learning with applications to compressed sensing of multichannel physiological signals. IEEE Trans Neural Syst Rehabil Eng. n.d.

Zhang Z, Rao BD. Sparse signal recovery with temporally correlated source vectors using sparse Bayesian learning. IEEE Journal of Selected Topics in Signal Processing. 2011 Sep;5(5):912–926. doi: 10.1109/JSTSP.2011.2159773.

7. National Chiao Tung University (with UCSD Collaboration)

The CaN CTA consortium founding members NCTU and UCSD have performed many research projects in tight collaboration. Two of their research projects are highlighted in this section with compilation of research plan objectives and progress reports.

7.1 Neurotechnologies: Effects of Vehicle Motion and Cognitive Fatigue (VMF)

Activity supported to overcome barriers included the following:

- Development of experimental paradigms that capture the unfolding nature of multisensory stimulus streams experienced in real-world environments.
- Discovery of models and novel methods for the identification and interpretation of statistical relationships among high-dimensional data sets characterizing the dynamics of environment, behavior, and brain function during complex task performance
- The acquisition and analysis of data from a large participant sample allowing characterization of inter- and intra-individual variation to systematically study relationships between individualized models derived for cognitive monitoring and for individual differences in performance, cognitive ability, and personality

7.1.1 VMF Year 1–2

VMF1: Drowsiness Assessment and Management (Y1-Y2).

We planned to use the lane-keeping driving experiments developed in our previous work (Huang et al. 2005, 2007) to develop and test a drowsiness assessment and management (DAM) system, based on the wearable and wireless dry-electrode (WWD) EEG system developed under Wearable EEG Development and Testing **(WDT)1**, for continuously and accurately estimating shifts in an individual's level of alertness, as indexed by changes in their level of task performance.

7.1.2 VMF Program Year 1 and 2 Accomplishments

In Year 1, we extended our previous work on developing an individualized alertness monitoring model to estimate the level of alertness, as indexed by changes in their level of task performance, to study inter-subject variability in the relationship between the EEG power spectrum and task performance. We recruited 10 right-handed, healthy volunteers (nine males, 18–28 years old) to participate the lane-

keeping driving experiments developed in our previous work (Huang et al. 2005, 2007). Each subject performed the experiment in the simulated realistic-driving environment. The four-lane road was separated by a median strip and the distance between the left and right sides of the road was equally divided into 250 points (digitized into values 0–250), where the width of each lane and the car was 60 and 32 units, respectively. The refresh rate of highway scene was set at 60 Hz, which can properly emulate a car driving at a fixed speed of 100 kph on the highway. All scenes were updated according to the displacement of the car and the subject's wheel handling. The car was randomly drifted away from the center of the cruising lane, which was controlled and triggered from the program, to mimic the consequences of a non-ideal road surface. The inter-deviation intervals were varied from 5 to 10 s and the car was deviated to either left or right side with the equal chance. This task required subjects to compensate the drifting by manipulating the steering to keep the car on the center of the third cruising lane (counted from left to right). EEG and behavioral data were simultaneously recorded during the experiments. Multi-channel EEG data were first decomposed into temporally independent brain processes using ICA. ICs were grouped based on similar scalp weight maps, dipole source locations, and power spectra across subjects.

Major Results

1) *Behavioral results*: Fluctuations in task performance. All subjects showed several periods of the fluctuated driving performances from small to large local driving errors (LDEs), sometime even abandoning control of the steering during the 100-min driving task. LDE values were distributed from 0 to 70 and the majority of the LDE values ranged between 0 and 30. Since only limited trials were with LDE values over 30 across 10 subjects, only trials with LDE values below 30 were selected for further analyzing. The responses to the drifting event were ranged from 500 to 6000 ms, which corresponded to the values of the LDE between 0 and 30. Thus, the LDE values lower than 3 indirectly indicated the subject was alert.

2) *EEG peak frequency shifting*: After the ICA of the EEG data, we found the detail changes at the alpha- and theta-band spectra in occipital component. The dominant frequency band is shifted from alpha to high theta band along with increases of the LDE indexes.

3) *Occipital component cluster*: For characterizing the temporal changes of the LDE-related power spectra at the alpha and theta band in detail, the temporal profile of the power changes at alpha and theta band are distributed against the LDE indexes. The changes of the alpha-band power showed a non-monotonic profile along with the decreases of the alertness.

Specifically, the alpha-band power is linearly increased for the LDE index lower than 20 and then the power is slightly decreased for the LDE indexes between 20 and 30. The theta-band power shows a monotonic increase from low LDEs to high LDEs.

4) *Parietal component cluster*: Similar changes on the LDE-sorted spectra are also observed at the parietal component, but the variations of the EEG activities are weaker than that observed at the occipital component. The peak intensities of the alpha- and theta-band power were significantly ($P < 0.05$) lower than those observed at the occipital component (alpha: 1.2 vs. 2.1; theta: 0.8 vs. 1.5). Additionally, the rate of the spectral power increases at the alpha- and theta-band power is lower than those at the occipital cluster (alpha: 5 vs. 8; theta: 10 vs. 13).

5) *Frontal component cluster*: As for the frontal cluster, a significant power increase is shown around 5 Hz at higher LDE values in the LDE-sorted spectra. Similar to the occipital and parietal clusters, the theta-band power is monotonically increased with the increases of the LDEs. The alpha-band power is only increasing slightly along with the decreases of alertness at the frontal cluster.

6) *Arousing feedback rectified lapse in performance and corresponding EEG power spectrum*: We have also explored EEG dynamics and behavioral changes in response to arousing auditory signals presented to individuals experiencing momentary cognitive lapses. In this study, arousing auditory feedback was delivered to the subjects in half of the non-responded lane-deviation events during a sustained-attention driving task, which immediately agitated the subject's responses to the events. The improved behavioral performance was accompanied by concurrent power suppression in the theta and alpha bands in the lateral occipital cortices. This study also demonstrated the feasibility of estimating the efficacy of arousing feedback presented to the drowsy subjects by monitoring the changes in EEG power spectra (Jung et al. 2010; Lin et al. 2010).

7.1.3 VMF Year 3

VMF1: The Effects of Vehicle Motion and Fatigue on Brain Effective Connectivity During Driving (Y3–Y5).

As mentioned above, we have made a lot of progress on assessing inter-subject EEG correlates of fatigue in Years 1 and 2. In Year 3, Dr Lin of NCTU will investigate the complex brain networking within multiple ICs to verify the effects of vehicle motion and neurocognitive fatigue on the driver's task performance in a

sustained-attention driving task. The causal relationship between ICs will be assessed by the multivariate vector autoregressive-based Granger causality model (GCM). Both time- and frequency-domain effective connectivity will be analyzed to explore dynamic information flows between different brain networks under different motions and cognitive states.

VMF2: Vehicle Motion Simulator for LSIE Experiments (Y3–Y4).

The VMF team will finish the installation and testing of a one-person version of the CES laboratory interface to allow parallel experiments at NCTU and UCSD. The major stimulus resource unique to the NCTU laboratory is the moving vehicle platform, which will pose additional stress on subjects not possible in the stationary CES at UCSD. Furthermore, we will adapt the UCSD Simulation Neuroscience and Application Platform (SNAP) experimental protocols programming environment to test the effects of vehicle motion and human fatigue on attention, decision-making, and situational awareness (see below). The goal of this task is to collect a large corpus of EEG and behavioral data that allow more robust training and testing of computational approaches to estimate the cognitive and behavioral states.

VMF 3: To Develop an Online Cognitive Monitoring System based on the WWD EEG (Y3–Y5).

Based on the results of the studies on cognitive-state assessment and management conducted in Years 1 and 2, we plan to develop an online cognitive monitoring system based on the WWD EEG. The system will be capable of automatically removing EEG artifacts, extracting performance-related EEG features, and continuously monitoring the neurocognitive states of the wearers. The envisioned system will be systematically validated in the LSIE experiments.

VMF 4: The Effects of Vehicle Motion and Fatigue on Attention, Decision-Making, and Situational Awareness (Y3–Y5).

Attention switching refers to the ability to shift the focus of attention quickly between different tasks. It is highly correlated to decision-making. Situation awareness is the perception of environmental elements with respect to time and/or space, the comprehension of their meaning, and the projection of their status after some variable has changed, such as time. Attention, decision-making, and situational awareness will be the main focus of LSIE. Under VMF, we plan to adapt the LSIE protocols developed at UCSD to explore the effects of vehicle motion and fatigue on attention, decision-making, and situational awareness. To this end, we will first explore brain dynamics associated with shift attention. In particular, we plan to explore the feasibility of continuously detecting the focus of attention of individuals performing multiple tasks. We will then investigate the effects of

vehicle motion and fatigue on the human performance and the accompanied EEG dynamics. Note that the vehicle motion might pose additional stress on subjects, which tends to have negative impacts on human performance, but also provides motion cues that might assist subjects in developing their spatial awareness or navigation. This study will assess both positive and negative impacts of vehicle motion on human performance in the LSIE experiments.

7.1.4 VMF Program Year 3 Accomplishments

Neural Correlates of Kinesthetic Stimuli Introduced by the Motion Platform.

We have studied the effect of the kinesthetic stimuli on the subject task performance and brain networks in a lane-keeping driving experiment on the NCTU motion vehicle simulator (MVS). Results of effective connectivity under the driving condition without kinesthetic inputs reveals the causal source of the brain network centered at the anterior and middle parts of the cingulate cortex (anterior cingulate cortex [ACC] and midcingulate cortex [MCC]) that connect with the contralateral sensorimotor cortex (SMC), PCC, and bilateral extrastriate cortex (ESC) by either unidirectional or bidirectional ways. Both regions co-modulate the activity of rest of the brain areas in deducing an extensive causality within the brain network responsible for the need on monitoring unexpected events during a pre-stimulus period. This finding can be explained by existing knowledge that the ACC is an interface of the motor control, performance monitoring, and attention response; the cingulated motor area in the MCC, one of the high-order motor areas, directly projects to the motor cortex and spinal cord and takes part in the processing of motor systems. Their underlying interaction with the prefrontal cortex forms a crucial communication between cognitive and motor systems to perform a given task, which supports the present causality toward the SMC.

When the driving task involved kinesthetic feedback, the effective connectivity has an apparent shift of the causal center from the anterior to the posterior region. This K^+ network shows a dominant causality at the PCC that receives causal information from the ACC and MCC and meanwhile sends causal information to the MCC, SMC, and ESC. This shift might be caused by the PCC taking charge of the evaluative function of monitoring sensory event and the processing of spatial information, thus to avoid perceptual ambiguity when the upcoming deviation event is present with both visual and kinesthetic forms. Sensory weighting interaction leads to increased activities in related regions processing attended information in one sensory modality and also deactivates the cortical regions associating with other sensory modalities when multiple stimuli are present simultaneously.

Vehicle Motion Simulator for LSIE Experiment.

The motivation of this study is to understand human behavioral decision-making and evaluate statistical and computational methods for assessing brain dynamics under stress, cognitive fatigue, and attention shift in complex operational environments. Thus, the goal of this study is to explore the principles and methods to enhance operator situational awareness and decision-making under several forms of stress, cognitive fatigue, and attention shift, and thereby, improve total human–system performance. During the third year, NCTU and UCSD collaborated to design the experiment to incorporate lane keeping and dynamic attention shifting tasks. The main simulation task was also modified from "navigation" to "deviation" to facilitate easier development within the short time and limited resources. In keeping with the UCSD LSIE design, audiovisual stimuli of spoken words, written words, icons, and tones were integrated in (with words in Taiwanese) with signals to subjects to shift attention differently at different points during the driving task. Piloting in this paradigm has been conducted.

Online cognitive monitoring system was based on the WWD EEG:

- We had proposed a new framework, the IC ensemble, to leverage neuroscience principles acquired from laboratory-oriented research into a truly automatic and online EEG-based BCI. The BCI includes 1) independent source separation using ICA, 2) automatic selection of the independent components of interest (ICis) associated with human behaviors, 3) multiple classifiers with a parallel constructing and processing structure, and 4) a simple fusion scheme to combine the decisions from multiple classifiers. Its implications in BCI are demonstrated through a sample application: cognitive-state monitoring of participants performing a realistic sustained-attention driving task. Empirical results showed that the proposed ensemble design could provide an improvement of 7%~15% in overall accuracy for monitoring the arousal state and the driving performance of the participants. In summary, constructing ICi-ensemble classifiers and fusing their outputs suggest a practical option for ICA-based BCIs to eliminate the need to manually select ICi and reduce the risk of not obtaining any desired independent source or selecting an inadequate component. Most importantly, the ICi-ensemble design for integrating neural information across multiple brain areas creates a potential for developing more sophisticated yet practical BCIs for real-world applications.

In the last year, our team completed the following works: 1) introduced the 4-channel Mindo4 EEG device to record EEG signals from the forehead regions

(AF8, FP2, FP1, and AF7), 2) proposed an effective system for analyzing EEG data and mapping them onto the arousal level, and 3) implement the proposed algorithm on a Java-based graphical user interface (GUI) for online analysis. To validate the performance of the proposed system, we recruited eight subjects to participate in a 90-min sustained-attention driving task in a VR-driving environment. The preliminary result of using the proposed system demonstrated the feasibility of predicting the arousal level of the driver. We won the best live demo award at the 2012 IEEE EMB/CAS/SMC Workshop on Brain-Machine-Body Interface (*Mobile and Wireless EEG System for Predicting Lapse in Driving Performance*). Next, the artifact removal technique will be implemented into this system to improve the performance of cognitive-state monitoring

The effects of vehicle motion and fatigue on attention, decision-making, and situational awareness were the following:

- Since distracted driving poses a serious threat to traffic safety, this study proposes an EEG-based BCI model to detect distraction/inattention. We designed five cases with different stimulus onset asynchrony (SOA) to investigate the distraction effects between the deviations and equations, and the experiment was based on a simulated driving experiment within an immersive the VR environment. The five different cases were math task 400 ms before lane deviation, math and deviation onset simultaneous, math task 400 ms after deviation, math task only, and finally deviation only. Fifteen healthy participants (all male), between 20 and 28 years of age, were recruited from the university population. Power increases in the theta and beta bands were observed in relation with distraction effects in the frontal cortex. In the motor area, alpha and beta power suppressions were also observed. All distracted and concentrated EEG epochs were recognized with a self-organizing map (SOM). The accuracy of the proposed system approached approximately 90% for the recognition of EEG epochs of distracted and concentrated driving according to the frontal and left motor components.

We also conducted a study to investigate the EEG correlates of attention shifts while driving and test the feasibility of monitoring drivers' focus of attention based on the EEG activities. The features were extracted from the selected six components include the frontal, central, parietal, occipital, left motor, and right motor to monitor drivers' attention. The samples extracted from pure lane-deviation and math conditions were selected to build a ML classifier, which was based on a support vector machine (SVM), to recognize the brain activities when subjects focused on solely on math or lane deviation. The performance of

classification on the testing data was 84.74 ± 6.47% and 85.59 ± 5.23% for the math and lane deviation, respectively. In the case of the math problem before deviation, the subjects were mainly focused on the math (blue patches) for the first 400 ms. After the onsets of the lane deviation, the outputs of the classifier remained low (blue) for the trials with short RT (the top portion of the plot), indicating the subjects focused on solving the math problems even as the lane deviation started.

7.1.5 VMF Year 4

VMF1: The Effects of Vehicle Motion and Fatigue on Brain Effective Connectivity during Driving.

Summary of Project Objectives

In Year 4, we applied Granger causality analysis on independent EEG sources using SIFT (developed by Tim Mullen, SCCN, UCSD) to construct the cortical effective connectivity. To study the effects of vehicle motion on brain effective connectivity during driving, each participant completed two driving sessions on separate days. One was denoted as the K^+ session, in which as real-road driving experience participants received visual information combined with the kinesthetic and vestibular sense commensurate with every lane departure. The other was denoted as the K^- session, in which the motion platform was deactivated and the participant had to take the initiative in visually detecting lane departures.

Achievements

1. **Effect of vehicle motion on brain effective connectivity**
    - Figure 7.1 shows the comparison of causal magnitudes under K^- and K^+ conditions when subjects exhibited optimal, suboptimal and poor performance. Edges indicate significant difference: either $K^- > K^+$ (bluish-dashed arrows) or $K^- < K^+$ (reddish arrows), and width of edges represents differential magnitude.
    - When subjects exhibited an optimal task performance, the causation in ACC→lSMC, MCC→PCC, ESC→lSMC, and ESC→ACC was stronger under the K^+ condition. When the task performance was suboptimal, magnitude of connectivity was greater in MCC→SMCs under the K^- condition and in ACC→PCC, PCC→SMCs, PCC→ESC, and ESC→lSMC under the K^+ condition. When the task performance was poor, most of links did not differ between the two conditions, and only the PCC→rSMC coupling exhibited a

greater magnitude of connectivity when driving with a kinesthetic feedback than driving without such feedback.

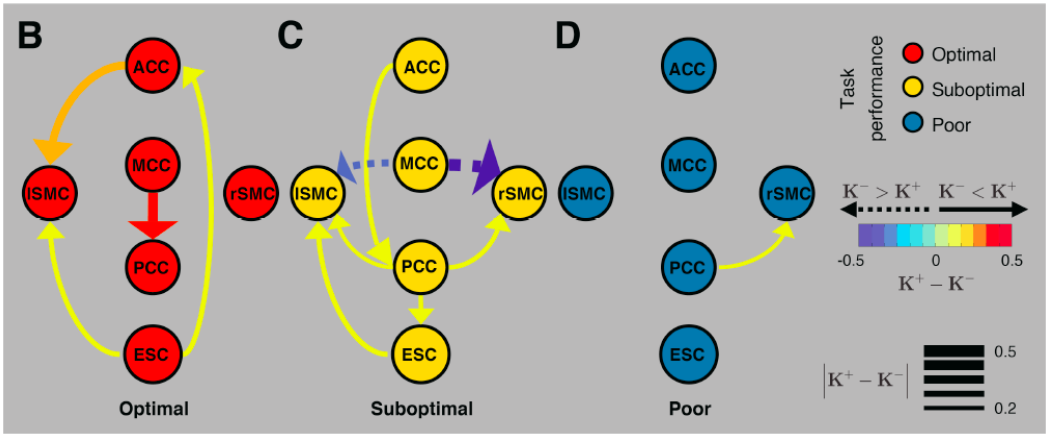


Fig. 7.1 Magnitude of connectivity observed in every pair of brain regions

2. Effect of fatigue on brain effective connectivity

- We applied ICA and partial directed coherence analysis to show the change of effective connectivity between distributed brain regions under different vigilance levels, including alertness, transition, drowsiness, and abrupt-awake, during the simulated driving.
- The results of alpha coupling (Fig. 7.2) showed that the ESC sent a causal outflow to the anterior region and received a causal inflow from the posterior region while being alert, compared to being drowsy. Regarding the transition state, the anterior region played a major source to affect the rest of the brain region with a cross-frequency coupling, and the connectivity magnitude had a relatively large causality, compared to other vigilance levels.
- Additionally, most of causal magnitudes declined as subjects progressed into a drowsy state. Interestingly, the subjects enabled a short RT in response to traffic events when they abruptly awakening from the drowsy state, however, the causal magnitude climbed to the level as the transition state, rather than the alert state.

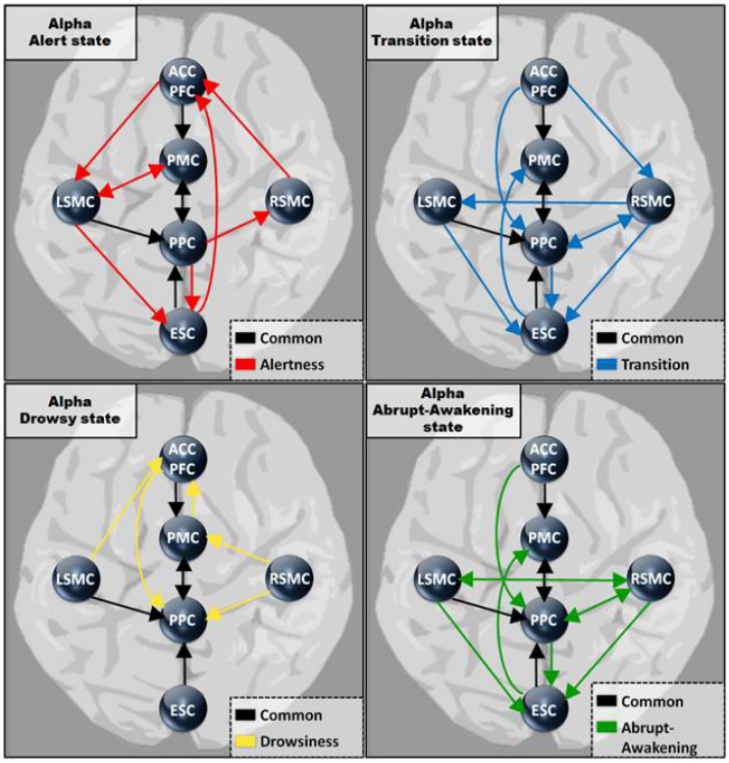


Fig. 7.2 Significant information flow of alpha band (8–12 Hz) in four different arousal levels

VMF2: Vehicle Motion Simulator for LSIE Experiments.

Summary of Project Objectives

The VMF team will finish the installation and testing of a one-person version of the CES laboratory interface to allow parallel experiments at NCTU and UCSD. The major stimulus resource unique to the NCTU laboratory is the moving vehicle platform will be able to pose additional stress on subjects not possible in the stationary CES at UCSD. Furthermore, we will adapt the UCSD DAS experimental protocols programming environment to test the effects of vehicle motion and human fatigue on attention, decision-making, and situational awareness. The goal of this task is to collect a large corpus of EEG and behavioral data that allow more robust training and testing of computational approaches to estimate the cognitive and behavioral states.

Achievements

- We have tested and modified the LSIE experiment and add the pure DAS task in each experimental session.
- We have collected 103 subjects in the revised LSIE experiment. Then there were 103 EEG and behavioral data and 61 eye-tracker data of LSIE.

- All EEG data will be denoised and decomposed into independent sources in the brain by ICA using EEGLAB. After applying ICA to total 103 EEG data, we will separate these independent sources to several clusters for future group analysis.
- In the preliminary analysis, the 31 behavioral data were separated into RT of DAS and Drive with auditory or visual shift attention task (Fig. 7.3). The results showed that the response times of DAS were no difference among all conditions of DAS with auditory task. The Drive task might increase the RTs for the DAS task, while the Drive task appeared after the DAS task with visual target. RTs of the Drive task would be the shortest in the pure condition and be the longest in the dual condition.
- The same subject were used to explore the dynamic of brain activation. Twenty-six EEG data (five were excluded for larger noise) were decomposed into independent sources in the brain by ICA using EEGLAB. These components (Fig. 7.4) were grouped to seven clusters by k-means from the information of scalp maps, dipoles, and power spectra. These data of clusters were applied ERSP analysis for observing the time-frequency phenomenon. The results shown that there was delta-band power increase to prepare response in the motor cluster. There were also delta and alpha suppression in the frontal cluster, and alpha and beta decrease in the motor and occipital clusters. To compare DAS task with visual and auditory target, the alpha and beta power suppression were more negative in the pure and mixed DAS task with a visual target.

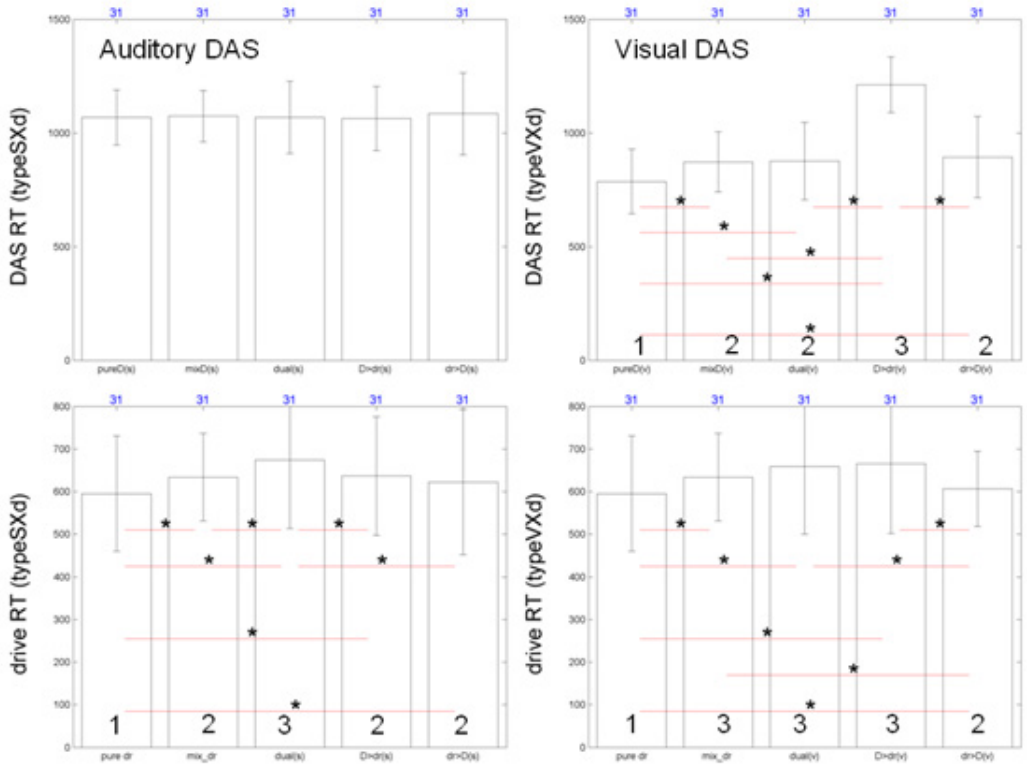


Fig. 7.3 The summary reaction time of 31 preliminary behavioral data. (Upper panel) Average RT for DAS and (lower panel) average RT for driving; (right) visual condition and (left) auditory condition.

Note: pureD: Pure DAS experiment; pure dr: Pure driving deviation (lane-keeping driving) experiment; mixD: DAS task appeared between two driving deviation experiments; mix_dr: Driving deviation experiments appeared between two DAS tasks; dual: DAS task and driving deviation experiment appeared at the same time; D>dr: DAS task appeared before driving deviation experiment; dr>D: DAS task appeared after driving deviation experiment; (v): visual DAS target; (s): auditory DAS target.

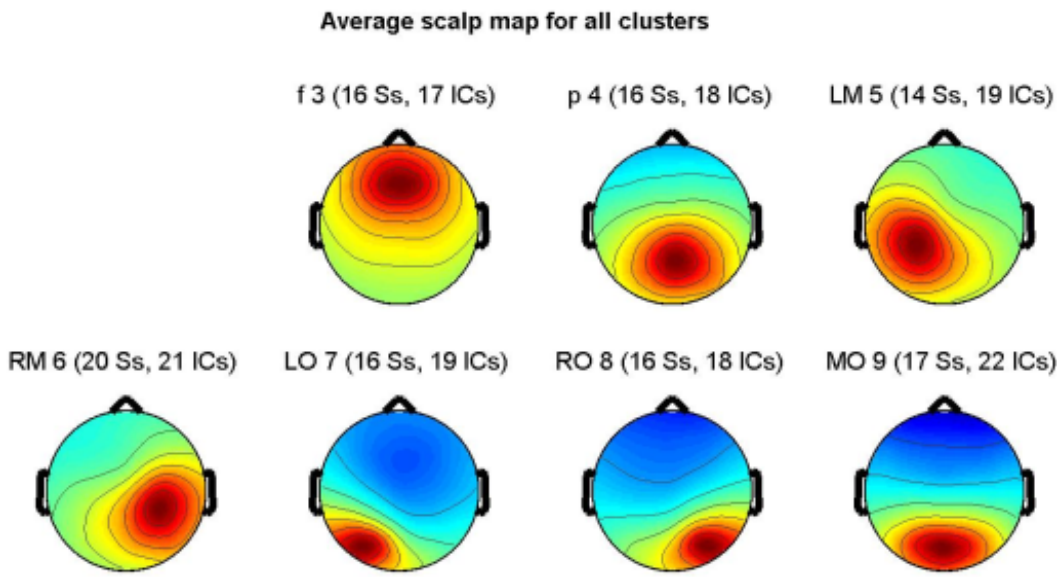


Fig. 7.4 EEG data were decomposed and grouped to some frontal, motor, parietal, and occipital clusters

VMF3: To Develop an Online Cognitive Monitoring System based on the WWD EEG.

Summary of Project Objectives

In Year 4, we have remodeled the framework of real-time drowsiness monitoring system (Fig. 7.5). After applying bandpass filter (0.5-50 Hz) and fast Fourier transformation (FFT), the pre-stimulus EEG spectra of all experimental trials were segmented and formed as a training data set of N samples. Each training sample was accompanying with the behavioral performance in response to the given task indicating the presumable vigilance of the driver.

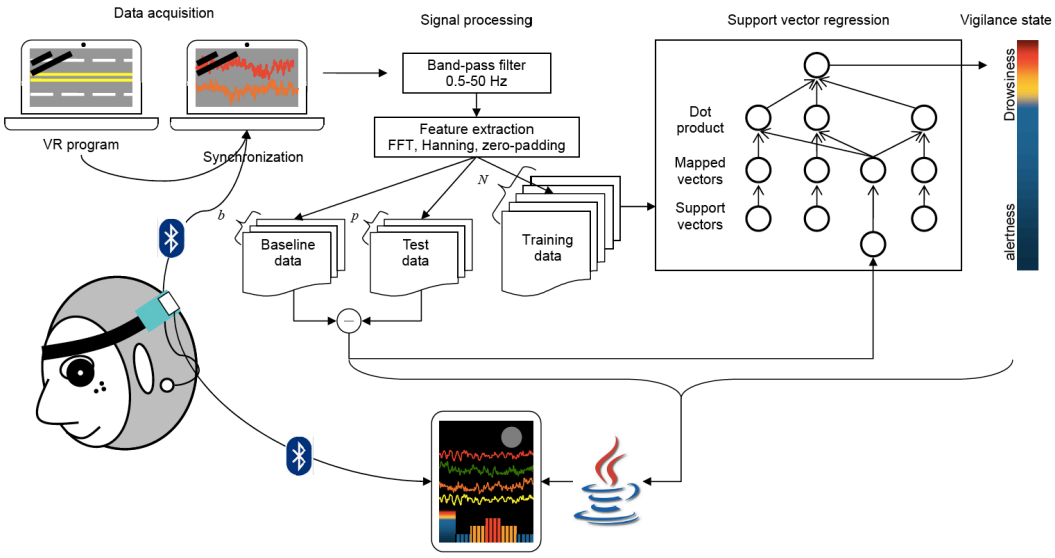


Fig. 7.5 Design of EEG signal acquisition, processing, and analysis system

Achievements

1) Build a real-time drowsiness monitoring system

- Regarding the core of the prediction system, the linear regression model was replaced by the SVR to model the relationship between EEG and behavior. Finally, the predicted outputs were converted to eight levels of vigilance. To obtain an accurate estimation, we proposed a weighted algorithm for online time-frequency analysis. The EEG signal was successively feed into weighted time-frequency analysis before applying SVR. As shown in Fig. 7.6, power spectral density (PSD) of the t-th EEG trial (a 2-s EEG signal) was the weighted average of spectral powers, which was calculated from {t-p+1}-th, …, {t-k-1}-th, …, t-th EEG trials, where $k \leq p$. Windowed 128-point epochs were extended to 256 points by zero-padding. The obtained EEG power spectra were further converted to a logarithmic scale prior to further analysis. Then, a weighted-averaging filter was used on all the PSDs to further obtain a smoothing a PSD estimation.

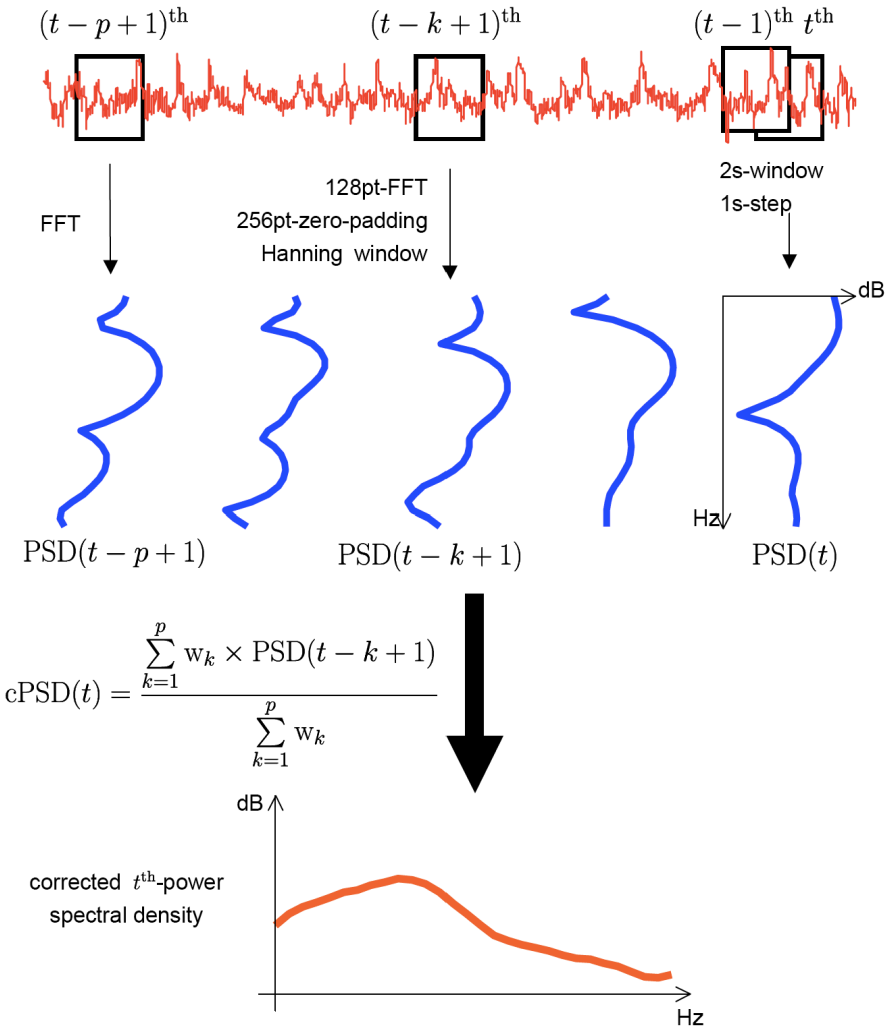


Fig. 7.6 Weighted spectral power estimation

2) Performance validation of online drowsiness monitoring system

- An attempt was also made in Year 4 to verify the feasibility of the proposed system by further implementing this new SVR model in Java language as an Android application. The parameters of the implemented model (including slack parameter of SVR, gamma value of radial basis function [RBF] kernel, and support vectors of the obtained model) were trained using MATLAB software. Figure 7.7 shows a temporal relationship between the vigilance levels predicted by the proposed system and driver's behavior in response to regular traffic events or emergencies when the participant performed the lane-departure driving task for approximately 70 min. The result showed that these two time-series data were highly correlated. Additionally, vigilance changes could be detected by the system, and the trend of the declining vigilance

could be considered as a useful index to alert drivers to the danger before server behavior lapses occurred.

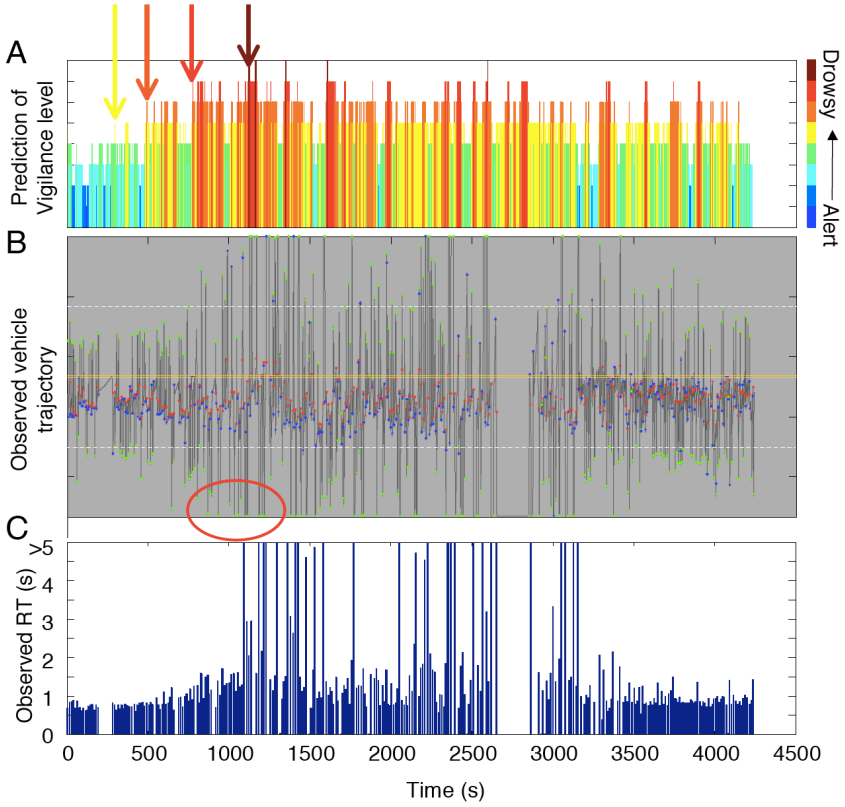


Fig. 7.7 Temporal changes in a) the vigilance level predicted by the proposed system, b) the vehicle trajectory, and c) the RT observed during a 70-min experiment.

VMF4: The Effects of Vehicle Motion and Fatigue on Attention, Decision-Making, and Situational Awareness.

Summary of Project Objectives

We reported differences in task performance and EEG spectra while participants performing two cognitive tasks separately and simultaneously: lane-keeping driving task and mathematical problem-solving tasks. The tonic changes associated with behavioral performance were highly related with the brain dynamics in the central area. The phasic brain dynamics related to driving and math tasks were clearly different, and can be accurately and continuously detected by ML classifiers (with the performance reached 84.80 ± 2.71% and 85.79 ± 1.34%, respectively). Finally, the relevance between the behavior performance and brain activity showed that the participants shifted their attention dynamically to achieve optimal performance in the dual-task conditions with two visual stimuli. We envision a practical, real-time attention detecting/tracking system to improve road safety.

Achievements

- Table 7.1 details the average behavioral performances of the math and driving tasks in the single- and dual-task conditions. Comparison of the STs for the math problems in the pure condition, the participants responded to the lane deviations faster and with less variation.

Table 7.1 Behavioral performances in the math and driving task

	Case 1 (D)	**Case 2 (M)**	**Case 3 (M/D)**	**Case 4 (D&M)**	**Case 5 (D/M)**
Math	X	1850.2(495.2)	2095.2(656.4)	1985.3(549.1)	1963.6(557.5)
Drive	708.4(97.4)	X	741.7(165.1)	746.5(119.7)	756.3(167.9)

- Figure 7.8 shows the (onset) RTs to the lane-deviation events (black line), (offset) RTs to the lane deviations (red line), and the solution times (STs) for the math problems (blue line). The behavioral performance of both tasks decreased in the dual-task conditions. Across all epochs in the three dual-task conditions, the participants achieved better performance in responding to lane deviations in Case 3 (M/D) and achieved shorter STs for the math problems in Case 5 (D/M). In Cases 3 (M/D) and 4 (D&M), the response offsets to lane deviations slowly declined as the STs for the math problems increased. In Case 5 (D/M), the RTs of the lane deviation were less sensitive to the STs for the math problems (i.e., the RTs were relatively flat across the variation in STs). The longest mean STs for the math problems were observed in Case 3 (M/D) in which the math equations were presented in the first 400 ms; during this time, the participants presumably concentrated only on the math problems.

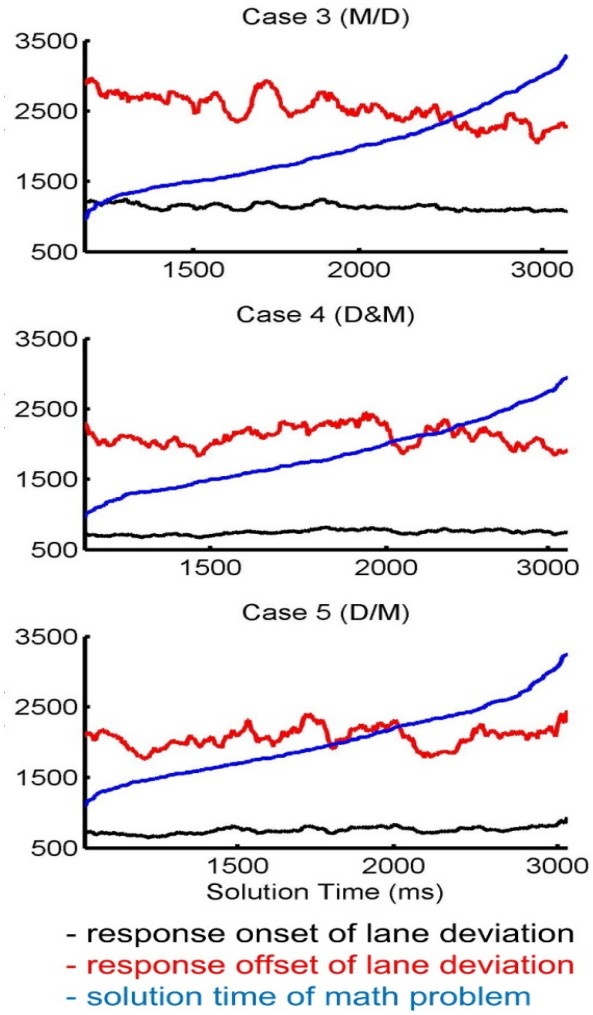


Fig. 7.8 The behavioral relationships between participants' responses to the lane-deviation and math problems in the distracted driving

- The lane deviation subsequently appeared on the screen and forced the participants to shift their attention to the driving events. In Cases 4 (D&M) and 5 (D/M), the average STs for the math problems and RTs to the lane deviations were also longer than those in the single-task conditions. In Case 5 (D/M), the response offsets to lane deviations were not noticeably different between the epochs with longer and shorter STs. In this condition, the lane deviation was displayed first, so the participants presumably concentrated on the driving task. The RTs to the lane deviations is averagely 756.3 ms. So, the participants could almost allocate more attention on math problems when the equation appeared.
- The performance-related tonic (pre-stimuli) changes the ICs located in frontal, central, parietal, and occipital while performing the driving or math tasks.

- The decreased wide bands in the central, alpha band in the parietal, alpha band in the occipital, and beta band in the occipital were significantly explored as the decreasing driving performance (RTs). The decreased wide bands in the central were significantly related to the increased STs of the math problem.
- The mainly significant differences of performance-related tonic spectral changes are plotted in Fig. 7.9. Here the central delta, central alpha, central beta, parietal alpha, occipital alpha, and occipital beta were selected. The mainly brain activity related to the behavioral performance was found in the central area. The curve in each figure reveals the oscillation in specific frequency bands.

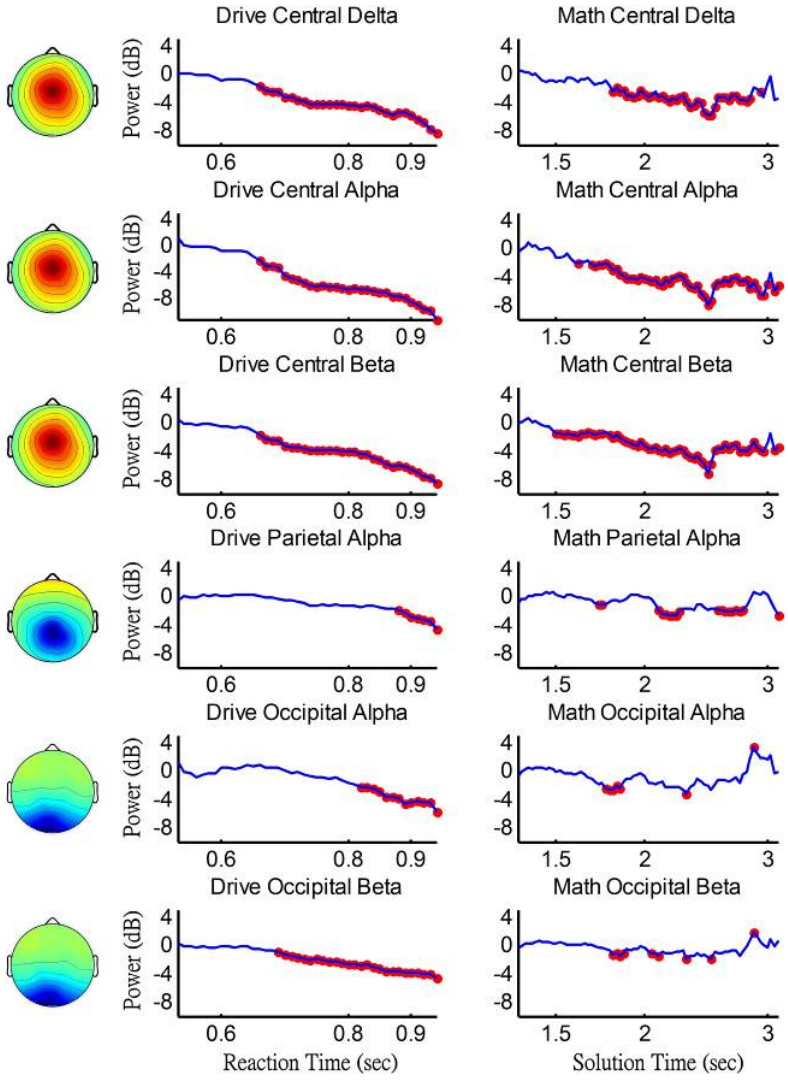


Fig. 7.9 The specific frequency bands in the lane-deviation driving and problem-solving mathematic tasks

The figures in left (right) panel were related to driving (math) task. The red lines indicate the significant difference compared with the epochs distributed in the Top 20%. When the behavioral performance of driving and math tasks decreased, the decreased power of the wide bands was explored in the central area. Especially, the occipital beta was also significantly decreased when the RT of the lane deviation was increased. The alpha band in the parietal and occipital was also found in those epochs with slower RTs of the driving task. When the STs of the math task was increased, the significantly decreased power of the wide bands was explored. In the other areas, there was no clear phenomenon related to the changes of STs. The dimension of features is 120 from six brain areas, and we apply LDA to select important features. Figure 7.10 shows the selected features and the significant different in the power spectrum while reacting to two types of tasks. The + represents selected bands and the * means significant different.

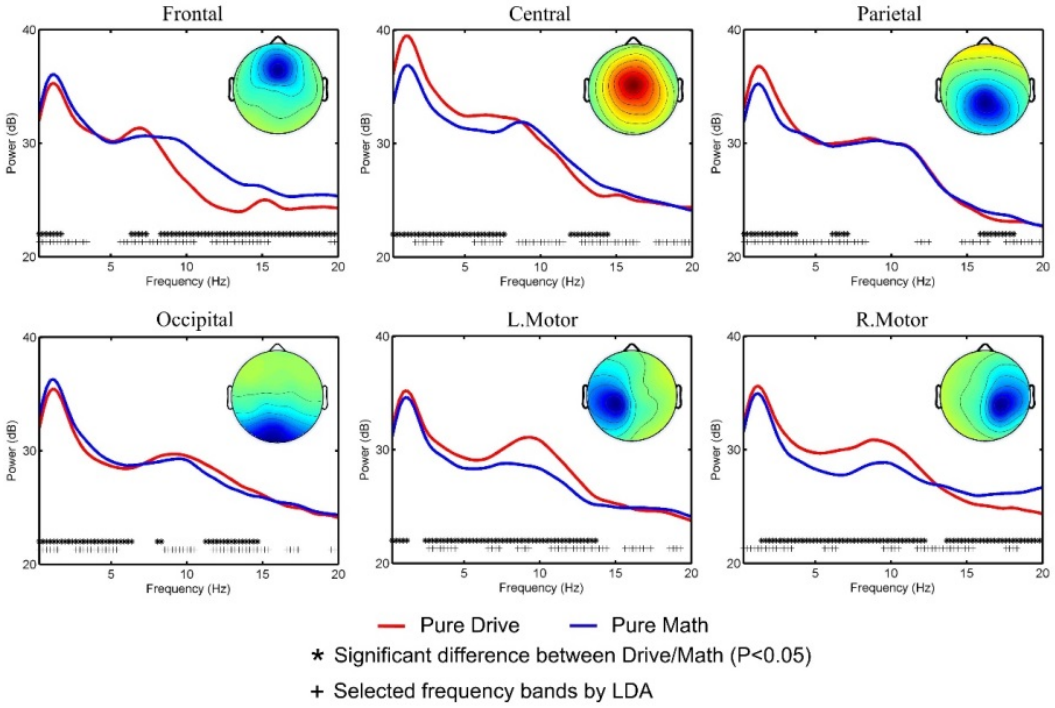


Fig. 7.10 The significant difference and selected frequency bands were marked in the PSD from six brain areas

- Relevance vector machines (RVMs) can improve the performance by fewer features than the previous study. We compare the performance by SVM with radio basis function kernel (SVMRBF) in Table 7.2 and RVM with linear kernel in Table 7.3. The classification performance decreased about

5% averagely by RVM. By SVM, the classification performance was 84.8 and 85.79 for recognizing math and driving, respectively.

Table 7.2 The classification performance by SVMRBF

	Subj 1	Subj 2	Subj 3	Subj 4	Subj 5	Subj 6	Average
Math	81.02(6.97)	86.58(6.47)	87.77(4.66)	82.25(7.34)	86.79(5.54)	84.43(6.97)	84.80(2.71)
Drive	87.27(4.79)	87.51(5.84)	85.16(6.12)	85.21(4.21)	85.56(5.96)	84.04(5.90)	85.79(1.34)

Table 7.3 The classification performance by RVM

	Subj 1	Subj 2	Subj 3	Subj 4	Subj 5	Subj 6	Average
Math	79.74(8.37)	77.93(8.93)	82.84(5.05)	78.45(7.56)	82.56(6.89)	76.75(8.04)	79.66(7.15)
Drive	83.12(5.8)	82.43(7.71)	78.10(6.79)	83.93(6.71)	82.02(7.06)	79.80(6.86)	81.56(6.32)

- One focus of attention (FOA) classifier based on SVMRBF was investigated to track the attentional states. Figure 7.11 (a–c) plots the estimated FOA. In each subplot, the first black vertical line represents the time point of the first event onset, and the second one represents the ST of arithmetic problem. Epochs were sorted by the ST of the math equations in each of the figures, so the longer ST epochs with longer ST were plotted at the lower part of the figures. The binary outputs of the FOA detection model were 1 (colored-coded with a warm color) (vs. –1) if the brain activity indicated that the subject was focusing on the driving task (vs. the math problem).
- To quantitatively investigate the relationship between the ST of math problems and duration of FOA on driving, Fig. 7.11 (d–f) plots the total numbers of 400-ms windows during which the FOA was on driving when the participants were supposed to solve the math problem for Case 3 (M/D), Case 4 (D&M), and Case 5 (D/M), respectively. Each point represented a single EEG epoch. As shown in Fig. 7.11 (d–f), the number of driving windows increased as the STs of the math task increased.

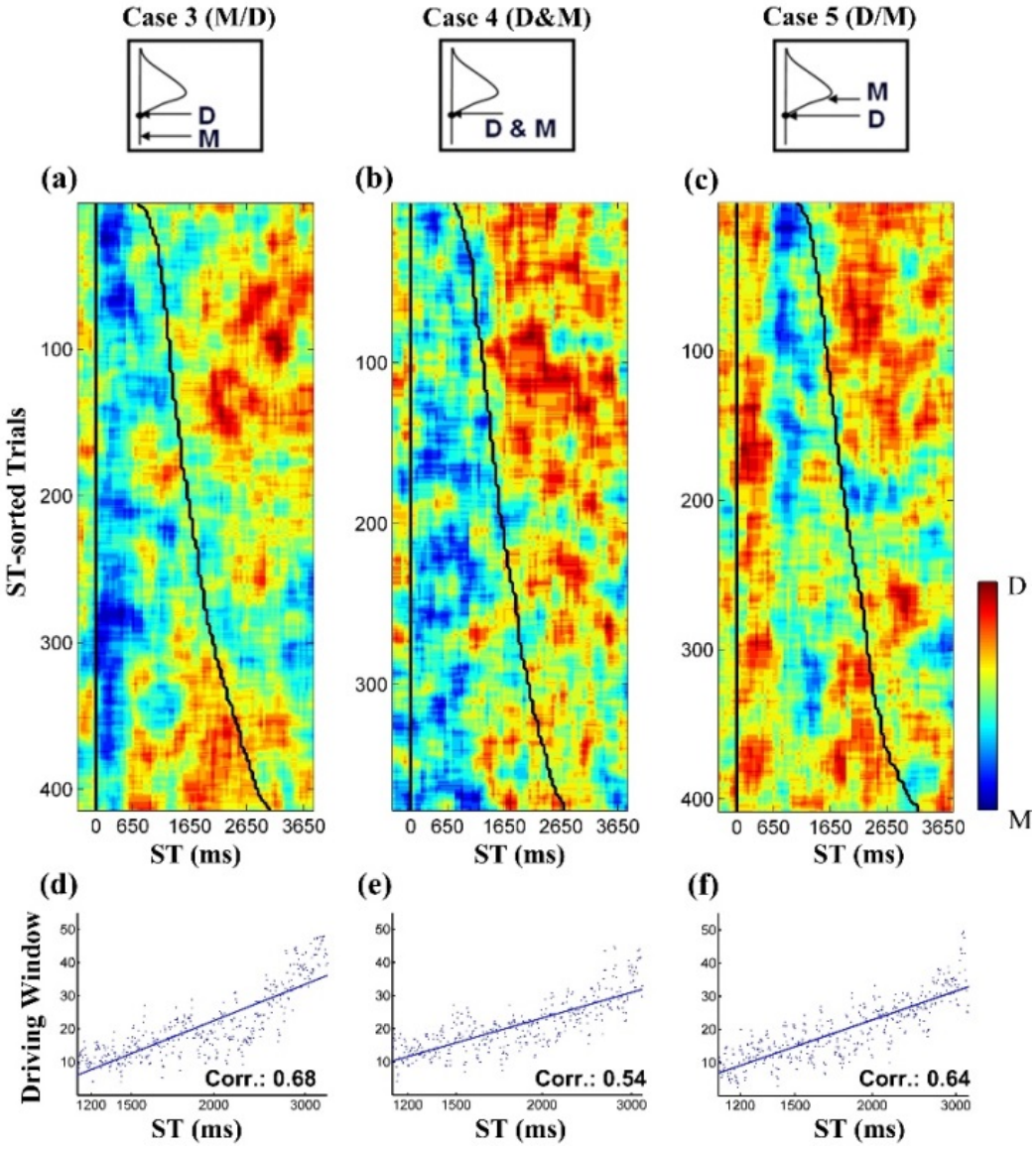


Fig. 7.11 The estimated FOA by the SVMRBF during the driving-math dual tasks and the relationship between the ST and the estimated FOA on driving

- The overall correlation coefficients between the numbers of the 400-ms window during which the FOA was on driving and the STs of the math problem were 0.68 and 0.64 in Case 3 (M/D) and Case 5 (D/M), respectively. The correlation coefficient was lower (0.54) in Case 4 (D&M) in which the lane-deviation events and math problems were presented simultaneously.

7.2 Neurotechnologies: Wearable EEG Development and Testing (WDT)

Activity supported to overcome barriers included the following:

- Development and employment of novel, wearable sensor suites for monitoring brain and body dynamics during naturalistic behavior, as well as software systems to enable integrated monitoring capabilities

7.2.1 WDT Research Goals

EEG is the only brain imaging modality with high temporal and fine (potentially cm^2-scale) spatial resolution that is lightweight enough to be worn in operational settings. Because of current limitations in size, weight, and cost of available EEG systems, early BCI systems have been designed to use a minimal number of recording channels. Our alliance includes collaborators from NCTU, Taiwan, who are designing, building, and testing ultra-lightweight, wearable, wireless, low-cost, whole-head, microelectronic EEG systems with successively higher sensor densities (Lin et al. 2008a; 2008b). The NCTU multi-channel dry-electrode wireless EEG system will be tested in parallel with standard EEG recording. Portable systems are already available and are in use by us to study the EEG dynamics accompanying motivated actions in normal 3-D environments (Makeig et al. 2009). The research we propose tests and demonstrates the value of wearable EEG system and other psychophysiological recording in neuroergonomic systems designed for operational use and its applications.

The goal of this research thrust is to design, develop, and test a wearable and WWD EEG human–machine interface that can allow assessment of brain activities of participants actively performing ordinary tasks in natural body positions and situations within a real operational environment. Monitoring the neurophysiological activities of Soldiers in an operational environment poses a severe measurement challenge using current laboratory-oriented biosensor technology. We recently demonstrated the feasibility of using dry EEG sensors and miniaturized supporting hardware/software to continuously collect EEG data recorded from four non-hairy forehead sites in a realistic VR-based dynamic driving simulator (Lin et al. 2008). Here, we further develop and test new methods of performing higher-density dry-electrode EEG acquisition and online/onboard signal processing for assessing cognitive performance of participants in operational environments.

7.2.2 WDT Year 1–2

We investigated and developed methods for assessing individual cognitive status and performance in military environments using the WWD EEG systems. Online neuroergonomic systems capable of measuring and processing concurrent neural, behavioral, psychophysiological, environmental, and system operational data could allow continuous estimation of subjects' cognitive state to design and operate systems that maximize operator cognitive capacity as well as overall human/system performance. Our overall research goal in this area was to develop and test a user-acceptable and wireless EEG-based cognitive state monitoring and management system capable of high-definition recording, online artifact cancellation and signal processing, and cognitive-performance detection without use of conductive gels applied to the scalp, in military environments.

WDT1: Developing Successively Higher-Density WWD EEG System (Y1–Y4).

During the first two years (Y1+Y2), Dr Lin's team at NCTU designed and fabricated a multi-channel WWD EEG system. During the following years, they designed and fabricated successively higher-density systems for acquiring EEG signals without requiring conductive paste or scalp preparation. Features of the target EEG system include 1) lightweight dry EEG sensors to measure EEG signals from the whole head; 2) a miniaturized, lightweight DAQ circuit board featuring bio-amp, analog-to-digital converter (ADC), filters, and wireless telemetry to maximize portability and wearability of the system; and 3) integration of the dry sensors and DAQ board into a quickly and easily donned and doffed electrode cap.

7.2.3 WDT Year 1–2 Accomplishments

Dry foam-based electrode: A novel dry foam-based electrode was developed for long-term EEG measurement at both non-hair and hair-covered sites. The dry foam electrode was fabricated by electrically conductive polymer foam covered with conductive fabric.

Impedance variation for long-term measurement: We conducted a series of experiments to test the skin–electrode impedance of the new foam-based sensor. The results of this study showed that the impedance between the skin and the dry foam electrode is similar to that of conventional wet electrodes with conductive gel.

Comparison of signals quality measured by using different electrodes: The linear correlation coefficient function in MATLAB (R2007a, The MathWorks) was used to evaluate the difference of EEG signals measured by different electrodes. The results showed the averaged correlation between conventional wet and new dry foam-based electrodes was very high.

Wireless DAQ circuit board: Electrical activity generated by large populations of active neurons has to penetrate through skin, skull, and several other layers before electrodes placed on the scalp can measure it. The measured signals need to be massively amplified before they can be analyzed and interpreted. Because the EEG signals are very feeble and the impedance between electrode and skin is quite high, the measurement system should have high impedance to reduce the loading effect. For this reason, we developed a wireless 16-channel EEG signal acquisition module consists of front-end amplifier (FEA) circuit, ADC, microprocessor, and wireless communication circuit in Year 1.

EEG cap (helmet) with 16 electrodes: We developed an easy-to-use EEG cap/helmet with the novel sensors. The EEG cap features 16 dry electrodes; a miniature, battery-powered DAQ; and wireless telemetry.

Collaboration: NCTU team provided a 16-channel spring-loaded dry electrode EEG cap (MINDO-16) along with software to ARL for testing in the US Army Tank Automotive Command (TARDEC) Experiment 17.

7.2.4 WDT Year 3 Accomplishments

WDT1: Developing New and Novel Dry Sensors (Y3–Y4)

During Year 3, in order to verify the biocompatibility of dry EEG sensors to avoid allergies or hypersensitivity from the users, we conducted a cytotoxicity test (Guidance: ISO 10993-5) and a skin irritation test (Guidance: ISO 10993-10) on the NCTU spring-loaded and Ag-silicon-based sensors.

WDT1.1: Searching for Better Conductive Materials for Dry Sensors.

In Year 3 we further designed and fabricated a new silicon-based dry sensor to alleviate the problems. This conductive poly rubber mixed with Ag particle materials does not cause any skin irritation and is also non-cytotoxic in vitro. The new sensors can be applied to different areas or devices for long-term recording. In addition, we also collected some data and compared the frequency responses and ERPs of the new dry sensors against that of wet sensors (Neuroscan).

WDT1.2: Integrating Active Sensor with Miniature Circuit Board Development of an Active Circuit with an Onboard Amplifier (WDT1.2 in Year 3).

To further reduce the noise level of EEG recording, we have developed an active sensor integrating a dry sensor and an active sensor circuit (diameter: 11.9 mm) consisting of a) a high gain (9752X) amplifier, and b) a low-noise design with a band-pass filter of 0.103~125 Hz. A bus circuit board for data transmission among all sensors has also been designed and fabricated. The bus circuit board reduces the

number of wires and, more importantly, the sensing noise. To test the effectiveness of the active sensor, a comparison between ERPs collected by an active-sensor system and Neuroscan system during a visual oddball task was conducted to evaluate the performance of active sensor. The result shows a high correlation (>90% in the time domain) between the signals measured by different sensors/systems.

WDT2: Developing Successively Higher-Density WWD EEG Systems (Y4).

WDT2.1: The Multi-Channel Mobile and Wireless EEG Systems (WDT2 in Year 3).

In Year 3, we developed several mobile and wireless EEG systems comprising a miniature battery, amplifiers, high-pass filters, ADCs, and a wireless controller. It is lightweight, miniature, and wireless. Currently, there are five form factors: 2-, 4-, 16-, 32-, and 64-channel EEG systems. The dimensions of circuits of 2/4- and 16-channel EEG system are 45 × 30 and 50 × 35 mm, respectively. The dimensions of circuit boards of the 32- and 64-channel EEG systems are 66 × 35 and 2 × 66 × 35 mm, respectively (for 64-channel EEG system, two circuits of 32-channel EEG system are integrated). The system can acquire high-quality EEG signals with a maximum sampling rate of 1,024 Hz and a maximum resolution of 24 bits. The EEG systems are stable and safe, and have passed CE and FCC certifications. Due to the bandwidth limitation of Bluetooth transmission, we have to make a compromise between sampling rate and resolution in a high-density wireless EEG. For the 32-channel systems, the two combinations of sampling rates and resolutions are 512 Hz/16 bits and 254 Hz/24 bits. For the 64-channel one, the best combination of the sampling rate and resolution is 128 Hz and 16 bits.

Several dry and wireless EEG/BCI devices have been developed and used to acquire user's EEG signals continuously. The active dry sensors amplify measured signals at a very early stage to improve SNRs. The novel head circumference adapted mechanical design reduces user setup time and extends the duration of system wearability. Wireless telemetry allows ubiquitous brain monitoring and increases user mobility. The systems can easily be used by technicians with limited experience and naïve participants.

Evaluating the EEG Signals Acquired by the WWD EEG Systems (WDT2 in Year 3).

We have conducted an experiment to evaluate the quality of EEG signals acquired by MINDO-32. In the experiment, participants were asked to blink, clinch their teeth, and close their eyes to verify the quality of EEG signals.

Evaluating the EEG Signals Acquired from Non-Hair-Bearing Sites (WDT2 in Year 3).

Even with the advances in spring-loaded dry EEG sensors, acquiring good-quality EEG signals from the hair-covered occipital sites is inevitably more difficult than from non-hair-bearing sites. We have systematically and quantitatively investigated the feasibility of measuring SSVEPs from non-hair-bearing regions, compared to those measured from the occipital areas. Empirical results showed that the signal quality of the SSVEPs from non-hair-bearing areas was comparable with, if not better than, those measured from hair-covered occipital areas. These results might significantly improve the practicality of a BCI system in real-life applications, especially when used in conjunction with dry foam-based EEG sensors. The results have been published in the Proceedings of the IEEE EBMC 2012.

WDT2.2: The Multi-Channel Mobile and Wireless EEG Recording Software (WDT2 in Year 3).

In Year 3, NCTU group developed EEG acquisition software for different platforms including Windows XP/7/8 and Android 2.1 or higher. The Windows platform software supports notch filter (50 and 60 Hz), data saving in different formats (txt/ edf/bdf), and event synchronization through RS232. Recording software for the Android platform incorporates all the functions on the Windows platform and an additional function to select channel and/or brain area of interest. We also incorporate an online ERP analysis package into the acquisition software. The software automatically averages and plots the ERPs time-locked to stimulus onsets.

WDT3: Applied the WWD EEG System to Study Human Cognition (Y3–Y5).

Since working memory is one of the important cognitive processes in human cognition and has been widely studied, in the past year, we modified a classic working memory paradigm—Sternberg working memory task—to verify the feasibility of using MINDO-32 for studying human cognition. Participants see black or green letters in uppercase appear in succession, and have to remember the letters that are presented in black and ignore green ones. Then, they have to make response by pressing the corresponding button to indicate whether a red letter, which is in lowercase, appears in the previous trial or not. Feedback will be given after each response. Thirteen subjects have participated in this working-memory experiment as of today, and seven of them wore MINDO-32 and the rest of them wore traditional wet electrodes (Neuroscan, Inc).

WDT3.1: Testing the WWD EEG System in Driving Experiments in MVS (Y3) Real-Time Dry-Sensor Based Cognitive-State Monitoring.

In Year 3, our team completed the following works: 1) use the MINDO4 EEG device to record EEG signals from the forehead regions (AF8, FP2, FP1, and AF7), 2) propose an effective system for processing EEG recordings and converting them into the arousal level, and 3) implement the proposed algorithm on a Java-based GUI for online analysis. To validate the performance of the proposed system, we had recruited eight voluntary subjects to participate a 90-min sustained-attention driving task in a virtual-realistic driving environment. The preliminary result of using the proposed system was able to predict the arousal level of the driver. We won the best live demo award at the 2012 IEEE EMB/CAS/SMC workshop on brain–machine–body interface (*Mobile and Wireless EEG System for Predicting Lapse in Driving Performance*). Next, the artifact removal technique will be implemented into this system to improve the performance of cognitive-state monitoring.

WDT4: Developing and Evaluating Online Signal-Processing Methods for Artifact Removal of the EEG Data Acquired by the WWD EEG System.

EEG recorded outside the laboratory using the new dry EEG must take into account and handle possible large increases in the magnitude and nonstationary character of EEG artifacts and/or system noise relative to laboratory recordings. Thus, for robust and maximally efficient EEG monitoring, explicit or implicit identification and separation of brain source signals of interest from non-brain and other less-relevant brain source signals are essential (Makeig et al. 2012). During the past 12 months, UCSD WDT team has developed and tested a new method, ASR, for online and real-time rejection of EEG artifacts that are localized to low-dimensional spatial subspaces on a short timescale (<1 s). ASR is a highly effective and robust spatial artifact rejection that intuitively can be thought of as projecting high-amplitude artifact subspaces out of the data.

WDT5: Developing and Evaluating a Wearable and wireless MoBI (WWMoBI) Apparatus for Motion-Artifact Removal of the EEG data.

UCSD WDT team has been working with NCTU collaborator Dr John Zao (currently not funded by CTA) to develop and test *BodyDyn,* a battery-powered, wearable and wireless motion and posture capture system based on 10- degree-of-freedom (DOF) microelectromechanical system (MEMS) sensors. The first prototype has been developed. The system consists of a single (2 inches × 1.4 inches × 0.5 inch) master device and up to four (0.75 inch × 0.5 inch × 0.15 inch) slave devices, each of which can be attached easily to user's body or clothing. Each slave device can capture a stream of 9-DOF motion data including the 3-D linear

accelerations, the 3-D angular accelerations, and the 3-D magnetic flux measurements up to a hundred samples per second while the master device can capture an additional 24-bit barometric pressure reading that can be used to detect altitude changes as little as 20 cm. Each of these devices is actually a miniature implementation of the attitude heading reference system (AHRS) that was used for inertial navigation in aviation. The master device is equipped with a powerful ARM-9 (cell phone) CPU and a Java virtual machine. Hence, it can run sophisticated signal-processing and application programs written in Java. The entire system can communicate with a smart phone via the Bluetooth 2.1 EDR+ Radio and integrate seamlessly with the Android mobile platform through the MIT FUNF Open Sensing Framework. Currently, we are integrating *BodyDyn* with NCTU MINDO EEG systems for motion-artifact removal.

7.2.5 WDT Year 4

WDT 1: Developing New and Novel Dry Sensor.

- We developed a novel dry sensor: Ag-silicon-based sensors and we have also performed auditory ERP test with Ag-silicon-based sensor to evaluate that MINDO system is able to catch P300 feature.

WDT 2: Developing Successively Higher-Density WWD EEG Systems.

- 4-channel headband
    - The new MINDO 4S jellyfish (Fig. 7.12) has replaceable electrode band mechanism that can be used on the frontal or occipital area with dry sensors (flat Ag-silicon or spring-loaded). In this updated version, we also integrated SD card into the system, allowing for over one day of data saving. Removable SD card slot provides the usability of data retrieving and management.



Fig. 7.12 4-channel MINDO headband

- 32-channel design
    - We modified MINDO-32 Trilobite form-factor design (Fig. 7.13) to make it more feasible and degrees of freedom to fit the many variations in head shape and size. The electrodes are now fitting the scalp better with easy-to-operate knobs and the net weight has reduced about 100 g. With metal electrode clips on earlobe, the headset used totally dry electrodes for EEG recording.



Fig. 7.13 MINDO 32

- 64-channel design
    - The MINDO 64 Coral (Wi-Fi) (Fig. 7.14) consists of a) an integrated circuit with PGA/filter/ADC, b) a low-power design: dynamic amplifier and ADC, and c) a low-noise design. Wi-Fi transmission provides a high-quality EEG signal and stable connection. User can adjust the size and structure of MINDO-64 EEG cap by correcting the angle of rubber mechanism with a good fit, and making the circumference of the movable mechanism wider to get better contact. With the detachable circuit box, the user can replace or recharge the system in an easy way. In addition, by replacing the inner soft cap, this EEG system can fit from children to adults regarding the several of head shape and sizes.



Fig. 7.14 64-channel MINDO-64

7.3 Publications and Transitions (UCSD, NCTU)

Throughout the life of the CaN CTA program, teams of collaborators at UCSD and NCTU, led by Drs Scott Makeig (UCSD), Tzzy-Ping Jung (UCSD), and Chen-Ting Lin (NCTU), have been extremely productive in all types of publications, tools transition, and talent transition. Some of the publications and transitions are mentioned in this section, but many are not. Some of the publications are highlighted in the publications compendium, and further search can be made through the Google scholar search: "W911NF-10-2-0022" - Google Scholar.

Chiu T-C, Gramann K, Ko L-W, Duann J-R, Jung T-P, Lin C-T. Alpha modulation in parietal and retrosplenial cortex correlates with navigation performance. Psychophysiology. 2012;1: 43–55.

Chuang CH, Huang CS, Ko LW, Lin CT. An EEG-based perceptual function integration network for application to drowsy driving. Knowledge-Based Systems. 2015;80:143–152.

Chuang CH, Ko LW, Jung TP, Lin CT. Kinesthesia in a sustained-attention driving task. NeuroImage. 2014;91:187–202.

Chuang CH, Ko LW, Lin YP, Lin CT, Jung TP. Independent component ensemble for brain-computer interface. IEEE Trans Neural Syst Rehabilitation Eng. 2014;22(2):230–238.

Chuang C-H, Huang C-S, Lin C-T, Ko L-W, Chang J-Y, Yang J-M. Mapping information flow of independent source to predict conscious level: a Granger causality based brain-computer interface. IEEE. 2012. https://doi.org/10.1109/IS3C.2012.209.

Chuang C-H, Liu Y-T, Wang J-M, Lin C-T. Changes in alertness and the EEG effective connectivity in a sustained-attention driving task. J Neurosciand Neuroeng. 2016.

Chuang S-W, Ko L-W, Lin Y-P, Huang R-S, Jung T-P, Lin C-T. Co-modulatory spectral changes in independent brain processes are correlated with task performance. NeuroImage. 2012;62(3):1469–1477.

Huang C-S, Pal NR, Chuang C-H, Lin C-T. Identifying changes in EEG information transfer during drowsy driving by transfer entropy. Front Neurosci. 2015.

Ko LW, Komarov O, Hairston WD, Jung TP, Lin CT. Sustained attention in real classroom settings: an EEG study. Front Hum Neurosci. 2017;11:388.

Ko LW, Wei CS, Chen SA, Lin CT. EEG-based motion sickness estimation using principal component regression. 2011.

Ko L-W, Kalyan S, Lin SC. Development of single channel hybrid BCI system using motor imagery and SSVEP. J Healthc Eng. 2017.

Lee H-E, Wang W-C, Lu S-W, Wu B-Y, Ko L-W. Home-based mobile cardio-pulmonary rehabilitation consultant system. IEEE; 2011. https://doi.org/10.1109/IEMBS.2011.6090229.

Li S-Y, Yang C-H, Ko L-W, Lin C-T, Ge Z-M. Implementation on electronic circuits and RTR pragmatical adaptive synchronization: time-reversed uncertain dynamical systems' analysis and applications. Abstr Appl Anal. 2013;1–10. https://doi.org/10.1155/2013/909721.

Li S-Y, Yang C-H, Lin C-T, Ko L-W, Chiu T-T. Chaotic motions in the real fuzzy electronic circuits. Abstr Appl Anal. 2013;1–8. https://doi.org/10.1155/2013/875965.

Liao LD, Chen BW, Tseng KC, Ko LW, Wang IJ, Chang JY, Lin CT. Design and implementation of a wearable and wireless multi-channel electroencephalography (EEG)-based brain-computer interface device with the novel dry sensors. Accepted by Sensor Letters. 2012.

Liao LD, Lai HY, Lin CT, Chen YY. Design and experimental verification of a novel light-addressable multi-electrode arrays chip for multi-channel neural signal recording. Accepted by Journal of Neuroscience and Neuroengineering. 2012.

Liao LD, Wang IJ, Chen SF, Chang JY, Lin CT. Design, fabrication and experimental validation of a novel dry contact sensor for measuring electroencephalography signals without skin preparation. Sensors. 2011;11(6):5819–5834.

Liao LD, Wu SL, Liou CH, Lu SW, Chen SA, Chen SF, Ko LW, L CT. A novel 16-channel wireless system for electroencephalography measurements with dry spring-loaded sensors. IEEE Trans Instrum Measure. 2014;63(6):1545–1555.

Liao L-D, Chang Y-J, Lai H-Y, Lin C-T, Tsang Z-M, Chen Y-Y. A novel light-addressable multi-electrode array chip for neural signal recording based on VCSEL diode arrays. J Neurosci Neuroeng. 2012;1(1):4–12.

Liao L-D, Chen C-Y, Wang I-J, Chen S-F, Li S-Y, Chen B-W, Chang J-Y, Lin C-T. Gaming control using a wearable and wireless EEG-based brain-computer interface device with novel dry foam sensors. J Neuroeng Rehabilitation. 2012;9(5).

Liao L-D, Lin C-T. Novel trends in biosensors used for electroencephalography measurements in neurocognitive engineering applications. J Neurosci Neuroeng. 2012;1(1):32–41.

Liao L-D, Lin C-T, McDowell K, Gramann K, Jung T-P, Ko L-W, Chang J-Y. Biosensor technologies for augmented brain–computer interfaces in the next decades. Proceedings of the IEEE. 2012;100:1553–1556.

Lin CTC, Huang CH, Tsai CS, Lu S-F, Chen SW, YH, Ko LW. Wireless and wearable EEG system for evaluating driver vigilance. IEEE Trans Biomedical Circuits Syst. 2014;8(2):165–176.

Lin CT, Huang KC, Chuang CH, Ko LW, Jung TP. Can arousing feedback rectify lapses in driving? Prediction from EEG power spectra. Accepted by Journal of Neural Engineering. 2013.

Lin CT, Pal NR, Wu SL, Liu YT, Lin YY. An interval type-2 neural fuzzy system for online system identification and feature elimination. IEEE Trans Neural Netw Learn Syst. 2014;26(7):1422–1455.

Lin CT, Wang YK, Fang CN, You YS, King JT. Extracting patterns of single-trial EEG using an adaptive learning algorithm. In accepted by IEEE EMBC 2015.

Lin C-T, Chuang C-H, Wang Y-K, Tsai S-F, Chiu T-C, Ko L-W. Neurocognitive characteristics of the driver: a review on drowsiness, distraction, navigation, and motion sickness. J Neurosci Neuroeng. 2012;1(1):61–81. https://doi.org/10.1166/jnsne.2012.1010.

Lin C-L, Shaw F-Z, Young K-Y, Lin C-T, Jung T-P. EEG correlates of haptic feedback in a visuomotor tracking task. NeuroImage. 2012;60(4):2258–2273. https://doi.org/10.1016/j.neuroimage.2012.02.008.

Lin C-L, Jung T-P, Chuang S-W, Duann J-R, Lin C-T, Chiu T-W. Self-adjustments may account for the contradictory correlations between HRV and Motion-Sickness Severity. Int J Psychophysiol. 2013;87(1):70–80.

Lin C-T, Chen S-A, Chiu T-T, Lin H-Z, Ko L-W. Spatial and temporal EEG dynamics of dual-task driving performance. J Neuroeng Rehabilitation. 2011;8(11). https://doi.org/10.1186/1743-0003-8-11.

Lin C-T, Chuang C-H, Kerick S, Mullen T, Jung T-P, Chen K, L-W, C, S-A, K, J-T, McDowell K. Mind-wandering tends to occur under low perceptual demands during driving. Sci Rep. 2016;6(213253).

Lin C-T, Chuang C-H, Wang Y-K, Liu Y-T, Huang S-H, King J-T, Chen S-A, Lu S-W. Novel neurotechnology and computational intelligence method applied to EEG-based brain-computer interfaces. Submitted to IEEE Systems, Man, and Cybernetics Magazine. 2015.

Lin C-T, Huang K-C, Chao C-F, Chen J-A, Chiu T-W, Ko L-W, Jung T-P. Tonic and phasic EEG and behavioral changes induced by arousing feedback. NeuroImage. 2010;52(2):633–42.

Lin C-T, Liao L-D, Liu Y-H, Wang I-J, Lin B-S, Chang J-Y. (2011). Novel dry polymer foam electrodes for long-term EEG measurement. IEEE Transactions on Biomedical Engineering, 58(5), 1200–1207.

Lin, C-T, McDowell K. Prolog to the section on neurotechnological systems: the brain-computer interface. Proceedings of the IEEE. 2012;100:1551–1552.

Lin C-T, Tsai S-F, Ko L-W. EEG-based learning system for online motion sickness level estimation in a dynamic vehicle environment. IEEE Trans Neural Netw Learning Syst. 2013;24(10):1689–1700.

Lin F-C, Ko L-W, Chuang C-H, Lin C-T. Generalized EEG-based drowsiness prediction system by using a self-organizing neural fuzzy system. IEEE Trans Circuits Syst I. 2012;59(9).

Liu Y-T, Lin Y-Y, Wu S-L, Chuang C-H, Lin C-T. Brain dynamics in predicting driving fatigue using a recurrent self-evolving fuzzy neural network. IEEE Trans Neural Netw Learn Syst. 2016;27(2):347–360.

Nascimben M, Wang YK, King JT, Jung TP, Touryan J, Lance BJ, Lin CT. Alpha correlates of practice during mental preparation for motor imagery. IEEE Trans Cogn Devel Syst. 2020.

Singh AK, Chen HT, Cheng YF, King JT, Ko LW, Gramann K, Lin CT. Visual appearance modulates prediction error in virtual reality. IEEE Access. 2018;6:24617–24624.

Wang YK, Chen SA, Lin CT. An EEG-based brain-computer interface for dual task driving detection. Neurocomputing. 2014;129:85–93.

Wang YK, Jung TP, Lin CT. EEG-based attention tracking during distracted driving. Accepted by IEEE trans. on Neural Systems and Rehabilitation Engineering. 2015

Wang YT, Huang KC, Wei CS, Huang TY, Ko LW, Lin CT, Cheng CK, Jung TP. Developing an EEG-based online closed-loop lapse detection and mitigation system. Front Neurosci. 2014;8:321.

Wu S-L, Liu Y-T, Heish T-Y, Lin Y-Y, Chen C-Y, Chuang C-H, Lin C-T. Fuzzy integral with particle swarm optimization for a motor-imagery-based brain-computer interface. IEEE Trans Fuzzy Syst. 2016.

Yang CL, Lee HC, Chen CC, Jung TP, Ho SY, Ko LW. Working memory performance and brain oscillations under stress. Accepted by Communications in Computer and Information Science (CCIS). 2013. Springer.

Yu YH, Lu SW, Liao LD, Lin CT. Design, fabrication, and experimental validation of novel flexible silicon-based dry sensors for EEG signal measurements. IEEE J Transl Eng Health and Med. 2014.

8. Three-Year Collaborative Research

Beginning in program Year 5, some of the major research themes in the refocused plan included three-year research projects that would span across two biennial program plans and integrated collaborative efforts across significant part of the consortium. Two such projects are highlighted in this section by compiling elements of the research plans and the progress reports from UCSD and NCTU. Some of contributions from other participating members, DCS, UTSA, Syntrogi, and Columbia are also discussed in the respective sections of these members.

8.1 Real-World Neuroimaging: Understanding Real-World Fatigue in Vehicle Driving Experiments RWN-VDE

DCS, UCSD, NCTU, UTSA, Syntrogi

Activities supported to overcome barriers included the following:

- Development of experimental paradigms that capture the unfolding nature of multisensory stimulus streams experienced in real-world environments
- Acquisition and processing of high-dimensional data sets that characterize physical, mental, and physiological behavior, as well as its environmental context, in sufficient detail and across a sufficient breadth of circumstances

8.1.1 RWN VDE Background

Soldiers performing sustained military operations often function for extended periods in stressful environments with fractionated or no sleep. It is well established that fatigue, whether due to acute or chronic sleep deprivation, extended time-on-task, or the interaction between sleep- and task-related factors, is associated with neurocognitive performance decrements across a broad range of perceptual, cognitive, and motor functions. Motor vehicle crashes account for nearly one-third of US military fatalities annually and are the leading cause of US military fatalities. Further, one of the leading causes of vehicle accidents is driver fatigue. Fatigue, as well as stress, has been shown to dysregulate executive attentional control mechanisms underlying performance.

Although much research has been devoted to understanding relations between brain activity and fatigue states of drivers, the vast majority of this research has been conducted in driving simulators (SIMs) under highly controlled laboratory conditions, so it is not known how well findings generalize to complex real-world (RW) driving. One issue with investigating fatigue in the laboratory is the artificial manipulation of sleep deprivation. Most researchers have employed full or partial

sleep deprivation paradigms. In full sleep deprivation paradigms, subjects are denied sleep continuously over a 24-h period or longer, whereas in partial sleep deprivation paradigms subjects are restricted to just a few hours of sleep (e.g., 2–6 h) over a period of 3–4 days. In the real world, full sleep deprivation is much less common than partial sleep deprivation. However, even partial sleep deprivation paradigms require control over the sleep restricted periods in a regimented manner, which do not accurately reflect sleep patterns of individuals in the real world. Therefore, we propose an alternative paradigm for investigating the effects of RW fatigue on performance in both SIM and RW driving experiments. Specifically, we will leverage a Daily Sampling System (DSS) developed in Program Year 4 to monitor and track subjects' daily variations in sleep patterns and perceived levels of stress and fatigue as experienced by subjects naturalistically on an everyday basis. The DSS will automatically evaluate each subject's daily levels of fatigue based on actigraphy, sleep diaries, and subjective reports and schedule subjects for experiments along a continuum of levels of fatigue. For the purposes of this research, note that while sleepiness may be considered an important component of fatigue, the terms are not synonymous.

Another issue with investigating fatigue in the laboratory is the artificial driving environment inherent in driving simulators. Realistic driving conditions are difficult to simulate because there's no element of danger or real consequences for degraded driving performance in SIM driving, as is evident in RW driving. To overcome this issue, we planned a series of SIM experiments designed to simulate increasingly more complex, realistic driving environments in a ride motion simulator, but under experimental control. We also planned an observational study in which we will examine data from subjects driving in the real world.

By addressing these two issues, we will be able to better understand how the brain functions during real driving under the demands of real fatigue. EEG, eye tracking, driving performance, and subjective report data will be recorded, integrated, and analyzed from a large number of subjects in both SIM and RW driving environments over repeated sessions across different driving conditions. Experiments composing this three-year effort will generate extensively large and complex data that will also be leveraged to generate a unique and unprecedented database in terms of the number and diversity of experiments, subjects, measures, and metadata (i.e., "Big Data"). The database will facilitate hypothesis-driven research focusing on brain–behavior relations in RW environments as well as data mining and exploratory research. The goals of this research is analysis of within- and between-subjects differences, analysis of SIM versus RW differences, comparisons of approaches in signal processing, statistics and multifactorial

analyses, data integration/fusion, feature extraction, data reduction, collaborative filtering and clustering, and modeling and prediction algorithms.

The RWN VDE research plan was for the program to be accomplished via two complementary approaches, executed in parallel:

- **Approach 1:** Image and interpret RW fatigue using a within-subjects longitudinal approach in a real vehicle and a motion simulated vehicle simulator.
- **Approach 2:** Utilize existing experimental driving data to interpret RW fatigue using a Big Data approach.

8.1.2 Real-World Driving Experiment Longitudinal Study

DCS/ARL/UPenn

DCS worked with ARL to determine the requirements for analyzing RW driving performance to provide context for the corresponding physiological data collected from the subject. In particular, we tried to identify, and account for, the key measures used in the analysis of driving simulation studies, to provide a consistent basis for comparison across environments. This set of data included vehicle control and status data, navigational data, near traffic data, road data, and driver/passenger physiological, neurophysiological, behavioral data, as well as subjective survey data. Based on this set of requirements, DCS integrated a sensor suite and DAQ system including custom software with a test vehicle. Figure 8.1 provides an overview of this effort.

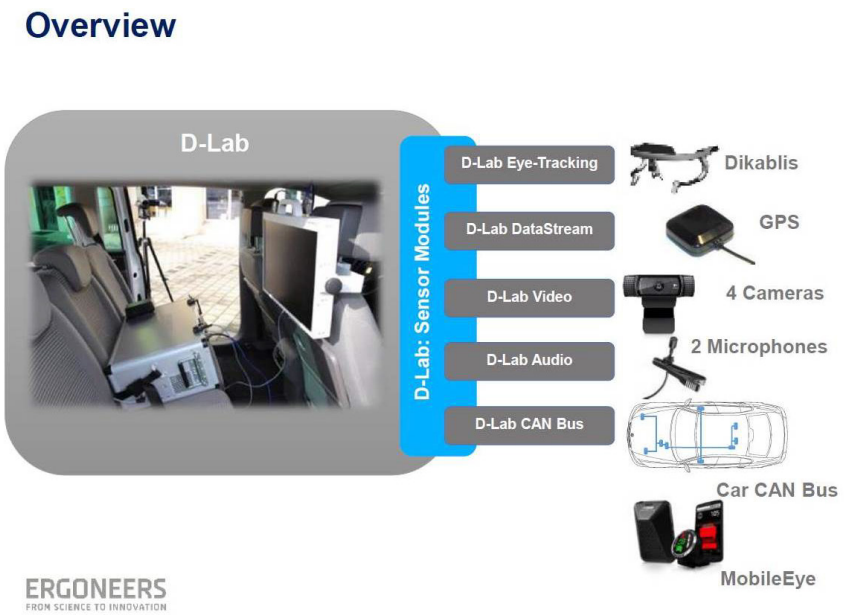


Fig. 8.1 RW vehicle driving DAQ

After the completion of the experiment apparatus, a RW driving experiment with driver/passenger dyad was designed in collaboration among ARL, DCS, and UPenn beginning in Year 7. Data collection was conducted through mid-2018, and analysis continues across different collaborators of the CaN CTA. Details of the experiment design and analysis results and publications are mentioned in the final report section of UPenn.

DCS engineers also provided significant assistance in the re-engineering and development of the DSS that was used to collect and assess fatigue data from the subjects recruited for the DF-DSS and MD-DSS experiments conducted at NCTU, Taiwan.

Using ARL's Multi-Aspect Real-world Integrated Neuroimaging (MARIN) system as the prototype, DCS worked with NCTU to refine the DSS user interfaces and provided MARIN source code to aid system development and align data formats. DCS also procured 100 Readiband devices for use with the DSS and assisted with the system implementation and validation process.

Analysis of the data collected in the driver/passenger dyad study has been conducted largely by UPenn team in collaboration with ARL. The results and publications are detailed in the final report section of UPenn.

8.1.3 Simulated Driving Experiment Longitudinal Study

NCTU

The "Simulated driving under conditions of real-world fatigue/stress" experimental was conducted at NCTU using the MVS (Fig. 8.2). A total of 15 participants were recruited to support data collection efforts over a five-month interval using two variations of experimental trials designed to study subjects performing a driving task under specific conditions of RW stress and fatigue, as determined by the DSS. All participants registered their stress and fatigue through a smartphone daily, and received notifications to report for experimental trials when the DSS deems their conditions to fit the experimental requirement.



Fig. 8.2 NCTU MVS

Previous studies have systematically established the brain–behavior relationship through the EEG signals recorded from human subjects when they performed a lane-keeping task in a simulated driving environment. However, it is unclear whether models derived under these conditions actually can translate into RW applications. Thus, in this project, we developed a DSS integrated with actigraphy and questionnaires to longitudinally assess and track objective and subjective fatigue level. When the fatigue met the criterion levels, subjects would be asked to participate in the driving experiment. Seventeen NCTU students were recruited for a longitudinal study over the NCTU 2014 fall semester. Averaged daily data (103–151 days) and session data (5–9 experiments) were collected for each subject. The relationships between subjective questionnaires and objective sleep measurements have been discussed and reported in PY5 part. The biomarker findings with RW fatigue were summarized in this report. Figure 8.3 shows the experimental design for the NCTU VDE.

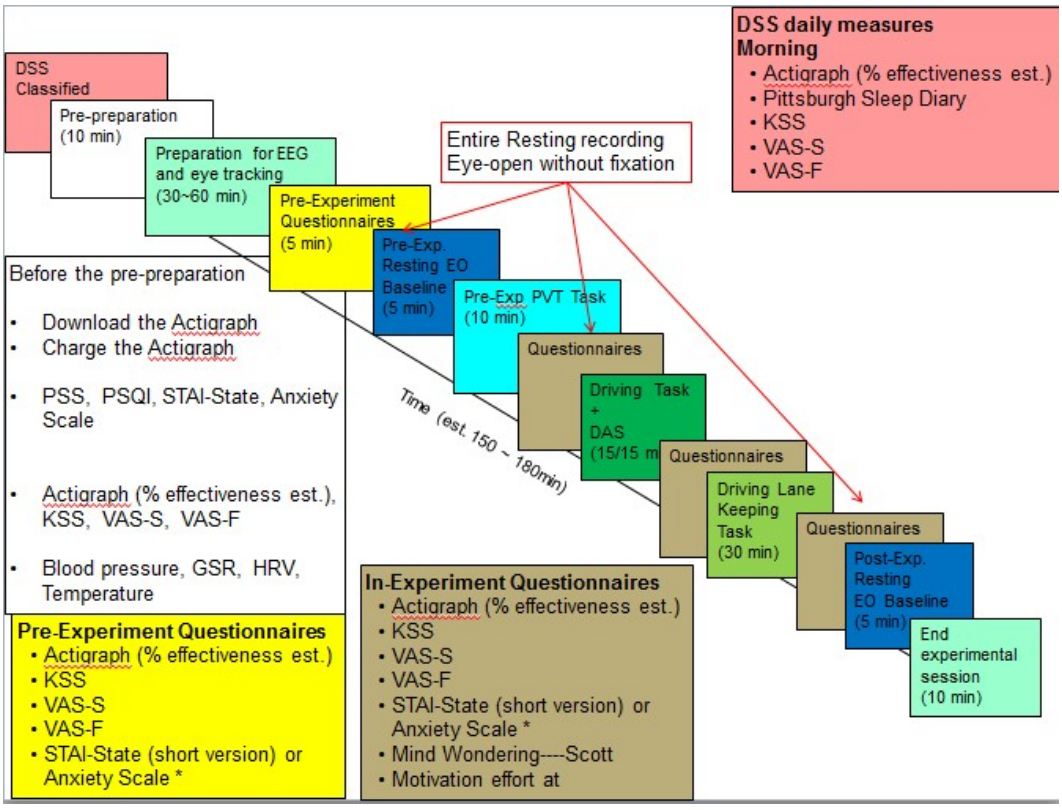


Fig. 8.3 NCTU VDE experiment design

In this part, we report the results of DF-DSS first. In this condition, subjects were required to perform NCTU lane-keeping task on the MVS. Throughout the experimental session, the vehicle randomly drifts from the center of the cruising lane, mimicking the consequences of driving on a non-ideal road surface.

Participants are required to maintain their attention, detect any lane-departure, and promptly steer the vehicle back to the center of the cruising lane. The RT and EEG features to the lane-departure event can be reflected the participant's task performance and vigilance state.

The tonic EEG change of different brain regions in three fatigue state groups is shown in the Fig. 8.4. Figures 8.5 and 8.6 display the trends of the parietal and occipital channels. The decrease of the high-risk group in the frontal low beta band (12–21 Hz) shifts to the occipital higher frequencies when normalized RTs are longer than 5.5 times the fastest 10% RT. The tonic EEG power of high-risk group shows increase in both the delta band (1~3 Hz) and theta band (4~7 Hz) when normalized RTs are longer than 5 times the fastest 10% RT. The increase of four brain regions in the alpha band (8~12 Hz) can be found in the reduced group when normalized RTs are longer than 4.5 times the fastest 10% RT. In addition, the same result can also be observed in the normal group, but it appears when normalized RT is longer than 3.5 times the fastest 10% RT.

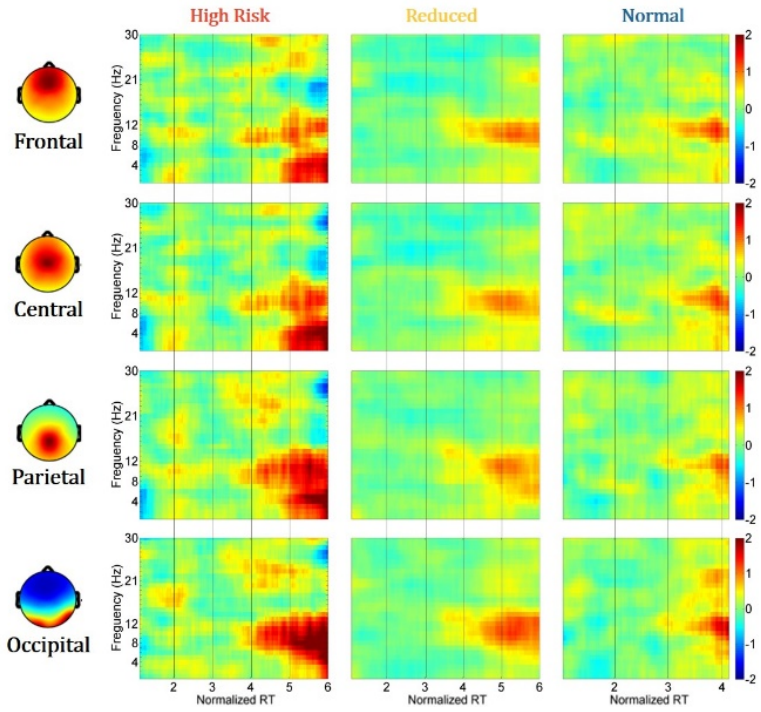


Fig. 8.4 The tonic EEG dynamics images with respect to normalized RT depicted for four brain components under three different fatigue groups, respectively (vertical axis, frequency, Hz; horizontal axis, RT-sorted index, and the corresponding normalized RT)

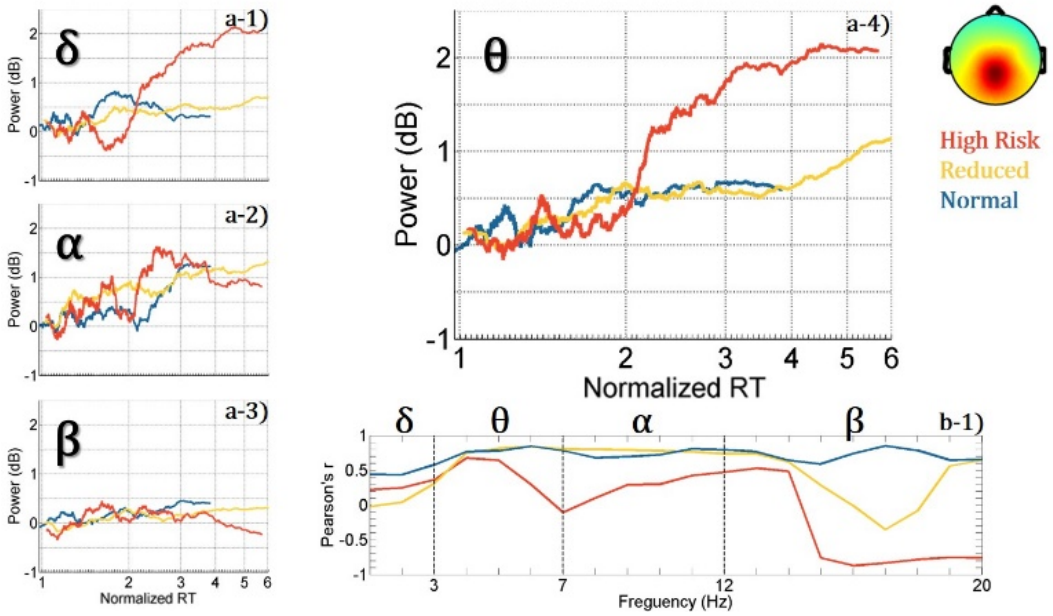


Fig. 8.5 The trends of parietal channels (P1, P2, and Pz) pre-stimulus EEG log power mean depicted for four frequency bands, respectively, and results of the correlation spectrum in parietal channels (vertical axis, Pearson's R-value; horizontal axis, frequency, Hz)

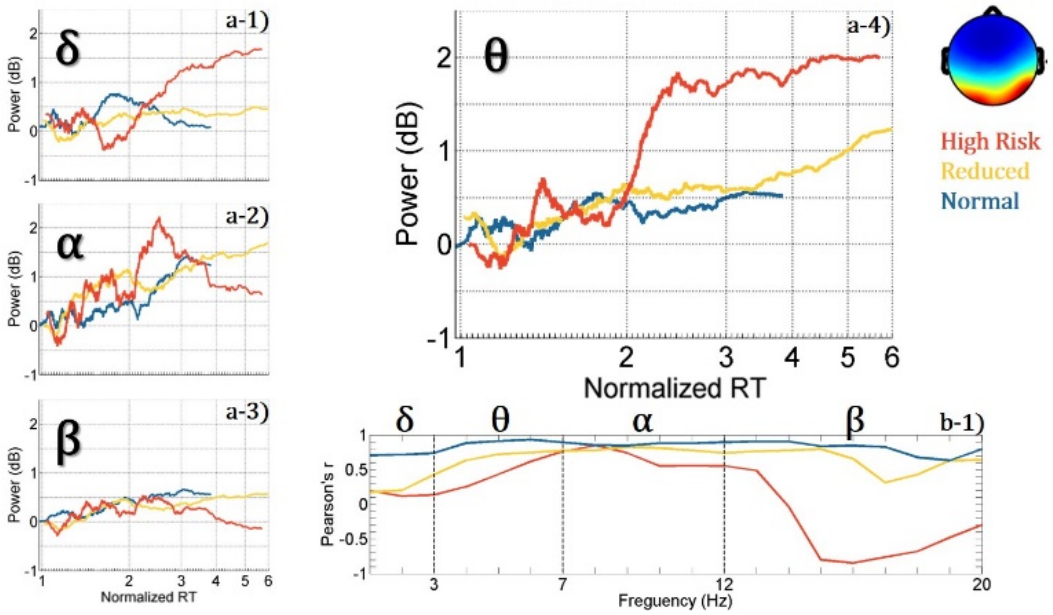


Fig. 8.6 The trends of occipital channels (O1, O2, and Oz) pre-stimulus EEG log power mean depicted in four frequency bands, respectively, and results of the correlation spectrum in occipital channels (vertical axis, Pearson's R-value; horizontal axis, frequency, Hz)

Regarding the effect of fatigue on brain–behavior relationship, the pre-stimulus brain activity showed that EEG theta and alpha powers of most of the brain regions observed in normal and reduced groups increased as the RT increased. In the high-

risk group, the theta power of posterior brain regions dramatically increased with the increased RT as compared with those in normal and reduced groups. Additionally, the alpha power of the occipital regions showed an inverted U-shaped change, which was observed only in the high-risk group. Taken together, fatigue significantly affects the brain–behavior relationship. Such findings could have major implication for understanding RW fatigue on drowsy driving and its model.

Re-defining and measuring alertness. The UCSD team developed a method to redefine and measure alertness for RW use. We define that alertness can be estimated by the prospective lapse rate (PLR), the probability of having slow responses (or no response) within an upcoming period. The PLR at a given time is estimated by the ratio of the number of slow-RT trials to the total number of trials within a certain time window in the near future (e.g., 90 s) using the entire data set of 79 lane-keeping-task (LKT) sessions. The non-causal PLR, as the ground truth of alertness, was found associated with two types of causal alertness indices (AIs), behavioral AI and EEG-based AI. Both behavioral and EEG-based AIs are assessable in near real time. However, the caveat of the behavioral AI is that it requires behavioral responses to frequent driving events, which is not practical in RW use. We thus model the association between the behavioral AI and EEG features to enable the estimation of the EEG-based AI with high temporal resolution in near real time. Our preliminary results suggest that the EEG-based AI effectively relates to the PLR, and thus validates this novel methodology of alertness estimation. The preliminary findings have been presented in *BCI Meeting 2018*.

Exploring nonlinear brain connectivity under different fatigue levels. UCSD and NCTU explored the use of nonlinear causality to model interactions among different brain networks. To be more specific, we use the causality concept, the convergent cross mapping 73 (CCM), a measure of the underlying deterministic causation of the system, to analyze the brain network outflows under high and low fatigue levels in an attempt to understand the changes in default mode network under different drowsiness and fatigue levels. CCM detects the causal relation strength and information exchanged between signals, assessing the synchronization features in the state space. CCM has provided new insight into physiological states, considering the brain as a complex network system. We analyzed the brain network changes of drivers by the shifts in the effective connectivity expressed in the CCM oscillations. For the LKT driving task, we analyzed the nonlinear causality in 1-s epochs before the lane-departure events. Study results showed distinct trends of nonlinear causality of alpha-band activity between the frontal and parietal areas in short- versus long-RT trials under different fatigue levels.

8.1.4 Big Data Approach

Syntrogi first laid the foundation of the CTA Data Repository by creating new versions of HED and ESS, suitable for RW neuroimaging. Syntrogi also defined the minimum necessary preprocessing steps that maximize the usability of data across diverse BCI and analysis workflows (ESS Standard Level 2 pipeline, preprocessing [PREP]). We then created tools (ESS tools and PREP toolbox, HED validation, CTAGGER), implementing and facilitating the use of these technologies. We placed legacy driving data (NCTU lane-keeping and eight BCIT studies) in ESS Levels 1 and 2 and trained CTA partners (DCS, UMI, and NCTU) to put the rest of RWN-related data in a standardized form in the CTA Repository. We also defined schemas for extending metadata encapsulation and provenance to custom pipelines (ESS level-derived data and derived-measure schema and file format), to be (further) implemented in PY6. Our research on EEG PREP was published in *Frontiers in Neuroinformatics* and we are currently working on a journal paper (ESS) and a conference paper (new version of CTAGGER).

DCS developed a central repository, the C3DS, to host all relevant vehicle driving data from within the alliance. DCS also developed a web-facing interface to facilitate access by alliance members. Additional detail of continued efforts and expansions of the Big Data approach are reported in the Syntrogi and UTSA final report sections.

Brain dynamics of task-positive and -negative networks during simulated driving: NCTU/UCSD VDE teams worked with Scott Kerick and Kaleb McDowell of ARL on the manuscript entitled "Brain network dynamics of mind-wandering during driving". This study examined whether changing the perceptual demand by manipulating amount of sensory inputs as the driver detected the lane-departure would promote a shift of brain activity between different modes of processing, reflected by brain network dynamics on EEG sources. Removing motion feedback during simulated driving deprives the driver of salient sensory information, and therefore imposes a relatively more perceptually demanding task, which activates the task-positive network. When the motion feedback is available, the drivers may rely on vehicle motion to perceive the perturbations, which reduce attentional load and result in higher activity of default mode network. We have published the study results in a high-impact journal *Scientific Reports* (Lin et al. 2016).

This paper demonstrates that brain network dynamics could have major implications for understanding fluctuations in driver attention and designing advance driver-assistance systems (Fig. 8.7). The present results further showed that participants are more likely to decouple their attention to sensory information

during the pre-stimulus time period in the environment under relatively lower task demand conditions, apparently even when sensory information is highly salient. The participants exhibited significantly more causal outflow from the MCC (node of task-positive network) versus PCC (node of default mode network) node during driving while deprived of salient sensory information (K^- condition in this study). Removing vehicle motion feedback during simulated driving deprives the driver of salient sensory information and, therefore, should impose relatively greater perceptual and executive demands on the driver to maintain vehicle control. Conversely, drivers succumbed to greater levels of inattention when the task is less demanding (K^+ condition), as evidenced by more causal outflow from the PCC versus MCC node when vehicle motion feedback was provided.

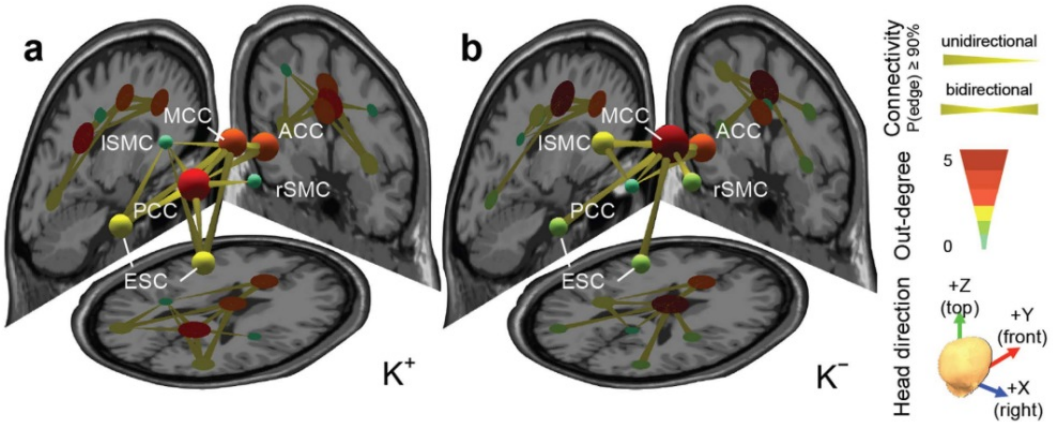


Fig. 8.7 MVS vehicle driver brain network dynamics

Effective connectivity between EEG independent processes estimated under a) K^+ and b) K^- conditions. A 3-D plot is formed with three anatomical MRI slices (left: sagittal view; right: coronal view; bottom: horizontal view) as background. Node represents the anatomical location of each independent process, localized using a single or dual-symmetric equivalent-current dipole model based on a four-shell spherical head model. Color of nodes represents the degree of outflow. Edges represent causality directions. A P(edge) $\geq$ 0.9 indicates that over 90% of participants have a significantly nonzero connectivity magnitude in that edge. Out-degree indicates the number of outgoing edges.

Compare EEG- and non-EEG-based fatigue monitoring systems: UCSD/NCTU teams have conducted a study to test the efficacy of arousing feedback triggered by EEG-based fatigue detection and mitigation system, compared to that of non-EEG-based counterpart. The study results were published in an article in *International Journal of Neural Systems* (Huang et al. 2016).

Another study demonstrates the feasibility of an online closed-loop EEG-based fatigue prediction and mitigation system that detects physiological change and can thereby prevent fatigue-related cognitive lapses. Figure 8.8 shows the flowchart of the experimental protocol (left panel) and the criteria for delivering warning feedback to drivers during driving tasks (right panel). In the first session, we determined a rational warning threshold for each subject. In the second session, a warning was delivered if the average alpha-band power exceeded the warning threshold.

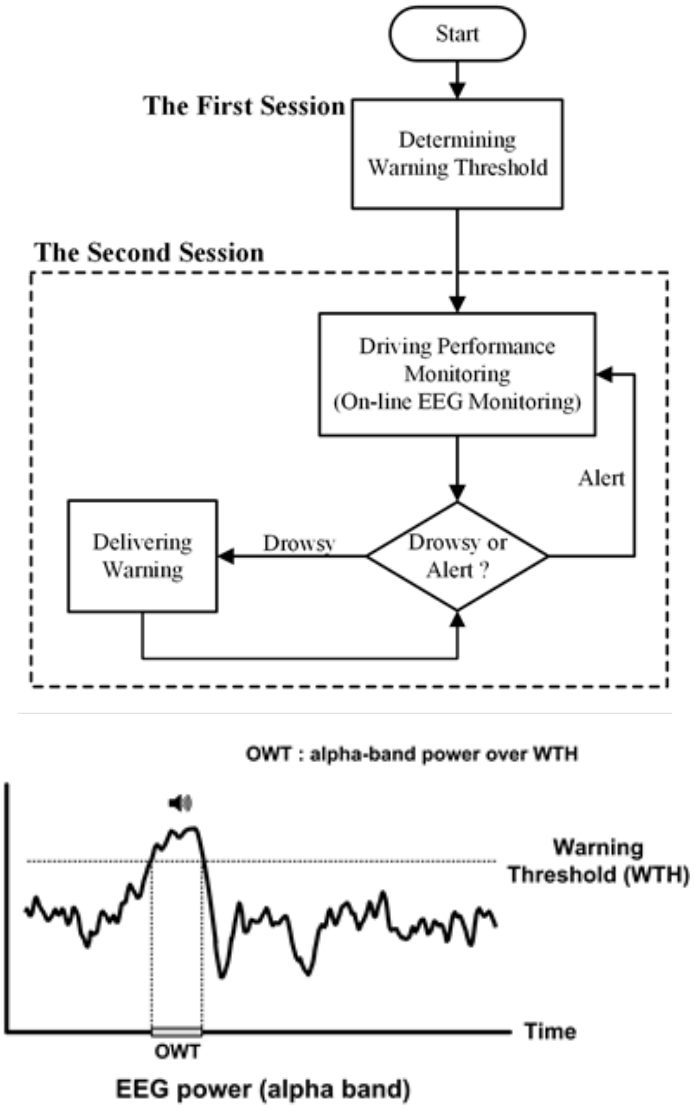


Fig. 8.8 The flowchart of the experimental protocol (left panel) and the criteria for delivering warning feedback to drivers during driving tasks (right panel)

8.2 Brain–Computer Interface: Effects of State Changes on BCI Technologies over Long Time Periods (BCI-GEM)

Columbia, DCS, NCTU, UCSD

Activities supported to overcome barriers included the following:

- Acquisition and processing of high-dimensional data sets that characterize physical, mental, and physiological behavior, as well as its environmental context, in sufficient detail and across a sufficient breadth of circumstances
- Discovery of models and novel methods for the identification and interpretation of statistical relationships among high-dimensional data sets characterizing the dynamics of environment, behavior, and brain function during complex task performance

8.2.1 BCI-GEM Goals

The goal of this project was to utilize a game scenario to investigate, longitudinally, how changes in user state affect a set of EEG signals that have been traditionally employed in BCI systems. We hypothesized that these signals will cause BCI performance to change over time but that much of this change is systematic and can be dealt with if appropriately characterized, modeled, and/or accounted for. If identifying and understanding these changes in neural signals and BCI performance over time proves feasible, we hypothesize that developing an adaptive approach that accounts for these changes during BCI usage over multiple timescales will enhance overall BCI performance. The specific aims of this three-year project are the following:

1) Explore the effect of fatigue on the neural signals underlying several standard BCI implementations and the resulting effect on BCI performance during long-term BCI use.
2) Gain insight into the neural correlates of the process of BCI skill acquisition and the effects of long-term BCI usage on human neural signals.
3) Develop an adaptive approach to BCI based on a characterization of neural state changes associated with long-term BCI use over multiple timescales.

To address these aims, this project collected a large amount of data from subjects using standard BCIs over a long period of time. To encourage subjects to use the BCIs, we embedded the BCIs into a game. This game design emphasized several key concepts, including entertainment, engagingness, replayability, and ease of development. We based the design of the game on a known genre that is entertaining, engaging, and highly popular, and then integrate BCIs into it. This

will result in a game that can be fun for hours, making the long-term data collection less onerous for the subjects, and thereby reducing subject attrition.

8.2.2 BCI-GEM Accomplishment

8.2.2.1 Game Development (NCTU)

The NCTU team developed the BCI-GEM game in which there were five designed BCI applications including attention, motor imagery, SSVEP, ERN, and RSVP. Figure 8.9 shows the layout of BCI-GEM. Behavior, eye movements, EEG, and other physiological information were acquired simultaneously.

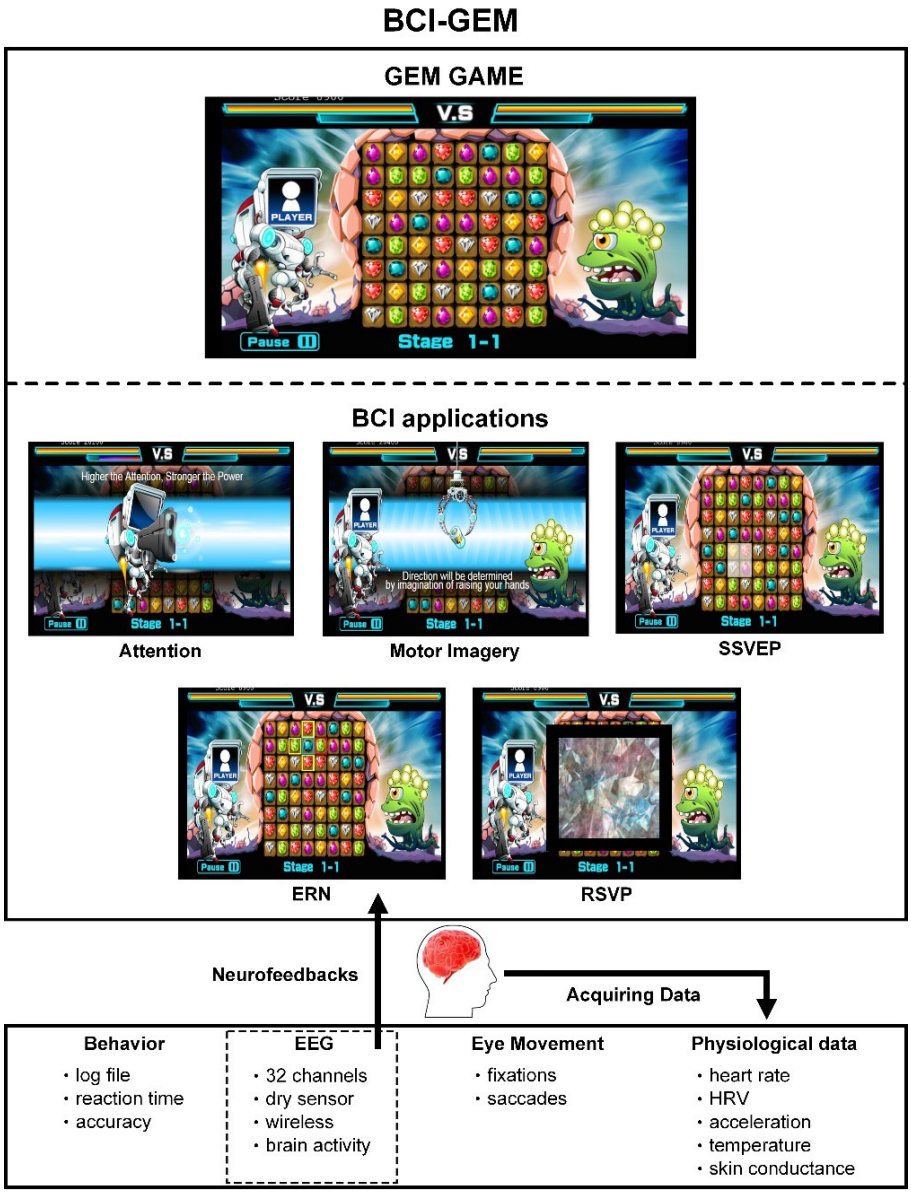


Fig. 8.9 Structure of the developed BCI-GEM and the acquired relative data

To acquire the EEG data, MINDO-32 was tested in NCTU. One classical RSVP paradigm was utilized in this testing as shown in Fig. 8.10a. The measured EEG data in Pz channel were shown in Fig. 8.10c. The red (blue) line represents the ERP induced by targets (non-target) as performing RSVP. One nonlinear algorithm called data-reused radial basis function network (DR-RBFN) was applied to the acquired EEG data for estimating the potentials. Figure 8.10d shows the estimated ERPs through different number of trials/epochs. To efficiently analyze the measured EEG data induced by RSVP, an automated pipeline was modeled for preprocessing, removing noise, and estimating the potentials.

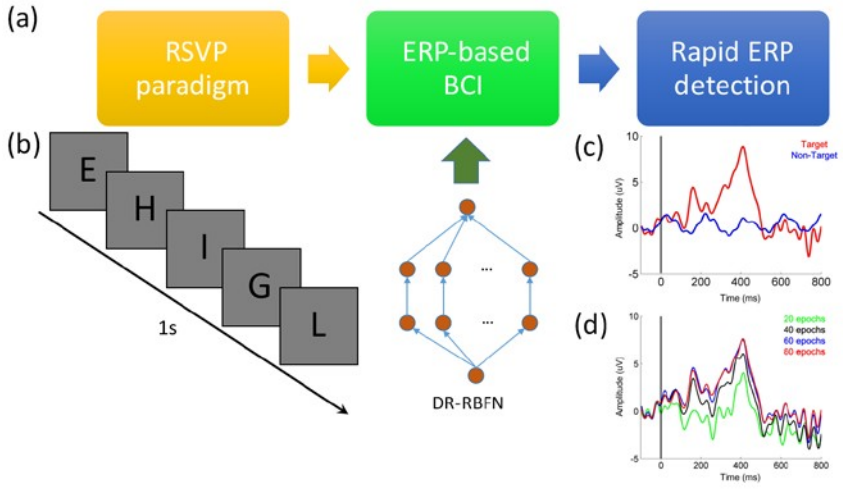


Fig. 8.10 Rapid ERP detection. a) Radial basis function network applied to ERP-based BCI. b) RSVP paradigm. The uppercase letters randomly present to subjects who are instructed to respond to the target (i.e., the letter "G"). Performance comparison of the ERP was estimated by evolutionary algorithm (EA) and DR-RBFN algorithm. c) ERP estimated by applying EA on 80 epochs. Red and blue traces represent the target- and non-target-evoked ERPs, respectively. d) Target-evoked ERP estimated by applying DR-RBFN on 20 (green), 40 (black), 60 (blue), and 80 (red) epochs.

Algorithm development: We have successfully developed a SSVEP algorithm based on CCA and implemented it into the BCI-GEM. Basically, the test performance of this algorithm can reach 90% accuracy in the low frequency band and different presentation durations (Table 8.1).

Table 8.1 Classified performances of SSVEP developed by NCTU

Time length / Subject	2	3	4	5
S1	88.54	95.83	96.88	97.92
S2	95.83	98.96	100.00	100.00
S3	93.75	95.83	97.92	97.92
S4	91.67	95.83	94.79	97.92
S5	88.54	91.67	96.88	98.96
S6	90.63	97.92	97.92	96.88
S7	87.50	93.75	95.83	96.88
S8	97.92	97.92	98.96	97.92
S9	98.96	98.96	98.96	98.96
s10	90.63	97.92	98.96	100.00
Avg	92.40± 3.84	96.46 ± 2.24	97.71± 1.53	98.33± 1.06

For longitudinal experiment, we set two identical platforms for acquiring physiologic and behavioral data during executing BCI-GEM. EyeTribe and EEG recording systems (cf. Figs. 8.11 and 8.12) were established in our platforms. In particular, all data were synchronized through LSL, which is an open-protocol proposed by SCCN of UCSD for synchronizing data collection.



Fig. 8.11 Two platforms were set for acquiring physiological data as executing BCI-GEM

Sampling rate	30Hz and 60Hz mode
Accuracy	0.5° - 1°
Spatial Resolution	0.1° (RMS)
Latency	<20ms at 60Hz
Calibration	9, 12 or 16 points
Operating range	45cm - 75cm
Tracking area	40cm x 30cm at 65cm distance (30Hz)
Screen sizes	Up to 24"
API/SDK	C++, C# and Java included
Data output	Binocular gaze data
Dimensions (W/H/D)	20 x 1.9 x 1.9 cm (7.9 x 0.75 x 0.75 inches)
Weight	70g
Connection	USB3.0 Superspeed



Fig. 8.12 EyeTribe tracker was tested for monitoring the eye movement

Four data sets were acquired through MINDO-32 and Neuroscan for pilot tests, and each participant performed one pilot session with 1 h. According to the results of pilot test, some issues included integrating the ABMx10 were addressed. For general purposes, the event can be outputted through the parallel port in the current version. The time issue was also tested. The event can be recorded with correct time information in the text file. All information during playing the GEM game was also recorded as one text file in the current file for further analysis.

One preliminary questionnaire was created. Each subject needed to fill it out prior to game playing and also made the feedbacks and comments about the BCI-GEM after finish the experimental session. According to the feedbacks and comments, the bugs in the BCI-GEM were fixed.

8.2.2.2 Analysis: Motor Imagery (UCSD, NCTU)

Analysis by Nascimben et al. (2016b) was focused on calibrations sessions before and after playing the game (untrained session) for 90 min. According to previous findings event-related desynchronization (ERD) seems unaffected by movement durations and brief movement imagery has a larger impact on pre-movement mu ERD rather than continuous movement. For this reason, the analysis window was extended from –1 s before arrow onset to 1 s after its appearance. EEG was preprocessed to extract epochs (–3 to +5 s from arrow appearance marker) and filter data (7–30 Hz) with a two-way least-squares finite impulse response (FIR). A preliminary screening on calibration data running a combination of CSP spatial filter for feature extraction and LDA as classifier was performed to include only participants able to perform a motor imagery (MI) task. During this offline procedure, only those who scored at least 70% of accuracy were included in the study (four subjects were excluded). To analyze EEG features, only the mu band (8–13 Hz) was isolated from data and only the C3 or C4 contralateral to movement was taken in consideration. Time interval between –3 to –1 s before onset of movement (i.e., time 0 s) of each epoch was considered as baseline and average power spectrum across subjects was calculated for each second.

While before playing BCI-GEM, the MI-related mu-band power decrease is sustained along all the interval from –1 to +1 s (–1 to 0 s 45% of ERD, 55% in 0 to +1 s), after 90 min of BCI-GEM playing, the MI ERD is concentrated in interval from 0 to 1 s (–1 to 0 s 10% of ERD, 90% of ERD in 0 to +1 s). In both situations at +2 s, EEG returned at the level reached in baseline. Focusing on 10–12 Hz mu-band same phenomenon is described with an ERD ending at +2 s in calibration data after playing BCI-GEM.

A study on baseline power composition was performed: in the 8–14 Hz band on the Cc electrode after playing the game, a relative decrease of lower mu representation (8–10 Hz) was found after playing BCI-GEM (L: –22%, R: –13%). If frequencies include an upper theta (6–8 Hz), the upper theta and lower mu decrease (T L: –15%, R: –11% lower mu L: –7.5%, R: –4%) in comparison to the upper mu bands (10–12 and 12–14 Hz) after playing BCI-GEM. In fact, dividing ERD in two subbands (8–11 and 11–14 Hz), the ERD is still less evident after playing BCI-GEM in the 8–11 Hz (L: –30% R: –76%) band, but an inverse behavior in the 11–14 Hz band is present compared to results before playing BCI-GEM. In the 11–14 Hz band, a power decrease is more evident after playing the game (L: +28%, R: +14%), reflecting higher frequency representation found in the baseline.

According to previous literature findings (Nascimben et al. 2016a), alpha oscillations can be related to cognitive performance both as tonic or phasic changes. Alpha band recorded during an eyes open resting EEG from C3 and C4 electrodes has already been applied as predictor of MI BCI feedback. Considering these two discoveries, we tried to verify if MI outcome can be predicted by alpha variations in a larger scalp area. To achieve this result, we extended data collection to 15 electrodes surrounding primary motor cortex.

Upper alpha (10–12 Hz) is the frequency range mainly involved in MI mechanism of primary motor cortex EEG desynchronization. We decided to verify if variations over time of the resting upper alpha derived from 15 electrodes have a correlation with intra-day changes of MI accuracy (Fig. 8.13). The non-parametric Spearman's correlation coefficient ($r = 0.675$, $n = 10$) between MI accuracy and upper alpha tonic changes is significant ($p = 0.032$) at the level $\alpha = 0.05$ (two tailed test).

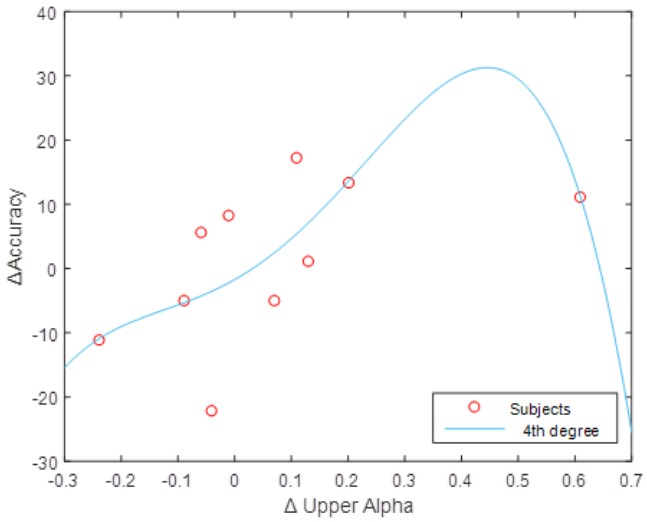


Fig. 8.13 Polynomial model ($r^2 = 0.41$ incl. all subjects) of resting upper alpha–MI accuracy relationship. On y-axis, MI Accuracy changes; on x-axis, resting upper alpha variations between sessions.

Training is fundamental in BCI systems to achieve a stable performance over time (Nascimben et al. in preparation). Mental preparation before MI can reveal some features able to characterize a trained BCI user. In areas surrounding primary motor cortex, neurophysiological correlates of training are found in alpha subbands as a decrease in electrical-field strengths (measured by global field power [GFP]), increase in signals similarity (with dynamic time warping [TW]), and decrease in their dependency (from mutual information [MutInf]). In addition, GFP values in lower alpha describe also a time-on-task effect.

To evaluate BCI-GEM state changes during mental preparation recordings have been divided in four preprocessed files, each one representing an experimental condition: "Untrained data set at the beginning of videogame", "Untrained data set at the end of videogame", "Trained data set at the beginning of videogame", and "Trained data set at the end of videogame" (Table 8.2). During mental preparation for MI, modifications in lower alpha/mu was discovered with GFP trends while alterations in upper alpha/mu arose from dynamic TW and MutInf analysis. Following table collects GFP values and results of statistical tests ran on GFP single scalar along mental preparation epoch (1 s).

Table 8.2 GFP during mental preparation recordings

GFP lower alpha / mu	Untrained data set at the beginning of videogame	Untrained data set at the end of videogame	Trained data set at the beginning of videogame	Trained data set at the end of videogame
F	101.6048	100.7976	107.012	80.9468
FC	111.5283	83.489	112.7795	80.3506
C	156.4035	92.1248	95.4633	81.4104
CP	193.7202	154.1129	145.1939	103.104
P	179.4251	175.3764	133.2048	88.6792
Mean±STD	148.5364±40.7116	121.1801±40.9331	118.7307±20.1489	86.8982±9.6722
Median	156.4035	100.7976	112.7795	81.4104

Creating a subset of central electrodes involved in motor task with values extracted every 200 ms during mental preparation epoch there is a joint inverse relationship between MutInf and dynamic TW in upper alpha (Fig 8.14).

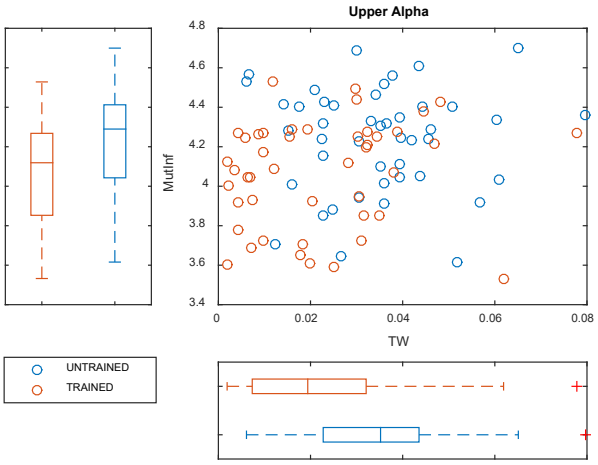


Fig. 8.14 Dynamic TW and MutInf relationship in upper alpha between untrained data set (blue) and trained (orange)

Findings are suggestive for a jointly influence of training in similarity and dependence over motor-related areas signals in upper alpha band. To summarize how training increases similarity and decreases dependency in this frequency range, descriptive statistics are collected in Table 8.3. We can conclude that training produces two effects: in lower alpha, GFP decays over time over the course of the experiment while, in upper alpha, there is a TW–MutInf inverse proportionality relationship.

Table 8.3 MutInf and dynamic TW in upper alpha

Upper alpha	TW (mean ± st dev)	MutInf (mean ± st dev)
Untrained data set	0.034618±0.015643	4.236691±0.267269
Trained data set	0.022302±0.017028	4.063707±0.269594

8.2.2.3 Analysis : Attention (UCSD, NCTU)

During BCI-GEM, EEG data from 1 s prior and 10 s following the onset attentional stimulus were segmented and epoched (Singh et al. 2016). A power spectrum time series was calculated using FFT, which was squared and average for individually frequency band to obtain a measure of the PSD from frontal channel (Fz) for each subject. ERD was also calculated on obtained PSD based on Pfurtscheller method. It is important to note that a positive value of ERD indicates power suppression, while a negative ERD means a decrease in power. Previous studies suggested that visual or other sensory task demand and visual attention in particular were main factors that lead to suppression of lower and upper alpha band power as well as an increase in theta band power. But our results in ERSP and ERD revealed much

more complex picture, where during the attentional processing theta, lower alpha, and upper alpha band power desynchronize simultaneously (Fig. 8.15).

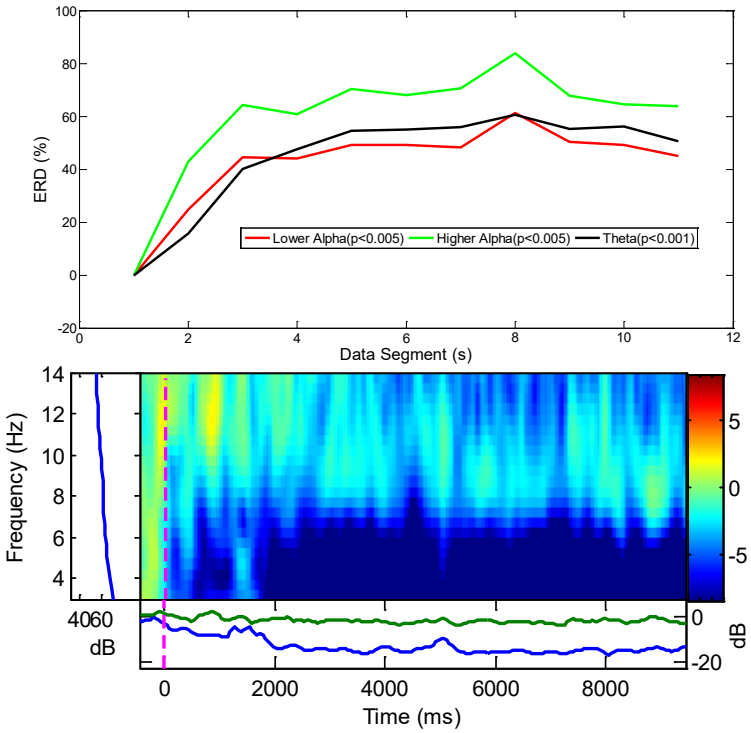


Fig. 8.15 (top) ERD and (bottom) ERSP

In the current study (Singh et al. in preparation), mental fatigue and effect of learning have been evaluated to see how it affect the performance of the subject. Ten subjects have been recruited to record EEG data during performing BCI-GEM experiment in two consecutive months with the gap of four weeks, during this period, subjects were playing BCI-GEM 3 h every week without recording.

Data collected from the subject were epoched for the attentional task and divided into two parts: the first half part and the remaining half part for analysis. Initially, ERP has been compared with the performance of the attentional task.

Figure 8.16 shows ERP changes in topography from the first half and remaining data from two months with the gap of four weeks. It was clearly seen that for the same subject, when they performed the experiment after four weeks of game playing, the training difference between the topography changed significantly ($p < 0.1$), which indicates that the subjects were showing some learning or adaptation effect. On the other hand, there was less evidence found in support of mental fatigue during the task based on the topography of the subjects. We also calculated the score obtained by the subjects (Fig. 8.17) in the first half and second half of game playing. It was found that 70% of subjects showed a 33.3% decline in

score, excluding one subject with a 90% decline in score. This suggests the decline in performance is not only due to mental fatigue, but possibly also due to motivation during the task.

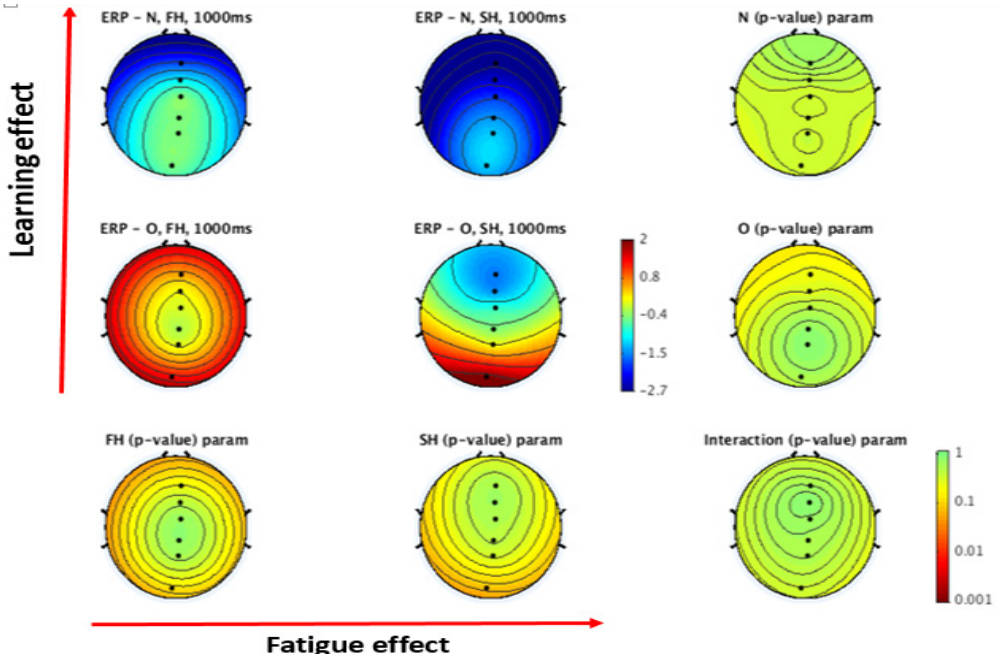


Fig. 8.16 ERP maps for learning and fatigue, where FH = first half data of session, SH = second half data of session; ERP – O (Oct) and ERP – N (Nov) are data from two continuous months with a gap of four weeks

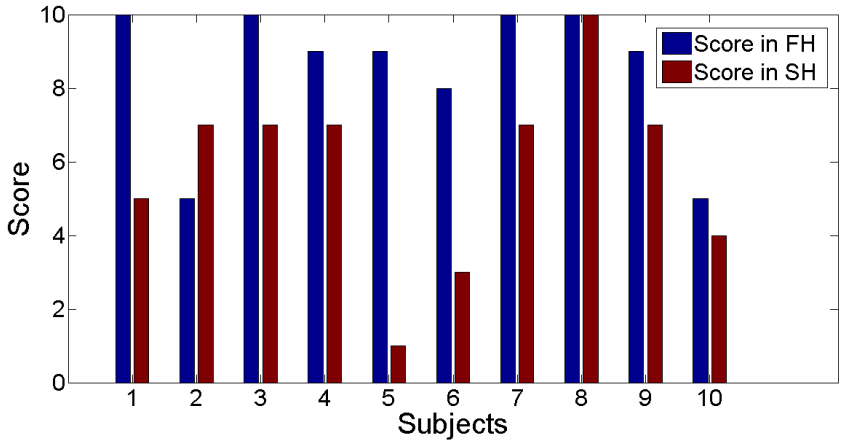


Fig. 8.17 Scores earned by subjects in the attention task

8.2.2.4 Analysis Training Effect

UCSD, NCTU

We studied the training effect on neural activity in the time interval of mental preparation right before MI. In areas close to the primary motor cortex, the neurophysiological correlates of training are observed in the alpha subbands as the

electrical-field strength/GFP declines, as presented in Fig. 8.18. In the low and high alpha band, the similarity of the signals increases with dynamic TW (Fig. 8.19) and their dependency from MutInf decreases (Fig. 8.20). In addition, GFP values in the lower alpha band exhibit a time-on-task effect. These statistical quantities derived from neural activity provide a measurable evaluation of the task-learning effect that can integrate the information theory performance indexes of EEG-based BCIs. These statistical quantities, derived from neural activity, measure the task-learning effect and can integrate the performance indexes of EEG-based BCIs from information theory. Moreover, instantaneous phase shifts between "at the beginning" and "at the end" inside the upper alpha band were calculated in support of this idea by applying a Hilbert transform on the signals of both data sets. From the output of the Hilbert transform, the phase angle difference was extracted. The results are shown in Fig. 8.21. To facilitate the understanding of the graph, a smoothing filter was applied to the data. Phase differences are more constant in the trained data set. This finding are being revised by ARL, UCSD, and NCTU, and a paper entitled "Alpha statistical correlates of learning and time-on-task during mental preparation for motor imagery".

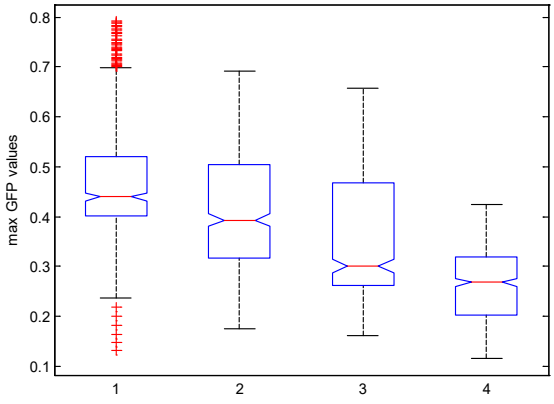


Fig. 8.18 Boxplot of maximal GFP values (y-axis) over experimental time course in lower alpha. Boxplot of maximal GFP values (y-axis) over experimental time course in lower alpha. The x-axis represents four experimental conditions: (from left to right) 1: untrained data set at beginning of gameplay, 2: untrained data set at end of gameplay, 3: trained data set at beginning of gameplay, and 4: trained data set at end of gameplay.

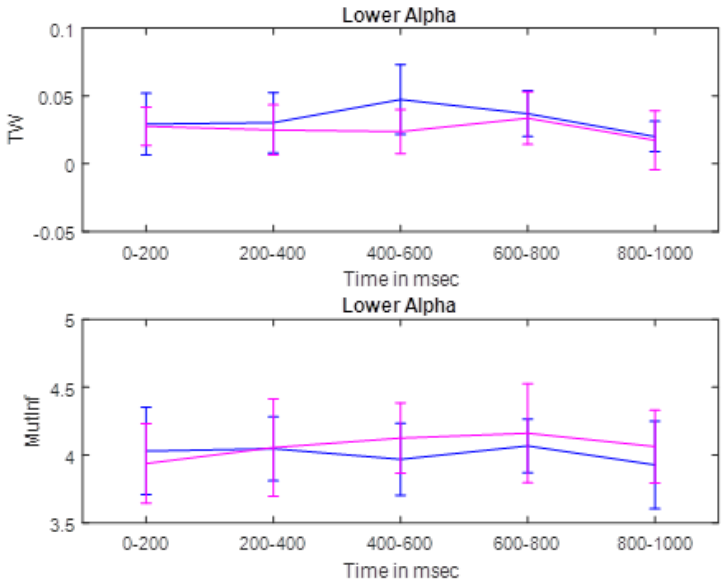


Fig. 8.19 Lower alpha: dynamic TW and MutInf. Lower alpha: dynamic TW and MutInf mean values across time (mean ± std from 15 scalp derivations). Untrained data set in blue, trained data set in violet.

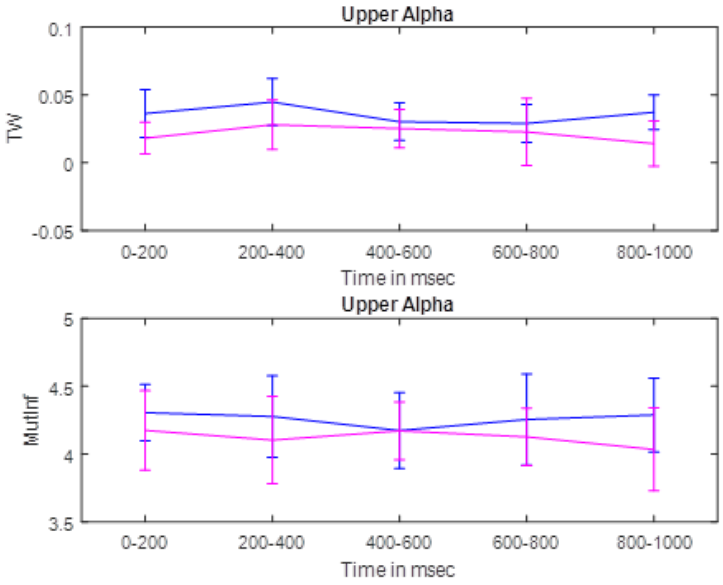


Fig. 8.20 Upper alpha: dynamic TW and MutInf. Upper alpha: dynamic TW and MutInf mean values across time (mean ± std from 15 scalp derivations). Untrained data set in blue, trained data set in violet.

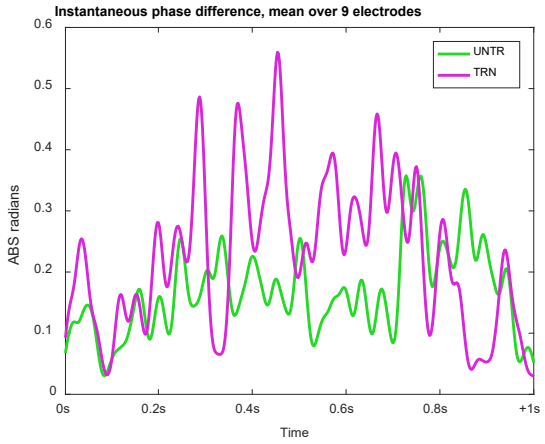


Fig. 8.21 Upper alpha mean of instantaneous phase shifts over FC3, FCz, FC4, C3, Cz, C4, CP3, CP4, and CPz. Upper alpha mean of instantaneous phase shifts over FC3, FCz, FC4, C3, Cz, C4, CP3, CP4, and CPz (same electrodes as Fig. 8.9). Phase differences seem to be more sustained in the intra-session variables of the trained data set (71% of epoch points in the trained data set have a higher instantaneous phase difference).

Developing new algorithms for SSVEP-based BCI: The UCSD BCI team developed a novel data-driven spatial filtering approach for enhancing SSVEP detection based on the task-related component analysis (TRCA), which can enhance reproducibility of SSVEPs across multiple trials. Furthermore, an ensemble method has been developed to combine TRCA filters that correspond to multiple stimulation frequencies. This study also compared BCI performance between the proposed TRCA-based method and the extended CCA-based method using a 40-class SSVEP data set recorded from 12 subjects. The results suggested the proposed TRCA-based approach could significantly improve the classification accuracy compared with the extended CCA-based method. Furthermore, an online BCI speller using the proposed approach achieved an averaged information transfer rate (ITR) of 325.33 ± 38.17 bits/min, a new world record in ITRs, from 20 subjects in a cue-guided target-selection task.

We submitted a manuscript for journal publication early this year. Reviewers requested an online validation of the proposed TRCA. During this reporting cycle, we have conducted online SSVEP BCI experiments across 10 subjects and incorporated the new results into the revision. The results have been published in *IEEE Transactions on Biomedical Engineering* (Nakanishi et al. 2018).

Inter- and intra-subject variability in SSVEP data: UCSD team has investigated the inter- and intra-subject variability in SSVEP data as a fundamental study to elucidate the EEG properties that are crucial for developing transfer-learning approaches. We conducted the first study that systematically and quantitatively assesses the variability in SSVEP data, where the sources of inter- and intra-subject variability were identified using Fisher's discriminant ratios (FDRs). We believe

that the inter-subject variability in the SSVEPs is mostly attributed to the low-frequency components, where we observed ERPs such as N1 at 200 ms after stimulus onset in most subjects. The low-frequency components exhibit different waveforms across subjects, but, intriguingly, they have small within-subject variability. In contrast, the high-frequency components seem to indicate a universal oscillatory pattern across subjects. The insights gained from this work could drive the future developments of transfer-learning approaches to minimize the calibration efforts in high-speed SSVEP BCIs. The results have been submitted to the *IEEE SMC 2018* (Wei et al. 2018).

8.3 References

Huang K-C, Huang T-Y, Chuang C-H, King J-T, Lin C-T, Jung T-P. Validating an EEG-based fatigue detection and mitigation system. Int J Neural Syst. 2016.

Lin C-T, Chuang C-H, Kerick S, Mullen T, Jung T-P, Chen Ko L-W, Chen S-A, King J-T, McDowell K. Mind-wandering tends to occur under low perceptual demands during driving. Sci Rep. 2016;17(6):213253.

Nakanishi M, Wang Y, Chen X, Wang Y-T, Gao X, Jung T-P. Enhancing detection of SSVEPs for a high-speed brain speller using task-related component analysis. IEEE Trans Biomed Eng. 2018;65(1):104–112.

Nascimben M, King JT, Lin CT. Resting upper alpha can predict motor imagery performance? EMBC 2016; 2016a Aug 16–20; Orlando, FL.

Nascimben M, Yu Y-H, Chi C-Y, Singh AK, King J-T, Wang Y-K, Chuang C-H, Chen S-A, Lin C-T. Effect of a cognitive involving videogame on MI task. 6th International Brain Computer Interface (BCI) Meeting; 2016b May 30–June 3; Pacific Grove, CA.

Nascimben M, King J-T, Huang C-S, Chuang C-H, Lin C-T. Alpha statistical correlates of learning and time-on-task during mental preparation for motor imagery. In preparation.

Singh AK, Wang YK, Chiu CY, Yu YH, Nascimben M, King JT, Chuang CH, Chen SA, Ko LW, Pal NR, Lin CT. Attention in complex environment of brain computer interface. Sixth International BCI Meeting; 2016 May 30–June 3; Pacific Grove, CA.

Singh AK, Chuang C-H, King J-T, Lin CT, Ko L-W. Effect of time on task in Attention task performance in Complex environment of brain computer interface. Under revision.

Wei, Chun-Shu, Masaki Nakanishi, Kuan-Jung Chiang, and Tzyy-Ping Jung. "Exploring human variability in steady-state visual evoked potentials." In *2018 IEEE International Conference on Systems, Man, and Cybernetics (SMC)*, pp. 474-479. IEEE. 2018.

9. University of Texas, San Antonio

9.1 ACA-NSST: ACA Improving EEG-Based Detection of Nonstationary Short-Term Spectral Features with Application to Attention and Fatigue (Robbins)

This work began with ARL-UTSA postdoctoral fellow Kenneth Ball in a previous funding cycle and continued with ARL-UTSA postdoctoral fellow John LaRocco. It is currently be pursued by Kay Robbins. The project has the following goals/hypotheses:

- Show matching pursuit can detect nonstationary features such as alpha spindles in driving data.
- Determine whether short-term attention lapses correlate with changes in spectral features such as alpha spindles and microsleeps in BCIT and NCTU data collections
- Detect gamma bursts in EEG using matching pursuit and relate to attention and shifts in cognitive state.

LaRocco and Robbins worked with ARL scientists Piotr Franaszczuk and Scott Kerick to develop spindle detection algorithms based on matching pursuit. A key contribution of this work was the development of methods to set the algorithm parameters based on the geometry of the spindle length and spindle rate curves. A major paper on this work was published in the *Journal of Neural Engineering* (LaRocco et al. 2018).

An open-source spindle toolbox was also released and can be found on GitHub at https://github.com/VisLab/EEG-Spindles. Aim 1 of this project has been completed. Some progress has been made on Aims 2 and 3. We have done some preliminary spindle detection and analysis on RWN VDE as part of Aim 2. In a previous funding cycle, we addressed removal of nonstationary line noise using matching pursuit by developing Band Limited Atomic Sampling With Spectral Tuning (BLASST) (Ball et al. 2017).

This open-source toolbox is available on GitHub at https://github.com/VisLab/blasst. A preliminary version of BLASST has also been incorporated in the PREP pipeline as an alternative to cleanline for line noise removal (https://github.com/VisLab/EEG-Clean-Tools). Removal of line noise without removing signal is an important step in improving the SNR of EEG in the gamma range. Work is ongoing on evaluating gamma bursts and relating bursts to other signal features. This work will continue after the end of the project.

9.2. ACA-SANDR: Standardized Annotated Neurophysiology Data Repository (Robbins)

This project had the following goals:

- Development of software tools for ARL and NCTU legacy data sets.
- Generate learning materials and other resources.
- Process and validate the remaining ARL and NCTU legacy data.
- Preserve, manage, review, and deliver data.

Over the course of the CTA, we have had many collaborative meetings and have done much work on curating the data for errors. We continue to develop many tools to support HED and event annotation. Our original data standard for organizing EEG, ESS, has been supplanted by the Brain Imaging Data Structure (BIDS), which recently incorporated EEG into its data standard. BIDS (https://github.com/bids-standard) has a large community working group. To support the evolution of standards, Joe Lambeth and Jonathan Balraj from our laboratory developed an *ess2bids* converter, which is now available at https://github.com/bids-standard/ess2bids. Robbins has produced a preliminary version of the BCIT data repository in BIDS format and is working to upload this data to openNeuro (https://openneuro.org).

BIDS has adopted HED as the event annotation standard for BIDS. Alexander Jones from our laboratory has developed both syntactic and semantic validators for HED written in JavaScript that have been incorporated into the bids-validator (https://github.com/bids-standard/bids-validator). We also have continued work and clean-up on the base HED validator, which is written in Python. Dung Truong of UCSD has taken over the development of the CTAGGER tools for MATLAB and has adapted them to now use the Python validator so that we only have to maintain one code base for validator. We also maintain an online web validator (https://visual.cs.utsa.edu/hed) and planned to transfer this online validator to a permanent home at the San Diego Supercomputer Center at UCSD during the summer of 2020. Figure 9.1 shows a screenshot of the online HED validator.

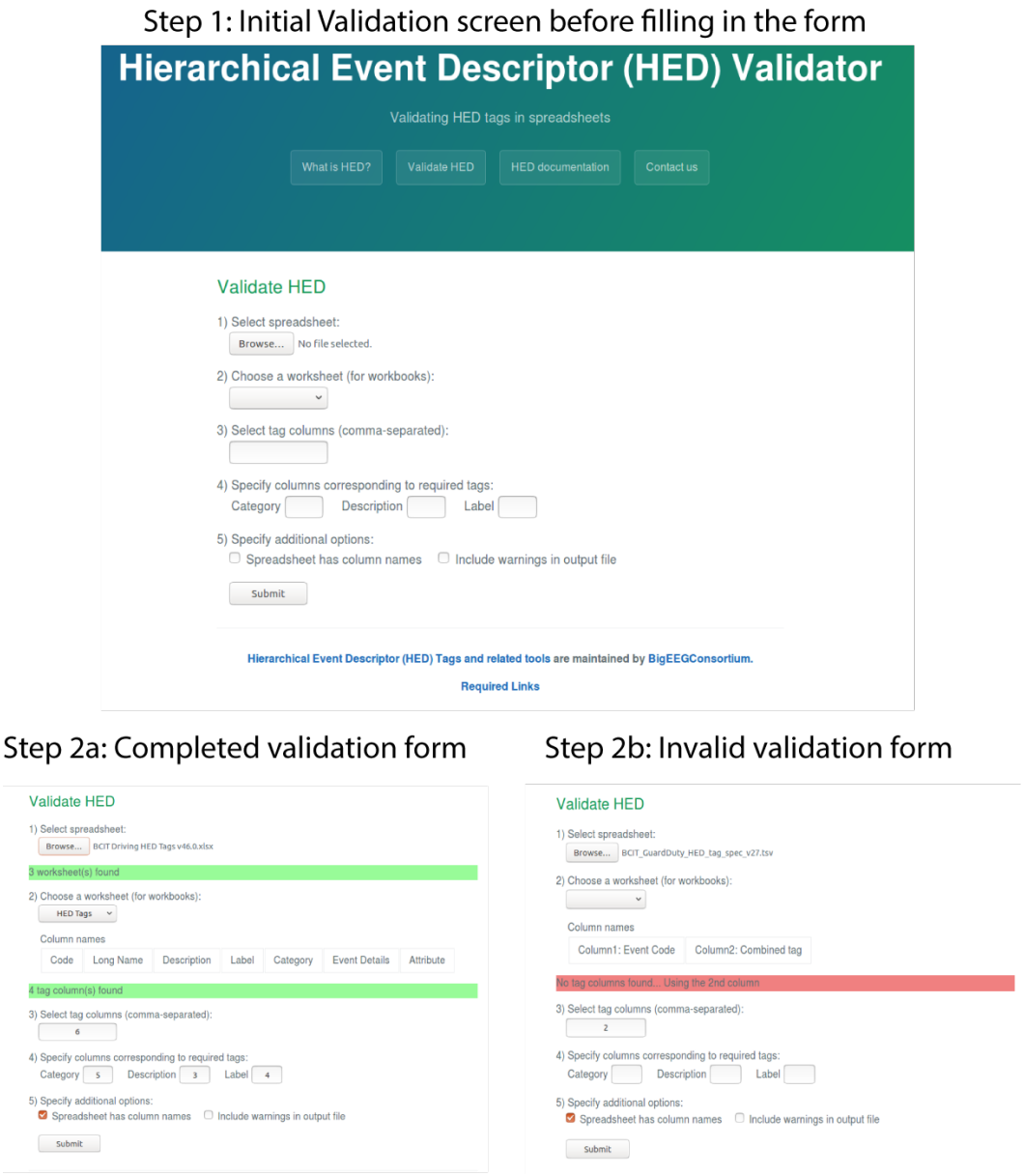


Fig. 9.1 Composite screenshots of the new online HED validator

For the last few months, Robbins has been meeting with a working group that includes Scott Makeig and Arno Delorme of UCSD about creating a community standardization group for HED and incorporating HED more integrally into EEGLAB and related efforts. Robbins has created https://github.com/hed-standard, which parallels the structure of https://github.com/bids-standard to host the HED community development. The repositories https://github.com/hed-standard/hed-specification, https://github.com/hed-standard/hed-javascript, https://github.com/hed-standard/hed-python, and https://github.com/hed-standard/hed-matlab are under active development.

9.3 ACA/BCI/RWN-LARG: Large-Scale EEG Analysis and Validation of Event Tags (Robbins)

The first phase of the LARG project was begun in the previous funding cycle. The original project aims were the following:

- Understand how event properties are related to EEG dynamics.
- Quantify the effect size.
- Develop and validate optimal methods for aggregating large-scale multi-study data.

The three main hypotheses associated these aims were verified on 18 studies from the CAN_CTA data repository:

- ARL_AdvancedGuard,
- ARL_AuditoryCue,
- ARL_BaselineDrive,
- ARL_BasicGuard,
- ARL_CalibrationDrive,
- ARL_MindWandering,
- ARL_RSVPBaseline,
- ARL_RSVPExpertise,
- ARL_SpeedControl,
- ARL_VEP,
- ARL_TrafficComplexity,
- NCTU_DAS,
- NCTU_DD,
- NCTU_LKwAF,
- TNO_ACC, and
- UCSD_RSVP.

This work resulted in the processing of more than 1000 EEG recordings with millions of event epochs. The work relied on being able to effectively automate the preprocessing pipeline, which strongly relies on our PREP for preprocessing and

our BLINKER tool for automatically identifying eye blinks in EEG signals. Papers describing these tools were published in the previous funding cycle and open-source tools were released and are currently being maintained on GitHub.

We published two major papers in *Neuroimage* describing this work during this funding cycle (Bigdely-Shamlo 2019a, 2019b).

Much of the revisions and editing of these papers occurred during the current funding cycle. These papers represent a collaboration of Robbins of UTSA with Jonathan Touryan of ARL, and Nima Bigdely-Shamlo, Tim Mullen, and Christian Kothe of Intheon.

In the LARG project, the Robbins lab also began working on automatic EEG annotation. Traditional time-locked EEG analysis tries to determine the neural response given a stimulus. Annotation looks at the inverse problem—trying to determine where in the signal particular neural responses occur. Using domain adaptation transfer learning techniques, we showed that automated EEG annotation is possible. This work was done in collaboration of W Dave Hairston of ARL and resulted in several publications (Su et al. 2016, 2018; Robbins et al. 2020).

In addition, we released an open-source annotation tool implementing these algorithms, available at https://github.com/VisLab/EEG-Annotate. This work has continued in the LARG II project as described in Section 9.4.

9.4 ACA Large-Scale Electroencephalography (EEG) Analysis and Exploration of Cognitive Aspects (LARG-II) (Robbins and Huang)

The LARG-II project is a continuation of LARG from the previous funding cycle, but has three additional aims:

1) Examine and quantify variability across studies. Included in this analysis is quantifying inter-subject and intra-subject variability.

2) Expanding the ERP and ERSP analysis of LARG to distributed source ROIs to systematically relate activations of canonical networks to cognitive aspects, as represented by HED tags and to behavior.

3) Capture discriminative features associated with behavior and cognitive aspects as represented by HED tags using large-scale semi-supervised and multitask learning based on generative adversarial networks (GANs) and other methods.

An important step in characterizing variability is to understand how the selection of processing methods and other factors influence variability across studies. The group working on this included Robbins of UTSA, Touryan of ARL, and Bigdely-Shamlo, Mullen, and Kothe of Intheon.

For each study-specific event code, we compare the correlation and the fraction variance explained of individual recording ERPs and ERSPs with the corresponding study-wide averages. We found that that z-scoring the event-related features before computing study-wide averages greatly improved the amount of variance explained by the study-wide averages. We also found that the Multiple Artifact Rejection Algorithm (MARA) had better correlation and variance explained than LARG when all event-codes were considered. However, when only event-codes corresponding to experimental stimuli were considered, there was no significant difference.

We expanded our analysis of how much difference the selection of processing methods made on downstream results and published an extensive analysis in Robbins et al. (2020).

Included with this analysis is an open-source repository with code implementing various pipelines (https://github.com/VisLab/EEG-Pipelines). An important conclusion of this work is that often 70% to 80% of the variability in ERPs and ERSPs can be attributed to often fairly minor differences in processing. We propose, as a general methodology, that researchers should select several automated processing methods to process their EEG and compare downstream results to understand how much differences in processing affect their results.

Robbins and her lab have also begun a more detailed characterization of variability due to subject using the NCTU RWN VDE corpus because the corpus includes up to 9 repeats on different days of 6 different tasks for 17 subjects. We have extracted blink indicators using our BLINKER tool and have done some preliminary analysis on alpha spindles and other signal characteristics. This data set also includes a signal recorded from an EEG sensor recorded on the chest. HRV, differences in the time between heartbeats, has shown to be a strong physiological measure of subject state. We decided to include HRV in our analysis of inter-/intra-subject variability. However, we found that existing tools could not adequately extract heart beats from EEG sensors without extensive manual intervention. We have developed an automated tool to extract this information on an entire study. We are in the final stages of validating the tool and developing the GUI for inclusion as an EEGLAB plug-in. We have a draft paper entitled “Automated extraction of physiological indicators based on heart rate variability (HVR) measures using EEG/ECG”.

Intheon has primary responsibility for Goal 2, which involves a large-scale study of connectivity and canonical networks. Robbins has provided processed data for this analysis and has participated in the writing of two extended abstracts and posters on this work presented at NER'19. She also participated in the writing of a short paper that was submitted to SMC'19 on this subject.

For Goal 3, Yufei Huang and his lab have been investigating the GAN models for generating the EEG signals. This work is a continuation of the development of deep learning approaches begun in previously funded projects to facilitate transfer learning across subjects and develop reliable biomarkers for stress and fatigue. We proposed a new up-sampling module for the generator, which combines the advantage of interpolation and deconvolution. This module preserves the advantage of bilinear interpolation by avoiding artifacts and at the same time provides a trainable deconvolutional kernel, which helps to match the amplitude of generated samples with real samples. We also adopted the conditional GAN architecture to address the mode collapsing. We have trained such a filter using BCIT X2 RSVP data and the results show that the proposed filter can generate samples mimicking the EEG signals for target and non-target events. Three papers were presented at SMC'19 Workshop on Deep Learning and Transfer Learning for BCI (Nayak et al. 2019; Panwar et al. 2019a, 2019b).

The GAN work was expanded and has been accepted to the special issue in *IEEE TNSRE* (Panwar et al. 2019c).

Robbins and her lab have also been continuing work related to goal 3 by incorporating self-supervised learning using contrastive predictive coding and deep networks to improve automated EEG annotation.

9.5 References

9.5.1 Journal Articles

Ball KR, Hairston WD, Franaszczuk PJ, Robbins KA. BLASST: Band Limited Atomic Sampling With Spectral Tuning with applications to utility line noise filtering. IEEE Trans Biomed Eng. 2017 Sep;64(9):2276-2287. doi: 10.1109/TBME.2016.2632119. Epub 2016 Nov 23. PMID: 27893379.

Bigdely-Shamlo N, Touryan J, Ojeda A, Kothe C, Mullen T, Robbins K. Automated EEG mega-analysis I: Spectral and amplitude characteristics across studies. Neuroimage. 2019a Nov 23:116361. doi: 10.1016/j.neuroimage.2019.116361, PMID: 31770636.

Bigdely-Shamlo N, Touryan J, Ojeda A, Kothe C, Mullen T, Robbins K. Automated EEG mega-analysis II: Cognitive aspects of event related features. Neuroimage. 2019b Sep 4:116054. doi: 10.1016/j.neuroimage.2019.116054, PMID: 31491523.

Chen J, Mao Z, Zheng R, Huang Y, He L. Feature selection of deep learning models for EEG-based RSVP target detection. IEICE Transactions on Information and Systems. 2019b;E102.D.:836–844. 10.1587/transinf.2018EDP7095.

Chen JX, Zhang PW, Mao ZJ, Huang YF, Jiang DM, Zhang YN. Accurate EEG-based emotion recognition on combined features using deep convolutional neural networks. IEEE Access. vol. 7, pp. 44317-44328, 2019a. doi: 10.1109/ACCESS.2019.2908285

LaRocco J, Franaszczuk P, Kerick S, Robbins K. Spindler: a framework for parametric analysis and detection of spindles in EEG with application to sleep spindles. J Neural Eng. 2018 Sep;15(6):066015. PMID: 30132445 DOI: 10.1088/1741-2552/aadc1c. PMID: 30132445 DOI: 10.1088/1741-2552/aadc1c.

Panwar S, Rad P, Jung T-P, Huang Y. Modeling EEG data distribution with a Wasserstein generative adversarial network to predict RSVP events. Accepted for IEEE Transactions on Neural Systems and Rehabilitation Engineering; 2020. http://arxiv.org/abs/1911.04379.

Robbins KA, Touryan J, Mullen T, Kothe C, Bigdely-Shamlo N. How sensitive are EEG results to preprocessing methods: A benchmarking study. IEEE Transactions on Neural Systems and Rehabilitation Engineering; 2020. doi: 10.1109/TNSRE.2020.2980223.

Su K-M, Hairston D, Robbins K. EEG-Annotate: Automated identification and labeling of events in continuous signals with applications to EEG. J Neurosci Methods. 2018;293:359–374.

9.5.2 Papers Submitted to Conferences

Hanada G, Wong C-K, Robbins K, Bigdely-Shamlo N, Touryan J, Mullen TR. Large-scale analysis of canonical cortical network dynamics across five visual target detection tasks. Submitted to IEEE 2019 International Conference on Systems, Man and Cybernetics; 2019; SMC'19.

Nayak T, Ko L-W, Jung T-P, Huang Y. Target classification in a novel SSVEP-RSVP based BCI gaming system. Submitted to IEEE 2019 International Conference on Systems, Man and Cybernetics; 2019. SMC'19.

Panwar S, Rad P, Quarles J, Huang Y. Generating EEG signals of an RSVP experiment by a class conditioned wasserstein generative adversarial network. Submitted to IEEE 2019 International Conference on Systems, Man and Cybernetics; 2019. SMC'19.

Panwar SJ, Rad P, Quarles J, Golob E, Huang Y. A semi-supervised Wasserstein generative adversarial network for classifying driving fatigue from EEG signals. Submitted to IEEE 2019 International Conference on Systems, Man and Cybernetics; 2019. SMC'19.

Su K-M, Hairston D, Robbins K. Adaptive thresholding and reweighting to improve domain transfer learning for unbalanced data with applications to EEG imbalance. 2016 15th IEEE International Conference on Machine Learning and Applications (ICMLA; 2016. pp. 320–325.

9.5.3 Extended Abstracts Presented

Bigdely-Shamlo N, Touryan J, Mullen T, Kothe C, Robbins K. Using large-scale ERP analysis to benchmark EEG preprocessing. 9th International IEEE EMBS Conference on Neural Engineering; 2019. NER'19.

Brief summary—We quantify the effect of preprocessing methods on downstream EEG analysis, using two simple measures: correlation of ERPs with z-scored study grand averages and fraction of variance explained by the z-scored respective study averages. We compare these measures for two preprocessing approaches (LARG and MARA) across 17 EEG studies.

Hanada G, Wong C-K, Robbins K, Bigdely-Shamlo N, Touryan J, Mullen T. Characterizing differential effects of cognitive aspect on canonical cortical network activity in a visual target detection task. 9th International IEEE EMBS Conference on Neural Engineering; 2019. NER'19.

Brief summary—We quantify effects of experimental events in an RSVP task on measures of functional integration and information flow within four canonical cortical networks.

Wong C-K, Hanada G, Bigdely-Shamlo N, Touryan J, Robbins K, Mullen T. Mega-analysis of event-related cortical source dynamics. 9th International IEEE EMBS Conference on Neural Engineering; 2019. NER'19.

Brief summary— We apply a large-scale analysis pipeline to quantify dependencies between experimental events and temporal and spectral EEG activity within cortical regions of interest across 1155 recordings in 17 studies.

10. University of Pennsylvania

10.1 Overall Contribution to the CaN CTA

The Falk Lab team joined the CaN CTA in 2015, contributing to the alliance's overall goal of applying neuroscience-based research and theory to complex operational settings by providing insight into the influence of social context on human decision-making and performance. Social influence is one of the most powerful determinants of human behavior, and understanding human performance in the real world must therefore account for the fact that social context shapes brain dynamics that account for human variability in learning and behavior. Understanding the performance of individuals in dyads, networks, and other social contexts is essential for predicting and improving performance in the naturalistic, operational contexts targeted by research at ARL.

In work under the CaN CTA, the Falk Lab team has integrated tools from neuroscience, network science, and social science to understand the interplay between social context and brain–behavior relationships. We collaborated with teams at ARL and DCS on the Real World Driving Project, and found effects of information framing (humor) on communication success and brain synchrony within dyads during retelling of the information (see Section 10.2).

Methodologically, we studied differences between metrics of neural synchrony between dyads in this realistic context. Our collaborations on this project also found that risk preferences are communicated within dyads, affecting real driving behavior as well as brain synchrony within dyads. Selected supported work on other data sets provided additional support for the ways that social context relates to brain function. For example, we found relationships between brain dynamics and social behaviors (Wasylyshyn et al. 2018; Lauharatanahirun et al. 2020; Tompson et al. 2018, 2019a, 2019b; Baek et al. in prep), such as opinion change in response to feedback from others; effects of social network structure on the brain and behavior (Schmälzle et al. 2017; Pei et al. in prep); and effects of information context on neural prediction of health behaviors (Cooper et al. 2018, 2019; Doré et al. 2019; Schmälzle et al. under review). This work has contributed to the development of ongoing programs at ARL, particularly the Strengthening Teamwork for Robust Operations in Novel Groups (STRONG) initiative. Together, these advances aid our ability to predict and improve performance in social contexts.

10.2 Real-World Neuroimaging Vehicle Driving Experiment

The Falk Lab team worked with the teams at ARL and DCS to design, develop, and conduct analysis of the Real World Driving Project. Our research objectives were to understand human variability during interaction with a vehicle traveling on roadways during regular traffic, as well as to understand inter- and intra-personal brain and behavioral dynamics during both laboratory tasks and real-world driving. Results for each specific aim are as follows.

10.2.1 Aim 1

Given that many key tasks require coordination between team members, one of whom may be operating a vehicle, it is critical to understand how successful communication is accomplished in this environment. In Aim 1, we have examined factors that facilitate successful communication (including information valence), and tested whether neural synchrony between driver and passenger during the drive predicts successful communication, as indexed by the driver's recall of task-related information communicated by passenger. Analysis for Aim 1 was led by former graduate student/now postdoc Dr Elisa Baek and current graduate student Prateekshit Pandey, in collaboration with Drs Jean Vettel, Javier Garcia, and Nina Lauharatanahirun.

> **H1a:** *Memory for information in the humorous framing condition would be greater than in the neutral condition.*

We found behavioral evidence to support the hypothesis that humor is more memorable than neutral information; passengers (communicators) and drivers (receivers) performed with better accuracy on the recognition memory task for humorous compared to neutral information (B = 0.197, z = 2.19, p = 0.028, n observations = 2756, n pairs = 43).

> **H1b:** *Greater levels of synchrony in language and neural activity (as indexed by inter-subject correlation in EEG signals) within a dyad would be associated with higher accuracy on the post-drive memory tasks.*

We explored trial-by-trial EEG activity as well as neural synchrony between passengers and drivers (indexed by phase locking value [PLV]) to test whether humorous information is encoded differently in the brain during initial exposure as well as during passenger (communicator) recall of the content to the driver (receiver). We found greater alpha PLVs, an indicator of neural synchrony, in anterior brain nodes between passengers and drivers during passenger recall of humorous versus neutral information (B = 0.004; t (538) = 3.269, p = 0.003). We further explored trial-by-trial EEG activity as well as neural synchrony to test

whether information that will be recognized with higher accuracy is encoded differently in the brain during initial exposure and recall. We found results that suggest that increased beta power within posterior brain nodes of passengers is associated with increased accuracy in the recognition memory task (B = 10.398, z = 2.081, p = 0.038). We also found that higher accuracy on the recognition memory task was related to increased alpha power within anterior brain nodes (B = 1.225, z = 1.810; p = 0.070), within posterior brain nodes (B = 1.073, z = 2.131, p = 0.033), within temporal brain nodes (B = 1.030, z = 2.012, p = 0.044), and globally throughout the brain (B = 1.165, z = 2.094, p = 0.036) while passengers were actively recalling news clips. We did not find support for the hypothesis that greater neural synchrony between the driver and passenger predicted accuracy on the memory tasks.

10.2.2 Aim 2

Aim 2 focused on linking language and neural synchrony measures collected during the driving dyad sessions to individual variability in real-world outcomes. Specifically, we focused on links between neural and linguistic synchrony during the drive, and later, real-world experiences related to objectively logged health behavior (specifically sleep and physical activity as measured by wrist-worn accelerometers), as well as daily social interactions.

> **H2a:** *Individuals who show stronger neural and linguistic synchrony with their dyad partner during the interaction portion of the drive will report more enjoyable and supportive social interactions in the weeks following the experiment.*

Data analysis for Aim 2a was led by Drs Bruce Doré and Matt O'Donnell. Drs Doré and O'Donnell completed automated language transcription and electromagnetic articulography (EMA) data cleaning, and developed a collaborative system for manual correction of transcripts by human coders in collaboration with Danny Forster, Steve Tompson, and Dr Vettel's team at ARL. Although there is considerable variation in the audio quality of the interaction portion of the drive and the resulting quality of automated transcripts, we were able to carry out some quantitative linguistic analyses of these transcripts. We experimented with a range of different text similarity measures using the whole transcript segmented by speaker (e.g., mean phrase and segment similarity using fuzzy string matching, and using categorical lexicon Linguistic Inquiry and Word Count [LIWC] proportions, bag-of-words/phrases and cosine similarity, proportion of shared contiguous words) and also taking conversation turn pairs as units of comparison. These measures operationalized as markers of interactional synchrony did not yield any notable patterns of association with the neural measures of synchrony. Because we

were not able to validate a measure of linguistic synchrony on these data, we did not test the predictive capacity of linguistic synchrony measures against social interactions (H2a) or physical activity and sleep behaviors (H2b).

> **H2b:** *Participants with neural and linguistic synchrony during sleep and physical activity messages will show similar trajectories in longitudinal, objectively logged changes in physical activity, sedentary behavior, and sleep patterns.*

Data analysis for Aim 2b was led by Dr Nicole Cooper. We have tested whether individuals who show more correlated neural responses to the health message podcasts delivered during the experimental session also show more similar levels of average sleep and physical activity during the longitudinal follow up period (based on Readiband data). We cleaned and created aggregate measures from Readiband data, in collaboration with Nick Wasylyshyn (formerly at ARL) and Dr O'Donnell. Self-report measures show increases in several positive beliefs toward sleep and exercise following the podcasts, and in perceived norms about sleep and exercise. Across participants, total activity levels and sleep durations before and after exposure to the podcasts did not significantly change. Explorations of whether individual differences in these changes over time relate to neural responses while listening to health podcasts have yielded null results. We examined the alpha and beta frequencies in each node in the frontal and parietal lobes, as well as aggregate measures across nodes. None of these measures relate significantly to changes in physical activity or sleep time.

We further examined PLVs to test whether the similarity of neural responses across individuals relates to similarity in behavior change. We examined mean PLVs in alpha, beta, and gamma frequency bands, within and between anterior, central, and posterior nodes. We related these dyad-wise PLVs to the dyad-wise difference between behavior change scores (% changes in average activity counts and total sleep time). Analyses have not found relationships between mean PLVs between the driver and passenger and changes in physical activity and sleep. Finally, we collaborated with UCLA-ARL trainee Nuttida Rungratsameetaweemana, who developed a measure of speech decoding accuracy from EEG signals during the podcasts. Across individuals, this decoding accuracy measure was not related to later changes in physical activity or sleep.

10.2.3 Further Exploration

We collaborated on work led by Dr Lauharatanahirun on analysis of the extent to which individual differences in social and non-social risk preferences can be explained by 1) previous social experiences and 2) similarity in resting state EEG

brain activity. Risk preferences were calculated for social and non-social conditions of an economic lottery choice task for 38 subjects using a constant relative risk aversion utility function, in which choices were fit to a logistic function using maximum likelihood estimation. A social risk sensitivity (SRS) index (SRS = RP social – RP non-social) has identified different risk preferences across subjects between social and non-social conditions. To account for this variability, we have computed 1) the density of participants' real-life social networks derived from a web-based application and 2) inter-brain similarity indexed by average PLV across pairwise EEG electrodes. Preliminary analyses indicate subjects with higher-density social networks showed lower SRS and those with lower-density social networks displayed higher SRS, with inter-brain similarity as a potential marker of this effect. Our results suggest real-world social experiences and global similarity in neural function may shape decision-making behavior in social exchange.

Graduate student Pandey is working with ARL scientist Drs Lauharatanahirun (now at Pennsylvania State University) and Garcia on implementing a variety of synchrony measures for evaluating dyad EEG synchrony. Synchrony measures include but are not limited to PLV, partial direct coherence (PDC), circular correlation coefficient, Kraskov MutInf, windowed cross-correlation, and CCA. This team is currently preparing a manuscript presenting similarities and differences between these measures using data from the real-world driving experiment (described further later).

10.3 Papers Submitted and Under Review

We have continued to work collaboratively with the team at ARL to co-mentor post-docs and conduct secondary analyses on multiple data sets, which has resulted in several paper drafts and submissions:

1. Schmälzle R, Cooper N, O'Donnell MB, Tompson S, Lee S, Cantrell J, Vettel JM, Falk EB. The effectiveness of online messages for promoting smoking cessation resources: predicting nationwide campaign effects from neural responses in the EX campaign. Frontiers in Human Neuroscience. 2020;14.

   We have submitted a paper titled *The effectiveness of online messages for promoting smoking cessation resources: Predicting nationwide campaign effects from neural responses in the EX campaign*. (with research director Nicole Cooper, former postdoc/new faculty Dr Ralf Schmälzle, and Drs Vettel and Falk) as an invited submission to a special issue of *Frontiers in Human Neuroscience.* We examined neural activity while a group of smokers watched anti-smoking video ads from the American Legacy Foundation's EX campaign. The same video ads were viewed online as banner ads, averaging

nearly 6 million impressions per ad. We related activation patterns for each ad to the click-through-rates resulting from ad impressions online, and found that banners whose brain response bears resemblance to an established negative emotion signature and to a vividness signature have lower population-level click-through-rates (Fig. 10.1). This multivariate "signature" pattern of negative emotion was more strongly predictive of click-through-rates than average univariate activity in a set of negative emotion ROIs.

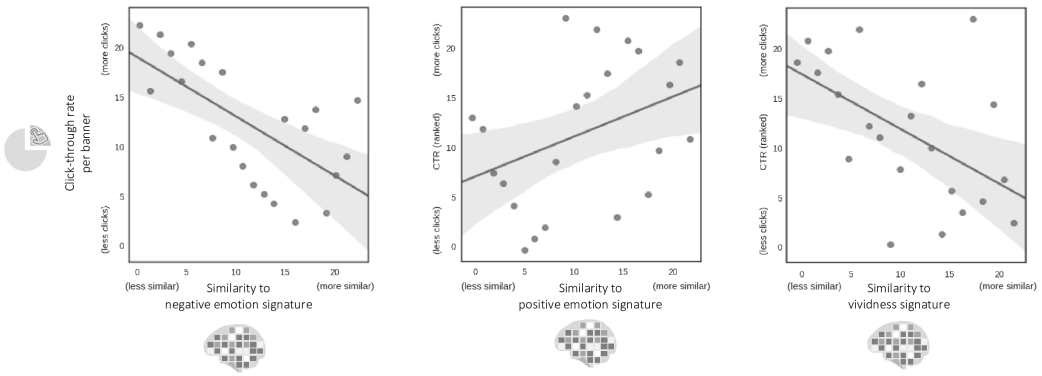


Fig. 10.1 The degree to which the pattern of brain activity for each individual banner matches predefined maps for negative and positive emotion, as well as vividness, is linked to the population-level click-through rate generated by the same banners. Banners that prompt brain activity patterns that better match negative emotion and vividness signatures tend to have lower population-level click-through-rates. All analyses are based on ranked similarity and click-through-rate scores, respectively.

2. Baek EC, Scholz C, O'Donnell MB, Garcia JO, Vettel JM, Falk EB. Mentalizing supports opinion change in response to negative social recommendations. In submission.

   This paper is in the process of being resubmitted to a peer-reviewed journal after additional analyses. This paper focuses on message propagation and successful social influence (with Drs Baek, O'Donnell, Vettel, and Garcia). Our findings show that mean activity within the brain's reward and mentalizing systems is engaged during opinion change in response to social recommendations. In a novel contribution to the field, we show that these effects depend on the valence of the recommendation and are stronger when the social recommendations are higher in negativity (i.e., "this mobile game app is really boring"). Further, negativity of recommendations is associated with mean activation in the brain's mentalizing system. We have also found that decreased functional connectivity between the brain's mentalizing and reward systems is associated with opinion change in response to social recommendations. These results provide important insights into how certain

contextual factors may moderate the processes that have previously been associated with successful social influence.

3. Pei R, Lauharatanahirun N, O'Donnell MB, Vettel JM, Falk EB. Neural risk sensitivity and the number of communities in adolescent's online social network. In preparation.

   We are in the process of preparing a paper (with graduate student Rui Pei, Dr Lauharatanahirun, and Drs O'Donnell and Vettel) in which we examined how adolescents' neural activity during a laboratory risk taking task may be related to their online social network structure (Fig. 10.2). We find that adolescents with higher mean reward-related neural activation during risk taking tend to have more clusters in their social network, and that this association is stronger for smaller clusters in a social network. We also find that greater functional connectivity between ventral striatum (VS) and ACC is associated with fewer social network clusters. These results highlight how contextual factors such as social network position can influence neural activation during decision-making, and that individual differences in neural reward sensitivity may shape their social network structure. This work was accepted for a poster presentation at the Biennial Meeting of the Society for Research on Adolescents (originally scheduled for March 2020 in San Diego, CA; however, the meeting was rescheduled to 2021 due to COVID-19).

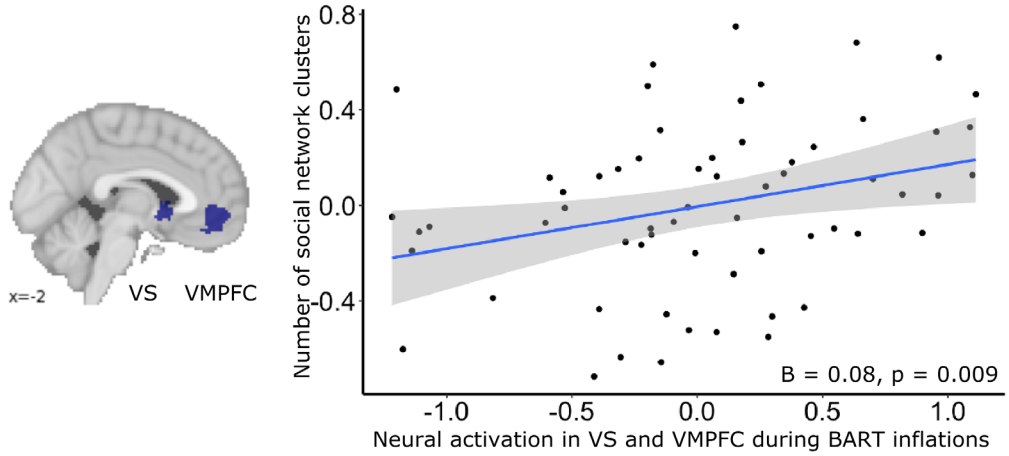


Fig. 10.2 Neural activation during Balloon Analogue Risk Task (BART) balloon inflation in the VS and the ventromedial prefrontal cortex (VMPFC) is associated with the number of social network clusters.

4. Pei R, Lauharatanahirun N, Andrews M, Waldzinska AN, Falk EB. Shared neural responses to health messages underlie similar message evaluation among adolescents. In preparation.

   In this work, led by graduate student Pei and supported by Dr Lauharatanahirun, we examine the association between individuals' evaluation of health messages and inter-subject correlation (ISC) in neural responses when viewing the health messages (Fig. 10.3). Health message evaluations were measured using self-report as well as participants' linguistic feedback. Our data demonstrated that higher ISC in multiple cortical and subcortical regions (i.e., posterior parietal cortex) was associated with higher similarity in message evaluation among participants, indicating that message evaluation is driven by high-level processing of health messages during message exposure. We are conducting further analyses to examine how these regions might work in conjunction with one another during health message processing, and how this relationship might be moderated by social network variables such as social network density and modularity.

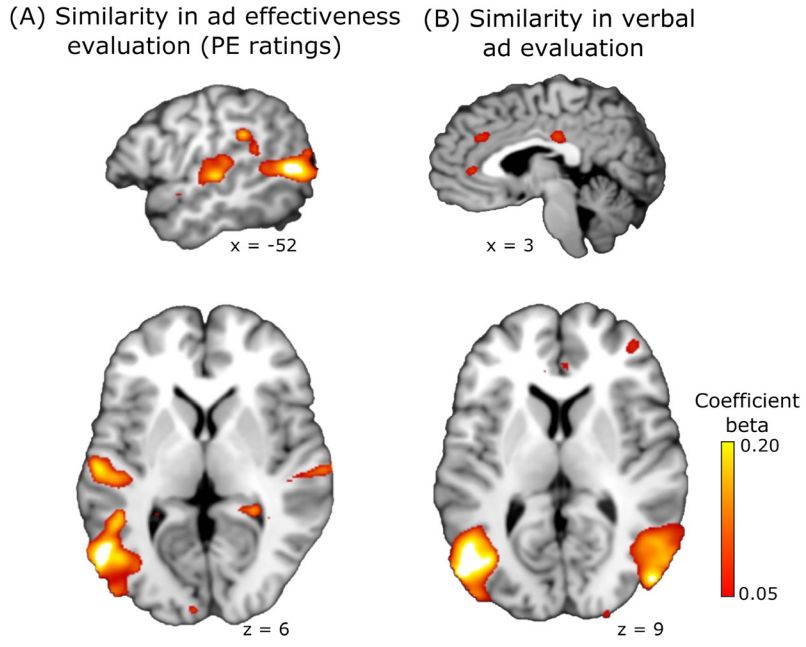


Fig. 10.3 Relationship between ISC in participants' neural activity during ad watching and similarity between participants' a) ad effectiveness ratings and b) verbal ad evaluation. a) Regions in which ISC was significantly associated with similarities in participants' ad effectiveness ratings. Significant clusters include regions associated with higher-order visual processing such as the occipital-temporal cortex and socio-semantic processing regions such as the temporoparietal junction. b) Regions in which ISC was significantly associated with similarities in participants' verbal ad evaluation. Significant clusters include regions associated with higher-order visual processing, as well as midline structures associated with self-related and valuation (e.g., VMPFC).

5. Pandey P, Garcia JO, Falk EB, Lauharatanahirun N. A comparison of neural synchrony measures in an EEG hyperscanning paradigm. In preparation.

   Social interaction and communication are foundational to the human experience, but the underlying neurophysiological processes that give rise to this interaction still remain elusive. Social neuroscience efforts have investigated the neural events from simultaneously monitored brains of interacting individuals, asking whether the underlying neurophysiological coordination between individuals may be at the core of social coordination, as well. Researchers have found that unique neural coordination, assessed via hyperscanning, between individuals is associated with a variety of social behaviors.

   Extant literature that employ hyperscanning techniques, however, use a range of measures to estimate inter-brain similarity and can very often give highly inconsistent results and lead to divergent conclusions. Using data from the Real World Driving experiment, graduate student Pandey compares many popular methods that include time-independent measures (e.g., correlation, Euclidean distance, cosine distance), frequency-based measures (e.g., coherence, directed partial coherence), and phase-based measures (e.g., PLVs, Kraskov's MutInf and circular correlation). Our results indicate that intercorrelations among metrics were highly variable with a large number of metrics being uncorrelated. These findings suggest that different metrics of synchrony may reflect unique features of interpersonal synchrony, and that caution must be taken when interpreting such metrics. Figure 10.4 shows the correlation between different synchrony measures between driver and passenger during free-conversation phase of driving.

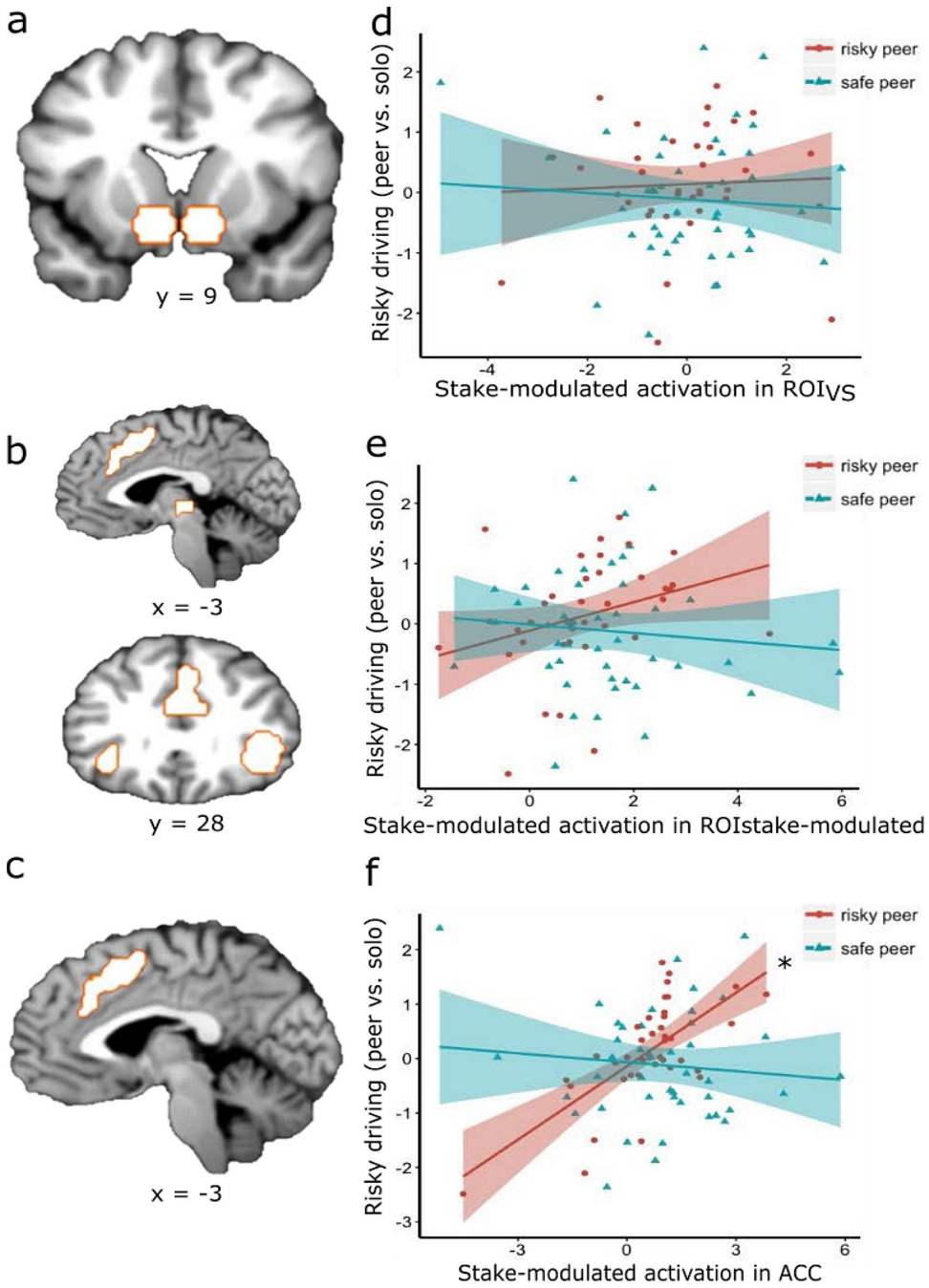


Fig. 10.4 ROIs and how their neural activation in the BART related to changes in risky driving in the simulated driving task. No relationship was found between stake-modulated VS activation and changes in risky driving: a) passenger type marginally moderated the relationship between stake-modulated neural activation and changes in risky driving; b) additional analyses that investigated each subcluster of stake-modulated separately showing a significant interaction between the ACC cluster of stake-modulated and passenger type, with a significant simple effect for the risky peer condition in that stake-modulated ACC activation is associated with more risky driving with a risky peer passenger; and c) *: simple effect $p < 0.05$.

6. Pei R, Lauharatanahirun N, Cascio C, O'Donnell MB, Shope J, Simons-Morton B, Vettel JM, Falk EB. Safety versus risk endorsing peer attitudes influence adolescent risk taking through distinct neural mechanisms. Developmental Cogn Neurosci. In press.

   Adolescents demonstrate both heightened sensitivity to peer influence and increased risk-taking. This study, led by graduate student Pei in collaboration with Drs. Lauharatanahirun and Vettel, provides a novel test of how these two phenomena are related at behavioral and neural levels. Our data shows that adolescents' neural responses to risky decision-making may modulate their behavioral conformity to different types of peer influence. In particular, neural activity in the ACC predicted conformity to risk-preferring peers while driving. We also found that connectivity between VS and risk-processing regions (including insula and ACC) predicted safer driving under risky influence. Together, these results suggest that adolescents' neural responses to risky decision-making may modulate their behavioral conformity to different types of peer influence on risk-taking.

7. Lauharatanahirun N, Pei R, Falk E, Vettel J. Intra-individual variability at the neural and behavioral levels predicts adolescents' risky behavior. Submitted.

   In this study, male adolescents (N = 88) between the ages of 16 and 17 completed the BART while undergoing functional neuroimaging. Our results show that intra-individual inflation variability in the BART captures strategic performance such that adolescents with higher variability were less likely to maximize rewards through risk-taking, while simultaneously banking a high number of balloons for monetary rewards. Combined, these findings suggest that higher behavioral variability is consistent with a risk-averse response strategy resulting in lower risk-taking. We also examined the extent to which neural variability in both anterior insular cortex (AIC) and ACC was dependent upon behavioral variability to predict risky driving behavior. Our findings show that for adolescents who show a relatively more risk-seeking strategy, lower AIC neural variability is associated with greater risk-taking, while the opposite was true for ACC. These novel findings are the first to show that AIC and ACC may serve distinct roles in responding to risk within adolescents who exhibit greater risky exploratory strategies. These results also highlight the different roles that behavioral and neural variability may play in contributing to adolescent risk taking behavior.

8. Tompson SH, Falk EB, O'Donnell MB, Cascio CN, Bayer JB, Vettel, JM, Bassett DS. Response inhibition in adolescents is moderated by brain connectivity and social network structure. Under revision.

   This manuscript, led by former ARL postdoc and Falk Lab member Tompson, in collaboration with several Falk Lab, ARL, and CaN CTA participants, is under revision with the journal *Social Cognitive and Affective Neuroscience*. The social environment an individual is embedded in influences their ability and motivation to engage self-control processes, but little is known about the neural mechanisms underlying this effect. Many individuals successfully regulate their behavior even when they do not show strong activation in canonical self-control brain regions. Thus, individuals may rely on other resources to compensate, including daily experiences navigating and managing complex social relationships that likely bolster self-control processes. Here, we employed a network neuroscience approach to investigate the role of social context and social brain systems in facilitating self-control in adolescents. We measured brain activation using fMRI as 62 adolescents completed a go/no-go response inhibition task. We found that social brain systems compensate for weaker activation in executive function brain systems, especially for adolescents with more friends and more communities in their social networks. Collectively, our results indicate a critical role for social brain systems during the developmental trajectory of self-control throughout adolescence.

9. Cascio CN, Lauharatanahirun N, Larson G, Farah M, Falk EB. Is socioeconomic status associated with differential engagement of neural pathways to cognitive control? In preparation.

   In this investigation, we examine how social variables relate to brain and behavioral performance during a response inhibition task. Response inhibition and socioeconomic status (SES) are critical predictors of many important outcomes in life, ranging from educational attainment to health behaviors and outcomes. The current study extends our understanding of SES and cognition by examining brain activity associated with response inhibition, during the key developmental period of adolescence. Adolescent males ($N = 81$), aged 16–17, completed a response inhibition task while undergoing fMRI brain imaging and reported on their SES. A brain ROI analysis showed that SES was associated with activation differences in the classic response inhibition network (rIFG+STN+BG) despite the absence of an SES-performance effect. A whole-brain analysis revealed effects of SES in several regions outside the classic response inhibition network, including the MTG and angular gyrus, which were, in turn, marginally associated with performance differences.

Taken together, these results suggest that high and low SES individuals engage key brain regions involved in response inhibition to differing degrees.

10.4 Development of Algorithms for Reading Real-World Brain States

In collaboration with Drs Vettel and Garcia, the Falk Lab team has begun developing predictive algorithms for reading out visual information from EEG signals. Graduate student Pandey worked with Alex Cohen, a professional artist, to develop an EEG-based ML model to predict the visuals being imagined by the artist.

Cohen participated in data collection using a 128-channel BioSemi EEG setup. We developed several tasks: 1) color imagination task: random colors were shown in blocks on a screen and Cohen was asked to imagine the colors in a given timeframe; 2) color picking task: same as the previous task, with the only difference being that Cohen chose the colors he will be imagining, instead of random assignment; 3) face task: Cohen viewed a rapid array of face images; and 4) movie task: viewing of a short movie clip. In addition to brain data, we also collected behavioral data including measures for mood (modified Differential Emotions Scale [mDES], Positive and Negative Affect Scale [PANAS], etc.), sleep (to also be measured by accelerometer), and his painting/sculpting activity.

The study team presented this work at the Society for Neuroscience annual conference, at San Diego, November 2018. The alpha and beta frequency bands were identified to be the most distinguishing bands for both hue and lightness color space (Fig. 10.5).

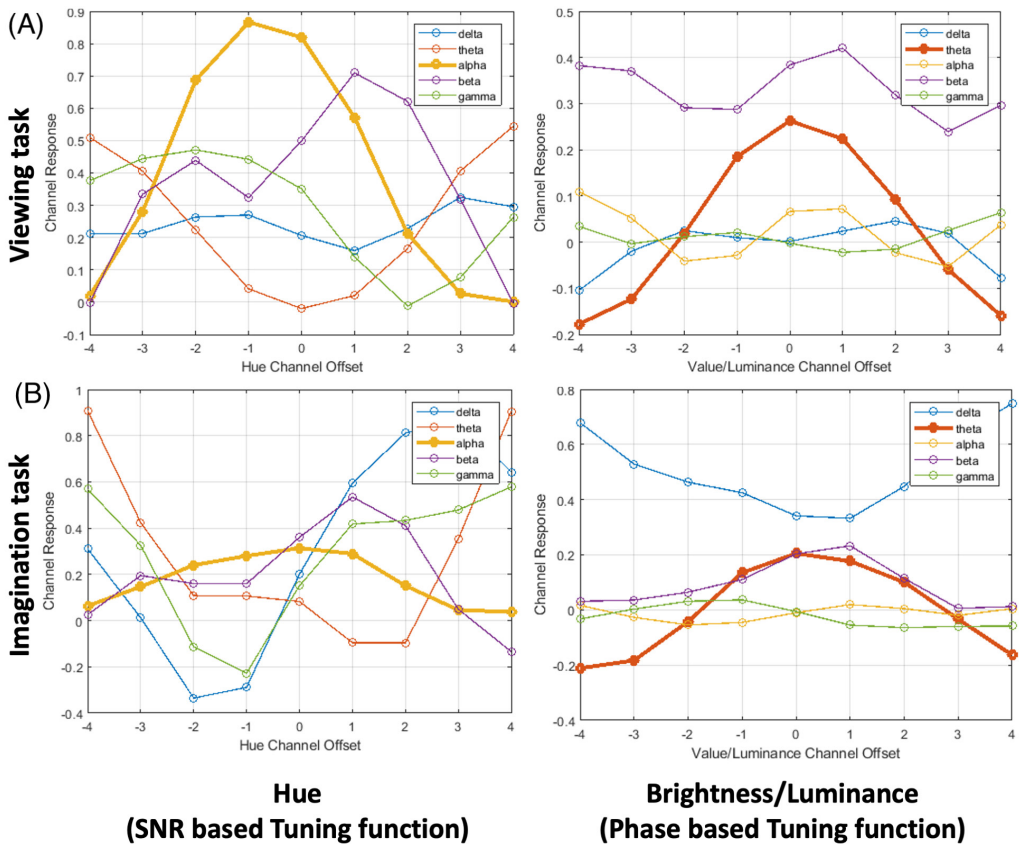


Fig. 10.5 Visualization of the strength of EEG signal responses to the hue and value/luminance of the color being shown on screen (Panel A) or being imagined (Panel B). Brain signals are divided into four frequency bands: delta (blue), theta (red), alpha (yellow), beta (purple), and gamma (green). Here, offset refers to a data manipulation technique to ensure that 0 value represents the target value to achieve and any deviation from 0 represents noise. Panel A represents the viewing task, where we showed solid colors on a screen to the participant. Panel B represents the imagination task, where the participant imagined a color of their own choice and then indicated the color on a color palette.

10.5 Conference Presentations (from 2018–2020 Supported by ARL Funding)

Cascio CN, Pei R, Falk EB. Are neural mechanisms associated with social feedback and conformity different among teens and young adults? Presented at the annual meeting of the International Communication Association; 2019, May Washington, D.C.

Lauharatanahirun N, Ball S, Kim-Spoon J, King-Casas B. Longitudinal changes in neurobehavioral risk sensitivity and associations with future health risk behaviors. Accepted for presentation at the Biennial Meeting of the Society for Research on Adolescence; 2020, Mar. (Conference canceled due to COVID-19).

Lauharatanahirun N, Garcia JO, Roy H, Bansal K, Metcalfe J, Falk EB, Vettel JM. Real world driving as a function of inter-individual similarity in neurobehavioral metrics of risk. Accepted for presentation at the annual meeting of the Social and Affective Neuroscience Society; 2020, May; Santa Barbara, CA. (Conference canceled due to COVID-19).

Lauharatanahirun N, Pei R, Cascio C, O'Donnell M, Shope J, Falk EB, Vettel JM. Intra-individual variability at the neural and behavioral levels predicts adolescents' risky behavior. Accepted for presentation at the Biennial Meeting of the Society for Research on Adolescence; 2020, Mar. (Conference canceled due to COVID-19).

Pandey P, Garcia JO, Lauharatanahirun N. A comparison of neural synchrony measures in EEG hyperscanning paradigm. Accepted for presentation at the annual meeting of the Social and Affective Neuroscience Society; 2020, May; Santa Barbara, CA. (Conference canceled due to COVID-19)

Pei R, Bayer J, Cascio CN, O'Donnell MB, Falk EB, Meshi D. Habitual social media use is associated with increased neural activity in the mentalizing network during social exclusion. Accepted for presentation at the annual meeting of the Social and Affective Neuroscience Society; 2020, May; Santa Barbara, CA. (Conference canceled due to COVID-19).

Pei R, Lauharatanahirun N, Cascio C, O'Donnell M, Falk EB. Neural activity during risky decision making reflects adolescents' online social network clustering structure. Accepted for presentation at the Biennial Meeting of the Society for Research on Adolescence; 2020, Mar. (Conference canceled due to COVID-19).

Pei R, Lauharatanahirun N, Cascio CN, O'Donnell MB, Vettel J, Falk EB. Neural activity during risky decision making reflects online social network clustering structure. Annual meeting of the Social and Affective Neuroscience Society; 2019, May; Miami, FL.

Pei R, Lauharatanahirun N, Falk EB. Adolescent's neural and self- report responses to fear vs. humor appeals in tobacco-prevention messages. International conference of Medicine, Humanity and Media: Health China & Health Communication; 2019, Nov; Beijing, China.

Pei R, Meshi D, Bayer J, Cascio CN, O'Donnell MB, Falk, EB. Habitual social media use is associated with increased neural activity in the mentalizing network during social exclusion. Annual meeting of the International Communication Association (virtual); 2020, May.

10.6 Top Paper Award

Cascio CN, Baek EC, O'Donnell MB, Falk EB. Social influence: a functional connectivity approach to conformity. Annual meeting of the International Communication Association; 2018, May; Prague, Czech Republic.

Cascio CN, Pei R, Falk EB. Neural correlates of social influence across development. Annual meeting of the Social and Affective Neuroscience Society; 2018, May; Brooklyn, NY.

Cascio CN, Wang X, O'Donnell MB, Falk EB. Neural correlates of social norms. Annual meeting of the International Communication Association; 2019, May; Washington, D.C.

Cooper N, Garcia JO, Tompson S, O'Donnell MB, Falk EB, Vettel JM. Time-evolving dynamics in brain networks forecast responses to health messaging. Annual meeting of the International Communication Association; 2018, May; Prague, Czech Republic.

Doré BP, Cooper N, Tompson S, Scholz CS, Baek EC, Falk EB**.** Population-level stimulus effects are reflected in distributed neural representations of affect and value. Presented at the annual meeting of the Social and Affective Neuroscience Society; 2019, May; Miami, FL. ****Top Poster Award****

Doré BP, Scholz CS, Baek EC, Falk EB. Information virality is reflected in a distributed neural representation of value. Presented at the annual meeting of the International Communication Association; 2019, May; Washington, D.C. ****Top Paper Award****

Garcia JO, Bansal K, Rungratsameetaweemana N, Wasylyshyn N, Roy H, Lauharatanahirun N, Johnson T, Fernandez R, O'Donnell MB, Falk EB, et al. Brain network communities between driver-passenger dyads capture successful communication while driving. Annual International IEEE EMBS Conference on Neural Engineering; 2019, Mar; San Francisco, CA.

Kang Y, Strecher VJ, Falk EB. Purpose in life and neural responses to health messages. Presented at the annual meeting of the Social and Affective Neuroscience Society; 2018, May; Brooklyn, NY.

Kranzler EC, Schmælzle R, Pei R, Hornik RC, Falk EB. Message-elicited brain response moderates relationship between opportunities for exposure to anti-smoking messages and message recall. Annual meeting of the International Communication Association; 2019, May; Washington, D.C.

Lauharatanahirun N, Garcia J, Wasylyshyn N, Roy H, Metcalfe J, Vettel J, Fernandez R, Johnson T, O'Donnell M, Falk EB. Social influence shapes neurobehavioral correlates of risky driving performance. Annual meeting of the International Communication Association; 2019, May; Washington, D.C.

Lauharatanahirun N, Garcia JO, Thurman S, Wasylyshyn N, Tompson SH, Cieslak M, Okafor G, Giesbrecht B, Grafton S, Flynn-Evans E, et al. Longitudinal examination of naturalistic sleep, global brain dynamics, and visual working memory performance in healthy adults. Presented at the annual meeting of the Society for Neuroscience; 2018, Nov; San Diego, CA.

Lauharatanahirun N, Garcia JO, Wasylyshyn N, Roy H, O'Donnell MB, Cooper N, Paul A, Fernandez R, Johnson T, Metcalfe J, Falk EB, Vettel JM. Social risk sensitivity in decision-making is linked to social network structure and inter-brain similarity. Annual meeting of the Society for Psychophysiological Research, Quebec City; 2018, October; Quebec, Canada.

Metcalfe J, Lauharatanahirun N, Wasylyshyn N, Garcia JO, Fernandez R, Roy H, O'Donnell MB, Johnson T, Falk EB, Vettel JM. Trust and communication in driver-passenger dyads during open interstate driving. International Conference on Applied Human Factors and Ergonomics; 2018, July; Orlando, FL.

Pandey P, Vettel JM, Cohen AJ, Paul A, Falk EB, Garcia JO. The precision and stability of imagination: reconstructing colors from oscillatory neural activity. Human Cognition and Behavior: Perception and Imagery session of the annual meeting of the Society for Neuroscience; 2018, November; San Diego, CA.

Pei R, Cascio C, Simons-Morton B, Falk EB. Safety versus risk endorsing peer attitudes influence adolescent risk taking through distinct neural mechanisms. Annual meeting of the International Communication Association; 2018, May; Prague, Czech Republic. ****Top Paper Award****

Pei R, Lauharatanahirun N, Cascio CN, O'Donnell MB, Vettel J, Falk EB. Neural activity during risky decision making reflects adolescents' online social network clustering structure. Annual meeting of the International Communication Association; 2019, May; Washington, D.C.

Rungratsameetaweemana N, Schmaelzle R, Cooper N, Bansal K, Wasylyshyn N, Roy H, Lauharatanahirun N, Johnson T, Fernandez R, O'Donnell MB. Capturing communication success of driver-passenger dyads during real-world driving. Presented at the annual International IEEE EMBS Conference on Neural Engineering; 2019, Mar; San Francisco, CA.

Tompson S, Vettel J, Falk EB, O'Donnell MB, Cascio CN, Bayer J, Bassett DS. Response Inhibition in Adolescents is Moderated by Brain Connectivity and Social Network Structure. Presented at the annual meeting of the International Communication Association; 2019, May; Washington, D.C. ****Top Paper Award****

Tompson SH, Kahn AE, Falk EB, Vettel JM, Bassett DS. Functional brain network architecture supporting the learning of social versus non- social networks. Presented at the annual conference or the Society for Personality and Social Psychology; 2019, Feb; Portland, OR.

Tompson SH, Kahn AE, Falk EB, Vettel, JM, Bassett DS. Functional brain network architecture supporting the learning of social versus non-social networks. Annual meeting of the Society for Neuroscience; 2018, November; San Diego, CA.

Vettel JM, Lauharatanahirun N, Wasylyshyn N, Roy H, Fernandez R, Cooper N, Paul A, O'Donnell MB, Johnson T, Metcalfe J, et al. Translating driving research from simulation to interstate driving with realistic traffic and passenger interactions. AHFE: 9th International Conference on Applied Human Factors and Ergonomics; 2018, July; Orlando, FL.

10.7 Publications (from 2018–2020 Supported by ARL Funding)

Baek, EC, Falk EB. Persuasion and influence: what makes a successful persuader? Cur Opin Psychol. 2018;24:53–57. https://doi.org/10.1016/j.copsyc.2018.05.004

Bayer JB, O'Donnell MB, Cascio CN, Falk EB. Brain sensitivity to exclusion is associated with core network closure. Sci Rep. 2018;8(1):16037. https://doi.org/10.1038/s41598-018-33624-3.

Cooper N, Garcia JO, Tompson SH, O'Donnell MB, Falk EB, Vettel JM. Time-evolving dynamics in brain networks forecast responses to health messaging. Netw Neurosci. 2019;3(1):138–156. https://doi.org/10.1162/netn_a_00058.

Cooper N, Tompson S, O'Donnell MB, Vettel JM, Bassett DS, Falk EB. Associations between coherent neural activity in the brain's value system during antismoking messages and reductions in smoking. Health Psychol. 2018;37(4):375–384. https://doi.org/10.1037/hea0000574.

Coronel JC, O'Donnell MB, Beard EC, Hamilton RH, Falk EB. Evaluating didactic and exemplar information: Noninvasive brain stimulation reveals message-processing mechanisms. Commun Res. 2019. https://doi.org/10.1177/0093650219876844.

Doré BP, Cooper N, Scholz C, O'Donnell MB, Falk EB. Cognitive regulation of ventromedial prefrontal activity evokes lasting change in the perceived self-relevance of persuasive messaging. Human Brain Mapping. 2019;40(9):2571–2580. https://doi.org/10.1002/hbm.24545.

Doré BP, Scholz C, Baek EC, Garcia JO, O'Donnell MB, Bassett DS, Vettel JM, Falk EB. Brain activity tracks population information sharing by capturing consensus judgments of value. Cerebral Cortex. 2018;bhy176. https://doi.org/10.1093/cercor/bhy176.

Doré BP, Tompson SH, O'Donnell MB, An L, Strecher V, Falk EB. Neural mechanisms of emotion regulation moderate the predictive value of affective and value-related brain responses to persuasive messages. J Neurosci. 2019;39(7):1293–1300. https://doi.org/10.1523/jneurosci.1651-18.2018.

Falk E, Scholz C. Persuasion, influence, and value: Perspectives from communication and social neuroscience. Ann Rev Psychol. 2018;69(18):329–356. doi:10.1146/annurev-psych-122216-011821.

Kang Y, Cooper N, Pandey P, Scholz C, O'Donnell MB, Lieberman MD, Taylor SE, Strecher VJ, Dal Cine S, Konrath S, et al. Effects of self-transcendence on neural responses to persuasive messages and health behavior change. Proc Natl Acad Sci USA. 2018;115(40)9974–9979. https://doi.org/10.1073/pnas.1805573115.

Kang Y, Strecher VJ, Kim E, Falk EB. Purpose in life and conflict- related neural responses during health decision-making. Health Psychol. 2019;38(6):545–552. http://doi.org/10.1037/hea0000729.

Kranzler EC, Schmälzle R, Pei R, Hornik RC, Falk EB. Message-elicited brain response moderates the relationship between opportunities for exposure to anti-smoking messages and self-reported message recall. J Commun. 2019;69(6):589–611. https://doi.org/10.1093/joc/jqz035.

Lydon-Staley DM, Falk EB, Bassett DS. Within-person variability in sensation-seeking during daily life: positive associations with alcohol use and self-defined risky behaviors. Psychol Addictive Behav. 2020;34(2):257–268. https://doi.org/10.1037/adb0000535.

Pei R, Lauharatanahirun N, Cascio C, O'Donnell MB, Shope J, Simons-Morton G, Vettel J, Falk EB. Neural processes during adolescent risky decision making are associated with conformity to peer influence. Developmental Cogn Neurosci. 2020 Aug;44:100794. https://doi.org/10.1016/j.dcn.2020.100794.

Pei R, Schmälzle R, Kranzler EC, O'Donnell MB, Falk EB. Adolescents' neural response to tobacco prevention messages and sharing engagement. Am J Prev Med. 2019;56(2, Supplement 1):S40–S48. https://doi.org/10.1016/j.amepre.2018.07.044.

Pei, R., Kranzler, E. C., Suileman, A. B., & Falk, E. B. (2019). Promoting adolescent health: insights from developmental and communication neuroscience. Behavioural Public Policy, 3(1), 47–71. https://doi.org/10.1017/bpp.2018.30

Scholz C, Baek EC, O'Donnell MB, Falk EB. Decision making about broad and narrowcasting a neuroscientific perspective. Media Psychol. 2020;23(1):131–155. https://doi.org/10.1080/15213269.2019.1572522

Scholz C, Jovanova M, Baek EC, Falk EB. Media content sharing as a value-based decision. Curr Opin Psychol. 2020;31:83–88. https://doi.org/10.1016/j.copsyc.2019.08.004.

Tompson SH, Falk EB, Bassett DS, Vettel JM. Using neuroimaging to predict behavior: an overview with a focus on the moderating role of sociocultural context. In: Davis PK, O'Mahony A, Pfautz J, Eds. Social-Behavioral Modeling for Complex Systems. John Wiley and Sons; 2019. p. 205–230.

Tompson SH, Falk EB, Vettel JM, Bassett DS. Network approaches to understand individual differences in brain connectivity: opportunities for personality neuroscience. Personality Neurosci. 2018;1(e5)1–12. https://doi.org/10.1017/pen.2018.4,

Tompson SH, Kahn AE, Falk EB, Vettel JM, Bassett DS. Functional brain network architecture supporting the learning of social networks in humans. NeuroImage. 2020;210:116498. https://doi.org/10.1016/j.neuroimage.2019.116498

Tompson SH, Kahn AE, Falk EB, Vettel JM, Bassett DS. Individual differences in learning social and non-social network structures. J Exp Psychol Learn Mem Cogn. 2018;45(2):253–271. https://doi.org/10.1037/xlm0000580,

Vettel JM, Lauharatanahirun N, Wasylyshyn N, Roy H, Fernandez R, Cooper N, Paul A, O'Donnell MB, Johnson T, Metcalfe J, et al. Translating driving research from simulation to interstate driving with realistic traffic and passenger interactions. In: Cassenti DN, editor. Advances in Human Factors in Simulation and Modeling; 2018. AISC. Vol. 780, p. 126–138. Springer, Cham. https://doi.org/10.1007/978-3-319-94223-0_12.

Wasylyshyn N, Hemenway Falk B, Garcia JO, Cascio CN, O'Donnell MB, Bingham CR, Simons-Morton B, Vettel JM, Falk EB. Global brain dynamics during social exclusion predict subsequent behavioral conformity. Soc Cogn Affec Neurosci. 2018;13(2):182–191. http://doi.org/10.1093/scan/nsy007.

11. Syntrogi Inc.

11.1 ACA Large-Scale Electroencephalography (EEG) Analysis and Exploration of Cognitive Aspects (LARG-II)

Activity supported to overcome barriers included the following:

- Discovery of models and novel methods for the identification and interpretation of statistical relationships among high-dimensional data sets characterizing the dynamics of environment, behavior, and brain function during complex task performance

The LARG-II project focuses on addressing the following three hypotheses:

- *H1 (LARG-II).* When the LARG methodology is expanded to encompass repeated sessions for individual subjects, then subject, task, and behavioral effects can be quantified and modeled in new ways that take advantage of data from other studies to provide insights into inter-subject and intra-subject variability.
- *H2 (LARG-II).* ERP and ERSP analysis can be expanded to distributed-source ROI connectivity analysis to show that activations of canonical networks can be systematically related to cognitive aspects as represented by HED tags and to different behavioral characterizations.
- *H3 (LARG-II).* Large-scale, automated, semi-supervised, and multitask learning using GANs can capture discriminative features associated with different behavioral characterizations and with cognitive aspects as represented by HED tags.

Key achievements during the final years of the program included the following:

- We published a series of two *NeuroImage* papers detailing key efforts under the LARG project (automated EEG mega-analysis I and II; Bigdely-Shamlo et al. [2019a, 2019b]). We worked closely with co-authors at UTSA and ARL to bring both papers through revisions, acceptance, and final publication. These papers bring together a number of CTA technologies developed over the lifetime of the CaN CTA including standardized preprocessing; data curation, containerization, and HED tagging; and temporal regression and multilevel hierarchical modeling to account for and characterize individual variability across individuals, recording hardware, experimental events, and experimental paradigms. Together they represent a significant milestone in CTA efforts toward enabling large-scale processing and generalizable analysis of heterogeneous EEG data.

- We extended the LARG methodology to encompass distributed-source ROI connectivity analysis to show that activations of canonical networks can be systematically related to cognitive aspects as represented by HED tags and to different behavioral characterizations. We presented these results in posters and short conference paper (Hanada et al. 2019) and are preparing a journal publication.
- We conducted a systematic investigation and validation of our connectivity pipeline in preparation for generating the final catalog of connectivity results applied to the full LARG corpus. In particular, using data from the LARG corpus, we studied the effect of the vector autoregressive model order and regularization parameter (used for estimating connectivity) on goodness-of-fit metrics such as residual variance, percent whiteness, and average whiteness. Results showed that both percent and average whiteness could achieve good model validation greater than 95% depending on the model versus lambda values selected. We further explored this relationship across a wide range of both model orders and lambda values, characterizing the surface shape to determine optimal model parameters. We additionally examined the residual autocorrelation and cross-correlation coefficient sequences for subsets of models and determined that the models appear to be adequately fitting to the data with rapidly decaying correlation over time, as would be expected for weakly correlated residuals. As a result of these experiments, we established a standard modeling procedure for LARG, which uses an autoregressive model order of 10 and applies a grid search across many values of the regularization parameter to select the one that produces the highest value of percent whiteness of the residuals. This procedure has been used to produce the LARG corpus connectivity data catalogue for archiving.
- It was brought to our attention that some of the channel mappings we had been provided for seven LARG studies were inaccurate. We conducted a thorough investigation into this issue and, after appropriate fixes were made, reran the source analysis and computed derived source-level features (ERPs, regressed ERPs, ERPSs, regressed ERSPs) and connectivity for affected subjects for the final data catalogue and archiving.
- We completed estimation of distributed source activity, ROI activations, and connectivity within canonical brain networks, including averaged and regressed source ERP, ERSP, and connectivity event-related responses (using the temporal hierarchical overlap regression [THOR] and general regression of aspects and details [GRAND] models) for the LARG corpus

(17 studies), and placing of data and results into standardized Baryon format.

- We presented a short conference paper on "Large-scale analysis of canonical cortical network dynamics across five visual target detection tasks" (Bigdely-Shamlo et al. 2019b) at IEEE SMC 2019 in Bari, Italy. The poster presentation is shown in Fig. 11.1.
- In addressing *H1*, we worked with UTSA and ARL to publish a *Transactions on Neural Systems and Rehabilitation Engineering* special issue journal paper titled "How sensitive are EEG results to preprocessing methods: a benchmarking study" (Robbins et al. 2020). This study examined data from 1000 EEG recordings from the LARG corpus, presenting an investigation into the effects of several preprocessing methods (LARG, MARA, and ASR) on ERP, ERSP, and spectral variability, topographical distributions, and blink characteristics. Based on our findings, we offer several recommendations and observation for researchers working with EEG data including the following:
    - Scaling by a recording-specific constant reduces inter-recording variability by approximately 40%.
    - Even with aggressive blink removal, careful consideration of residual blink artifacts is necessary, as well as consideration of potential neural origins of blink-locked EEG responses. Blink-locked signal analysis with temporal overlap regression methods can help to address this.
    - A "federation" of well-documented automated processing approaches may be better than a single "gold standard".
    - Small differences in preprocessing methods can change the distribution of neural features, with significant differences in outlier characteristics.
    - Using a diverse set of events (with an appropriate tagging ontology) and separating temporally adjacent events with temporal overlap regression can help to improve generalization power when evaluating and comparing preprocessing methods.

Approved for public release; Distribution is unlimited

Large-Scale Analysis of Canonical Cortical Network Dynamics Across Five Visual Target Detection Tasks

Grant Hanada[1], Chung-Ki Wong[1], Kay Robbins[2**], Nima Bigdely-Shamlo[1,2], Jonathan Touryan[3*], Tim Mullen[1*]
[1]Intheon, [2]University of Texas at San Antonio, [3]Army Research Laboratory
*Member, IEEE **Senior Member, IEEE

INTRODUCTION:

In recent work [1] we demonstrated the feasibility of performing large-scale multi-study EEG analyses using a pipeline that includes annotating experiment-specific event codes using a common Hierarchical Event Descriptor (HED) ontology, facilitating the analysis of brain activity related to cognitive aspects (i.e. groups of events that share common properties). We analyzed event-related functional brain network measures and quantified effects of cognitive aspects on global efficiency within four canonical cortical networks in five Rapid Serial Visual Presentation (RSVP) tasks. We compare these results to event-related potentials (rERP) and event-related spectral perturbation (rERSP) measures for channels and cortical sources.

METHODS:

Data

- 64-channel EEG data from 80 subjects (225 recordings) from five RSVP datasets described in [1]. Data curation and pre-processing were performed as described in [1].

Source Connectivity Estimation:

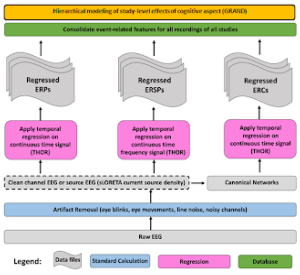
- Cortical current source density (CSD) estimated using sLORETA and averaged within each of a set of 20 regions of interest (ROIs) constructed from the Destrieux cortical atlas and comprising the nodes of four canonical cortical networks adapted from [2]: Attention, Salience, Default Mode, and Cognitive Control.
- Time-varying Direct Directed Transfer Function (dDTF) computed using a 500ms sliding window applied to continuous ROI CSD time-series.
- dDTF averaged within delta (1-3Hz), theta (4-7Hz), alpha (8-13Hz), beta (14-25Hz), and gamma (26-45Hz) frequency bands and computed Global Efficiency (GE), a measure of information exchange efficiency in a network [3].

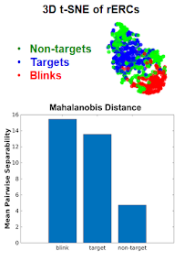
Statistical Modeling of Event-related Responses:

- Modeled event-related responses of GE to each of several cognitive aspects using Temporal Overlap Regression (TOR). Each TOR pattern was smoothed using a 10-point moving average, followed by mean subtraction over 750ms pre-event baseline. We denote this metric as regressed event-related connectivity (rERC).
- Modeled the study-level effects of each cognitive aspect on rERC measures using a second-level (hierarchical) linear regression modeling approach called General Regression of Aspects and Details (GRAND).

Cognitive Aspect Separability Analysis:

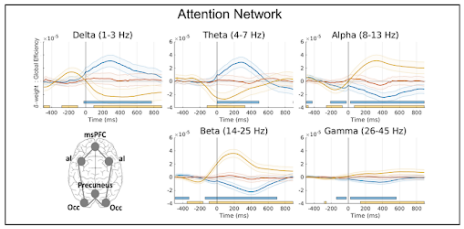
- Applied 3D *t*-SNE (t-distributed stochastic neighbor embedding) to visualize separability of each cognitive aspect and quantified using Mahalanobis distance.
- Applied same 3D *t*-SNE metric to channel and source rERP and rERSP measures.
- Concatenated all features for the given measure (e.g. all ROIs, or all channels, or all networks + bands) into a single measurement vector prior to applying *t*-SNE.
- Quantified classification accuracy using a support vector machine (SVM) with 10-fold cross validation.
- Compared separability of rERC, and channel and source rERPs and rERSPs. One-way ANOVA was applied to determine if classification performance was significantly different across the three types of measures.

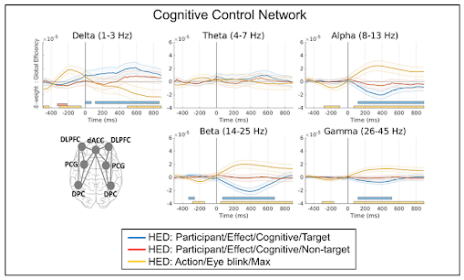


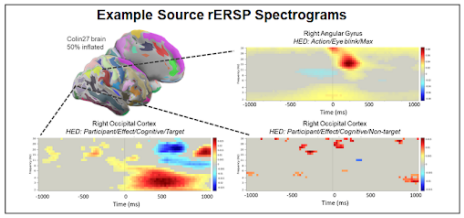


RESULTS:

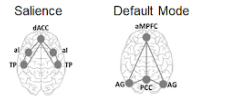
- RSVP visual target presentations resulted in significantly increased network Global Efficiency in delta and theta bands for the Attention and Default Mode Networks, with decreased alpha, beta, and gamma GE for all networks. This was not observed for non-target presentations. Generally, similar rERC patterns were observed for DMN and Attention networks and for Salience and Cognitive Control networks.
- Spontaneous blinks were associated with decreased GE in delta band, and increases in alpha, beta, and gamma bands across all networks.
- t-SNE produced distinct clusters for target, non-target, and blink events with similar or greater separability of cognitive aspects for rERC measures as for channel or source level ERP and ERSP features, as measured by Mahalanobis distance and SVM classification accuracy following 3D t-SNE feature projection.

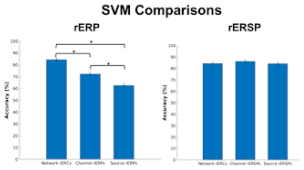






- SVM classification accuracy:
  rERC on GE 84.35%
  channel rERP 72.25%
  source rERP 62.49%
- Significant effect of type of measure on classification accuracy ($F = 70.87$, $p<0.001$) with greater accuracy for network rERCs than both channel ($p<0.001$) and source rERPs ($p<0.001$).
- No significant differences in classification accuracy between rERC measures and channel rERSP or source rERSP measures.





Acknowledgments
We acknowledge Tony Johnson and Michael Dunkel of DCS Corporation for their careful assembly and curation of the ARL data. This research was sponsored by the Army Research Laboratory and was accomplished under Cooperative Agreement Number W911NF-10-2-0022 (CAST 0709102270001). The views and the conclusions contained in this document are those of the authors and should not be interpreted as representing the official policies, either expressed or implied, of the Army Research Laboratory or the U.S Government. The U.S Government is authorized to reproduce and distribute reprints for Government purposes notwithstanding any copyright notation herein.

References:
[1] N. Bigdely-Shamlo, J. Touryan, A. Ojeda, C. Kothe, T. Mullen, K. Robbins, "Automated EEG mega-analysis I: Spectral and amplitude characteristics across studies," bioRxiv, p. 405631, Sep 2018.
[2] L. M. Williams. "Precision psychiatry: a neural circuit taxonomy for depression and anxiety." Lancet Psychiatry. Vol.3(5) pp. 472-80. May, 2016.
[3] M. Rubinov, O. Sporns. "Complex network measures of brain connectivity: Uses and interpretations." NeuroImage, vol. 52, 2010, pp. 1059-69

Fig. 11.1 LARG-II poster presented at IEEE SMC 2019

Our tasks included a significant contribution of data analyses, code, and manuscript text for the draft and revisions, engaging in discussions with UTSA and ARL co-authors regarding content, and conducting of a

systematic evaluation of the preprocessing methods used, particularly ASR, and processing of the LARG corpus data using Intheon's recommended ASR parameters and pre-filters.

We conducted a detailed investigation into HED tag distributions among the LARG corpus to better understand how they are grouped and which key tags are used the most as well as which are shared the most across studies of different types.

Figure 11.1 showed the most prevalent HED tags using a criteria of at least 20 subjects from a given study, with at least 30 trials of the given tag, present across at least 7 of the 18 LARG corpus studies. Table 11.1 shows the breakdown of each of these HED tags that met all criteria.

Table 11.1 HED tags meeting minimum criteria

HED tag	No. of studies	No. of total subjects	No. of subjects with at least 30 trial instances	Median number of trials per subject
Event/category/incidental	18	1166	1160	501
Action/button press	8	245	215	93
Attribute/direction/left	8	806	540	41
Attribute/direction/right	8	809	542	41
Attribute/object control/perturb	9	828	694	78
Event/category/experimental stimulus	18	1168	1130	270
Event/category/incidental	18	1166	1160	501
Event/category/participant response	18	1130	1092	177
Item/object	18	1168	1168	407
Item/object/vehicle	11	886	886	352
Item/object/vehicle/car	10	872	846	350
Item/symbolic	10	621	444	67
Participant ~ action/control vehicle/drive ~ item/object/vehicle/car	9	827	827	284
Participant ~ action/control vehicle/drive/correct ~ item/object/vehicle/car	9	827	827	186
Participant/effect/cognitive/non-target	9	461	461	694
Participant/effect/cognitive/target	9	460	369	51
Participant/effect/visual	10	557	556	371
Sensory presentation/visual	16	858	699	344
Sensory presentation/visual/rendering type/screen/2-D	10	557	556	421

We observed that while the number of total HED tags used in the LARG corpus is large and varied, there is only a small subset that is used across multiple studies. This gives us insight into which HED tags to focus on for

future analyses as well as understand better which studies might have contributed the most toward previous findings reported in the LARG manuscripts. Importantly, only the most high-level, generalized HED tags such as participant response, visual presentations, and stimulus descriptions are common across a majority of the LARG corpus. Most of the LARG Corpus tasks fall into either using a simulated driving paradigm or a RSVP paradigm, and similarly many of the HED tags with the most usage are split between those two groups.

- *Investigation of alternative ASR variants:* We additionally worked on improving the ASR automated adaptive artifact removal technique originally developed under CTA. This method is used extensively throughout the CTA and in the scientific community, as well as in the LARG project. In recent years, improvements have been proposed by other groups (e.g., Blum et al. 2019) with the Riemannian ASR (rASR) method (Bigdely-Shamlo et al. 2019a) emerging as a method that is claimed to be more robust to outliers and enjoys improved performance under small-sample situations. We sought to further validate the rASR method and determine conditions under which it outperforms ASR. In doing so, we identified several serious issues with the published description of the rASR method and major differences between the paper and the available reference rASR MATLAB implementation. We conducted a side-band analysis to investigate these issues using data from several studies, and we implemented a more general and more efficient update for the Riemannian exponential moving average in order to be able to perform more fine-grained and larger-scale comparisons efficiently. We also implemented and tested a robust Riemannian average for covariance matrices (including a recursive variant), which allows us to perform also ASR's calibration algorithm in a Riemannian-correct fashion (something that the rASR method did not attempt to do). We determined that our modifications led to improved artifact removal performance. However, as this was a side project, this benchmark evaluation is not yet complete and will be continued in a subsequent quarter. We have notified the EEGLAB maintainers of our findings with respect to the rASR implementation by Blum et al. (2019), and we are planning to summarize the results of our forthcoming benchmark in a short paper.

11.2 Lab Streaming Layer Development and Maintenance (LSL-DM)

Activity supported to overcome barriers included the following:

- Development and employment of novel, wearable sensor suites for monitoring brain and body dynamics during naturalistic behavior, as well as software systems to enable integrated monitoring capabilities
- Acquisition and processing of high-dimensional data sets that characterize physical, mental, and physiological behavior, as well as its environmental context, in sufficient detail and across a sufficient breadth of circumstances

This one-year project focused on the establishment of much-needed core library improvements and extensions, and long-term support and maintenance infrastructure for the LSL software, including the core technology (the LSL library, core tools, and programming language bindings), its surrounding applications (e.g., device integrations), as well as community resources such as the website and forum as well as examples and documentation. Some effort is also allocated to maintaining the closely related XDF data storage format and associated tools.

11.2.1 Development and Maintenance

We developed some initial tools to aid management of files in the XDF format:

- *xdf-tagger*: a command-line (CLI) tagging tool for XDF files that allow for adding, removing, replacing, and listing of metadata tags in XDF files (this tool is initially hosted on Intheon's GitHub during initial development, but will be migrated to the XDF repository). This tool has been designed for either direct use via the CLI or use with automation scripts or other programmatic means, and can process multiple groups of files in a batched fashion. Note: Not to be confused with the CTAGGER tool, which is for manual event annotation, this program is for per-file XDF metadata tags (e.g., subject age, name, device manufacturer, and so on).
- A diagnostic toolkit for XDF files (implemented in Python) that includes the following capabilities:
    - Robust or least-squares linearization of timestamps and moving-window quality-of-fit diagnostics that include the mean and standard deviation of the sampling rate over time (to quantify sampling rate drift or wobble); mean, standard deviation, and mean absolute deviation of the per-sample jitter (in seconds and samples); the maximum timestamp error versus the optimal fit across the

whole data; maximum gap length; and maximum sampling rate error.

  - Warnings in case certain prespecified limits are exceeded
  - Optional processing of sample or frame counter information with support for wrap-around counters and detection of data gaps (e.g., packet loss) based on sample counters, as well as gap-aware timestamp linearization, and warnings in case sample counters being inconsistent with observed timestamp gaps
  - Warnings for excessive packet loss
  - Optional detection of subsample shifts in DAQ timing without packet loss (requires a sufficiently regular sampling interval)
  - This toolkit will be made available in the form of a CLI for XDF diagnostic inspection.

- An implementation of the CCA method for automatic post-hoc time alignment of multi-channel data streams based on their contained correlated activity, which we have initially tested on EEG and eye-tracking data, although applications to other modalities, such as EMG, EOG, and fNIRS (based on movement artifacts), are envisioned. The method supports pairs of regularly and irregularly sampled time series, with matching or non-matching sampling rates, and is fully automatic within certain default limits without requiring channels to be specified. Traditionally, time-alignment via cross-correlation requires candidate channels to be manually selected by the user, requiring a fair amount of judgement or trial-and-error; CCA solves this problem, but would be prohibitively expensive (on the order of hours) if run in a brute-force fashion (due to the need to perform a full sweep over possible shifts). We solved this by using Bayesian optimization, which is known for its use of very few iterative updates until the optimum is reached compared to other optimizers. This algorithm will be packaged up into a library of post-editing tools for XDF files.
- We have begun work on a refactoring of the XDF Python importer that allows it to efficiently extract only the header information without parsing or loading into memory the bulk time-series data, in a single pass. This is to support workflows in which folders of XDF files are efficiently scanned for certain metadata tags before the desired subset of files is loaded in full.
- We have also updated the official MATLAB XDF importer repository, which was temporarily broken by a new MATLAB version that dropped

some mex-file backward compatibility, and have tested the current importer on Windows, Linux, and Mac OSs against several recent MATLAB versions.

11.2.2 Application Development

- We have started implementation of an LSL integration for Empatica E4 devices in C++, using the current application template. In the process, we anticipate to make improvements to and add documentation for this template to improve the experience for first-time developers of LSL device integration applications (specifically GUI applications).
- We have cleaned up, retested, documented, and rereleased the Wearable Sensing LSL integration (currently on Intheon's GitHub, but slated for publishing on the labstreaminglayer GitHub organization).
- We have begun drafting an LSL multi-stream, time-series viewer, and in the process, have reviewed several candidate starting points (including SigViewer, OpenEphys, and several others).

11.2.3 Journal Paper

- We worked on the LSL journal paper, including organizing meetings with lead authors, and established key task assignments. We have produced an initial draft, but we are currently awaiting some additional validation data in order to proceed with the final paper drafts.

11.2.4 Community and Standardization Efforts

- We organized, chaired, and taught a half-day workshop titled "Introduction to LSL" at the IEEE Systems, Man, and Cybernetics Conference 2019. The workshop presented the history, philosophy, and architecture of the LSL project; technical overviews; a hands-on practicum; and insights into practical considerations and use cases presented by key LSL developers and "power users" followed by open Q&A and round-table discussions.
- We organized and prepared educational and demonstrative materials for a full-day 2nd International Hands-On LSL Workshop scheduled to follow the EEGLAB 2020 workshop in San Diego and immediately preceding the MoBI Workshop. The workshop has, however, been postponed due to COVID-19.
- We have continued to work closely with the core LSL developers and SCCN to coordinate the organization of GitHub repositories, continuous

integration system, and improvement of documentation. We have also engaged engineers at ARL and held a roundtable videoconference discussion with ARL and DCS engineers and scientists who are using LSL to better understand their use cases and to address their needs.

- We have engaged IEEE and community members regarding establishing a working group to create an IEEE Standard for LSL. We have initiated work on an IEEE Project Authorization Request to create the working group.
- We have begun work on designing the new LSL website and forum systems.

11.2.5 Transition Opportunities/Standards Initiatives

We have engaged IEEE and community members regarding establishing a working group to create an IEEE Standard for LSL. We have initiated work on an IEEE Project Authorization Request to create the working group.

11.2.6 Synergistic Projects

NeuroPype Suite Academic Edition

Throughout PY10, we completed two major version releases of NeuroPype Academic Edition and a number of minor point releases. These releases include a number of new modules for processing multimodal biosensor data, including data from EMG, PPG, and ECG sensors, and eye trackers, as well as a new suite of statistics modules. Support for implanted electrodes and executing deep neural network models within workflows is forthcoming in a new release. Throughout PY10, NeuroPype Academic Edition usage grew to over 320 academic and scientific *institutions* in over 45 countries.

NeuroScale Insights Beta Release

Intheon has opened up its beta program for the NeuroScale (NS) Insights platform, representing a major step forward in standardized automated processing and analytics and report generation for neural and other biosignal data. NS Insights enables turnkey, cloud-based, or local processing of data recorded using various file formats and organized using various containerization schemes (including BIDS, but also simple folder-based organizational schema). Individual or group data is processed using standardized (albeit configurable) NeuroPype pipelines, including data cleaning and quality analysis; continuous or event-related spectral, temporal, and spatial feature extraction at the channel or cortical region of interest level; statistical modeling using GLM/(M)AN(C)OVA, paired statistics, or hierarchical/mixed-effects models; and ML. Insights supports various statistical designs (N-way, N x M, repeated measures, individual vs. group comparisons, etc.).

Results are presented in interactive graphical reports as well as standardized Baryon data structures in HDF5 and MATLAB formats. Insights is currently being used to support CTA/DCS/ARL projects, as well as a number of other industry, academic, and government partners.

Real-time Tracking of Brain Networks and Task Performance Prediction during Driving

We published and presented a paper entitled "Online tracking of canonical brain network activation and behavioral prediction using Bayesian filtering" (Fazel-Rezai and Mullen 2019) at the IEEE SMC 2019 conference in Bari, Italy. In this paper, we extended previous CaN CTA work and applied the two-stage block sparse Bayesian learning (BSBL-2S) method developed and refined under previous CaN CTA projects to both simulated and real EEG data for online tracking of the relative evidence of activation of groups of cortical ROIs comprising the nodes of two brain networks, the task-positive network (TPN) and default-mode network (DMN). This was used to predict RT to unexpected lane departure events in simulated lane-keeping driving data from eight subjects (data from NCTU; collected under the CTA RWN VDE project). The estimated Bayes factors (BFs) showed significant linear and quadratic predictive relationships with RT, with the poorest task performance associated with decreasing BF (increased DMN activation, relative to TPN) (Fig. 11.2). These results confirm prior results showing that online estimation of a BF for cortical network activation could be useful in the development of neuroscientifically grounded adaptive BMI systems for tracking and predicting task performance.

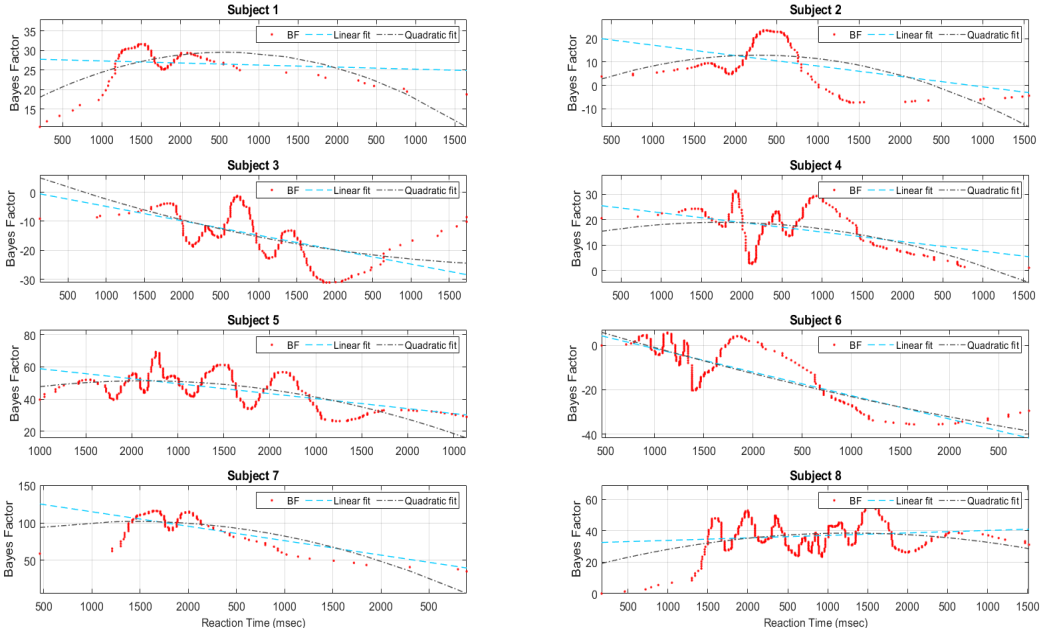


Fig. 11.2 Scatter plots of estimated BFs (red traces) vs. RT for each of eight subjects. Dotted lines show linear and quadratic polynomial functions fit to the (BF, RT) data. Larger values of the BF indicate greater evidence for TPN activation relative to that of the DMN.

Real-time Neuroimaging and Task Performance Prediction in Aircraft Pilots during Real Flight

We conducted research with ISAE-SUPAERO (the most prestigious aerospace engineering school in France) using NeuroPype and several methods we developed under the CTA for artifact removal and real-time error prediction during real aircraft operation. We co-authored a paper titled "A pBCI to predict attentional error before it happens in real flight conditions" (Frederic Dehais, Rida Imad, Raphaelle Roy, Iversen John, Tim Mullen, and Daniel Callan), which we presented at IEEE SMC 2019 where it was awarded the *IEEE Brain Best Paper Award* (Dehais et al. 2019).

11.2.7 Community Outreach

- Intheon members co-organized and/or participated in a number of workshops, summits, research topics, and think-tanks throughout PY10.
- T Mullen and C Kothe served as Special Session Co-chairs and Associate Editors for the 9th Workshop on Brain-Machine Interface Systems (BMI) at the IEEE Systems, Man and Cybernetics Conference in October 2019. We co-organized and taught a half-day workshop on LSL, a Brain Hackathon, a neurotech/industry panel, as well as served as chairs for the following special sessions on neurotechnology:

    - Brain Connectivity and Neuronal System Identification: Theory and Applications to Brain State Decoding
    - Neuroadaptive Technologies and Passive BCI.
    - Deep Learning and Transfer Learning for Brain–Machine Interface
    - Mobile Brain/Body Imaging and Multi-Modal BMI http://musaelab.ca/bmi19/smc2019_bmi.html

- Mullen and Kothe worked on tasks related to their roles as Special Session Co-chairs and Associate Editors for the 10th Workshop on Brain-Machine Interface Systems (BMI) at the IEEE Systems, Man and Cybernetics Conference (scheduled for October 2020). We submitted several (accepted) special session proposals:
    - Deep Learning and Transfer Learning for Brain–Machine Interfacing
    - Mobile Brain/Body Imaging and BMI
    - Advances in Neurotechnology for Human Performance Optimization
- Intheon participated as invited members of the highly curated BrainMind Summit at Stanford, October 12–13 (https://brainmind.org/). We demonstrated NeuroPype and NeuroScale platforms as well as various real-world neuroimaging and BCI technologies.
- Intheon participated in the IEEE EMBS Symposium on Brain, Mind and Body – Cognitive Neuroengineering for Health and Wellness (Dec 19–20, 2019). Intheon was presented with an *IEEE EMBS Demonstration Award*. Mullen participated in an industry-academic panel "Towards more effective and sustainable healthcare through synergy between unobtrusive neurotechnology and holistic medicine".
- Mullen worked on tasks related to his role as an Associate Editor for the *Frontiers in Human Neuroscience* Research Topic titled "Brain-Computer Interfaces and Augmented/Virtual Reality." The Research Topic was finalized and closed this quarter.
- Mullen served as a member of the BrainMind National Neuroethics Advisory Board and participated in a summit meeting of the neuroethics advisory board at Duke University (https://brainmind.org/neuroethics).

- Mullen worked on finalizing a draft of a journal paper titled "Multiview hierarchical Bayesian learning for multi-subject M/EEG source connectivity" detailing and validating a novel method previously developed under the CaN CTA.
- Our team worked on poster and demonstration preparations for the CTA Capstone Meeting.

11.3 Publication Summary for PY10

Papers:

1. Bigdely-Shamlo N, Touryan J, Ojeda A, Kothe C, Mullen T, Robbins K. Automated EEG mega-analysis I: spectral and amplitude characteristics across studies. NeuroImage. 2019;207(15). https://doi.org/10.1016/ j.neuroimage.2019.116361.
2. Bigdely-Shamlo N, Touryan J, Ojeda A, Kothe C, Mullen T, Robbins K. Automated EEG mega- analysis II: cognitive aspects of event related features. NeuroImage. 2019;207. https://doi.org/10.1016/j.neuroimage.2019.116054.
3. Robbins K, Touryan J, Mullen T, Kothe C, Bigdely-Shamlo N. How sensitive are EEG results to preprocessing methods: a benchmarking study. IEEE Trans Neural Syst Rehabil Eng. 2020 Mar;28(5):1081–1090.
4. Hanada G, Wong C-K, Robbins K, Bigdely-Shamlo N, Touryan J, Mullen T. Large-scale analysis of canonical cortical network dynamics across five visual target detection tasks. IEEE Conference on Systems, Man, and Cybernetics; 2019.
5. Fazel-Rezai R, Mullen T. Online Bayesian state space filtering for tracking canonical cortical network activity from EEG. IEEE Conference on Systems, Man, and Cybernetics; 2019.
6. Dehais F, Imad R, Roy R, Iversen J, Mullen T, Callan D. A pBCI to predict attentional error before it happens in real flight conditions. IEEE Conference on Systems, Man, and Cybernetics; 2019. IEEE Brain Best Paper Award.

Selected Invited Talks:

1. Mullen T. Using the NeuroScale & NeuroPype platforms for multi-modal neuroscience and BCI. Invited presentation. National Chiao Tung University / Brain Research Center; 2019.

2. Mullen T. Tools for multi-modal neuroscience data analysis and brain computer interfacing. 1st mbt workshop on Mobile EEG; 2019; Belgrade, Serbia.

3. Mullen T. Online Bayesian state space filtering for tracking canonical cortical network activity from EEG. IEEE Conference on Systems, Man, and Cybernetics; 2019.

4. Kothe C. The Lab Streaming Layer. 9th International Workshop on Brain-Machine Interface Systems. IEEE SMC; 2019.

5. Mullen T. Accelerating multi-modal neuroscience data analysis and brain computer interfacing. UCLA Brain Research Institute Affinity Speaker Series; 2019 Dec 9.

6. Mullen T. Towards more effective and sustainable healthcare through synergy between unobtrusive neurotechnology and holistic medicine. IEEE EMBS Symposium on Brain, Mind and Body -- Cognitive Neuroengineering for Health and Wellness; 2019 Dec 20. Panelist.

7. Mullen T. Keynote. Past, present, and future of brain-computer interface technologies. IPI Winter Forum; 2020 Feb 4; San Francisco, CA.

8. Mullen T. Neural interface technologies: promises, pitfalls, and possibilities for transforming human potential. Katapult Future Fest 2020 Virtual Summit; 2020 May 19. Keynote.

11.4 References

Bigdely-Shamlo N, Touryan J, Ojeda A, Kothe C, Mullen T, Robbins K. Automated EEG mega-analysis I: spectral and amplitude characteristics across studies. NeuroImage. 2019a;207. https://doi.org/10.1016/j.neuroimage.2019.116361.

Bigdely-Shamlo N, Touryan J, Ojeda A, Kothe C, Mullen T, Robbins K. Automated EEG mega- analysis II: cognitive aspects of event related features. NeuroImage. 2019b;207. https://doi.org/10.1016/j.neuroimage.2019.116054.

Blum S, Jacobsen NSJ, Bleichner MG, Debener S. A Riemannian modification of artifact subspace reconstruction for EEG artifact handling. Front Hum Neurosci. 2019 Apr 26. https://doi.org/10.3389/fnhum.2019.00141.

Dehais F, Imad R, Roy R, Iversen J, Mullen T, Callan D. A pBCI to predict attentional error before it happens in real flight conditions. IEEE Conference on Systems, Man, and Cybernetics; 2019. IEEE Brain Best Paper Award.

Hanada G, Wong C-K, Robbins K, Bigdely-Shamlo N, Touryan J, Mullen T. Large-scale analysis of canonical cortical network dynamics across five visual target detection tasks. IEEE Conference on Systems, Man, and Cybernetics; 2019.

Fazel-Rezai R, Mullen T. Online Bayesian state space filtering for tracking canonical cortical network activity from EEG. IEEE Conference on Systems, Man, and Cybernetics; 2019.

Robbins K, Touryan J, Mullen T, Kothe C, Bigdely-Shamlo N. How sensitive are EEG results to preprocessing methods: a benchmarking study. IEEE Trans Neural Syst Rehabil Eng. 2020 March;28(5):1081–1090.

12. University of Maryland, Baltimore County

12.1 Human-in-the-Loop Model Refinement for Efficient Deep Reinforcement Learning

The objective of this project was to develop novel techniques to integrate human intervention in deep reinforcement learning (DRL) to improve learning sample efficiency and implemented the proposed techniques in embedded low-power environments. DRL methods have seen recent success in difficult tasks as different as learning to play video games at superhuman levels from raw images and learning to beat the best human Go players. But like all RL methods, DRL is hungry for data. Atari video games can be "played" much faster than real time, but interactions with the physical world cannot. Therefore, tasks such as learning to control robots or drones can benefit substantially from human intervention. Humans can help reduce RL sample complexity by injecting knowledge, typically directed at the emerging policy. In the past few years, we made a significant progress toward implementing techniques for improving DRL in complex and realistic environments. We also worked closely with ARL researcher Dr Nicholas Waytowich to develop new environments and co-author several papers during past two years. The details of our accomplishments are highlighted here.

The major outcome of this project was the development and enhancement of at least five real-world environments and hardware implementation using our proposed techniques (Fig. 12.1). We demonstrated the efficiency of learning and low-power embedded implementation of the proposed techniques using the majority of these environments in six peer-review conferences.



Fig. 12.1 Demonstration of five real-world environments with our proposed techniques in RL

12.2 Publications

- Manjunath NK, Shiri A, Hosseini M, Prakash B, Waytowich NR, Mohsenin T. An energy efficient EdgeAI autoencoder accelerator for reinforcement learning. IEEE Journal of Circuits and Systems. In review.

In this work, we developed very-low-power autoencoder hardware to be used in autonomous systems. The key novelty is that we represented the trained model in ternarized (2-bit) and binarized (1-bit) instead of the 32-bit floating point that existing work uses. We evaluated the energy efficiency, accuracy, and training of the proposed work using three different environments: Donkey Car autonomous car, Mini World Side Walk, and Object Pickup. We implemented the proposed ternarized autoencoder hardware on an field-programmable gate array (FPGA) that consumes only 370 mW and 0.28 mJ to classify one image.

- Gandhi S, Oates T, Mohsenin T, Waytowich N. Learning behaviors from a single video demonstration using human feedback. International Conference on Autonomous Agents and Multiagent Systems (AAMAS); 2019. Extended abstract.

  In this work, we proposed a method for learning from video demonstrations by using human feedback to construct a mapping between the standard representation of the agent and the visual representation of the demonstration. In this way, we leverage the advantages of both (i.e., we learn the policy using standard state representations, but are able to specify the expected behavior using video demonstration). We train an autonomous agent using a single video demonstration and use human feedback (using a numerical similarity rating) to map the standard representation to the visual representation with a neural network. We show the effectiveness of our method by teaching a hopper agent in the Multi-Joint Dynamics with Contact (MuJoCo) to perform a backflip using a single video demonstration generated in MuJoCo as well as from a real-world YouTube video of a person performing a backflip (Fig. 12.2). Additionally, we show that our method can transfer to new tasks, such as hopping, with very little human feedback.

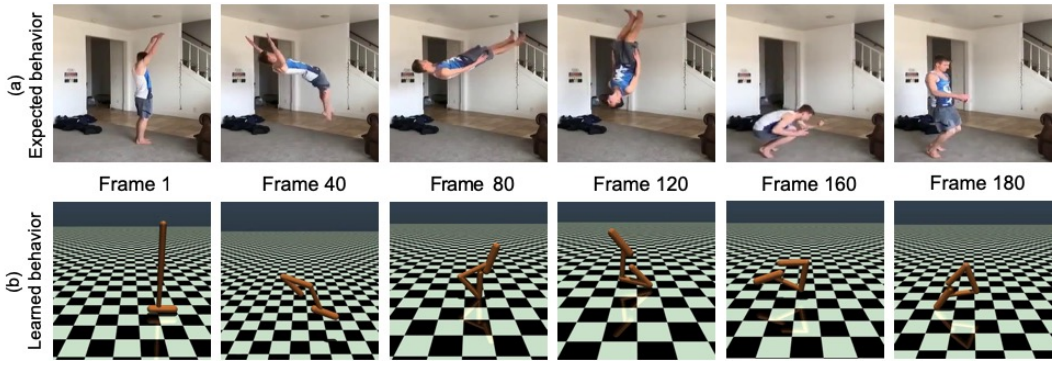


Fig. 12.2 Autonomous agent training with video input and human feedback. Comparison of the backflip in the real-world video demonstration and by our agent. a) Frames of YouTube video of person performing backflip, b) backflip performed by our agent (AAMAS 2019).

- Prakash B, Khatwani M, Waytowich N, Mohsenin T. Improving safety in reinforcement learning using model-based architectures and human intervention. 32nd International FLAIRS conference (AAAI); 2019.

  In this paper, we present a hybrid method for reducing the human intervention time by combining model-based approaches and training a supervised learner to improve sample efficiency while also ensuring safety. We evaluate these methods on various grid-world environments using both standard and visual representations, and show that our approach achieves better performance in terms of sample efficiency, number of catastrophic states reached, as well as overall task performance compared to traditional model-free approaches.

- Prakash B, Horton M, Waytowich N, Hairston WD, Oates T, Mohsenin T. On the use of deep autoencoders for efficient embedded reinforcement learning. 29th Edition of the Great Lakes Symposium on VLSI (GLSVLSI); 2019.

  Training RL agents from high-dimensional image representations can be very expensive and time consuming. We use autoencoders to efficiently learn policies, especially when learning on embedded systems. We have implemented this model on the NVidia Jetson TX2 embedded GPU, and evaluated the power consumption, throughput, and energy consumption of the autoencoders for various CPU/GPU core combinations, frequencies, and model parameters.

- Prakash B, Waytowich N, Ganesan A, Oates T, Mohsenin T. Guiding safe reinforcement learning policies using structured language constraints. SafeAI Workshop in the 34th AAAI conference; 2020.

  We propose a framework to train RL agents conditioned on constraints that are in the form of structured language, thus reducing effort to design and integrate specialized rewards into the environment. In our experiments, we show that this method can be used to ground the language to behaviors and enable the agent to solve tasks while following the constraints. We also show how the agent can transfer these skills to other tasks.

- Shiri A, Mazumder AN, Prakash B, Manjunath NK, Homayoun H, Sasan A, Waytowich NR, Mohsenin R. Energy-efficient hardware for language guided reinforcement learning. 30th Edition of the Great Lakes Symposium on VLSI (GLSVLSI); 2020.

  In this paper, we propose an energy-efficient architecture that is designed to receive both images and text inputs as a step toward designing RL agents

that can understand human language and act in real-world environments. Different configurations are proposed to illustrate the tradeoff between the number of parameters and the model accuracy, and a custom low-power hardware is designed and implemented on an FPGA based on the best configuration. Compared to the similar works using FPGAs for hardware implementation, our design is more energy efficient and needs less energy for generating each output.

13. Bibliography of Representative Publications

The following is a listing of a sample of publications produced by the CaN CTA. The list is in chronological order with earliest publications on top. Links to these publications can found on the ARL CaN CTA website: https://www.arl.army.mil/cast/CaNCTA_PP/#Bibliography.

1. Delorme A, Kothe C, Vankov A, Bigdely-Shamlo N, Oostenveld R, Zander TO, Makeig S. MATLAB-based tools for BCI research. brain-computer interfaces: applying our minds to human-computer interaction. In: Tan DS, Nijholt A; Editors. London: Springer; 2010. p. 241–259.

2. Delorme A, Mullen T, Kothe C, Acar ZA, Bigdely-Shamlo N, Vankov A, Makeig S. EEGLAB, SIFT, NFT, BCILAB, and ERICA: new tools for advanced EEG processing. Intell Neurosci. 2011 Jan;2011:10:10. doi: 10.1155/2011/130714.

3. Lau TM, Gwin JT, McDowell KG, Ferris DP. Weighted phase lag index stability as an artifact resistant measure to detect cognitive EEG activity during locomotion. J Neuro Eng Rehabil. 2012 Jul;9(1):47. doi: 10.1186/1743-0003-9-47.

4. Lawhern V, Hairston WD, McDowell K, Westerfield M, Robbins K. Detection and classification of subject-generated artifacts in EEG signals using autoregressive models. J Neurosci Meth. 2012 Jul;208(2):181–189. doi: 10.1016/j.jneumeth.2012.05.017.

5. Liao L-D, Lin C-T, MacDowell K, Wickenden AE, Gramann K, Jung T-P, Ko L-W, Chang J-Y. Biosensor technologies for augmented brain–computer interfaces in the next decades. Proceedings of the IEEE. 2012 May;100(Special Centennial Issue):1553–1566. doi: 10.1109/JPROC.2012.2184829.

6. Makeig S, Kothe C, Mullen T, Bigdely-Shamlo N, Zhang Z, Kreutz-Delgado K. Evolving signal processing for brain–computer interfaces. Proceedings of the IEEE. 2012 May;100(Special Centennial Issue):1567–1584. doi: 10.1109/JPROC.2012.2185009.

7. Plöchl M, Ossandón JP, König P. Combining EEG and eye tracking: identification, characterization, and correction of eye movement artifacts in electroencephalographic data. Front Hum Neurosci. 2012;6. doi: 10.3389/fnhum.2012.00278.

8. Bigdely-Shamlo N, Mullen T, Kreutz-Delgado K, Makeig S. Measure projection analysis: a probabilistic approach to EEG source comparison and multi-subject inference. NeuroImage, 2013 May;72:287–303. doi: 10.1016/ j.neuroimage.2013.01.040.

9. Kothe CA, Makeig S. BCILAB: a platform for brain–computer interface development. J Neural Eng. 2013 Aug;10(5):056014. doi: 10.1088/1741-2560/10/5/056014.

10. Mcdowell K, Lin C-T, Oie KS, Jung T-P, Gordon S, Whitaker KW, Li S-Y, Lu S-W, Hairston WD. Real-world neuroimaging technologies. IEEE Access. 2013;1:131–149. doi: 10.1109/ACCESS.2013.2260791.

11. Sipp AR, Gwin JT, Makeig S, Ferris DP. Loss of balance during balance beam walking elicits a multifocal theta band electrocortical response. J Neurophysiol. 2013 Aug;110(9):2050–2060. doi: 10.1152/jn.00744.2012.

12. Chuang C-H, Ko L-W, Lin Y-P, Jung T-P, Lin C-T. Independent component ensemble of EEG for brain–computer interface. IEEE Trans Neural Syst Rehabil Eng. 2014 Mar;22(2):230–238. doi: 10.1109/TNSRE.2013.2293139.

13. Gramann K, Ferris DP, Gwin J, Makeig S. Imaging natural cognition in action. Int J Psychophysiol. 2014 Jan;91(1):22–29. doi: 10.1016/ j.ijpsycho.2013.09.003.

14. Gramann K, Jung T-P, Ferris DP, Lin C-T, Makeig S. Toward a new cognitive neuroscience: modeling natural brain dynamics. Front Hum Neurosci. 2014; 8. doi: 10.3389/fnhum.2014.00444.

15. Jangraw DC, Wang J, Lance BJ, Chang S-F, Sajda P. Neurally and ocularly informed graph-based models for searching 3D environments. J Neural Eng. 2014 Jun;11(4):046003. doi: 10.1088/1741-2560/11/4/046003.

16. Lin Y-Y, Liao S-H, Chang J-Y, Lin C-T. Simplified interval type-2 fuzzy neural networks. IEEE Trans Neural Netw Learn Syst. 2014 May;25(5):959–969. doi: 10.1109/TNNLS.2013.2284603.

17. Ojeda A, Bigdely-Shamlo N, Makeig S. MoBILAB: an open source toolbox for analysis and visualization of mobile brain/body imaging data. Front Hum Neurosci. 2014;8. doi: 10.3389/fnhum.2014.00121.

18. Bradford JC, Lukos JR, Ferris DP. Electrocortical activity distinguishes between uphill and level walking in humans. J Neurophysiol. 2015 Dec;115(2):958–966. doi: 10.1152/jn.00089.2015.

19. Chen X, Wang Y, Nakanishi M, Gao X, Jung T-P, Gao S. High-speed spelling with a noninvasive brain–computer interface. PNAS. 2015 Nov;112(44):E6058–E6067. doi: 10.1073/pnas.1508080112.

20. Jarbo K, Verstynen TD. Converging Structural and functional connectivity of orbitofrontal, dorsolateral prefrontal, and posterior parietal cortex in the human striatum. J Neurosci. 2015 Mar;35(9):3865–3878. doi: 10.1523/JNEUROSCI.2636-14.2015.

21. Kline JE, Huang HJ, Snyder KL, Ferris DP. Isolating gait-related movement artifacts in electroencephalography during human walking. J Neural Eng. 3015 Jun;12(4):046022. doi: 10.1088/1741-2560/12/4/046022.

22. Muraskin J, Sherwin J, Sajda P. Knowing when not to swing: EEG evidence that enhanced perception–action coupling underlies baseball batter expertise. NeuroImage. 2015 Dec;123:1–10. doi: 10.1016/j.neuroimage.2015.08.028.

23. Betzel RF, Gu S, Medaglia JD, Pasqualetti F, Bassett DS. Optimally controlling the human connectome: the role of network topology. Sci Rep. 2016 Jul;6(1):1–14. doi: 10.1038/srep30770.

24. Bigdely-Shamlo N, Cockfield K, Makeig S, Rognon T, La Valle C, Miyakoshi M, Robbins KA. Hierarchical event descriptors (HED): semi-structured tagging for real-world events in large-Scale EEG. Front Neuroinform. 2016;10. doi: 10.3389/fninf.2016.00042.

25. Cole MW, Ito T, Bassett DS, Schultz DH. Activity flow over resting-state networks shapes cognitive task activations. Nat Neurosci. 2016 Dec;19(12):1718–1726. doi: 10.1038/nn.4406.

26. Lin C-T, Chuang C-H, Kerick S, Mullen T, Jung T-P, Ko L-W, Chen S-A, King J-T, McDowell K. Mind-wandering tends to occur under low perceptual demands during driving. Sci Rep. 2016 Feb;6(1):1–11. doi: 10.1038/srep21353.

27. Muldoon SF, Bridgeford EW, Bassett DS. Small-world propensity and weighted brain networks. Sci Rep. 2016 Feb;6(1):1–13. doi: 10.1038/srep22057.

28. Oliveira AS, Schlink BR, Hairston WD, König P, Ferris DP. Proposing metrics for benchmarking novel EEG technologies towards real-world measurements. Front Hum Neurosci. 2016;10. doi: 10.3389/fnhum.2016.00188.

29. Tzelesford QK, Lynall M-E, Vettel J, Miller MB, Grafton ST, Bassett DS. Detection of functional brain network reconfiguration during task-driven cognitive states. NeuroImage. 2016 Nov;142:198–210. doi: 10.1016/j.neuroimage.2016.05.078.

30. Wu D, Lawhern VJ, Hairston WD, Lance BJ. Switching EEG headsets made easy: reducing offline calibration effort using active weighted adaptation regularization. IEEE Trans Neural Syst Rehabil Eng. 2016 Nov;24(11):1125–1137. doi: 10.1109/TNSRE.2016.2544108.

31. Baek EC, Scholz C, O'Donnell MB, Falk EB. The value of sharing information: a neural account of information transmission. Psychol Sci. 2017 Jul;28(7):851–861. doi: 10.1177/0956797617695073.

32. Garcia JO, Brooks J, Kerick S, Johnson T, Mullen TR, Vettel JM. Estimating direction in brain-behavior interactions: Proactive and reactive brain states in driving. NeuroImage. 2017 Apr;150:239–249. doi: 10.1016/j.neuroimage.2017.02.057.

33. Melnik A, Hairston WD, Ferris DP, König P. EEG correlates of sensorimotor processing: independent components involved in sensory and motor processing. Sci Rep. 2017 Jun;7(1):1–15. doi: 10.1038/s41598-017-04757-8.

34. Melnik A, Legkov P, Izdebski K, Kärcher S, Hairston WD, Ferris DP, König P. Systems, subjects, sessions: to what extent do these factors influence EEG data? Front Hum Neurosci. 2017;11. doi: 10.3389/fnhum.2017.00150.

35. Schlink BR, Peterson SM, Hairston WD, König P, Kerick SE, Ferris DP. Independent component analysis and source localization on mobile EEG Data can identify increased levels of acute stress. Front Hum Neurosci. 2017;11. doi: 10.3389/fnhum.2017.00310.

36. Schmälzle R, O'Donnell MB, Garcia JO, Cascio CN, Bayer J, Bassett DS, Vettel JM, Falk EB. Brain connectivity dynamics during social interaction reflect social network structure. PNAS. 2017 May;114(20):5153–5158. doi: 10.1073/pnas.1616130114.

37. Tu T, Schneck N, Muraskin J, Sajda P. Network configurations in the human brain reflect choice bias during rapid face processing. J Neurosci. 2017 Dec;37(50):12226–12237. doi: 10.1523/JNEUROSCI.1677-17.2017.

38. Wu D, Lance BJ, Lawhern VJ, Gordon S, Jung T-P, Lin C-T. EEG-based user reaction time estimation using riemannian geometry features. IEEE Trans Neural Syst Rehabil Eng. 2017 Nov;25(11):2157–2168. doi: 10.1109/TNSRE.2017.2699784.

39. Cooper N, Garcia JO, Tompson SH, O'Donnell MB, Falk EB, Vettel JM. Time-evolving dynamics in brain networks forecast responses to health messaging. Netw Neurosci. 2018 May;3(1):138–156. doi: 10.1162/ netn_a_00058.

40. Dmochowski JP, Ki JJ, DeGuzman P, Sajda P, Parra LC. Extracting multidimensional stimulus-response correlations using hybrid encoding-decoding of neural activity. NeuroImage. 2018 Oct;180:134–146. doi: 10.1016/j.neuroimage.2017.05.037.

41. Garcia JO, Ashourvan A, Muldoon S, Vettel JM, Bassett DS. Applications of community detection techniques to brain graphs: algorithmic considerations and implications for neural function. Proceedings of the IEEE. 2018 May;106(5):846–867. doi: 10.1109/JPROC.2017.2786710.

42. Lawhern VJ, Solon AJ, Waytowich NR, Gordon SM, Hung CP, Lance BJ. EEGNet: a compact convolutional neural network for EEG-based brain–computer interfaces. J Neural Eng. 2018 Jul;15(5):056013. doi: 10.1088/1741-2552/aace8c.

43. Wasylyshyn N, Hemenway B, Garcia JO, Cascio CN, O'Donnell MB, Bingham CR, Simons-Morton B, Vettel JM, Falk EB. Global brain dynamics during social exclusion predict subsequent behavioral conformity. Soc Cogn Affect Neurosci. 2018 Feb;13(2): 82–191. doi: 10.1093/scan/nsy007.

44. Waytowich N, Lawhern V, Garcia JO, Cummings J, Faller J, Sajda P, Vettel JM. Compact convolutional neural networks for classification of asynchronous steady-state visual evoked potentials. J Neural Eng. 2018 Oct;15(6):066031;2018. doi: 10.1088/1741-2552/aae5d8.

45. Bigdely-Shamlo N, Touryan J, Ojeda A, Kothe C, Mullen T, Robbins K. Automated EEG mega-analysis I: spectral and amplitude characteristics across studies. NeuroImage. 2019 Nov;116361. doi: 10.1016/ j.neuroimage.2019.116361.

46. Bigdely-Shamlo N, Touryan J, Ojeda A, Kothe C, Mullen T, Robbins K. Automated EEG mega-analysis II: cognitive aspects of event related features. NeuroImage, 2019 Sep:116054. doi: 10.1016/j.neuroimage.2019.116054.

47. Chang C-Y, Hsu S-H, Pion-Tonachini L, Jung T-P. Evaluation of artifact subspace reconstruction for automatic artifact components removal in multi-channel EEG recordings. IEEE Trans Biomed Eng. 2019:1–1. doi: 10.1109/TBME.2019.2930186.

48. Faller J, Cummings J, Saproo S, Sajda P**.** Regulation of arousal via online neurofeedback improves human performance in a demanding sensory-motor task. PNAS. 2019 Mar;116(13):6482–6490. doi: 10.1073/pnas.1817207116.

49. Madsen J, Margulis EH, Simchy-Gross R, Parra LC. Music synchronizes brainwaves across listeners with strong effects of repetition, familiarity and training. Sci Rep. 2019 Mar;9(1):1–8. doi: 10.1038/s41598-019-40254-w.

50. Solon AJ, Lawhern VJ, Touryan J, McDaniel JR, Ries AJ, Gordon SM. Decoding P300 variability using convolutional neural networks. Front Hum Neurosci. 2019;13. doi: 10.3389/fnhum.2019.00201.

14. CaN CTA Research Contributors

Last name	First name	Affiliation
Acar	Zeynep	UCSD
Adali	Tulay	UMBC
Apker	Greg	ARL
Arsiwalla	Xerxes	UPF
Balkan	Ozgur	UCSD
Ball	Kenneth	UTSA
Banerjee	Nilanjan	UMBC
Bassett	Danielle	UPenn
Beukema	Patrick	CMU
Bigdely-Shamlo	Nima	UCSD
Bin Hossain	Arif	UTSA
Boatman	Dana	JHU
Buffington	Robert	UCSD
Cao	Ze-Hong	UTS
Cervenka	M	JHU
Chang	Hao-Yen	NCTU
Chang	Yu-Cheng	UTS
Chao	Tze-Yand	NCTU
Chen	Sheng-Fu	NCTU
Chen	Shi-An	UTS
Cheng	Tze-Kuan	NCTU
Chiu	Ching-Yu	NCTU
Chiu	Chin-Yu	UTS
Choe	YJ	CMU
Chuang	Chun-Hsiang	UTS
Chuang	Wanli	NCTU
Chuang	Ya-Ting	NCTU
Cockfield	Jeremy	UTSA
Cooper	Nicole	UPenn
DeGuzman	Paul	Neuromatters
Dunkel	Michael	DCS
Ebert	Manuel	UOs
Ehtiati	Neda	Syntrogi
Falk	Emily	UPenn
Faller	Josef	Columbia
Feltch	Cody	DCS
Ferris	Daniel	UMI
Flascher	Oded	DCS
Franaszczuk	Piotr	ARL
Gameriro	Ricardo	Uos
Geary	Robert	UMI
Goeke	Caspar	IBEC
Gordon	Stephen	DCS
Gramann	Klaus	UCSD

Last name	First name	Affiliation
Hairston	David	ARL
Hajinoroozi	Mehdi	UTSA
Hanada	Grant	UMI/UFL
Hong	Linbi	Columbia
Hsu	Sheng-Hsiou	UCSD
Hsu	Wen-Cheng	NCTU
Huang	Chih-Sheng	UTS
Huang	He	UCSD
Huang	Teng-Yi	NCTU
Huang	Yufei	UTSA
Izdebski	Kryzysztof	UOs
Jarbo	Kevin	CMU
Jaswa	Matthew	DCS
Jung	Tzzy-Ping	UCSD
Kalyan	Sai	NCTU
Kannan	Nandini	UTSA
Kellihan	Bret	DCS
Kerick	Scott	ARL
King	Jung-Tai	NCTU
Ko	Li-Wei	NCTU
Komarov	Oleksii	NCTU
König	Peter	UOs
Kothe	Christian	UCSD
Kreutz-Delgado	Kenneth	UCSD
Kuester	Falko	UCSD
Lance	Brent	ARL
LaRocco	John	UTSA
Lawhern	Vernon	UTSA DCS ARL
Lee	Timothy	DCS
Levy	Roger	UCSD
Liang	Chung-Wei	NCTU
Liao	Lun-De	NCTU
Lin	Chin-Teng	NCTU
Liu	Shih-Hua	NCTU
Liu	Yu-Ting	UTS
Lou	Bin	Columbia
Lu	Shao-Wei	NCTU
Lukos	Jamie	ARL
Makeig	Scott	UCSD
Mattar	Marcelo	UPenn
McDaniel	Jonathan	DCS
McDowell	Kaleb	ARL
Meng	Jia	UTSA
Metcalfe	Jason	DCS/ARL
Meyer	David	UMI
Ming	Yu-Rui	UTS

Last name	First name	Affiliation
Mohsenin	Tinoosh	UMBC
Molesworth	Tara	CMU
Mrozek	Randy	ARL
Muil	Robert	UOs
Muraskin	Jordan	Columbia
Nascimben	Mauro	NCTU
Nayak	Tapsya	UTSA
Netto	Derek	Neuromatters
Nikanishi	Masaki	UCSD
Nonte	Michael	DCS
Nordin	Andrew	UMI/UFL
O'Donnell	Matt	UPenn
Oates	Timothy	UMBC
Oie	Kelvin	ARL
Oliveira	Anderson	UMI
Omedas	Pedro	UPF
Palmer	Jason	UCSD
Passaro	Tony	DCS/ARL
Ploechl	Michael	UOs
Poczos	Barnabas	CMU
Riordan	Rick	Syntrogi
Robbins	Kay	UTSA
Robucci	Ryan	UMBC
Sajda	Paul	Columbia
Saproo	Sameer	Columbia
Schilz	Joseph	UCSD
Schlink	Bryan	UMI
Shenoy	Pradeep	UCSD
Sheulk	Lei	CMU
Shi	Chao	UTSA
Shih	Benjamin	UCSD
Siddharth	Siddharth	UCSD
Singh	Aarti	CMU
Singh	Avinash	NCTU
Sipp	Amy	U MI
Smith	Nathaniel	UCSD
Solon	Amelia	DCS
Song	Meng Shue	NCTU
Stretcu	Otilia	CMU
Su	Kyung Min	UTSA
Telesford	Qawi	UPenn
Touryan	Jonathan	ARL
Townsend	Jean	UCSD
Tseng	Kevin	NCTU
Tu	Tao	Columbia
Valenti	James	CMU

Last name	First name	Affiliation
Vankov	Andrey	UCSD
Veljkovic-Perez	Dragana	UTSA
Verschure	Paul	UPF
Verstynen	Timothy	CMU
Vettel	Jean	ARL
Wahn	Basil	UOs
Walker	Anthony	DCS
Wan	I-Jan	NCTU
Wang	Yijung	UCSD
Wang	Yu-Te	UCSD
Waytowitch	Nick	Columbia
Wei	Chun-Shu	UCSD
Wei	Min	DCS
Weiss	Neil	Columbia
Wells	Nicole	UCSD
Whitaker	Keith	ARL
Wu	Dongrui	DataNova
Wu	Ying	UCSD
Yang	Yin Lin	NCTU
Yeh	Frank	CMU
Yu	Alfred	ARL
Yu	Angela	UCSD
Yu	Yi-Hsin	NCTU
Yun	Chen	NCTU
Zucca	Riccardo	UPF

List of Symbols, Abbreviations, and Acronyms

3-D	three-dimensional
9-DOF	nine degrees-of-freedom
AAMAS	Autonomous Agents and Multiagent Systems
ACA	advanced computational approaches
ACC	anterior cingulate cortex
ADC	analog-to-digital converter
Ag	silver
AgCl	silver chloride
AHRS	attitude heading reference system
AI	alertness index
AIC	anterior insular cortex
ANOVA	analysis of variance
API	application programming interface
APP	Annual Program Plan
AR	augmented reality
ARL	Army Research Laboratory
ASR	Artifact Subspace Reconstruction
AUC	area under receiver operator curve
BART	Balloon Analogue Risk Task
BAT	boundary avoidance task
BCG	ballistocardiogram
BCI	brain–computer interaction/interface
BCIT	brain–computer interaction technology
BEM	boundary element method
BF	Bayes factor
BIDS	Brain Imaging Data Structure
BLASST	Band Limited Atomic Sampling With Spectral Tuning
BOLD	blood oxygen level-dependent

BSBL	block sparse Bayesian learning
C3DS	CaN CTA Consortium Data Server
CaN CTA	Cognition and Neuroergonomics Collaborative Technology Alliance
CCA	canonical correlation analysis
CCM	convergent cross mapping
CES	Command Environment Simulator
CI	confidence interval
CL	classification
CMU	Carnegie Mellon University
CNN	convolutional neural network
CNN4EEG	New CNN architecture designed specifically for capturing the spatial and temporal correlations in EEG.
CNS	central nervous system
CNV	contingent negative variation
CPU	central processing unit
CRASH	Cognitive Resilience And Sleep History
CSA	cognitive state assessment
CSP	common spatial pattern
CSR-LAR	Comparison of Stress Responses under Laboratory, Ambulatory, and Real-World Environments
CT2WS	Cognitive Technology Threat Warning System
CTAGGER	Tool for user community to populate hierarchical event tags for neurophysiology data collection
CV	cross-validation
DAM	drowsiness assessment and management
DAN	dorsal attention
DAQ	data acquisition
DAS	dynamic attention-shifting
DASS	Depression Anxiety Stress Scale
DCM	dynamic casual modeling

DCS	DCS Corporation
DD	diverse density
dDTF	direct directed transfer function
DEVCOM	US Army Combat Capabilities Development Command
DFT	discrete Fourier transform
DIPFIT	equivalent dipole source localization of independent components
DL	deep learning
DLPFC	dorsal lateral prefrontal cortex
DMM	deep Markov model
DMN	default mode network
dMRI	dynamic magnetic resonance imaging
DP	driving performance
DRL	deep reinforcement learning
DRN	deep relationship network
DR-RBFN	data-reused radial basis function network
DRV	driving-related variable
DSS	Daily Sampling System
DTF	directed transfer function
DTI	diffusion tensor imaging
EA	evolutionary algorithm
ECG	electrocardiography
ECoG	electrocorticography
EDA	electrodermal activity
EEG	electroencephalography
EMA	electromagnetic articulography
EMBC	Engineering in Medicine and Biology Conference
EMG	electromyography
EOG	electrooculography
ERD	event-related desynchronization

ERICA	Experimental Recording, Interactive Control and Analysis
ERP	event-related potential
ERSP	event-related spectrum perturbation
ESC	extrastriate cortex
ESS	EEG Study Schema
FC	functional connectivity
FDR	Fisher's discriminant ratio
FE	feature extraction
FEA	front-end amplifier
FEM	finite-element method
FFT	fast Fourier transform
FG	fusiform gyrus
FH	first half
FIR	finite impulse response
fMRI	functional magnetic resonance imaging
fNIRS	functional near-infrared spectroscopy
FOA	focus of attention
FPGA	field-programmable gate array
FRP	fixation-related potential
Fz	frontal brain region
GA	genetic algorithm
GAN	generative adversarial network
GCM	Granger causality model
GFP	global field power
GLM	general linear model
GLZ	generalized linear model
GPU	graphics processing unit
GRAND	general regression of aspects and details
GSR	galvanic skin response
GUI	graphical user interface

hBCI	hybrid brain-computer interface
HDCA	hierarchical discriminate component analysis
HED	hierarchical event descriptor
HF	Huynh–Feldt
HEOG	horizontal EOG
HID	human interest detector
HRV	heart-rate variability
IC	independent component
ICA	independent component analysis
ICi	independent components of interest
ICSD	independent component sparse decomposition
IEEE	Institute of Electrical and Electronic Engineers
IG	information gain
IMAI	Integrating Multi-Aspect Information
IMU	inertial measurement unit
IPL	inferior parietal lobule
IR	infrared
IRB	institutional review board
IRW	instrumented real-world
ISC	inter-subject correlation
ITC	inter-trial coherence
ITR	information transfer rate
JADE	Joint Approximation Diagonalization of Eigenmatrices
JHU	Johns Hopkins University
jICA	joint independent component analysis
KSS	Karolinska sleepiness scale
LC	locus coeruleus
LDA	linear discriminant analysis
LDEs	local driving errors
LED	light-emitting diode

LF	low frequency
LIM	limbic
LIWC	Linguistic Inquiry and Word Count
LKT	lane-keeping task
LORETA	low resolution electromagnetic tomography
LSE	Large-Scale Experiment
LSIE	Large-Scale Integration Experiment
LSL	lab streaming layer
LSSM	latent state space modeling
LSTM	long short-term memory
MAP	maximum a posteriori
MARA	Multiple Artifact Rejection Algorithm
MARIN	Multi-Aspect Real-world Integrated Neuroimaging
MCC	midcingulate cortex
MCCA	multiset canonical correlation analysis
mDES	modified Differential Emotions Scale
MDL	Minimum Description Length
MDRM	minimum distance to Riemannian mean
MDS	multivariate dynamical systems
MEG	magnetoencephalography
MEMS	microelectromechanical system
MI	motor imagery
mIRW	minimally instrumented real-world
ML	machine learning
MoBI	mobile brain/body imaging
MPFC	medial prefrontal cortex
MPT	Measure Projection Toolbox
MRCP	movement-related cortical potential
MRI	magnetic resonance imaging
MuJoCo	Multi-Joint dynamics with Contact

MutInf	mutual information
mwCSSP	multi-window Common Spatio-Spectral Patterns
mwFBCSP	multi-window Filter-Bank Common Spatial Patterns
NCTU	National Chiao Tung University (Taiwan)
NCP	neurocomputation
NEDE	naturalistic experimental design environment; open-source scripting suite for developing experiments in 3-D virtual environments.
NFT	Neuroelectromagnetic Forward Head Modeling Toolbox
NNI	Nearest Neighbor Index
ODE	operator dynamics of event
P300	positive component of the event-related potential
PANAS	Positive and Negative Affect Scale
PCA	principal component analysis
PCC	posterior cingulate cortex
pCCA	phase-constrained canonical correlation analysis
PDC	partial directed coherence
PI	principal investigator
PLR	prospective lapse rate
PLV	phase locking value
PREP	preprocessing
PSD	power spectral density
PSN	pre-stimulus noise
PY	program year
Pz	parietal brain region
QUSP	formerly Syntrogi, Inc.
rASR	Riemannian ASR
RBF	radial basis function
RG	Riemannian geometry
RL	reinforcement learning

RM-ANOVA	repeated measures analysis of variance
RMS	root-mean-square
ROI	region of interest
RPCA	robust principal component analysis
RSA	representational similarity analysis
RSSD	Regularized Spatio-Spectral Dynamics
RSVP	rapid serial visual presentation
RT	reaction/response time
RVM	relevance vector machine
RW	real world
RWN	real-world neuroimaging
SANDR	Standardized Annotated Neurophysiology Data Repository
SCCN	Swartz Center for Computational Neuroscience
SCR	skin conductance response
SES	socioeconomic status
SE-SSM	Simon effect SSM
SH	second half
SIFT	Source Information Flow Toolbox
SIM	simulator
SL	shallow learning
SMC	sensorimotor cortex
SMA	supplementary motor area
SMPC	Society for Music Perception and Cognition Conference
sMRI	structural magnetic resonance imaging
SMSE	standardized mean square error
SNAP	Simulation Neuroscience and Application Platform
SNR	signal-to-noise ratio
SOA	stimulus onset asynchrony
SOBI	Second Order Blind Identification
SOM	self-organizing map

SRS	social risk sensitivity
SSM	sequential sampling model
SSVEP	steady-state visually evoked potential
ST	solution time
STRONG	Strengthening Teamwork for Robust Operations in Novel Groups
STRUM	Small Team Reconnaissance and Urban Surveillance Missions
stTFCE	spatiotemporal threshold-free cluster enhancement
SVM	support vector machine
SVMRBF	SVM with radio basis function kernel
TARDEC	US Army Tank Automotive Command
THOR	temporal hierarchical overlap regression
TPN	task-positive network
TR	temporal resolution
TRCA	task-related component analysis
TW	time warping
TX16	TARDEC experiment 16
UCSD	University of California, San Diego
UMI	University of Michigan
UMBC	University of Maryland Baltimore County
UOs	University of Osnabruck
UPenn	University of Pennsylvania
UPF	Universitat Pompeu Fabra
UTS	University of Technology Sydney
UTSA	University of Texas at San Antonio
VEOG	vertical EOG
VDE	vehicle driving experiment
VEP	visually evoked potential
VMF	Vehicle Motion and Cognitive Fatigue
VMPFC	ventromedial prefrontal cortex

VR	virtual reality
VS	ventral striatum
WDAS	wearable daily assessment system
WDT	Wearable EEG Development and Testing
WWD	wearable and wireless dry-electrode
XDF	Extensible Data Format

1 (PDF) DEFENSE TECHNICAL INFORMATION CTR DTIC OCA

1 (PDF) DEVCOM ARL FCDD RLD DCI TECH LIB

1 (PDF) DEVCOM ARL FCDD RLH B T DAVIS BLDG 5400 RM C242 REDSTONE ARSENAL AL 35898-7290

1 (PDF) DEVCOM ARL FCDD HSI J THOMAS 6662 GUNNER CIRCLE ABERDEEN PROVING GROUND MD 21005-5201

1 (PDF) USAF 711 HPW 711 HPW/RH K GEISS 2698 G ST BLDG 190 WRIGHT PATTERSON AFB OH 45433-7604

1 (PDF) USN ONR ONR CODE 341 J TANGNEY 875 N RANDOLPH STREET BLDG 87 ARLINGTON VA 22203-1986

1 (PDF) USA NSRDEC RDNS D D TAMILIO 10 GENERAL GREENE AVE NATICK MA 01760-2642

1 (PDF) OSD OUSD ATL HPT&B B PETRO 4800 MARK CENTER DRIVE SUITE 17E08 ALEXANDRIA VA 22350

ABERDEEN PROVING GROUND

14 (PDF) DEVCOM ARL FCDD RLH J LANE Y CHEN P FRANASZCZUK A MARATHE K MCDOWELL K OIE FCDD RLH F J GASTON (A) FCDD RLH FA A DECOSTANZA FCDD RLH FB D BOOTHE (A) FCDD RLH FC K COX (A) J TOURYAN T LEE FCDD RLH FD A FOOTS (A) FCDD RLH FE D HEADLEY